PHD

The Sonochemical Remediation of Phthalate Esters
An investigation into products and kinetics

Vandenburg, Daniel

Award date:
2012

Awarding institution:
University of Bath

The Sonochemical Remediation of Phthalate Esters:

An investigation into products and kinetics

Volume 1 of 1

Daniel Martin VandenBurg

A thesis submitted for the degree of Doctor of Philosophy

University of Bath

Department of Chemistry

November 2011

Signed_____

Abstract

Phthalate esters or phthalates have become ubiquitous water pollutants. They are used as plasticisers in several plastics. Due to them not being bound to the plastic material they leach out over time. Thus phthalate esters have entered the planet's aquasphere. Phthalates are stable in the environment and also recalcitrant to most standard water processing methods. Due to their being linked to endocrine disruption and cancer they have been classed as a pollutant of concern by the EU and the American EPA.

Previous work had shown that ultrasound of frequency between 20 kHz and 500 kHz can be used to remove phthalate esters from aqueous solutions as an advanced oxidation process. These works studied the effects of various parameters on the sonolysis. They however, did not perform a satisfactory analysis of the degradation products of the esters studied. These too may be biologically active and need to be ascertained for ultrasound to be considered for their removal from water in industrial and municipal processing centres.

Therefore this work describes the study of additional parameters known to be pertinent to ultrasound science, namely the acoustic power, the type of gas dissolved in the solution and the initial concentration of phthalate on the sonolysis of DBP as a model for the family of phthalate esters. Work was performed using 20 kHz and 515 kHz ultrasound. The performance of these two systems is compared and contrasted throughout. A detailed analysis of the products of the degradation of DBP was then performed using LC-MS based methods.

Finally the degradation of other alkyl phthalates was examined as well as the effect of DBP on the quenching of aqueous sonoluminescence. This last topic was performed hoping it would give some insight into the way DBP partitions in the bubble-water interface.

Acknowledgements

I would firstly like to thank my parents without whose financial support the last several months I would not have been able to finish my PhD as comfortably as I have done so.

Secondly I would like to thank my supervisor Prof. Gareth Price for his advice, patience, support, encouragement and where needed discipline these past five years.

I would like to thank Dr Anneke Lubben for her excellent support and advice in the mass spectrometry work needed for this project. Mass spectrometry was fairly new to me and I knew little about it before starting this project. The increase in my knowledge has mainly occurred thanks to the suggestion and guidance of you, Anneke.

Similarly I would like to thank Dr Matt Jones for his help with the GC and GC-MS experiments and the use of said equipment.

Next I would like to thank all members of Price group during my PhD. Especial thanks to Dr David King and Dr Ursula Laska for making me feel welcome when I first started and helping me find my feet in the field of ultrasonics.

Many thanks to members of Edler and Roser research groups, to Jim Holdaway, Rob Barker, Dr Bin Yang and to Dr Karen Edler and Dr Steve Roser. I learnt a lot during our group meetings as a triumvirate. To Jim and Rob many thanks for your social activities the past 4 years and to your ongoing support as friends.

I would lastly like to thank all my friends from the department who are too many to name, bust special thanks to Dr Claire Thompson for your emotional support while writing this thesis, I couldn't have finished it without you all.

List of Acronyms and Abbreviations

AOP: Advanced Oxidation Process

BBP: Butylbenzyl phthalate

CMC: Critical Micelle Concentration

DBP: Dibutyl phthalate

DBP: Dodecyl benzene sulfonate

DEHP: Diethylhexyl phthalate

DEP: Diethyl phthalate

DHP: Diheptyl phthalate

DMP: Dimethyl phthalate

DNP: Dinonyl phthalate

DOC: Dissolved Organic Content

DOM: Dissolved Organic Matter

DOP: Dioctyl phthalate

DPP: Diptopyl phthalate

EPA: Environment Protection Agency (USA)

ESI-TOF: Electrospray Ionisation – Time of Flight

EU: European Union

GC: Gas Chromatography

GC-MS: Gas Chromatography - Mass Spectrometry

HPLC: High Performance Liquid Chromatography

HTA: Hydroxyterephthalic acid

LC: Liquid Chromatography

LC-MS: Liquid Chromatography – Mass Spectrometry

MBP: Monobutyl phthalate

MEP: Monoethyl phthalate

MO: Methyl Orange

MS: Mass Spectrometry

MS-MS: Mass Spectrometry – Mass Spectrometry

NMR: Nuclear Magnetic Resonance

NOM: Natural Organic Matter

OBS: Octylbenzene sulfonate

pK_{OW}: Octanol-Water Partition Coefficient

PTFE: polytetrafluroethane

PVC: Polyvinylchloride

SDS: Sodium dodecyl sulfonate

SL: Sonoluminescence

SPME: Solid Phase Micro-extraction

STS: Sodium 4-toluene sulfonate

TBZ: Thiabendazole

TNT: Trinitrotoluene

TOC: Total Organic Content

TOF: Time of Flight

UV: Ultraviolet

UV-Vis: Ultraviolet – Visible

W/V: Weight *per* Volume

Contents Page

Contents

Abstract....2
Acknowledgements....3
List of Acronyms and Abbreviations....4
Chapter 1: General Introduction to ultrasound....10
1.1: Definition of Ultrasound....10
1.2: The nature of the ultrasonic wave....11
1.3: Definition of terms used in ultrasound science....13
1.4: How ultrasound causes cavitation to occur....15
1.5: The influence of the ultrasound wave on cavitation bubbles....16
1.6: Stable and transient cavitation....18
1.7: The productive consequences of cavitation....21
1.8: Factors that influence the effects of cavitation....22
1.9: How a sound wave can produce chemistry....25
1.10: Chapter References....29
Chapter 2: Introduction to water treatment processes....31
2.1: Behaviour of ultrasound in water....31
2.2: Current methods employed for water treatment....34
2.3: Advanced oxidation processes....38
2.4: Use of ultrasound as an AOP for aqueous remediation chemistries....44
2.5: Phthalate esters....59
2.6: Previous work on phthalate ester remediation using ultrasound....64
2.7: Aims and goals....68
2.8: Chapter References....69
Chapter 3: Experimental....72

3.1: Ultrasonic Equipment....72
3.2 Liquid Chromatography - Mass Spectrometry 91
3.3: Methods for kinetic analyses of phthalate degradations. 94
3.4: Methods for assessments of phthalate degradation products.....98
3.5: Method of analyses of reaction model 101
3.6: Measuring surface tension of DBP solutions 103
3.7: Materials Used....104
3.8: Calculation of best fit lines and fitted data calculated from such lines ..105
3.9: Chapter References....106
Chapter 4: Method Development 107
4.1: Handling requirements and user precautions 107
4.2: Solution preparation....108
4.3: Internal standards 109
4.4: Sampling and processing of solutions 110
4.5: Quantification procedures....112
4.6: Method validation....114
4.7: Why DBP was chosen as a model....116
4.8: Chapter references 119
Chapter 5: Results and discussion of dibutyl phthalate degradation kinetics experiments. 120
5.1: Starting work; a basic check of the sonolysis of DBP 120
5.2: Varying ultrasonic power. 124
5.3: Changing the gas dissolved in solution....132
5.4: Varying the initial concentration of DBP....146
5.5: Relating the rate of degradation of DBP to the ·OH radical yield....163
5.6: Addition of additives to DBP degradation experiments 166
5.7: Drawing up a model for the degradation of DBP 170

5.8: Chapter references 175
Chapter 6: Studies on the products of the degradation of DBP 177
6.1: Chapter summary and initial explanations 177
6.2: The products of DBP degradation under argon: liquid phase 178
6.3: Finding gas phase products using GC and GC-MS 196
6.4: A semi quantitative study into the effect of frequency on degradation product distributions 197
6.5: .. A semi quantitative study into the effect of different gas compositions on the degradation products and their distributions 206
6.6: ..... Chapter references 224
Chapter 7: Collected Experiments 225
7.1: Aqueous sonoluminescence quenching by DBP 225
7.2: Degradation studies on other phthalate esters 230
7.3: Chapter References 239
Chapter 8: Conclusions and Future Work 240
8.1: Conclusions arising from chapter 5, kinetic results 240
8.2 Conclusions from chapter 6, product analysis 242
8.3: Conclusions from chapter 7, collected data 244
8.4: Proposals for future work 246
8.5 Chapter references 247
Appendix I : LC-MS Spectra of products found to occur from DBP degradation 248

Chapter 1: General Introduction to ultrasound

1.1: Definition of Ultrasound

Ultrasound is defined as any sound which is beyond human hearing. The limit of human hearing is generally considered to be about 16 kHz[1], therefore ultrasound ranges from ~17 kHz upwards.

There are two general forms of ultrasound in use today, diagnostic ultrasound and power ultrasound. They are defined both by their frequency, acoustic intensity and their uses. Typically power ultrasound is less than 800 kHz in frequency, whereas diagnostic ultrasound is >1 MHz in frequency.

Diagnostic Ultrasound

Diagnostic ultrasound, also known as imaging ultrasound, is generally low in acoustic intensity and is used not only by mankind to produce the ultrasound images that are familiar in medicine[2-4] but also by bats and whales as a method of locating objects, known as echolocation[5, 6].

The frequency of diagnostic/imaging ultrasound generally ranges from 1-10 MHz but sometimes frequencies as low as 100 kHz are used in echolocation and frequencies as high as 100 MHz are sometimes used in diagnostic imaging[7].

Power Ultrasound

Power ultrasound is of much higher acoustic intensities than diagnostic ultrasound as is implied by its name. Power ultrasound makes use of a narrower range of frequencies than diagnostic ultrasound, typically ranging from 20 kHz[8] to 1MHz[9]. However, frequencies higher than 800 kHz are not often used.

Like diagnostic ultrasound, power ultrasound varies in its uses. Almost all chemists are familiar with ultrasonic cleaning baths which make use of low intensity power ultrasound to clean the surfaces of lab glassware. Power ultrasound is used in the materials industry for, as examples, the dispersal of solids[10], atomization of particles[11] and to induce crystallisation[12], particularly of pharmaceuticals[13]. Recently power ultrasound has also been popular in the food and beverage industry. For example it has been used in the manufacture of mousses[14] and for improving the character and flavour of wines[15].

Power ultrasound is also responsible for the process of cavitation; the nucleation, growth and violent collapse of microscopic bubbles whose effects bring about the processes of sonochemistry, the chemistry created as a result of power ultrasound.

1.2: The nature of the ultrasonic wave

Ultrasound whether it be diagnostic or power ultrasound is a longitudinal wave. This means that particles under the influence of the sound wave are moved parallel to the direction of movement of the sound wave[16]. These particles do not travel freely with the wave however but merely oscillate as the wave changes from positive to negative pressure phases[17].

Figure 1.1 shows a diagram of an ultrasonic wave travelling along the positive X direction (to the right). It can be seen that the wave is sinusoidal and consists of positive and negative pressure phases.

The top of figure 1.1 shows the influence of the sound wave on the molecules which make up the transmitting fluid. These are shown as bobs of a certain mass connected by massless springs. As such after being perturbed by the sound wave they move back to their original positions when the sound wave is discontinued i.e. the fluid is both compressible, elastic and also possesses inertia. These last two factors are prerequisites for the propagation of sound waves in any fluid.

In the positive pressure phases of the ultrasound wave the particles are compressed together and in the negative pressure phases they are moved apart or rarefied. It is this action on the fluid which eventually gives rise to cavitation given a large enough negative pressure phase[18].

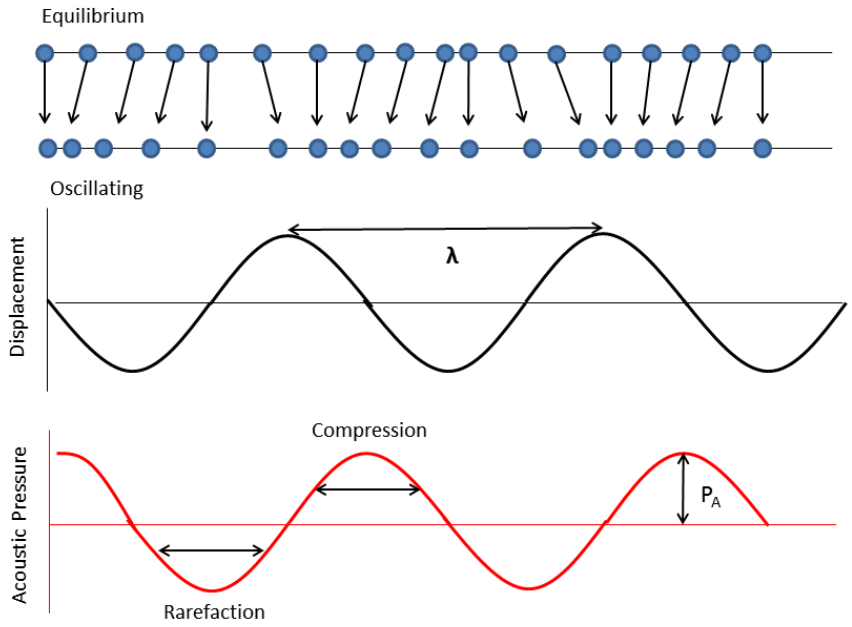

Figure 1.1: The ultrasound wave and its effect on fluid particles. Adapted from T.G Leighton "The acoustic bubble"[16]

It can also be noted from figure 1.1 that the displacement of the sound wave and the resulting pressure exerted on the fluid are not in tandem but are in quadrature[19]. That is that pressure wave in the lower half of the image is one quarter phase behind that of the displacement wave. This means that ultrasound waves give rise to effects which show hysteresis. That is, the effects follow some amount of time after the corresponding pressure phase.

It is also important to note that although figure 1.1 shows the wave as a 2d sine wave, ultrasound waves are actually spherical in three dimensions and move out in all three directions from their source of origin[19].

As shown in figure 1.1 the wavelength of the wave is given as the distance between two adjacent peak maxima and/or minima. This wavelength can be converted into the frequency of the sound wave which is more commonly used to describe the nature of an ultrasound field.

This is done by dividing the velocity of the wave, *c*, by its wavelength, λ, as shown in equation 1.1

$$v = \frac{c}{\lambda} \tag{1.1}$$

This frequency, *v*, describes not only the movement of the ultrasound wave but also the oscillation of the particles being influenced by the ultrasound wave and is described in units of Hertz (Hz) or cycles per second. Therefore to describe the frequency of an ultrasound wave we need to know its velocity through the fluid medium. Using pure water as the fluid medium, calculations have found the velocity of sound to be 1496 m s^{-1} at 298 K and 1 atmosphere pressure[20].

1.3: Definition of terms used in ultrasound science

Having described two parameters of a sound wave; its wavelength and its frequency other terms commonly referred to both in ultrasound science and in this work shall be explained and defined.

Amplitude

This is a measure of the power of the ultrasound wave and can also be derived from figure 1.1, generally the amplitude of a wave is the height of its peaks. It is denoted as P_A.

Acoustic pressure

This is defined as the pressure exerted on the fluid medium as a result of the transmittance of the sound wave. It typically is referred to in units of bar and denoted as P_a. It can be calculated as shown in equation 1.2[21]

$$P_a = P_0 - P_A \sin 2\pi f t \quad (1.2)$$

Where P_0 is the ambient pressure of the fluid and t is the amount of time which has passed since the start of the ultrasound wave. The acoustic pressure is therefore both time dependant and sinusoidal as is shown in figure 1.1.

More practically, the acoustic pressure amplitude can also be calculated using equation 1.3, where I is the intensity of the ultrasound being generated, ρ is the density of the fluid medium and c is the speed of sound in the fluid.

$$P_a = (2I\rho c)^{1/2} \quad (1.3)$$

Acoustic Intensity

The acoustic intensity is defined as the total ultrasonic power transmitted into the fluid medium divided by the radiating area being used. As such it has units of W m^{-2} or given the scale of most power ultrasound transmitting devices, W cm^{-2}. It can be calculated using equation 1.4 where I is the acoustic intensity, P is the electrical power dissipated into solution (usually measured using calorimetry to measure the increase in temperature of the fluid in question as a result of sonication) and A is the transmitting area.

$$I = \frac{P}{A} \quad (1.4)$$

1.4: How ultrasound causes cavitation to occur

Figure 1.1 shows that the ultrasound wave has both positive and negative pressure phases. In section 1.2 it was stated that the pressure phases of the wave cause the fluid medium to compress and rarify. This causes the density of the fluid to increase (during compressions) and to decrease (during rarefactions). If the negative pressure phase exerted by the ultrasound wave on the fluid is strong enough then it can cause voids and ruptures in the fluid structure. This rupturing starts the process of cavitation where the voids created are essentially microscopic bubbles.

For cavitation to occur the negative pressure exerted by ultrasound has to exceed the tensile strength of the fluid. The pressure which successfully overcomes this cohesive force is known as the cavitation threshold pressure. For pure water this threshold pressure has been calculated to be roughly 10,000 atmospheres[22]. This threshold can be reduced somewhat, by allowing for the formation of vapour filled bubbles, to 1000 atmospheres[23]. More recently Caupin *et al* have calculated the pressure required to be -24 MPa at 20℃[24].

In reality however, water is not completely pure and contains various impurities such as pre-existing gas bubbles, dust motes and organic species which lower the tensile strength of the fluid allowing for cavitation to occur at much lower pressures. These existing impurities are collectively referred to as *cavitation nuclei* since they aid the formation of cavitation bubbles. Because of this weakening of the water fluid structure, cavitation has been noted to occur at a range of much more moderate negative pressures, ranging from +0.1 MPa to –1 MPa[24].

Once formed these small bubbles are stabilised by a pressure known as the Laplace pressure which is derived from the surface tension of the bubble as in equation 1.5. The surface tension and therefore the Laplace pressure exert an overall inwards force on the newly created bubble. This force is greater the smaller the bubble size, so upon creation, or inception, the newly formed small cavitation bubbles are subject to a large surface tension/ Laplacian force.

$$p_L = \frac{2\sigma}{R} \quad (1.5)$$

The surface tension and Laplace pressures are balanced out by the pressure exerted on the inside of the bubble wall by its contents; gas and (water) vapour. Otherwise the bubble would collapse in on itself and dissolve rapidly. Thus the contents of the bubble exerts an overall outwards pressure which prevents the bubble from being dissolved.

1.5: The influence of the ultrasound wave on cavitation bubbles

The ultrasound wave passing through a fluid, from now on always assumed to be water, is not only responsible for the formation of cavitation bubbles but also for their growth, oscillation and eventual collapse.

Just as the water particles' position oscillates due to the ultrasound wave, the bubble wall is also influenced. If the negative pressure of the ultrasound is great enough the bubble can grow without being limited by its' containing surface tension. The threshold acoustic pressure which is the requirement for this unbounded growth is the Blake threshold pressure[25] and is given in equation 1.6.

$$P_B = p_0 + 0.77\,\frac{\sigma}{R_0} \quad (1.6)$$

Where p_0 is the ambient pressure exerted on the fluid, and R_0 is initial radius of the cavitation bubble.

When the negative pressure is greater than the Blake threshold, during negative ultrasound pressure phases the wall expands. This has an effect that the bubble wall grows in size. In response to the drop in internal pressure water vapour and

gas molecules evaporate into the bubble. During positive pressure phases the bubble wall recedes in on itself. This has the effect of shrinking the bubble size and forcing the contents out of the bubble as the bubble shrinks.

During several oscillations of growth and shrinking the bubble has a net increase in size due to rectified diffusion. Simply put, the bubble is able to grow and expand more during negative pressure phases than it shrinks during positive pressure phases. So over time cavitation bubbles increase in size and also become more filled with water vapour and gas.

The reason for this is that during growth phases the bubble has a larger overall wall surface area than it does during collapse phases and so there is more interface for gas diffusion for expansion phases than contraction phases. This allows for the influx of more gas and vapour than the amount which leaves during collapse phases.

Several works have attempted to deduce the equilibrium sizes of cavitation bubbles at various different frequencies. Using a pulsed ultrasound – bubble dissolution method Lee *et al* calculated the equilibrium radius of bubbles resonating in a 515 kHz sound field to be 2.8 – 3.7μm[26]. Brotchie *et al* expanded on this work and covered frequencies of 20 kHz to 1.1MHz[27]. At 213 kHz frequencies a bubbles radius of 2.9 μm was calculated and at ~1 MHz the bubble radius was 2.0 μm. In the same work Brotchie also concluded that the bubble equilibrium radius decreased with increasing applied ultrasound frequency and increased with increasing acoustic power. Ultrasound with a frequency of 20 kHz has been previously calculated to initiate bubbles with an equilibrium radius between 2 and 5 μm[28].

So once formed cavitation bubbles grow steadily due to rectified diffusion and also become more filled with gas and water vapour over time. During this oscillation period the bubble is fairly stable but once the bubble grows beyond a specific size its growth phase becomes unstable. This causes the bubble to grow suddenly and very rapidly. Once the ultrasound phase reverts back to a positive pressure mode this overgrown bubble then collapses in on itself.

During this collapse the speed of the moving bubble wall is thought to be able to sometimes (but importantly not always) exceed the speed of sound. The bubble radius at which this explosive growth and collapse is triggered is known as the critical radius and can be calculated for a given bubble using equation 1.7.

$$R_c = \frac{4\sigma}{3(P_v - P_L)} \quad (1.7)$$

Where R_c is the critical bubble radius, P_v is the vapour pressure inside the bubble and P_L is the pressure exerted on the bubble by the surrounding liquid.

This picture of a stable growing bubble which suddenly destabilises is an idealised image. To most sonochemists cavitation is thought to exist in two regimens, stable cavitation and transient cavitation.

1.6: Stable and transient cavitation

1.6.1: Stable cavitation

The example described in the above section describes well the process known as stable cavitation. As implied by its name, stable cavitation bubbles exist for many acoustic cycles. This allows them to grow and shrink many times within their lifetime and so become filled with gas and water vapour. Once their collapse is triggered due to their size exceeding the critical radius it is cushioned by the bubble contents and so is not as explosive or as fast as collapses by transient cavitation bubbles.

It is thought that stable cavitation is produced mainly by low intensity ultrasound and also by ultrasound of higher frequencies. The reason for higher ultrasound frequencies producing mainly stable cavitation is that the frequency of the wave is higher so the wavelength is smaller. This means there is less time between positive and negative pressure phases and so less time for growth and subsequent collapse.

This produces rapidly oscillating bubbles which grow slowly due to the time limit on growth phases. Therefore it takes longer for these bubbles to reach R_c and so their lifetime is longer. For similar reasons cavitation is also harder to induce when using higher frequencies. The higher the frequency used higher intensities i.e. higher the acoustic pressures (more negative) have to be used to successfully initiate cavitation.

1.6.2: Transient cavitation

As implied by its name transient cavitation is the formation and explosive growth and collapse of short lived cavitation bubbles. Transient cavitation is thought to occur mainly for lower frequencies of ultrasound and for higher acoustic intensities.

The reasoning for this is that there is now more time for growth of the bubble before the mode of the ultrasound wave changes to a positive pressure phase. Higher acoustic intensities allow for faster bubble wall movement and again the bubble grows faster and so reaches R_c quicker and then implodes.

This short lived, fast growing and collapsing behaviour also means that transient cavitation bubbles contain less gas and vapour than stable cavitation bubbles. This leads to their collapse being much more explosive as it is damped less by the bubble contents.

These two regimens of cavitation are pictorialized in figure 1.2 below.

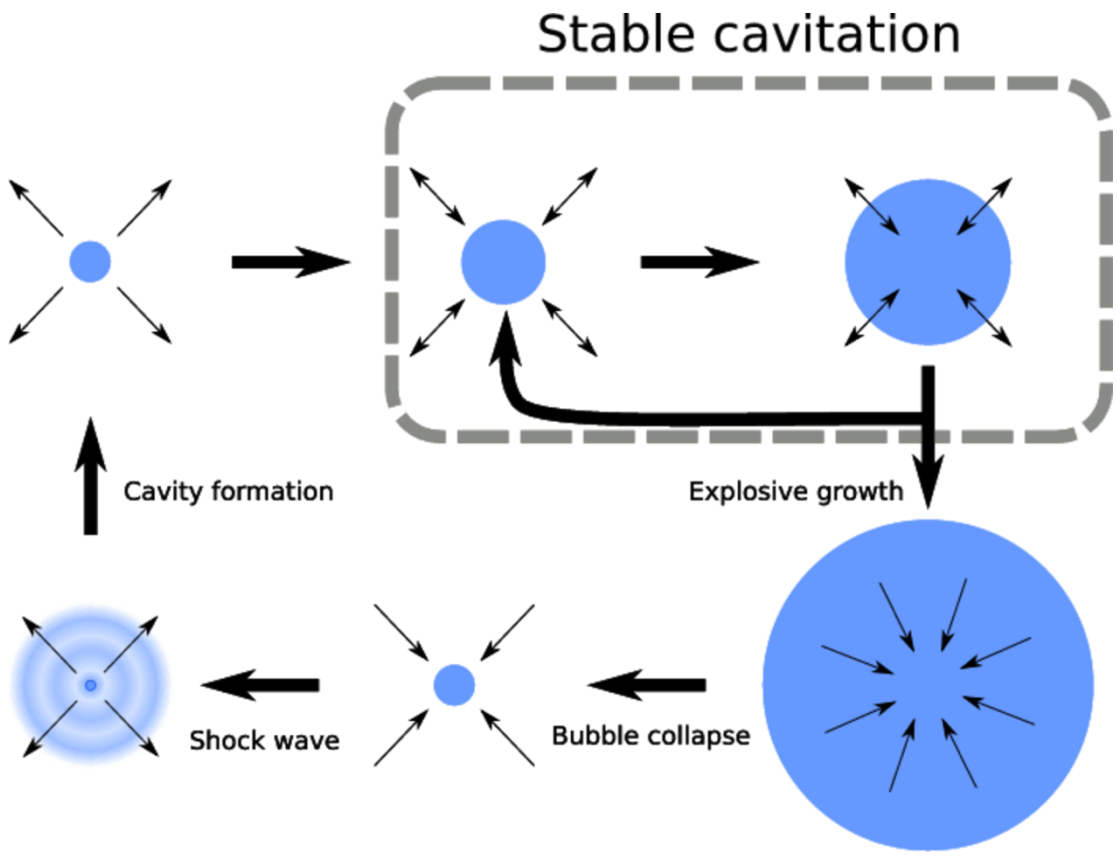

Figure 1.2: Diagram describing stable and transient modes of cavtitation. Adapted from PhD thesis of David King, 2010.

Until recently it was thought that these two regimes were fairly well separated and work by Apfel showed phase diagrams of bubble radius *verses* acoustic pressure describing the transition from one regime to the other[29]. However in a 2009 dated paper Ashokkumar has shown that stable cavitation bubbles can exist alongside transient bubbles as a minority species and *vice versa*[30].

1.7: The productive consequences of cavitation

Once a cavitation bubble collapses several processes occur. During the collapse phase the bubble implodes without heat transfer to the outside water i.e. the collapse is adiabatic. This means that as the bubble contents becomes more pressurised it increases in temperature. The maximum temperatures attained during bubble collapse have been modelled and calculated by several groups. Temperatures of up to 5000 K and several hundred Bar in pressure have been calculated by Suslick e*t al*[31]. Most recently Suslick *et al* have conclusively shown from spectroscopic data that temperatures of 1400 to 9000 K can be observed with pressures of up to 300 Bar[32].

The maximum temperature which should theoretically be attained can be calculated by equation 1.8, where T_{max} is the maximum temperature attained, T_0 is the initial temperature, P_m is the pressure of the liquid at the time of collapse, γ is the so called polytropic ratio (the ratio of the specific heats of the gas contents of the bubble) and P is the pressure in the bubble at its maximum size.

$$T_{max} = T_0 \left(\frac{P_m(\gamma-1)}{P}\right) \tag{1.8}$$

Similarly the maximum pressure attained upon collapse can be estimated using equation 1.9, where P_{max} is the maximum pressure attained.

$$P_{max} = P \left(\frac{P_m(\gamma-1)}{P}\right)^{\gamma/(\gamma-1)} \tag{1.9}$$

As a result of the high temperatures and pressures produced the gas contents is thermally excited. These species can decay by emitting photons and hence the collapse triggers the release of a pulse of light (or periodic pulses for stable cavitation oscillations) known as sonoluminescence.

Also as a consequence of the temperatures created within the collapsed bubbles transient core a plasma is created which is thought to be both opaque and confined by its own inertia[33].

The contents of the bubble is readily converted into radical species and/or pyrrolised. For this work the sonolysis of water is most important as it creates both ·OH radicals and ·H radicals, which can be used to degrade pollutants such as dibutyl phthalate (DBP). These can recombine into water but can also form H_2 and H_2O_2, hydrogen peroxide.

As with macroscopic bubbles, microscopic cavitation bubbles “pop” upon collapse and so on the final stage of collapse sound is created. The final effect of bubble collapse is that a shockwave is emitted around the same time as the sound is produced. These can be very fast (*circa* 200 m s^{-1} up to half the speed of sound[34]) and are the cause for the sonochemical cleaning effects present in the aforementioned cleaning baths.

The final product of bubble collapse is further bubble nucleation. The collapsed bubble often splits into smaller micro or nanobubbles which can then serve as further bubble nuclei and so grow to equilibrium sizes during the following acoustic cycles.

1.8: Factors that influence the effects of cavitation

Having described the physical and chemical products of cavitation bubble’s collapse the primary factors which are known to affect bubble collapse and hence the productivity of the bubble collapse will now be described. The effects are important in understanding how a change in experiment conditions may affect the bubble dynamics and hence the sonochemistry of the experiment. They also aid in experimental design; how to create the desired chemistry and consequences.

1.8.1: Ultrasonic frequency

It has already been stated above that cavitation is harder to induce at higher frequencies than it is at lower frequencies. This is due to the amount of time available in the rarefaction half cycle being small and so there is less time for bubble growth. Therefore the bubble wall of gas nuclei for, example, have to be expanded more quickly in the shorter amount of time available. This means that the amplitude of the ultrasonic wave needs to be higher i.e. higher acoustic intensities and pressures have to be used. As an example, it has been found that ten times more power is needed to induce cavitation in water at 400 kHz than at 10 kHz ultrasonic frequency[35].

1.8.2: Choice of solvent

Since cavitation occurs due to rupture of the fluid structure, cavitation is harder to induce in more viscous liquids which have stronger cohesive forces. Conversely the use of low surface tension fluids allows for cavitation to be induced at lower acoustic intensities.

Liquids that have high vapour pressures lead to lessened sonochemical effects. This is due to the bubble collapse being more damped by its contents which being more volatile easily evaporates into the bubble core. This can be seen numerically from equation 1.8. An increase in the internal bubble pressure at maximum size decreases the maximum temperature attainable for the system in question. As an illustration of the converse of this Suslick *et al* have used liquids with very low vapour pressures to initiate bubble collapses which lead to very bright sonoluminescence (SL) which is even visible to the naked eye[33].

1.8.3: Liquid Temperature

The temperature of the liquid being irradiated by ultrasound is known to affect both the amount of bubbles undergoing cavitation and the violence of bubble collapse. Rosenburg found that moderate increases in temperature (-10℃ to +50℃) aided the ultrasonic erosion of aluminium[36]. This was hypothesised to be due to the amount of nuclei being increased as the temperature was raised. In the same work it was also found that beyond 50℃ the cavitation intensity

decreased. This was found to be due to the increase in vapour pressure leading to more cushioned bubble collapse as described above in section 1.5.2.

1.8.4: Gas contents

Most sonochemical consequences of bubble collapse are dependent on the heat produced and focussed by the collapsing bubble. From equation 1.8 it can be seen that one of the determining parameters in the T_{max} produced during bubble collapse is the polytropic ratio of the gas contents, γ.

From equation 1.8 gases with high values of γ will produce higher maximum temperatures upon being compressed adiabatically. Monoatomic gases such as the noble gases have high values of γ. Polyatomic gases such as carbon dioxide have much lower values of γ and so bubbles filled with these gases lead to collapses which are less hot. The main reason for this is that polyatomic gases can consume heat energy and convert it into molecular rotations and vibrations. These are endothermic processes and so the temperature attained in the bubble core is lessened.

Another property of the gaseous contents of a bubble which is important in generation of T_{max} is its' thermal conductivity. Sonochemistry is most efficient when a small, very hot core is obtained just after collapse. A gas with high thermal conductivity will lead to a larger more diffuse less hot core whereas one with a low thermal conductivity will lead to the heat energy remaining focussed on the collapse site rather than be allowed to conduct away.

Therefore the most efficient gases for sonochemistry tend to be the noble gases such as Ar, Xe and Kr, which are monoatomic, have high γ values and also have low thermal conductivities.

1.8.5: External (ambient / applied) pressure

An increase in the pressure applied to a liquid such as water will increase the cavitation threshold for that liquid. This is because increasing the amount of external pressure increases the amount of work that needs to be done on a nucleus such as a pre-existing bubble for it to produce a cavitation microbubble. This process requires expansion of the microbubble wall and the applied

pressure increases the force in the opposite direction and so higher acoustic intensities are needed to cavitate the liquid.

However once cavitation is successfully induced it can be seen from equation 1.7 that the bubbles collapsing under the force of an applied overpressure will also be more violent. This is due to the applied pressure increasing the P_m parameter thus increasing T_{max}.

1.8.6: Acoustic Intensity

Increasing the acoustic intensity *I* applied to a liquid increases the cavitation events occurring in the liquid i.e. an increase in the production of microbubbles. This is due to the generated acoustic pressure being higher and higher above the Blake threshold and so a higher percentage of the fluid forms voids (microbubbles).

An increase in the intensity applied also increases the violence of collapse of microbubbles. This behaviour reaches a limit however when the growth of the bubble is much greater its rarefaction and so there is not enough time for bubble collapse during the negative pressure cycle of the ultrasound wave. The fate of such bubbles is that they grow and form buoyant bubbles which then migrate to the surface air-water interface.

1.9: How a sound wave can produce chemistry

In the previous section, 8 productive consequences of microbubble collapse were described. Several of these effects can give rise to chemistry. Therefore it is due to the action of the ultrasound wave on cavitation bubbles and their eventual collapse that ultrasound can initiate chemistry. There is no direct coupling of ultrasound to the molecular systems which undergo sonochemistry, chemistry brought about by sound. This is because the wavelength of the sound is too large to directly couple with molecules. And so the microbubble acts as a “middle-man” bringing about the chemical effects of ultrasound *via* bubble collapse.

This subsection aims to present several examples of sonochemistry to show its rich and diverse nature.

1.9.1: Radical based chemistry

As mentioned in section 1.7 the production of radicals is a common side effect of cavitation bubble collapse. The contents of a bubble can be readily pyrolysed and radical formation can occur. It is also not uncommon for these primary radicals to react with species in the interfacial area of the bubble to produce secondary radicals.

1.9.2: Polymer chain scission

It has been known since the 1930s that ultrasound can reduce the viscosity of polymers[37]. Initially natural polymers were studied but to date several important and widely used man made polymers have been studied. These include polystyrene[38], poly vinyl acetate[39], polypropylene[40] and poly(methyl methacrylate)[41]. From this wide range of studies it has been found that this reduction in viscosity occurs by chain scission in the middle of polymer chains *via* the most labile bond available.

1.9.3: Radical induced polymerisation

As well as inducing degradation of polymers ultrasound is known to also be able polymerise monomers to polymers[41, 42]. Most of the published work concentrates on the polymerisation of vinyl monomers either in bulk solution or as an emulsion[43]. The attractiveness of using ultrasound to initiate polymerisations is that no initiator is required. This combined with the fact that ultrasound will degrade polymers above a certain size / weight makes ultrasound attractive for the formation of controlled weight polymers.

1.9.4: Organic Couplings

As well as being able to initiate polymerisations ultrasound has been shown to be effective at inducing 1 to 1 cross couplings of organic moieties an example being Wurtz coupling of two haloorganics in the presence of lithium[44-47].

1.9.5: Radical initiated Nanoparticle formation

A modern “hot topic” in which ultrasound is also useful is the formation of nanoparticles. Several kinds of particles have been formed by action of ultrasound including those of gold[48], iron[49] and palladium[50].

1.9.6: Sonochemiluminescence

In section 1.7 it was stated that the collapse of cavitation microbubbles can give rise to light being emitted, sonoluminescence. This is not the only possible way by which ultrasound can give rise to light formation, sonochemiluminescence also exists. Sonochemiluminescence can be described as the augmentation of sonoluminescence by the addition of a chemical which luminesces when it has reacted with the products formed from cavitation bubble collapse. Possibly the best known example of this is the reaction of luminol (3-aminophthalichydrazide) with the hydroxyl radicals formed by sonolysis of water[51].

In this example of sonochemiluminescence the luminescence of luminol comes from its partial decomposition to a dicarbonyl species, the final step of which forms the stable dicarbonyl and a photon. The emitted photon has energy in the blue band of the colour spectrum. This complex process is illustrated in scheme 1.1 and is initiated by the reaction of a hydroxyl radical with the luminol species. It should be noted that when used, luminol solutions are basic in nature hence the equilibrium shown in the top left hand of scheme 1.1

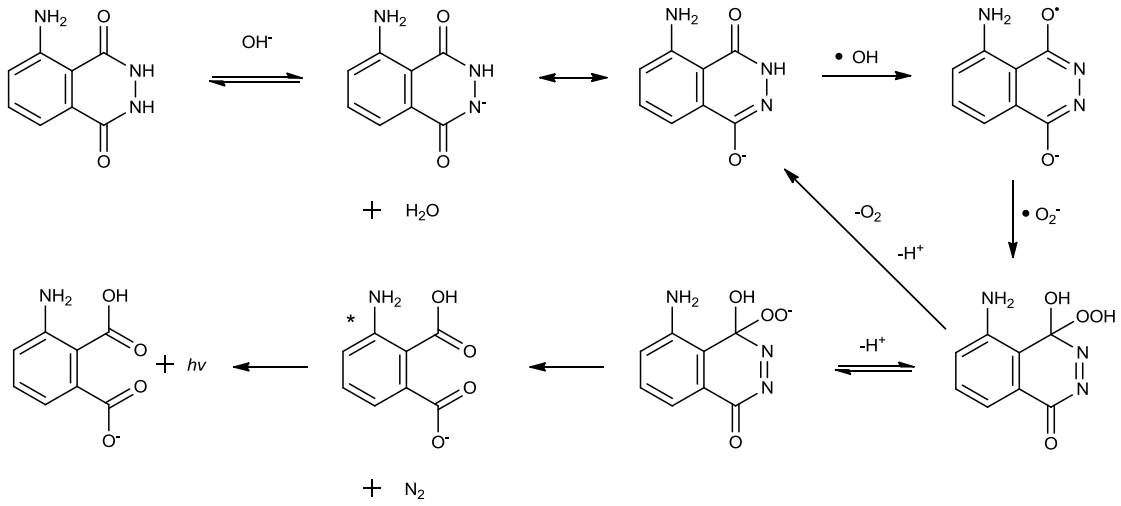

Scheme 1.1: The partial decomposition of Luminol giving rise to sonochemiluminescence

1.9.7: Tribochemistry

Tribochemistry is the initiation of chemistry by pressure or force. Since cavitation bubbles generate very high pressures locally to the collapsed bubble, shockwaves which originate from the collapsed bubble and also strong sheer forces due to motion of fluid over the rapidly oscillating cavitation bubbles, it is perhaps not surprising that ultrasound has been used to initiate tribochemistry.

Suslick *et al* have studied the light emitted from argon saturated crystal slurries of sucrose and resorcinol as a result of the slurry being irradiated with power ultrasound[52, 53]. It was found that light was emitted which was consistent with argon gas excitement.

1.9.8: Sonophotochemistry

There also exists a third way by which ultrasound and cavitation bubble collapse can give rise to light emission. This is sonophotoluminescence, where photons from sonoluminescence are used to vibronically excite a species which then decays to ground state emitting a photon of differing energy. This process was discovered by Ashokkumar and Grieser in which they used 515 kHz ultrasound to induce sonophotoluminescence of pyranine[54] and later fluorescein, pyrene and eosin[55].

1.10: Chapter References

1. S. Takeda, I. Morioka, K. Miyashita, A. Okumura, Y. Yoshida and K. Matsumoto, *European Journal of Applied Physiology and Occupational Physiology*, 1992, **65**, 403-408.
2. P. N. T. Wells and H.-D. Liang, *Journal of the Royal Society, Interface / the Royal Society*, 2011, **8**, 1521-1549.
3. S. Farruggia and D. S. Babcock, *Radiology*, 1981, **139**, 147-150.
4. A. Monteagudo, T. Tharakan and I. E. Timor-Tritsch, *Journal of the Association for Academic Minority Physicians : the official publication of the Association for Academic Minority Physicians*, 1995, **6**, 34-37.
5. K. Koselj, H.-U. Schnitzler and B. M. Siemers, *Proceedings of the Royal Society B-Biological Sciences*, 2011, **278**, 3034-3041.
6. A. Y. Supin, P. E. Nachtigall and M. Breese, *Journal of the Acoustical Society of America*, 2011, **130**, 1711-1720.
7. T. G. Leighton, *Progress in biophysics and molecular biology*, 2007, **93**, 3-83.
8. S. Rup, M. Sindt and N. Oget, *Tetrahedron Letters*, 2010, **51**, 3123-3126.
9. L. Somaglino, G. Bouchoux, J. L. Mestas and C. Lafon, *Ultrasonics Sonochemistry*, 2011, **18**, 577-588.
10. M. Habib, G. Baroud, F. Gitzhofer and M. Bohner, *Acta Biomater.*, 2010, **6**, 250-256.
11. D. M. Kirpalani and K. Suzuki, *Ultrasonics Sonochemistry*, 2011, **18**, 1012-1017.
12. A. L. Pirozerskii, E. V. Charnaya, E. N. Latysheva, A. I. Nedbai, Y. A. Kumzerov and A. S. Bugaev, *Acoustical Physics*, 2011, **57**, 637-641.
13. R. Ambrus, N. N. Amirzadi, P. Sipos and P. Szabo-Revesz, *Chemical Engineering & Technology*, 2010, **33**, 827-832.
14. D. Pingret, A. S. Fabiano-Tixier, E. Petitcolas, J. P. Canselier and F. Chemat, *J. Food Sci.*, 2011, **76**, C287-C292.
15. D. Bates and A. Patist, in *Case Studies in Novel Food Processing Technologies: Innovations in Processing, Packaging, and Predictive Modelling*, ed. C. J. K. K. F. F. E. Doona, 2010, vol. 197, pp. 119-138.
16. T.G.Leighton, in *The Acoustic Bubble*, Academic Press Limited, London, 1997, p. 3.
17. P.A.Tipler, in *Physics for Scientists and Engineers*, W.H.Freeman and Company, New York, USA, 1999.
18. J. P. Lorimer and T. J. Mason, *Chemical Society Reviews*, 1987, **16**, 239-274.
19. T.G.Leighton, in *The Acoustic Bubble*, Academic Press Ltd, London, 1997, p. 5.
20. W. Marczak, *Journal of the Acoustical Society of America*, 1997, **102**, 2776-2779.
21. T. Leighton, *The Acoustic Bubble*, Academic Press, London, 1994.
22. L. A. Crum, IEEE Ultrasound Symposium, 1982.
23. Y. B. Zel'dovich, *Zhurnal E'Ksp. Tevr. Flz*, 1942, **12**, 525.
24. F. Caupin and E. Herbert, *Comptes Rendus Physique*, 2006, **7**, 1000-1017.
25. F. G. Blake, in *tech memo 12 Acoustic Research Lab*, Harvard University, Cambridge MA, 1949.
26. J. Lee, M. Ashokkumar, S. Kentish and F. Grieser, *Journal of the American Chemical Society*, 2005, **127**, 16810-16811.
27. A. Brotchie, F. Grieser and M. Ashokkumar, *Physical Review Letters*, 2009, **102**.
28. S. L. a. W. L. R. Mettin, Proceedings of the 2nd Conference on Applications of Power Ultrasound in Physical and Chemical Processing, Toulouse, France, 1999.
29. A. R.E, in *Methods in Experimental Physics*, Academic Press, New York, USA, 1981, pp. 355-413.
30. M. Ashokkumar, J. Lee, Y. Iida, K. Yasui, T. Kozuka, T. Tuziuti and A. Towata, *Physical chemistry chemical physics : PCCP*, 2009, **11**, 10118-10121.

31. K. S. Suslick, Y. Didenko, M. M. Fang, T. Hyeon, K. J. Kolbeck, W. B. McNamara, M. M. Mdleleni and M. Wong, *Philosophical Transactions of the Royal Society of London Series a-Mathematical Physical and Engineering Sciences*, 1999, **357**, 335-353.
32. K. S. Suslick, N. C. Eddingsaas, D. J. Flannigan, S. D. Hopkins and H. Xu, *Ultrason Sonochem*, 2011, **18**, 842-846.
33. K. S. Suslick and D. J. Flannigan, *Nat Phys*, 2010, **6**, 598-601.
34. T. Prozorov, R. Prozorov and K. S. Suslick, *Journal of the American Chemical Society*, 2004, **126**, 13890-13891.
35. J. P. L. a. T. J. Mason, in *Sonochemistry: Application and uses of ultrasound in chemistry*, Ellis Horwood Ltd, 1989, p. 248.
36. L.Rosenberg, *Ultrasonics News*, 1960, **4**, 4.
37. G. J. Price, P. J. West and P. F. Smith, *Ultrasonics Sonochemistry*, 1994, **1**, S51-S57.
38. G. J. Price and P. F. Smith, *Polymer*, 1993, **34**, 4111-4117.
39. G. Madras and S. Chattopadhyay, *Polymer Degradation and Stability*, 2001, **73**, 33-38.
40. J. Chakraborty, J. Sarkar, R. Kumar and G. Madras, *Polymer Degradation and Stability*, 2004, **85**, 555-558.
41. G. J. Price, D. J. Norris and P. J. West, *Macromolecules*, 1992, **25**, 6447-6454.
42. M. A. Bradley, S. W. Prescott, H. A. S. Schoonbrood, K. Landfester and F. Grieser, *Macromolecules*, 2005, **38**, 6346-6351.
43. B. M. Teo, S. W. Prescott, G. J. Price, F. Grieser and M. Ashokkumar, *Journal of Physical Chemistry B*, 2010, **114**, 3178-3184.
44. A. G. Osborne, K. J. Glass and M. L. Staley, *Tetrahedron Letters*, 1989, **30**, 3567-3568.
45. D. VandenBurg and G. J. Price, *Ultrasonics Sonochemistry*, 2012, **19**, 5-8.
46. B. H. Han and P. Boudjouk, *Tetrahedron Letters*, 1981, **22**, 2757-2758.
47. T. D. Boudjouk P, *Organometallics*, 1986, **5**.
48. K. Okitsu, M. Ashokkumar and F. Grieser, *Journal of Physical Chemistry B*, 2005, **109**, 20673-20675.
49. D. L. Huber, *Small*, 2005, **1**, 482-501.
50. A. Nemamcha, J. L. Rehspringer and D. Khatmi, *Journal of Physical Chemistry B*, 2006, **110**, 383-387.
51. F. R.D, *Ultrasonics*, **1**, 87-98.
52. N. C. Eddingsaas and K. S. Suslick, *Nature*, 2006, **444**, 163.
53. N. C. Eddingsaas and K. S. Suslick, *Journal of the American Chemical Society*, 2007, **129**, 6718-+.
54. M. Ashokkumar and F. Grieser, *Chemical Communications*, 1998, 561-562.
55. M. Ashokkumar and F. Grieser, *Ultrasonics Sonochemistry*, 1999, **6**, 1-5.

Chapter 2: Introduction to water treatment processes

2.1: Behaviour of ultrasound in water

Water is a fluid which possesses both inertia and elasticity, it therefore is capable of propagating ultrasound waves. Three properties that are important when considering the sound field present in a fluid are the speed of sound in the fluid, the fluids specific acoustic impedance and the amplitude attenuation coefficient of the fluid.

The speed of sound in a fluid is an important parameter in calculating the wave length of the sound as shown in the previous chapter. Water is known to travel at a speed of 1480 m s^{-1} in water[1].

The specific acoustic impedance is the ratio of the acoustic pressure applied to the system and the particle oscillation velocity, and can also be calculated by multiplying the density of the fluid (water) by the speed of sound in water. The density of water at standard pressure and temperature is 1000 kg m^{-3} therefore the specific acoustic impedance of ultrasound in water[1] is 1.5 x10^{6} kg m^{-2} s^{-1}.

The last parameter is the amplitude attenuation coefficient. This is a measure of how much amplitude is lost from the sound wave as it propagates through the fluid. In water this happens at a rate of 0.0253 Np m^{-1} at 1 MHz[1]. Defining the frequency of the measured attenuation is very important as the attenuation rate of ultrasound increases with increasing frequency of sound. Water is a good transmitter of sound with quite a low attenuation coefficient. Other fluids attenuate sound much more than water. Examples include castor oil (10.9 Np m^{-1}) and air at standard temperature and pressure (138 Np m^{-1})[1].

2.1.1: Attenuation of ultrasound in water

The movement of sound waves through fluids causes their amplitudes to diminish over time or more correctly with the amount of distance travelled[2]. As mentioned above, water is a very good transmitter of sound. An identical sound

wave will travel much further in water than in air, due to the lower attenuation coefficient of water detailed above.

The process of attenuation occurs since the sound wave loses energy to the medium it is passing through. The decay of the sound wave through a medium in the positive X direction can be described by equation 2.1, where *A* is the rate of attenuation and *b* is the attenuation coefficient mentioned in the previous section.

$$A = e^{-2bx} \tag{2.1}$$

There are several mechanisms for attenuation of sound in water. Firstly amplitude can be lost as the wave does mechanical work against the viscous forces of the fluid as it causes the fluid particles to oscillate[2]. Secondly heat flow can occur between the compression and rarefaction cycles of the sound wave which dissipates energy[2]. Thirdly heat can be radiated from compression phases to rarefaction phases[3]. In cavitating fluids the bubbly nature of the fluid can also scatter the sound wave which causes energy loss[2]. Lastly if there are several species present in the fluid as is the case for aqueous solutions the relative motions between species can also cause energy loss and therefore attenuation of the sound wave[2].

From these descriptions it can be seen that several of the attenuation mechanisms relate to energy exchange or flow between compression and rarefaction phases. As the frequency of the sound wave increases the closeness in space of these two phases increases and it is this along with the reduction of the time per cycle that causes the attenuation effects to increase with increasing frequency.

2.1.2: Cavitation in water

Ultrasound can readily cause cavitation in water and has been shown to occur for moderate negative pressures between +0.1 and -1 MPa[4]. These negative pressures exert enough force to create voids in the fluid structure, overcoming

water's viscous forces. These voids as described in the previous section are microbubbles and it is these which are responsible for generating the effects of sonochemistry.

2.1.3: The sonolysis of pure water

As described in section 2.5 in the previous chapter the oscillation of growth and shrinking cycles causes the bubbles formed to fill with gas and water vapour over time due to the processes of rectified diffusion. Once the bubble does collapse the water content of the bubble is converted into ·OH and ·H radicals through homolysis of a water O-H bond due to the high temperatures and pressures attained during bubble collapse[5]. These can then undergo several reactions with themselves and each other to produce hydrogen, water and hydrogen peroxide as shown in scheme 2.1, where the use of))) denotes the use of ultrasound.

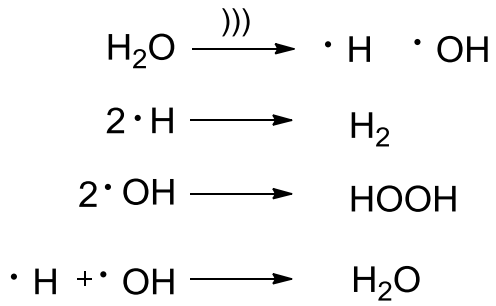

Scheme 2.1: The formation of ·OH and ·H radicals and their interaction to produce other oxidising species.

Of these species produced ·OH, ·H and H_2O_2 are highly oxidising and are expelled from the bubble after collapse. It is these reactive species formed from water homolysis which allow ultrasound to be used as an advanced oxidising process (AOP) for the remediation of pollutants. The reactive species expelled can react with and subsequently oxidise pollutant molecules present either in the bubble core, the bubble interfacial region or the bulk solution.

2.2: Current methods employed for water treatment

Before considering the advanced oxidation processes which are attracting much interest in water processing research, the methods currently employed by the water industry for the cleaning and processing of water will be described. This section has been largely adapted from “Water Chemistry” by S.E.Manahan, 2011, CRC Press, Boca Raton, USA

The type of processing water undergoes is heavily dependent on its intended use. Water for consumption in towns and cities needs to be thoroughly disinfected and have high quality levels of colour, odour and suspended solids. Water for industrial use may contain high levels of microbes but may need to be very soft, containing only trace levels of dissolved inorganics. Water which is to be discharged into a large river or natural water supply may require less rigorous treatment (rightly or wrongly) than water headed to the taps of a large town. This sections aims to introduce some of the processes and technologies used in water processing centers today for a variety of intended supply purposes.

2.2.1: A typical treatment process of water for municipal use

Figure 2.1 shows a representation of a typical water processing centre for the treatment of water for municipal (domestic) use. This particular plant serves to process water from a well for supply to a large city. There are several stages each designed to remove a particular pollutant or undesirable chemical species from the water being supplied.

The first stage which is employed is aeration. This serves to remove volatile organic species and other volatile species such as hydrogen sulphide, carbon dioxide, methane, methane thiols (which are also odorous and therefore undesirable in domestic water supplies) and other chemicals which are the metabolites of bacteria living in the well water. Contact with the oxygen content in the pumped-in air also serves to oxidise Fe(II) to insoluble Fe(III).

After aeration lime is added to the water to raise the pH. This is commonly in forms such as CaO or $Ca(OH)_2$. The raised pH serves to precipitate out Ca^{2+}

and Mg^{2+} which add hardness to the water. It is the hardness of the water which causes the build-up of limescale in sinks, baths, boilers and dishwashers and so it is desirable to reduce it. The water is then fed to a primary basin where the precipitates are allowed to settle out.

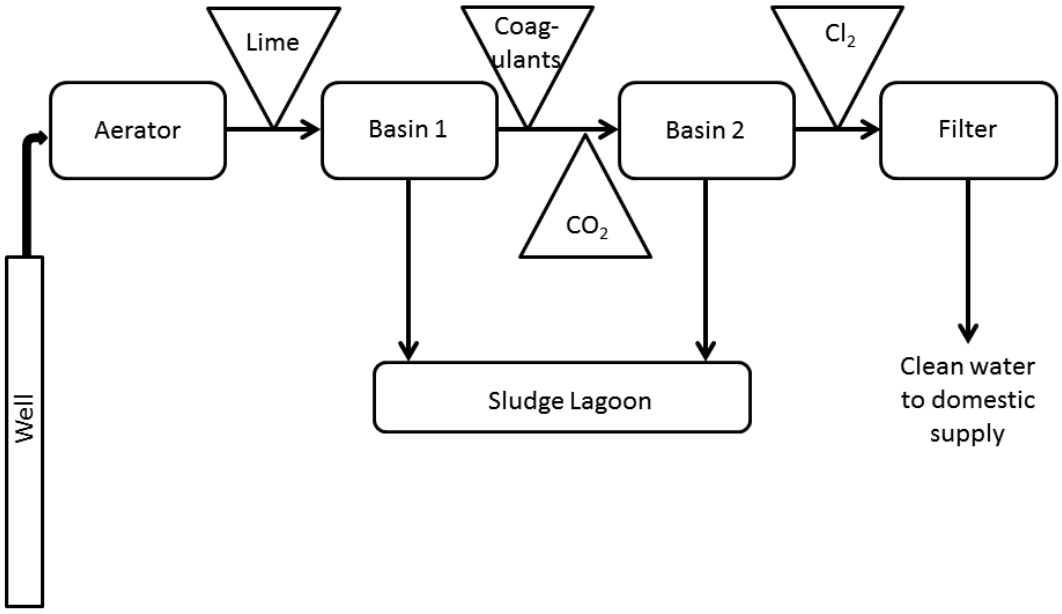

Figure 2.1: A schematic of a typical water processing facility providing water for domestic use. Adapted from S. Manahan Environmental Chemistry, 9th ed, Taylor and Francis, Boca Raton 2010. Permission requested.

A large amount of the solid content of the precipitates and other solids present in the water are suspended and so do not settle out easily. To aid the removal of such solids coagulants are added. These may be simple inorganics such as Fe(III) and $AlSO_4$, both of which form gels trapping the suspended solids, or they may be more complex additives such as activated silicas or synthetic polyelectrolye polymers both of which attract charged solid particles to their solid bulk aiding removal of the suspended particles. These solids/gels/particles are then allowed to settle out in a secondary basin once CO_2 has been added to lower the pH back to neutral (pH 7) again. The sludge formed from these

settling and flocculation steps is then syphoned off into a sludge lagoon where it is processed separately.

The final steps in the treatment process are firstly filtration which removes fine suspended particles which were not removed by either of the previous coagulation / precipitation steps. Chlorination is then used to disinfect the water.

2.2.2: Tertiary water treatment

In areas of the world such as Western Europe about 50% of water has been recycled from sewage waste. This level of water recycling makes it crucial that toxic and disease causing species are removed effectively from the water.

These tertiary or advanced waste treatments remove refractory dissolved and suspended substances which are harmful for human consumption. These may be suspended solids, dissolved organic materials (such as pesticides, pharmaceutical metabolites, synthetic and natural hormones and personal care products) or dissolved inorganic species of which phosphates and nitrates are of the most concern as they promote algal growth.

In development are advanced oxidation processes (AOPs) which in general produce high concentrations of ·OH radicals for chemical oxidation. These are of great promise in the tertiary treatment of the aforementioned species, particularly non- biodegradable organic species which are difficult to remove by the aforementioned standard techniques. Three major classes of AOP are described in section 2.3.

2.2.3: Removal of dissolved organics

One of the major problems present in modern treatment of waste water is the dissolved organic content of the water. These compounds are typically present in very low concentrations (µM – nM) and are linked to cancer, are toxic and are possibly mutagenic.

Dissolved organics may be present in the water due to the water's previous use as is the case for personal care related organics and natural and synthetic hormones. They may also be created by secondary water treatment or by disinfection of the water as is the case for the many chlorinated species formed

by chlorination of water. They may also enter the aquasphere due to contamination of part of the water cycle for an area, as is the case for phthalate esters.

The dissolved organic content of the water has typically survived biodegradation and contains classes of chemicals such as *n*-alkanes, biphenyls, phenols, substituted phenols, napthalenes, pharmaceutical products and endocrine disruptors such as bisphenol A and phthalate esters.

The main method used currently for the removal of dissolved organic species is activated carbon adsorption / filtration. Activated carbon is made by charring carbonaceous materials (such as wood, peat and lignite) anoxically around 600℃. The prepared material is then partially oxidised by treatment with either CO_2 or steam. The finished material has a massive surface area to volume ratio and is highly porous and so makes a good material for the removal of most organic species. Since the material requires a lot of energy to prepare it is reused many times over. Activated carbon can be regenerated once used by steam-air treatment at 950℃, although this does strip *circa* 10% of the carbon content.

The removal of organic species may also be performed by polymers such as Amberlite-XAD-4 which is hydrophobic and so strongly adsorbs more insoluble organic species such as chlorinated pesticides. They too can be regenerated by treatment with organic solvents such as isopropanol and acetone.

Recently oxidation processes have been investigated for their potential to remove organic species using less energy overall than the adsorption processes mentioned above (where the main energy and materials requirement is in the adsorption materials' formation and recycling). These include use of ozone, H_2O_2, O_2, permanganates, ferrates, electrochemical processes, UV light driven processes and the use of ultrasound.

2.3: Advanced oxidation processes

Advanced oxidation processes (AOPs) are advanced chemical methods that generate high concentrations of OH radicals *in situ*[6]. Unlike many other radical species the hydroxyl radical is highly reactive and unselective. Aside from fluorine radicals it is one of the most oxidising species known with an oxidising potential of 2.80 V[7]. This means it is able to attack and oxidise a wide range of chemical moieties and structures. This results in the oxidation, fragmentation, and remediation / mineralisation of the organic species over time. AOPs therefore are a useful tool for transforming harmful organic species into less complex and (hopefully) less harmful organic species.

Given the right operating conditions and enough time most AOPs are capable of completely mineralising the organic content of contaminated real or test waters. By mineralisation it is meant that the organic content of the water is converted completely into CO_2. Percentage of mineralisation therefore describes the percentage of the original organic content of the contaminated water which is converted into CO_2 at a given time.

The principle benefit of AOP technology is that it completely removes the hazard related to the organic contamination by oxidising the species present to CO_2. Most other waste water treatments transfer the hazard from one phase to another, as is the case for activated carbon adsorption. AOPs also do not produce large amounts of hazardous waste, just CO_2, which aside from being a greenhouse gas is environmentally benign and also safe to handle. Therefore AOP technologies are remarkably environmentally friendly and a potential green tool for the water processing industry.

In this section 2 major AOP technologies will be introduced, UV light action and the use of ultrasound. Ozonation is also discussed as it is a cost effective low energy method to mineralise DOC.

2.3.1: UV light

The use of ultraviolet light is one of the most widely spread AOPs in the water processing industry. Strangely enough its installed purpose is commonly not for the removal of recalcitrant organics from the water which is being treated but as a disinfection tool. Some 3000 applications for UV as a disinfection tool are commercially available today[7]. UV action (photolysis) is also the major abiotic route for organic matter oxidation in the environment.

UV light generates reactive species such as ·OH by photolysis. This process involves the outermost electron in a compounds electronic configuration absorbing a photon from a UV light source and becoming electronically excited. In photolysis this destabilises the compound causing it to split into two or more other species which are usually reactive.

UV light is capable of producing high energy intermediates as a result of excitement of species present in the water by photons. An important oxidising species produced by UV light is the superoxide radical ion $\cdot O_2^-$. This species is produced in solution by reaction of UV photons with dissolved oxygen. UV oxidation by the superoxide radical ion can be coupled with the Fenton reaction as shown in scheme 2.2 to also produce ·OH.

$$2H_2O + 2\cdot O_2^- \rightarrow 2H_2O_2 + O_2$$

$$Fe^{2+} + H_2O_2 \rightarrow Fe^{3+} + OH^- + \cdot OH$$

Scheme 2.2: The Fenton process as initiated by superoxide radical ions.

UV light can also be coupled with hydrogen peroxide to generate *in situ* ·OH. This method is much more common and useful than using UV light in water by itself. The overall and half reactions which make up this process are described in scheme 2.3.

$$H_2O_2 + h\nu \rightarrow 2\cdot OH$$

$$H_2O \rightarrow \cdot OH + H^+ + e^-$$

$$H_2O_2 + 2H^+ + 2e^- \rightarrow 2H_2O$$

Scheme 2.3: The overall and half reactions governing the photolysis of hydrogen peroxide by UV light to yield ·OH.

These half reactions give an overall reaction potential of -0.827 V. This can be used to calculated the optimum frequency of UV light to initiate the reaction with, in this case a maximum frequency of 750 nM is best.

While H_2O_2 / UV treatment yields high concentrations of ·OH and is therefore effective at degrading DOC of water samples there are issues with its use that have limited it's uptake in potable water treatment. The process requires high concentrations of H_2O_2 since the peroxide is actually quite poor at absorbing UV photons. This results in the affluent also containing substantial H_2O_2. Aside from the direct health consequences of this, residual H_2O_2 would react with the chlorine used later for disinfection and reduce the effectiveness of this process. One method to reduce this issue is to irradiate the system for longer than required for substrate conversion. This reduces the residual H_2O_2 concentrations to acceptable levels but also results in higher operation costs.

Ozone may also be added to UV initiated systems to enhance degradation of DOC. Photolysis of ozone in water yields H_2O_2 as shown below in scheme 2.4. As above the subsequent photolysis of H_2O_2 yields hydroxyl radicals which act to degrade DOC. This process is overall quite efficient yielding approx.
1 mol ·OH / 1 mol O_3. The high cost of ozone generation is largely offset by the cheapness of H_2O_2.

$$O_3 + H_2O + h\nu \rightarrow O_2 + H_2O_2$$

Scheme 2.4: Generation of H_2O_2 using O_3 and UV light.

In remediation research UV light is also often (but not always) coupled with titanium dioxide catalysts. Aqueous suspensions of TiO_2 are photochemically active, when a photon strikes the TiO_2 surface conduction band electrons and valence band holes are produced. These species are capable of performing photoreduction of species (free conduction band electrons) and photooxidations of species (holes). Therefore UV and UV / TiO_2 systems have garnered significant research interest as a water remediation technology[6, 8-11].

The holes produced in such materials are able to react with water molecules to form ·OH as shown in scheme 2.5, h^+ denotes a hole. The electrons generated can combine with O_2 to form the superoxide radical mentioned earlier which is also useful as an oxidant.

$$h^+ + H_2O \rightarrow H^+ + \cdot OH$$

Scheme 2.5: Production of ·OH from reaction between holes and water in materials such as TiO_2.

2.3.2: Ozonation

The use of ozone has been widely investigated for the removal of a wide range of organic pollutants from water[6, 12-14]. This was driven by the fact that ozone is already employed in the water processing industry for the clarification and disinfection of water[6]

Two mechanisms exist for ozone to react with dissolved organic matter, named the direct route and the indirect route.

In direct ozonation molecular ozone oxidises the organic matter leading to oxidation of the molecule. In indirect ozonation the oxidising species are ·OH and ·OOH radicals formed when ozone degrades in alkaline conditions. It is these which form the main oxidising species in the ozonation process. These reactions are shown in scheme 2.6[15].

$$O_3 + OH^- \rightarrow HO_2^- + O_2$$

$$HO_2^- + O_3 \rightarrow \cdot O_3^- + HO_2\cdot$$

$$HO_2\cdot \rightarrow \cdot O_2\text{-} + H^+$$

$$\cdot O_2^- + O_3 \rightarrow \cdot O_3^- + O_2$$

$$\cdot O_3^- + H^+ \rightarrow HO_3\cdot$$

$$HO_3\cdot \rightarrow O_2 + \cdot OH$$

Scheme 2.6: The chemical reactions involved in indirect ozonation to form oxidising radicals.

The overall stoichiometry of the first reaction set is given in scheme 2.7. From this it can be seen that the high pH (>11) conversion of ozone to ·OH is inefficient needing 1.5 mol O_3 / 1 mol ·OH.

$$3O_3 + OH^- + H^+ \rightarrow 4O_2 + 2\cdot OH$$

Scheme 2.7: The high pH conversion of O_3 to ·OH.

Ozonation reactions also occur in natural waters when dissolved oxygen is excited by UV light hitting the water surface forming ozone. It is thought that direct ozonation is primarily responsible for ozonation reactions in natural waters due to the complex water matrix screening out the reactive hydroxyl radicals.

Ozone for water treatment is generated on-site as required due to its rapid decomposition into oxygen. O_3 is generated when passing oxygen through a dielectric discharge gap with a high voltage alternating current applied (6 to 20 kV)[15]. Once generated the ozone is applied to the water as either diffusing bubble or by using a turbine mixer. Only ozone which dissolves in the water can be chemically active, this accounts for about 95% of the total ozone. The rest is lost as off-gas.

2.3.3: Ultrasound

As mentioned in section 1 and this chapter in section 2.1.3, ultrasound can also be classed as an AOP since it stimulates the formation of ·OH radicals via the process of microbubble formation, growth and collapse.

Unlike the other two AOPs mentioned in this section, ultrasound is not already employed in the water processing industry for some purpose, this may put it at a disadvantage when the water industry considers which AOP or combination of AOPs to use for dissolved organic pollutant oxidation.

Ultrasound's advantage however is a direct consequence of its active process of bubble cavitation. Ultrasound is much more useful a choice for the degradation of volatile and hydrophobic species. Volatile species will partition effectively into the bubble core and be pyrolysed. Hydrophobic species will be present in high concentrations close to the bubble and therefore oxidised quickly due to the high concentration of radical species close to the bubble upon its collapse.

A review of examples of the use of ultrasound in water remediation research now follows, focussed on 3 broad pollutant categories, dyestuffs, surfactants and hydrophobic species.

2.4: Use of ultrasound as an AOP for aqueous remediation chemistries

Upon bubble collapse the gas and water vapour contents of the bubble are pyrolysed. The main consequence of this from the point of view of using ultrasound as an AOP is the formation of hydroxyl radicals from the sonolysis of water. These hydroxyl radicals recombine to some extent within the collapsing bubble but high concentrations are ejected from the collapsed bubble into the surrounding fluid. These can then react with chemicals present around the bubble and degrade them.

2.4.1: The three sites of sonochemical degradation of pollutants

There are three sites for sonochemical degradation of pollutants; the bubble core, the interfacial region of the bubble and the bulk solution. Which reaction site a given chemical degrades in will be decided by its physicochemical properties.

Volatile species especially volatile hydrophobes will degrade in the bubble core. Due to the chemicals volatility it is able to evaporate into the bubble core during the growth period(s) of the bubble lifetime. Upon bubble collapse the species is pyrollised and also attacked by the high radical density formed within the bubble core.

Hydrophobic and surface active chemicals which are not volatile will degrade in the bubble interfacial region. This region is demarked by the bubble interface and the surrounding fluid. Hydrophobic and surface active chemicals will be attracted to the bubble interface and accumulate onto it. Upon bubble collapse the chemicals present in this region are degraded by the high radical density ejected from the bubble into the interfacial region. This region is also subject to high bubble temperatures and pressures (although not as high as in the bubble core) and so hydrolysis of pollutants chemicals in this region may also occur.

Hydrophilic non-volatile species will be degraded in the bulk solution since they are not volatile enough to penetrate the bubble core nor are they hydrophobic nor surface active and so are not attracted to the bubble interface. In the bulk solution they are degraded solely by radical attack since the temperature and

pressure of the bulk solution remains ambient. The radical density moving from the collapsed bubble into the bulk solution diminishes rapidly however, and so ultrasound is less effective at removing this class of pollutant. These three reaction sites are portrayed in figure 2.2.

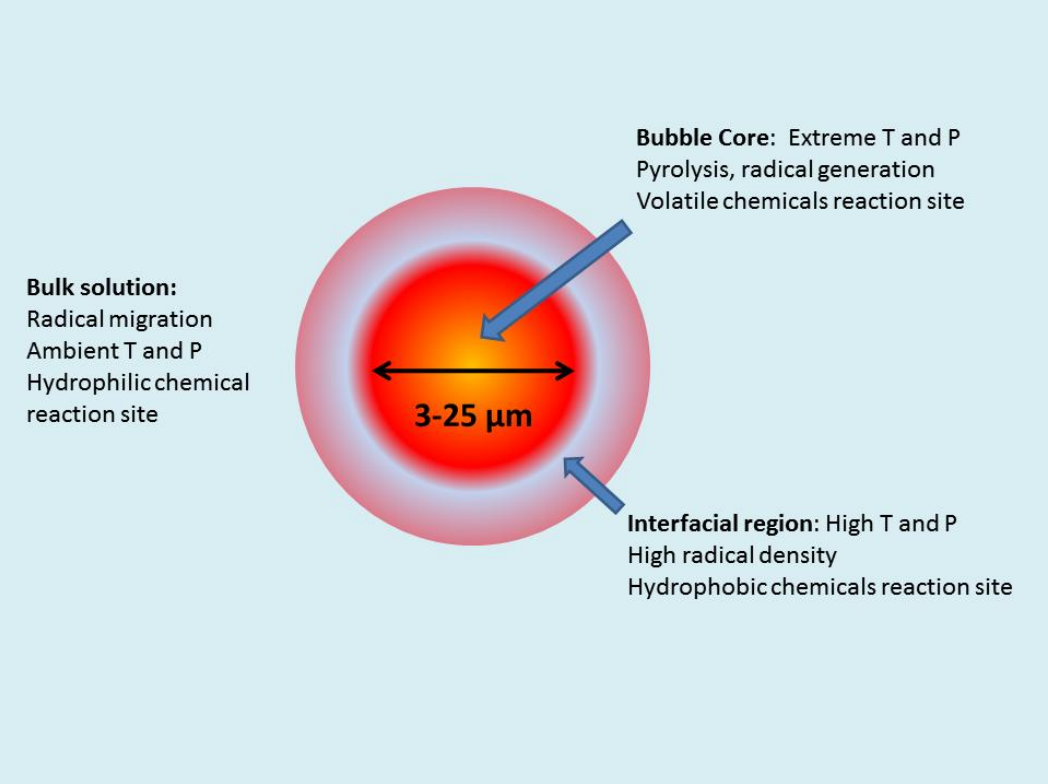

Figure 2.2: The three degradation sites for the sonolysis of pollutants in water. T denotes temperature and P pressure.

Sets of example degradations using ultrasound now follows for three classes of pollutant; dyestuffs, surfactants and hydrophobic pollutants. These 3 classes were chosen since they are both widely encountered problem pollutants in water processing and also their degradation by ultrasound is well researched.

2.4.2: Examples of removal of dyestuffs

In the last 12 years there has been a great deal of work on the use of ultrasound to destroy dyestuffs in aqueous solution. Most of the published work has concentrated on the kinetic process of degradation and its acceleration / intensification. Few studies have looked at the mechanism of the degradation and degradation products.

An early paper to study this topic was that of Hong *et al*[16]. The dyes studied were alizarin (5 µM solutions) and Procion Blue (4 µM) using 20 kHz ultrasound. They found that the degradation of alizarin followed a first order rate law degradation process. They observed that the rate constants observed decreased with solution volume which was attributed to the main sonolytic effect occurring close to the horn tip. The rate constants calculated were in the order of 4.1×10^{-5} s^{-1} in the presence of air and reduced to 3.6×10^{-5} s^{-1} under argon, indicating that the presence of some oxygen is important for the degradation process. They found that alizarin degraded more slowly than cyanide which was also studied in the same paper and attributed this to the lower diffusion coefficient of alizarin compared to cyanide.

The degradation of alizarin was attributed to ·OH radicals formed from sonolysis of water by cavitation bubbles. The possibility of degradation by hydrogen peroxide formed in the interfacial region was discounted due to the discrepancy between rate constant of the known hydrogen peroxide bleaching process and the measured rate constant for sonochemical degradation of alizarin (the bleaching process degradation was second order and too low to account for the degradation rates found).

The degradation of Procion Blue, a recalcitrant reactive dye used for covalent binding to fabrics, was also found to degrade by simple first order kinetics. Its measured rate constants of degradation were 5.1×10^{-5} s^{-1}.

Much of the work on dyestuffs has concentrated on the use of ultrasound in tandem with another oxidising technology. Stock *et al* combined ultrasonic degradation using 640 kHz ultrasound with photocatalysis using TiO_2 for the degradation of the azo dye Napthol Blue Black (50 µM)[17]. Three experiments were performed using ultrasound alone, photocatalsysis alone and the two combined. For all three processes the degradation was found to follow first order kinetics. The sonochemical degradation (1.04×10^{-2} min^{-1}) was found to be about two times faster than the photochemical process (0.56×10^{-2} min^{-1}). The two combined was found to be faster than the sum of the two processes (1.83×10^{-2} min^{-1}).

As with the work by Hong[16], the degradation by both solo processes and their combination was attributed to ·OH radical attack. The work also studied the total organic content of the solutions over time and at best found that 90% of the dye could be degraded within 6h using the combined treatment. The synergistic (non linear) combination of the two technologies was attributed to ultrasound acting to constantly regenerate the TiO_2 surface and improve mass transport within the solution as well as degradation of the dye directly.

Destaillats *et al* combined sonolysis using 500 kHz ultrasound with ozonolysis in their work on the degradation of Methyl Orange solutions (10 μM)[18]. They found that sonolysis or ozonolysis alone was only able to remove 50% of the total organic carbon (TOC) (dye + degradation product concentration) but the combined methodology was able to remove over 80% of the solution TOC. This synergism was proved by first degrading the solution by ozonation and then subsequently performing sonolysis on the same solution. They found that the products formed from ozonolysis could not be further degraded using sonolysis and the TOC remained the same. These products were identified as partially oxidised saturated mono and dicarboxylic acids. The degradation products of MO were studied and found to include phenol, hydroquinone. benzoquinone, oxalic acid, maleic acid, formic acid and formaldehyde.

Abdelsalam *et al* combined sonolysis using 124 kHz ultrasound with electrochemical formation of hydrogen peroxide at -0.7 V (sonoelectrolysis) for the degradation of Meldola Blue solutions (100 μM)[19]. Electrolysis alone was found to be ineffective and did not degrade the dye. Sonolysis alone did degrade the dye with a pseudo first order rate constant of 4.4 $x10^{-3}$ min^{-1}. The combined process was much more efficient at degrading the dye than either method alone, affecting a degradation rate constant of 12.6 $x10^{-3}$ min^{-1}.

The use of Fenton type catalysis was also studied by the addition of $FeSO_4$ (0.5 mmol dm^{-3}). In all cases the degradation was enhanced and the highest rate constant observed was 23.7 $x10^{-3}$ min^{-1} when using Fenton reagent, electrochemical peroxide formation and sonolysis simultaneously. As with the other studies described the degradation was attributed to OH radicals. The

mechanism by which Fenton-type catalysis enhances the degradation of H_2O_2 into ·OH is shown in equation 2.2.

$$Fe^{2+} + H_2O_2 \rightarrow Fe^{3+} + OH^- + \cdot OH \qquad (2.2)$$

The calculation of the degradation rates described relied on the colour of the solution since the degradation was followed spectrophotometrically. Therefore the rate constants were for the decolourisation process. To ascertain the rate of the complete degradation of Meldola Blue, the chemical oxygen demand of the solution was followed. Chemical oxygen demand measures the amount of oxygen required to completely oxidise the organic matter in aqueous solution using a strong oxidant and therefore is an indicator of the complete degradation of organic substrates including Meldola Blue. The rate of degradation was found to be slower than the decolourisation process with a rate constant of $1x10^{-2}$ min^{-1}, compared with a rate constant of 2.5×10^{-2} min^{-1} for the decolourisation process.

Voncina combined use of 20 kHz ultrasound with hydrogen peroxide for the decolourisation of six vinylsulfone reactive dye solutions (10 mg /L)[20]. Rate constants were not measured but using ultrasound alone the dyes were all decolourised to between 57% decolourisation for C.I. Reactive Blue 28 and 95% decolourisation for C.I. Reactive Black 5 after 7 hours of sonication. With the addition of 0.23 mol L^{-1} hydrogen peroxide sonication times could be reduced to 4 hours and decolourisation occurred to above 91% for all the dyes studied.

2.4.3: Examples of removal of surfactants

Surfactants have not been examined as thoroughly as dyes to date. A few examples are discussed below.

The first paper on the sonolytic destruction of surfactants was by Suzuki *et al* in 1999[21]. They studied the decomposition of polyoxyethylene alkyl ether. Four ultrasonic frequencies were studied for the degradation of solutions with an initial concentration of 50 ppm namely 26 kHz, 38 kHz, 100 kHz and 300 kHz

ultrasonic frequencies. The order of degradation rate magnitude increased along the series 38 kHz < 26 kHz < 100 kHz < 300 kHz with the fastest degradation removing all of the surfactant within 60 minutes as measured by HPLC analysis. Rate constants were not measured for the data nor were the actual rates of degradation. The TOC of the solution was found to decrease much more slowly however with the TOC reducing from ~60 ppm to ~40 ppm after as long as 24 hours of sonication.

Vinodgopal *et al* studied the sonolysis of the polydisperse nonylphenol ethoxylate (NPE) Teric GN9, a non-ionic surfactant using 363 kHz frequency ultrasound[22]. It was found that using just 2 W cm^{-2} ultrasonic intensity that the NPE was destroyed after 2 hours. The effect of initial surfactant concentration was assessed and it was found that the degradation rate constant increased with decreasing concentration. The first order kinetics were explained to be present due to the inclusion of pyrolysis in the degradation mechanism. The initial degradation rate was found to initially increase with concentration between initial concentrations of 0 – 40 µM. After this the rate became constant and even decreased slightly with increasing concentration. The maximum rate was 4.3 µM min^{-1} at a concentration which approximated the critical micelle concentration of Teric GN9 (50 µM).

A mechanism of surfactant adsorption onto the bubble interface was proposed to explain the degradation of Teric GN9. In this model the hydrophilic ethoxylate portion resides in the solution bulk and the hydrophobic phenyl moiety exists inside the bubble core.

The plateauing of degradation rate around the micelle formation point was explained by the flux of Teric GN9 to the bubble interface increasing up to the CMC point with increasing concentration but becoming constant at the CMC where there now exists a dynamic equilibrium between the amount of Teric GN9 traversing the bubble interface and the amount in micelles.

Degradation of Teric GN9 was postulated to occur by both thermal and radical attack based degradation pathways. The thermal degradation occurs due to the proximity of the surfactant to the hot collapsing core of the bubble. The radical

attack occurs due to the high concentration of ·OH radicals formed and expelled from the collapsing bubble.

The initial degradation products were then postulated to be pyrolysed in the bubble core since they are volatile. It is the build up of these decomposition products that were used to explain the increasing sonoluminescence quenching found with increasing Teric GN9 concentration up to the CMC after which the quenching rate became constant. This last point was used as further proof of the amount of surfactant on the bubble interface becoming constant past the CMC point.

The accumulation of surfactant around the bubble interface was also used as a model by Yim *et al*[23]. Yim studied the degradation of the surfactants sodium dodecylbenzenesulfonate(DBS), sodium dodecylsulfate (SDS), polyethylene glycol monostearate, sodium 4-toluenesulfonate and the hydrophobic species 1-hexanol as 100 µM solutions. The degradation rates when using 200 kHz frequency ultrasound were 1-hexanol > DBS = SDS> STS. The fact that these surfactants scavenged the formed hydrogen peroxide in the same order was used to support the proposal that the surfactants accumulated in differing degrees around the bubble interface depending on their physico-chemical properties.

From the rate constant of the recombination of ·OH radicals to form hydrogen peroxide, the rate constant of the addition of a ·OH radical to the surfactant species and the concentration of ·OH radicals, Yim calculated accumulation ratios for the species studied. These were in the order 1-hexanol > SDS> DBS> STS and were used to explain the degradation rates found. The major gaseous degradation products were found to be CO and methane. No solution phase degradation products were identified.

Manousaki *et a*l in 2004 reported the use of ultrasound to degrade sodium dodecylbenzene sulfonate as an alternative technology for the removal of linear alkylbenzene sulfonates present at high concentration, at which biodegradation is inhibited[24].

Manousaki studied the use of 20 kHz and 80 kHz ultrasound for the degradation process, and found that the process was enhanced by using higher frequency ultrasound. The explanations given for this were the combined effects of an increase in bubble lifetime and interfacial area increasing the amount of surfactant on the bubble interface along with the increased number of cavitational events occurring and collapsing due to increasing frequency.

An increase in initial surfactant concentration was examined and it was found that in accordance with previous work that the degradation rate increased with increasing surfactant concentration.

The effect of addition of radical scavengers was also studied using KBr and 1-butanol as the scavenging species. It was found that 1- butanol was much more effective than KBr at preventing the degradation of surfactant. The reason given for this is that the ionic KBr only scavenges radicals in the bulk phase whereas butanol scavenges radicals in the interfacial region of the bubble. Since this was the proposed reaction zone the findings that 1-butanol at 1 g L^{-1} completely quenched the sonodegradation reaction supported this hypothesis.

The addition of salt, which effectively increases the hydrophobicity of organic species dissolved in water was found to have a negative albeit minor effect on the degradation efficiency. The use of combining ultrasound with a peroxide / Fenton process was also examined and it was found that both Fe^{2+} and Fe^{2+} with hydrogen peroxide added increased the degradation efficiency.

2.4.4: Examples of removal of hydrophobic species

In 2004 Psillakis *et al* reported the use of ultrasound to destroy 11 nitroaromatic explosives in water[25]. For the chemical analysis and quantification of the experiments hollow fibre liquid phase micro extraction was used. This method involves the use of a hollow porous fibre tube into which organic solvent was injected prior to immersing the tube and solvent (3 µL) into the aqueous solution which is to be analysed. The solution with the suspended fibre-solvent assembly is then stirred and the chemicals in the aqueous phase are

concentrated into the organic phase within the tube. Half of this solvent was then removed via microsyringe and analysed using GC-MS.

Using this extraction – sampling method the degradation of 11 nitroaromatics were studied using 80 kHz ultrasound with a power input of 150 W and controlled at a temperature of 20℃ using a thermostatted water bath. Solutions containing 100 μg L^{-1} of each contaminant were irradiated for 300 minutes under an atmosphere of air. To avoid photochemical reactions a glass cylindrical vessel was used. It was found that several of the nitroaromatics were removed easily within 300 minutes while others proved recalcitrant. TNT for example was not degraded at all by ultrasonic action. No rate constants for the degradation were studied nor were any degradation products confirmed.

Also in 2004 Chen *et al* studied the use of ultrasound for the reduction in TOC of natural organic matter in aqueous solution[26]. Natural organic matter are naturally occurring organic substances which may be present in both surface, ground and to some extent municipal water supplies due to the decay of plant and animal matter in water supplies. The organic content of such organic matter is highly complex and ill-defined but consists of phenolic, aromatic, aliphatic and carboxylic macromolecular species[27]. As such their presence may affect water treatment processes designed to remove other pollutants such as the organic species mentioned in this chapter.

Two types of dissolved organic matter (DOM) were studied by Chen; Aldrich humic acid, which is base extracted from coal and Pahokee peat which is formed in freshwater marshes. The degradations of DOM were affected using both 20 kHz and 354 kHz ultrasonic frequencies. The initial TOC of the DOM solutions was 22.5 mg / L. It was found that for both types of DOM studied 20 kHz ultrasound was ineffective at removing the TOC of the solutions even when using a power density as high as 450 W L^{-1}. Conversely the 354 kHz system at the same power density the TOC decreased to 15 mg L^{-1} and 18.2 mg L^{-1} for the Aldrich DOM and the Pahokee DOM respectively therefore it was found that the Aldrich DOM was mineralised more effectively. Using the same parameters it was also found that the colour of the solutions due to the dissolved DOM was much more greatly removed when using 354 kHz ultrasound. It was also found

that the molecular weight of the two types of DOM were reduced through ultrasonic irradiation, with the higher frequency again being more effective. This result is analogous to the chain scission that occurs for polymer solutions subjected to power ultrasound.

Shemer *et al* in 2005 used 20 kHz ultrasound with an acoustic intensity of 3.75 W cm^{-2} to degrade solutions of the trihalomethanes $CHCl_3$, $CHBrCl_2$, $CHBr_2Cl$, $CHBr_3$ and CHI_3[28]. The experiments were performed under air and with an initial solution loading of 10 mg L^{-1} of trihalo species. Under these conditions it was found that the percentage of removal within 180 minutes was in the order $CHCl_3$ > $CHBrCl_2$ > $CHBr_2Cl$ > $CHBr_3$ > CHI_3 and that pseudo first order kinetics were found to occur. Rate constants were calculated for the degradations and were calculated as being between 2.48 x 10^{-2} min^{-1} ($CHCl_3$) and 5.1 x 10^{-3} min^{-1} (CHI_3).

For the trihalomethanes studied it was found that the physicochemical properties of the species were important. The rate of degradation increased with increasing vapour pressure signifying that the degradation occurred within the bubble core. The half life of the species studied was found to increase with increasing octanol partition coefficient of the halomethanes. The authors stated that this meant that the degradation process was limited by both the concentration of halomethane around the bubble compared to the bulk and the diffusion of the species in water.

Parathion is a recalcitrant pesticide and its' sonolytic degradation has been studied by several groups. First of all in 1992 Kotronarou *et al* published a short communication on the degradation of parathion by 20 kHz ultrasound running at an ultrasonic intensity of 75 W cm^{-2} under an atmosphere of air[29]. For the sonolysis experiments saturated solutions of parathion were used (24 mg L^{-1}). The paper was mainly a discussion of the products formed from parathion sonolysis. These products were found to be sulphate, nitrite, nitrate and phosphate ions, oxalate and paranitrophenol were the organic species found as degradation products. Hoffman *et al* had already shown that paranitrophenol was susceptible to sonolysis and so this mechanism was used to finish the

degradation mechanism of parathion, where the final products were phosphate, sulphate, nitrate, carbon dioxide and protons.

Secondly in 2010 parathion degradation by ultrasound was studied in two papers by Yao *et al*[30, 31]. The first covered the effects of frequency, power and initial concentration of parathion on the degradation kinetics. The effect of two radical scavengers, t-BuOH (to scavenge radicals in the bubble contents and interfacial zone of the bubble) and sodium bicarbonate (to scavenge the bulk solution of radicals) was studied on the degradation of parathion. A complete degradation product analysis was also carried out using solid phase microextraction (SPE) to pre concentrate the aqueous samples followed by GC-MS and ion chromatography analysis.

For the experiments on the effect of ultrasonic frequency on the degradation 200, 400 600 and 800 kHz ultrasound frequencies were used with 2.9 µM solutions of parathion being degraded under air. The ordering of the resulting rates of degradation were 600 kHz > 400 kHz > 800 kHz > 200 kHz with the fastest pseudo first order rate constant being 0.150 min^{-1} when inputting 45 W of power. An increase in power was found to increase the degradation rate of parathion with the fastest degradation occurring for 55.2 W of inputted power effecting almost complete degradation of parathion within 30 minutes with a rate constant of 0.254 min^{-1}. Three initial concentrations of parathion were studied these were 0.8 µM, 2.9 µM and 5.2 µM solutions. For each solution three power settings were studied namely 55.2 W, 37.8 W and 17.4 W. It was found that the rate constants increased with increasing power at each given concentration but that the rate constants also increased with decreasing parathion concentration. The highest rate constant measured was 0.254 min^{-1} when using 0.8 µM solutions with 55.2 W of ultrasonic power.

Addition of differing amounts of t-BuOH was found to quench the degradation of parathion, with almost no degradation occurring when 0.1M of t-BuOH was added. Conversely to this the addition of sodium bicarbonate was found to have little effect on the degradation of parathion. This showed that parathion is degraded around the interfacial region of the cavitation bubbles and not in the solution bulk since t-BuOH partitions to the interfacial region of the bubble and

so scavenges radicals preventing the degradation of parathion. Conversely the sodium bicarbonate would partition into the bulk solution and hence does not scavenge the radicals which degrade parathion.

To model the degradation of parathion a Langmuir – Hinshelwood kinetic model was used. This type of kinetics is most often used to describe the catalysis of heterogeneous gas/solid reactions. By using this kind of kinetics Yao *et al* stated that the surface boundary of a bubble acts as a heterogenous surface with a fixed number of reaction sites for parathion to absorb onto and consequently degrade due to ·OH radicals and hydrolysis. It was found that these types of kinetics modelled well the data from degradation of 6 solutions of parathion of differing concentration confirming that parathion degrades at the interfacial surface of the formed cavitation bubbles.

Using GC-MS 10 products were confirmed to be formed by parathion sonolysis. These were p-benzoquinone, diethyl phosphite, triethylephosphate, O,O,O-triethyl thiophosphate, O,O,S-triethyl phosphorothioate, 1-ethoxy-4-nitro-benzene, 2,4-dinitrophenol, 4-nitrophenol, 4-nitro catechol and paraoxon. These products were formed by hydrophysis of the initial parathion and subsequent ·OH radical attacks as well as attack by $\cdot NO_2$ radicals formed from the sonolysis of nitrogen in the air atmosphere used.

The second paper published on the same topic covered the effects of ultrasonic intensity, different dissolved gases, the addition of different anions, and the addition of natural organic matter (NOM) on the degradation of parathion. An ultrasonic frequency of 600 kHz was used with 2.9 µM solutions of parathion being degraded. An increase in ultrasonic intensity was found to increase the rate constants and hence the rate of the degradation of parathion. The intensity range covered was 0.1 – 0.69 W cm^{-2} with the resultant pseudo first order rate constants ranging between 0.020 min^{-1} – 0.192 min^{-1}.

The effects of dissolving O_2, N_2 and air into the parathion solutions were investigated. The reactions were all found to be pseudo first order in their degradation kinetics with oxygen producing the fastest degradations (k = 0.288 min^{-1}), then air (k = 0.211 min^{-1}) then no added gas (k = 0.186 min^{-1}) and lastly nitrogen (k = 0.123 min^{-1}). The acceleratory effect of oxygen addition was

explained by oxygen forming additional ·OH radicals by direct reaction with ·H but also by the reaction of the oxygen diradical with water to form additional ·OH. These extra radicals boosted the degradation rate of parathion. Conversely to this the retarding effect of nitrogen was explained by its ability to act as an ·OH radical scavenger inside the bubble core.

The addition of 4 different anions to the parathion solutions was then studied. Of these it was found that CO_3^{2-}, HCO_3^- and Cl^- had a retarding effect on the degradation rate with the inhibition following the series $CO_3^{2-} > HCO_3^- > Cl^-$. This trend was explained by the fact that CO_3^{2-} and HCO_3^- can act as ·OH radical scavengers whereas chloride tends not to react as much with ·OH due to the instability of the product $·ClOH^-$. The addition of bromide ions was found to accelerate the degradation of parathion and that this acceleration increased with increasing concentration of bromide. This effect was explained by recognising that bromide can react with ·OH to form $·Br_2^-$ which is more stable and sulphur selective in its oxidation chemistry than ·OH. This more stable radical is able to diffuse more easily from the cavitation bubble and degrade parathion by attack on its sulphur moiety to form paraoxon re-releasing Br^- thus forming a catalytic system for paraoxon formation. The authors stated that this effect was similar to the increase in rate of the degradation of CCl_4 by addition of iodide ions as studied by Kotronarou *et al*[29].

To study the effect of natural organic matter (NOM) on the degradation two types of NOM (hydrophilic NOM and hydrophobic NOM) were added in an amount of 10 mg L^{-1}. The both types of NOM retarded the degradation of parathion with the retardation being greater for the hydrophobic NOM. Since both parathion and this type of NOM are hydrophobic it was suggested that the NOM competed successfully with parathion for ·OH radicals at the bubble interface reaction sites.

Finally in this paper a model was used to fit the kinetic data for the degradation of parathion and also for the formation of paraoxon and 4-nitrophenol. An excellent fit was found between the data and the model.

Most recently Shriwas *et al* studied the effects of solution pH, addition of solids, addition of CCl_4, addition of peroxide, use of Fenton type chemistry and the effect of the scale of the process on the degradation of methyl parathion[32] For all experiments 20 kHz ultrasonic frequency was used either as an immersion probe or as an ultrasonic bath for the scale up experiments. Methyl parathion solutions were always made as 20 ppm.

For the experiments probing the effect of the solution pH a pH range between 2.5 and 7 was studied. Solutions were irradiated for 60 minutes at each pH point studied. It was found that acidic pH favoured the sonolysis of methylparathion with a degradation percentage of 10.2% at pH 2.5, a rate constant of 1.75×10^{-3} min^{-1} was calculated for this pH point. At pH higher than 2.5 the degradation percentage decreased linearly with increasing pH up to a pH of 7. No explanation for this was given, although work by other authors has found that sonolysis is favoured at a pH where the solute substrate is in a neutral rather than an ionic form as this favours accumulation around the bubble surface[33].

To study the influence of suspended solids TiO_2 was added to methyl parathion solutions at varying ratios of TiO_2 to the concentration of methyl parathion. Using a 1:1 suspension a degradation percentage of 32.5% was achieved, at a loading of 20:1 40% degradation was achieved and when using a rather excessive 500:1 suspension the degradation was reduced from this value. The results were explained by stating that the addition of solids increased the amount of cavitation events in the solution and completely disregarded the ability of TiO_2 to act as a sonochemical catalyst for additional ·OH radical production[34].

The effect of the addition of CCl_4 was then studied. With a CCl_4 range of 200 ppm to 1000 ppm the fastest degradation was found to occur with a 25:1 ratio of CCl_4 to methyl parathion. This enhancement is explained by the carbon tetrachloride being sonolysed in the cavitation bubble to form chlorine atoms which can also degrade the methyl parathion species, so in essence the radical density of the solution is increased by increasing amounts of CCl_4 up to the optimum mentioned. This paper is not the first to use CCl_4 as an intensification

method for sonolytic reactions. It is the opinion of the author of this work that this method is not valid for study since CCl_4 is itself an extremely dangerous, toxic and carcinogenic chemical and its addition as an intensifier in the context of water purification works does not make sense on this basis.

A much less hazardous chemical was then studied as an intensifier of the radical yield of the system: hydrogen peroxide. Shriwas *et al* studied a concentration range between 60 and 400 ppm of H_2O_2 and found that the optimum ratio was 10:1 peroxide to methyl parathion[32]. The rate constant at this optimal point was 2.51 $x10^{-3}$ min^{-1}. It was also found that the degradation of methylparathion continued after the sonication period. Samples were left to stand after the sonication period and it was found that 48 hours after sonication the degradation had increased to 70%. This was explained by a latent effect whereby the radicals produced by ultrasound continue to react with remaining peroxide in a radical chain reaction manner, continuing to degrade pollutant over time.

To study the effect of Fenton type chemistry $FeSO_4$: H_2O_2 was added to methyl parathion solutions. This was done between 1:1 and 4:1 ratios with a fixed amount of peroxide (200 ppm). It was found that a 3:1 ratio of $FeSO_4$: H_2O_2 was optimum degrading 96% of the methylparathion in the 1 hour reaction time with a rate constant of 5.36 x 10^{-2} min^{-1}. Using this optimum ratio a TOC reduction of 74% was achieved.

Lastly the scale of the process was considered by using a bath reactor also running at 20 kHz. Using just the sonochemical reaction without any additives a slower degradation was found using the bath (8%). This was attributed to the lower power density (72 W / L) compared to the horn (2700 W / L). However the reduction in degradation percentage is not as great as the reduction in power density and this was explained by the bath being more effective per unit power density due to a more even amount of cavitation occurring throughout the volume the bath due to the spreading of multiple transducers.

2.5: Phthalate esters

This section describes the context for the work in this thesis, phthalate esters and why they are a problem for mankind.

2.5.1: What are phthalate esters?

Figure 2.3 shows the structures of three phthalate esters (now referred to simply as phthalates). As can be seen phthalates are benzoic diesters with the ester groups *ortho* to each other. The ester groups can be dialkyl and is the case for diethyl and diethylhexyl ether or they can be mixed as is the case for benzylbutyl phthalate. The alkyl chains can also be linear or they can be branched as is the case for the widely used phthalate diethylhexyl phthalate. There are therefore a wide range of phthalates used industrially as there are many possible combinations of the ester chains. In fact there are known to be over 60 phthalates manufactured and in industrial use worldwide[6]. The majority of phthalates however are dialkyl species and benzyl butyl phthalate is the most widely used mixed phthalate.

Phthalate esters were originally developed for use as plasticisers by the Kodak company. To the present date they have been used extensively as plasticisers for PVC resins and for cellulose film coatings with an estimated 5 million tonnes a year being produced[35]. The role of a plasticiser is to improve the flexibility, workability and extensibility of the plastic material[36]. The stability, fluidity and very low volatility of phthalates make them highly suitable for use as plasticisers[37].

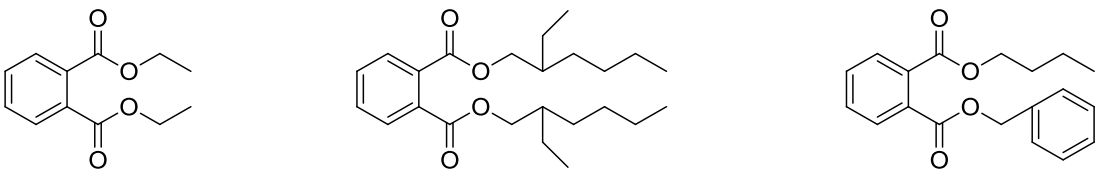

Figure 2.3: The structures of three phthalate esters. Diethyl phthalate, diethylhexyl phthalate and butylbenzyl phthalate.

In terms of production and consumption the most important phthalate is diethylhexyl phthalate (DEHP), which is used as a plasticiser in PVC and also used in cosmetics, adhesives and paints. Other prominent phthalates include butyl benzyl phthalate (BBP) and dibutyl phthalate (DBP) which were both used extensively in vinyl flooring tiles[38]. The short chain dimethyl (DMP) and diethyl phthalates (DEP) are used in cellulose ester based plastics such as cellulose acetate and cellulose butyrate[37].

Phthalate esters are largely hydrophobic compounds. This hydrophobicity increases with the carbon count of the ester chain groups. Therefore dimethyl phthalate is more hydrophilic than dibutyl phthalate which is more hydrophilic than butylbenzyl phthalate. Their solubility in water also decreases with increasing carbon chain length. Phthalates also exhibit low volatility. The physico-chemical properties of the phthalates used in this study are shown in table 2.1

Phthalate	Solubility in water / mg L^{-1}	Vapour Pressure / mm Hg	Henry Constant / Pa m^3 mol^{-1}	Octanol Partition coefficient
Diethyl Phthalate (DEP)	1130.0 [39]	8.11 x 10^{-4} [40]	0.0269 [40]	2.42 [41]
Dipropyl Phthalate (DPP)	47.0 [40]	1.04 x10^{-3} [40]	0.0309 [40]	3.57
Dibutyl Phthalate (DBP)	11.2 [40]	4.40 x 10^{-5} [42]	0.0895 [40]	4.61 [40]
Butylbenzyl Phthalate (BBP)	2.4 [40]	9.10 x 10^{-5} [40]	0.0771 [40]	4.77 [40]
Diheptyl Phthalate (DHP)	0.001 [41]	-	-	8.17 [41]
Dioctyl Phthalate (DOP)	0.00 [40]	1.3 x 10^{-5} [40]	10.4365 [40]	8.54 [40]
Dinonyl Phthalate (DNP)	0.130 [43]	5x10^{-5} [44]	-	9.27 [41]

Table 2.1: Physico-chemical properties of phthalate esters pertinent to removal *via* ultrasound. Where blanks are present the data is not available in the literature.

2.5.2: Phthalate esters in the environment

In their use as a plasticiser phthalate esters are not covalently bound to the plastic. This is so that the necessary flexibility of the plastic is maintained[45]. This has however meant that phthalate esters have become a ubiquitous pollutant of land, water and air largely through the manufacture, use and disposal of plastic materials and goods.

Since they are used in aerosols phthalates have entered into the air around the world. Through the disposal of plastic materials to landfill sites phthalates have contaminated ground water flows and also the earth around such sites as the phthalate is able to leech out in nanogram quantities over time. Phthalates enter water supplies during their production and also the production of the plastic material.

As an example of the ubiquitous nature of this pollutant the short chain phthalates dimethyl and diethyl phthalate are commonly found in many kinds of environmental sample. This is largely due to the fact that these phthalates are the most soluble of the phthalates and are also widely used. These types of sample include surface marine waters[46, 47], freshwaters[48] and sediments[49].

The quantities of various phthalates in water supplies vary within the ng to µg per litre levels. In Californian raw (pre-treatment) drinking water dimethyl, diethyl and dibutyl phthalates have been identified in amounts of 0.04µg L^{-1}, 0.49 µg L^{-1} and 1.35 µg L^{-1} respectively[50]. After treatment these levels actually rose. In reclaimed Californian waste water the same phthalates were found in amounts of 0.04 µg L^{-1}, 0.97 µg L^{-1} and 2.70 µg L^{-1} [50].

In a processing facility in China, influent reclaimed waste water was found to contain an average of 0.78 µg L^{-1} of DBP and 1.80 µg L^{-1} of diethylhexyl phthalate (DEHP). After processing these levels dropped to 0.54 µg L^{-1} and 0.40 µg L^{-1} [51].

In Germany a study in three regions found that surface water concentrations varied between 0.33 and 97.80 µg L^{-1} of DEHP. These three examples show that phthalates are a widespread pollutant of several different kinds of water, and that they are not adequately removed using conventional water processing techniques. Even bottled drinking water, often marketed heavily for its purity and health aspects, has been found to contain phthalates[52].

Phthalates have been described as recalcitrant water pollutants. This is because they biodegrade very slowly. For hydrolysis in the natural environment half lives of phthalate degradation are expected to range between 3 years for dimethyl phthalate to 2000 years for diethylhexyl phthalate[37]. Photodegradation can also occur as sunlight falls on natural waters. Half lives for this degradation route have been calculated to range between 2.4 and 12 years for dimethyl and dibutyl phthalates and 0.12 to 1.5 years for DEHP[53].

Phthalates have also been shown to bioaccumulate and bioconcentrate. These two terms describe the accumulation of a chemical in biological organisms compared to the concentrations found in the environment. Bioaccumulation is

the concentration in tissues due to all exposure routes and bioconcentration is the accumulation of the species in tissues due to just aqueous exposure routes. These factors are usually calculated from fish since they are the most prone and sensitive organisms to aqueous pollutants[54]. As an example of such a study English Sole exposed to 30 – 200 µg L-1 of DEP was found to contain 177 times more DEP in its fatty tissues[55]. Similarly Bluegill Sunfish had 449 times more butylbenzyl phthalate in their tissue than what was found in their test environment[56]. As a final example Mullet had 270 times more DEHP in their system than did the water they were kept in[57].

2.5.3: Effects of phthalate esters on animal health

The bioaccumulation of phthalate esters in organisms would not be a problem if they were innocuous. Sadly this has been found to not be the case. Overall phthalates are classed as endocrine disrupting compounds and have been shown to have a wide range of effects on different animal species.

In rodents DEHP has been shown to be a known reproductive and sexual toxin. Effects of exposures to DEHP have included reduced testosterone levels, reduced testis weight and overall lowered sexual productivity, especially for developing males as opposed to sexually mature males[58].

Similarly DBP, again in rodent studies, caused abnormalities in the reproductive tracts, was found to affect testicular growth with foetus and immature animals being the most sensitive to intoxication. At high concentrations DBP also caused lowering of female rat fertility. DBP was also found to be a developmental toxin causing lesions to appear on the kidneys and liver of the rats tested[59].

2.5.4: Effects of phthalate esters on human health

Due to these displayed effects on animal health there have been concerns about human health. Some reports controversially claim from the given data that there is little-to-no risk to humans[58-61]. However in recent studies there have been displays of reduction in semen quality[62], links to breast cancer in males[63], effects found on thyroid counts in teenagers[64], links to self-diagnosed

diabetes[65] and other metabolism disruptions which have been linked to the modern rise of diabetes[66].

Human exposure to phthalates comes mainly from food and drink[67]. Since phthalates are largely hydrophobic, fatty foods can transmit phthalates which can be garnished into the food during its growth (from use of contaminated water and contamination from equipment) and also from food packaging (plastic is widely used for this task)[67]. Exposure to dibutyl phthalate has been estimated as 7 µg / kg bodyweight / day[67] for adults, 2.3 µg / kg bodyweight / day for 12-19 year olds and 5.0 µg / kg bodyweight / day for children up to the age of 4[68].

Due to the recalcitrant nature and biological activity of phthalates the USA Environmental Protection Agency in 1991 classified phthalates as a top priority pollutant mandating risk assessment and their removal from the environment. The European Union passed a similar decree in 1993.

2.6: Previous work on phthalate ester remediation using ultrasound

Due to the actions by the EPA and the EU there has been a great incentive for the study of improved methods of water purification and the removal of pollutants of concern from water supplies. Phthalates are listed among these pollutants and so there has been a great amount of work in the study of their removal by a wide range of AOPs and other linked processes. This section will discuss the work done previously to this work in the use of ultrasound for removing phthalate esters from aqueous solutions.

2.6.1: The work of Yim *et al*

The first work to examine the degradation of phthalate esters was that of Yim *et al* in 2002[69]. Using high frequency ultrasound (200 kHz) dimethyl, diethyl and dibutyl phthalate solutions (100 µM) were degraded while testing various parameters. Using an atmosphere of argon and a fixed pH of 7 the following pseudo first order rate constants were calculated: 0.039 min^{-1} (DMP), 0.110 min^{-1} (DEP) and 0.059 min^{-1}(DBP).

Having found that DEP was degraded more quickly than the other phthalates the effect of pH was ascertained for DEP degradation using pH of 7 and 12 under argon gas. At pH 7 the rate was observed to be 7.9 µM min^{-1}. At a pH of 12 the rate increased to 11.6 µM min^{-1}. Tert-butanol was added to solution to evaluate the proportion of free radical attack. It was found that DEP degradation was suppressed by 66% at pH 7 and by 44% at pH 12 in a 30 minute experiment.

In a brief product , Yim *et al* detected CO, CH_4, C_2H_6, C_2H_4 and C_2H_2 in the gas headspace of the sonochemical reactor used. It was found that CO was the main gas phase product and that [CO] increased over time whereas the other hydrocarbon gas concentrations did not. This was attributed to these larger hydrocarbons being pyrollised themselves by the cavitation process. In the solution phase, monoethyl phthalate (MEP) was found as the only reported liquid phase product and the amounts of MEP measured was 3.3 times higher at pH 12 than at pH 7.

Yim *et al* then continued to measure the degradation rate constants between pH 4 and pH 12. It was found that the rate constants increased with increasing pH in a pseudo exponential function and that the rate constants for DEP were consistently around 7 times greater than those of MEP. This difference was attributed to the low hydrolytic activity of MEP.

Using the physical chemical properties of DEP (low vapour pressure, moderately phydrophobic and susceptible to hydrolysis) Yim *et al* concluded that DEP degradation could occur by thermal reaction (pyrolysis), ·OH radical attack, and hydrolysis in the interfacial region. Yim *et al* then calculated the contribution of these three pathways to the degradation of DEP between pH 4 and 11.

It was found that the predominant pathway for degradation was ·OH radical attack (c.80%) and that its proportion remained unchanged between ph 4 and 11. At pH higher than 11 the contribution of radical attack to the degradation of DEP decreased. Within the same pH frame the contribution to degradation by hydrolysis increased (<20% up to c.65%). The amount of pyrolysis was calculated to always be below 20% and decreased slightly as the pH increased.

The overall mass balance calculated was constant at c. 96%. No explanation for this behaviour was given.

Finally Yim *et al* studied the effect of pH on the amount of MEP formation via the hydrolysis pathway between pH 11 and 12.5. This was done using ultrasound irradiation and by stirring which acted as a control experiment. It was found the the amount of hydrolysis occurring as calculated from the amount of MEP formed was 2-5 times higher for ultrasonic action. No good explanation was given for this other than the “chemical effects of ultrasound”.

2.6.2: The work of Psillakis *et al*

In 2004 Psillakis *et al* studied the sonolysis of DMP, DEP, DBP, BBP,DEHP and dioctyl phthalate (DOP) *via* solid phase micro extraction (SPME) coupled with GC-MS[70]. The use of this technique allowed Psillakis *et al* to study the degradation of much lower concentrations of phthalates then the methods used by Yim *et al* (HPLC and GC), aqueous solutions containing 40 μg L^{-1} of each phthalate as a mixture were used.

Using 80 kHz ultrasound and an experiment time of 240 minutes Psillakis *et al* found that all 6 phthalates were essentially destroyed as signified by the GC-MS peaks of their parent ions. The degradation was explained to happen mainly in the “interfacial sheath” of the cavitation bubble due to the phthalates low volatility and high hydrophobicity. This model was used to rationalise the fact that the more hydrophobic phthalates DBP, BBP, DEHP and DOP were rapidly destroyed within the first 30-60 minutes where as the more hydrophilic DMP and DEP were much more recalcitrant to sonolysis, requiring longer irradiation times (180 – 240 minutes) to effect complete degradation of the phthalate. It was also found that DEP was degraded more slowly than DBP which conflicts with the findings of Yim *et al*.

The effect of several parameters on the degradation of the phthalates were then studied, the first being the addition of salt. Adding salt to a solution of organic compounds essentially makes the dissolved species more hydrophobic since less water is now available to solvate the organic species[71]. It was found that the addition of 10% w:v of NaCl improved the degradation rates of DMP DEP

DBP and BBP but decreased the degradation rate of DEHP and DOP. The first group were classified as polar by Psillakis *et al* due to their shorter ester chain moieties and the “salting out effect” increased their transport to the interfacial region of the bubble and so aided their degradation. Conversely DEHP and DOP were classified as nonpolar and the effect of the salt reducing the vapour pressure and increasing the surface tension of the system. These two factors should decrease the amount of cavitation bubbles in the solution[72] and this was used to explain the decreased degradation of DEHP and DOP due to a decrease in the amount of available bubble surface area to bind to.

A limited study of the effect of the ultrasonic power was carried out using 150 W and 75 W powers. It was found that reducing the power input decreased the removal rate of all phthalates. This was attributed to the increase in power increasing the amount of cavitation bubbles in the solution.

The effect of temperature was also studied by performing three experiments: an original run with the temperature controlled to be 21℃, an experiment where the temperature was controlled at 50℃ and a final experiment which was uncontrolled and started at 21℃ but ended at 51℃. It was found that a detrimental effect was seen as the temperature was increased. This was explained by the increase in temperature allowing the formation of bubbles filled with more vapour. These bubbles have their collapse cushioned more by their increasing gas and vapour contents with increasing temperature and so the collapse is less violent and less ·OH radicals and other chemical effects are produced as the temperature is increased.

Psillakis *et al* attempted to ascertain the liquid phase degradation products of the sonolysis of phthalate esters but problems with their SPME fibre being too selective for phthalates prevented them from doing so. One product was identified, phthalic acid. Psillakis *et al* were unable to confirm the formation of monoesters which was originally found as the major degradation product by Yim *et al*. This was attributed to Psillakis working at much lower concentrations of phthalates than Yim *et al* and so the monoester products if formed were thought to be below the detection limits of the GC-MS system used.

2.7: Aims and goals

Based on the previous work carried out on the degradation of phthalate esters there were several aims for this work

1. The main aim was to establish the degradation products for the sonolysis of phthalate esters.Previous work had not carried out a sufficient examination of the degradation process. In the case of Yim *et al* this was due to his instrumentation, HPLC was not specific enough. In the case of Psillakis *et al* the use of the SPME method ultimately got in the way of their carrying out a proper product analysis.

2. Develop a simplistic yet effective analysis method to allow for the quantification of phthalate esters and phthalate degradation products without worry of contamination by phthalate present in the lab environment or by contamination by handling / sample preparation etc.

3. Study whether the sonolysis products change as a result of changing the conditions of the sonolysis e.g. dissolved gas content.

4. Expand the selection of phthalate esters which had been studied since only short chain phthalates had been studied to date.

5. Study other factors affecting phthalate kinetics which had not yet been studied.

6. Study the effect of phthalate ester addition on sonoluminesce quenching

2.8: Chapter References

1. P. N. T. Wells, in *Biomedical Ultrasonics*, Academic Press, London, 1977, p. 14 and 136.
2. T.G.Leighton, in *The Acoustic Bubble*, Academic Press, London, 1997, p. 28.
3. A. Wood, in *Acoustics*, Blackie, London, 1960 reissue, p. p124.
4. F. Caupin and E. Herbert, *Comptes Rendus Physique*, 2006, **7**, 1000-1017.
5. Haissins.M and R. Klein, *Journal De Chimie Physique Et De Physico-Chimie Biologique*, 1968, **65**, 336-&.
6. I. Gultekin and N. H. Ince, *J Environ Manage*, 2007, **85**, 816-832.
7. S. A. P. a. M. Williams, in *Advanced Oxidation Processes for Water and Wastewater Treatment*, IWA Publishing, London, 2004, pp. 1-6.
8. T. K. Lau, W. Chu and N. Graham, *Chemosphere*, 2005, **60**, 1045-1053.
9. R. A. Torres, C. Petrier, E. Combet, F. Moulet and C. Pulgarin, *Environmental Science & Technology*, 2007, **41**, 297-302.
10. J. Madhavan, P. S. Kumar, S. Anandan, M. Zhou, F. Grieser and M. Ashokkumar, *Chemosphere*, 2010, **80**, 747-752.
11. R. Kidak and N. H. Ince, *Ultrasonics Sonochemistry*, 2006, **13**, 195-199.
12. G. Wen, J. Ma, Z.-Q. Liu and L. Zhao, *Journal of Hazardous Materials*, 2011, **195**, 371-377.
13. L. K. Weavers, N. Malmstadt and M. R. Hoffmann, *Environmental Science & Technology*, 2000, **34**, 1280-1285.
14. K. Ayoub, E. D. van Hullebusch, M. Cassir and A. Bermond, *Journal of Hazardous Materials*, 2010, **178**, 10-28.
15. I. Wojtenko, M. K. Stinson and R. Field, *Critical Reviews in Environmental Science and Technology*, 2001, **31**, 295-309.
16. Q. Hong, J. L. Hardcastle, R. A. J. McKeown, F. Marken and R. G. Compton, *New Journal of Chemistry*, 1999, **23**, 845-849.
17. N. L. Stock, J. Peller, K. Vinodgopal and P. V. Kamat, *Environmental Science & Technology*, 2000, **34**, 1747-1750.
18. H. Destaillats, A. J. Colussi, J. M. Joseph and M. R. Hoffmann, *Journal of Physical Chemistry A*, 2000, **104**, 8930-8935.
19. M. E. Abdelsalam and P. R. Birkin, *Physical Chemistry Chemical Physics*, 2002, **4**, 5340-5345.
20. D. Voncina, *Dyes and Pigments*, 2003, **59**, 173-179.
21. Y. Suzuki, Warsito, A. Maezawa and S. Uchida, *Chemical Engineering & Technology*, 1999, **22**, 507-510.
22. K. Vinodgopal, M. Ashokkumar and F. Grieser, *Journal of Physical Chemistry B*, 2001, **105**, 3338-3342.
23. B. Yim, H. Okuno, Y. Nagata, R. Nishimura and Y. Maeda, *Ultrasonics Sonochemistry*, 2002, **9**, 209-213.
24. E. Manousaki, E. Psillakis, N. Kalogerakis and D. Mantzavinos, *Water Res*, 2004, **38**, 3751-3759.
25. E. Psillakis, *Analytica Chimica Acta*, 2004, **501**, 3-10.
26. D. Chen, Z. Q. He, L. K. Weavers, Y. P. Chin, H. W. Walker and P. G. Hatcher, *Research on Chemical Intermediates*, 2004, **30**, 735-753.
27. F. J. Stevenson, in *Humus Chemistry. Genesis, Compositions, Reactions*, Wiley, New York, NY, USA, 1994, p. 212.
28. H. Shemer and N. Narkis, *Ultrason Sonochem*, 2005, **12**, 495-499.
29. A. Kotronarou, G. Mills and M. R. Hoffmann, *Environmental Science & Technology*, 1992, **26**, 1460-1462.
30. J. J. Yao, N. Y. Gao, C. Li, L. Li and B. Xu, *J Hazard Mater*, 2010, **175**, 138-145.

31. J. J. Yao, N. Y. Gao, Y. Deng, Y. Ma, H. J. Li, B. Xu and L. Li, *Ultrason Sonochem*, 2010, **17**, 802-809.
32. A. K. Shriwas and P. R. Gogate, *Separation and Purification Technology*, 2011, **79**, 1-7.
33. G. J. Price, M. Ashokkumar, T. D. Cowan and F. Grieser, *Chemical Communications*, 2002, 1740-1741.
34. J. Wang, T. Ma, Z. Zhang, X. Zhang, Y. Jiang, D. Dong, P. Zhang and Y. Li, *J Hazard Mater*, 2006, **137**, 972-980.
35. , 2011, vol. 2011.
36. A. A. C.S. Giam, J.M. Powers, A. Leonard, in *Handbook of Environmental Chemistry*, ed. O. Hutzinger, Spinger-Verlag, New York, 1984.
37. C. A. Staples, D. R. Peterson, T. F. Parkerton and W. J. Adams, *Chemosphere*, 1997, **35**, 667-749.
38. M. M. a. E. Pfeiffer, in *Endocrine Disruptors Part 1*, ed. M. Metzler, Springer, Germany, 2001, pp. 63-80.
39. M. Thomsen, L. Carlsen and S. Hvidt, *Environmental Toxicology and Chemistry*, 2001, **20**, 127-132.
40. D. R. P. C.A. Staples, T.F. Parkerton, W.J. Adams, *Chemosphere*, 1997, **35**, 667-749.
41. J. J. Ellington, *Journal of Chemical and Engineering Data*, 1999, **44**, 1414-1418.
42. D. A. Hinckley, T. F. Bidleman, W. T. Foreman and J. R. Tuschall, *Journal of Chemical and Engineering Data*, 1990, **35**, 232-237.
43. D. J. Letinski, M. J. Connelly, D. R. Peterson and T. F. Parkerton, *Chemosphere*, 2002, **48**, 257-265.
44. W. J. Frissell, *Industrial and Engineering Chemistry*, 1956, **48**, 1096-1099.
45. C. Nilsson, *Swedish National Chemcials Inspectorate, Solna*, 1994.
46. G. H. Tan, *Bulletin of Environmental Contamination and Toxicology*, 1995, **54**, 171-176.
47. O. S. Fatoki and F. Vernon, *Science of the Total Environment*, 1990, **95**, 227-232.
48. M. Vitali, M. Guidotti, G. Macilenti and C. Cremisini, *Environment International*, 1997, **23**, 337-347.
49. A. Thuren, *Bulletin of Environmental Contamination and Toxicology*, 1986, **36**, 33-40.
50. G. A. Loraine and M. E. Pettigrove, *Environmental Science & Technology*, 2006, **40**, 687-695.
51. Y. Q. Wang, W. Hu, Z. H. Cao, X. Q. Fu and T. Zhu, *Analytical and Bioanalytical Chemistry*, 2005, **383**, 857-863.
52. D. Amiridou and D. Voutsa, *J Hazard Mater*, 2011, **185**, 281-286.
53. P. H. Howard, in *Handbook of Environmental degradation rates*, Lewis Publishers Inc., Chelsea, MI, 1991, p. p725.
54. H. O. Sanders, F. L. Mayer and D. F. Walsh, *Environmental Research*, 1973, **6**, 84-90.
55. B. L. Boese, *Canadian Journal of Fisheries and Aquatic Sciences*, 1984, **41**, 1713-1718.
56. G. T. C. K.H. Carr, R.A. Kimerle, in *13th annual Society of Environmental Toxicology and Chemistry Meeting*, Seattle, Washington, USA, 1992.
57. C. W. Park, H. Imamura and T. Yoshida, *Journal of the Korean Fisheries Society*, 1990, **22**, 424-428.
58. R. Kavlock, K. Boekelheide, R. Chapin, M. Cunningham, E. Faustman, P. Foster, M. Golub, R. Henderson, I. Hinberg, R. Little, J. Seed, K. Shea, S. Tabacova, R. Tyl, P. Williams and T. Zacharewski, *Reproductive Toxicology*, 2002, **16**, 529-653.
59. R. Kavlock, K. Boekelheide, R. Chapin, M. Cunningham, E. Faustman, P. Foster, M. Golub, R. Henderson, I. Hinberg, R. Little, J. Seed, K. Shea, S. Tabacova, R. Tyl, P. Williams and T. Zacharewski, *Reproductive Toxicology*, 2002, **16**, 489-527.
60. R. Kavlock, K. Boekelheide, R. Chapin, M. Cunningham, E. Faustman, P. Foster, M. Golub, R. Henderson, I. Hinberg, R. Little, J. Seed, K. Shea, S. Tabacova, R. Tyl, P. Williams and T. Zacharewski, *Reproductive Toxicology*, 2002, **16**, 453-487.

61. R. Kavlock, K. Boekelheide, R. Chapin, M. Cunningham, E. Fuastman, P. Foster, M. Golub, R. Henderson, I. Hinberg, R. Little, J. Seed, K. Shea, S. Tabacova, R. Tyl, P. Williams and T. Zacharewski, *Reproductive Toxicology*, 2002, **16**, 655-678.
62. L.-P. Huang, C.-C. Lee, P.-C. Hsu and T.-S. Shih, *Fertility and Sterility*, 2011, **96**, 90-94.
63. S. Villeneuve, D. Cyr, E. Lynge, L. Orsi, S. Sabroe, F. Merletti, G. Gorini, M. Morales-Suarez-Varela, W. Ahrens, C. Baumgardt-Elms, L. Kaerlev, M. Eriksson, L. Hardell, J. Fevotte and P. Guenel, *Occupational and Environmental Medicine*, 2010, **67**, 837-844.
64. J. D. Meeker and K. K. Ferguson, *Environmental Health Perspectives*, 2011, **119**, 1396-1402.
65. K. Svensson, R. U. Hernandez-Ramirez, A. Burguete-Garcia, M. E. Cebrian, A. M. Calafat, L. L. Needham, L. Claudio and L. Lopez-Carrillo, *Environmental Research*, 2011, **111**, 792-796.
66. B. A. Neel and R. M. Sargis, *Diabetes*, 2011, **60**, 1838-1848.
67. I. P. o. C. Safety, *Environmenal Health Criteria 189 di-n-butyl phthalate*, World Health Organisiation, Geneva, 1997.
68. J. Mes and D. S. Campbell, *Bulletin of Environmental Contamination and Toxicology*, 1976, **16**, 53-60.
69. B. Yim, Y. Nagata and Y. Maeda, *Journal of Physical Chemistry A*, 2002, **106**, 104-107.
70. E. Psillakis, D. Mantzavinos and N. Kalogerakis, *Chemosphere*, 2004, **54**, 849-857.
71. H. Lord and J. Pawliszyn, *Journal of Chromatography A*, 2000, **902**, 17-63.
72. Y. C. Chen and P. Smirniotis, *Industrial & Engineering Chemistry Research*, 2002, **41**, 5958-5965.

Chapter 3: Experimental

3.1: Ultrasonic Equipment

3.1.1: 20 kHz system

All sonication experiments performed at 20 kHz used a Sonic Systems L500-20 system. This unit runs at a nominal frequency of 20 kHz and is capable of delivering up to 500 W of power. The operating frequency and the power delivered from the generator are readable from a digital display and an analogue needle dial respectively.

The generator was connected to a typical ultrasonic horn. This was composed of 3 increasingly wider sections and ended in the head which housed the transducer for converting the output of the generator. The 3 horn sections measured 72 mm (length) x 12 mm (width), 40 mm x 29 mm and 63 mm x 36 mm. The housing for the transducer measured 128 mm x 65 mm. The radiating surface area of the horn tip was 1.1cm^2. A photo of the setup used for all degradations apart from gas phase product examination experiments is shown below in figure 3.1.

Figure 3.1: Photo of the setup typically used for degradation studies at 20 kHz.

The reactor was a glass pear shaped vessel with an external water jacket for cooling purposes. The reactor has 4 necks, 3 B19 “Quickfit”® joints arranged in an evenly spaced triad around a larger central neck measuring 40 mm across with a length of 104 mm. This neck was used to introduce the ultrasonic horn into the reactor. The neck had 2 grooves up its length designed to hold o-rings to form air tight seals between the reactor and the horn. In practice only the lower groove housed an O-ring. The reactor was capable of holding a volume of liquid up to 220 cm^3.

One of the three joints was plugged with a “Subaseal”® rubber joint and used to introduce appropriate gases into the reactor via a stainless steel needle. A second needle in the seal provided an outlet for gas flow. The other two joints were plugged with non-greased ground glass stoppers, one of which was fixed with a joint clip while the other was unclipped to prevent excess gas pressure build up. This neck was used for collection of samples from the reactor. Cooling water was introduced from the underside of the reactor via a grooved port and

flowed out of the jacket at the base of the reactor neck through a similar port. The width of the jacket was typically 6 mm, although this varied slightly around the reactor. The internal base of the reactor had a convex shaping to enhance reflection of sound waves.

The O-rings used were made from black Viton® rubber with an external diameter of 34.52 mm and a ring thickness of 3.53 mm (British Standard size BS220V75).

When inserting the horn into the reactor, the O-ring was first slid onto the horn so that it was in line with the horizon of the horn tip. The horn was then inserted into the neck of the reactor until the head of the horn made flat contact with the top of the reactor neck. The width of the horn and O-ring was sufficient to form an air and water tight seal between the horn and the reactor neck. The horn and reactor were then affixed with clamps so that the horn tip was straight and in line with the reflector at the reactor base. The cooling water used was ring mains water and had a temperature of 21 ± 2°C throughout all experiments.

3.1.2: 515 kHz System

All sonication experiments performed at 515 kHz used an Undatim UL03/1reactor. This generator has two switchable modes which can deliver a maximum power output of 25 W and 100 W. The power delivered was controlled by a rotary dial, and the power outputted by the generator was readable on an analogue needle gauge.

The generator connected to a separate cylindrical stainless steel transducer embedded in PTFE. The radio frequency input and also an air input for cooling of the transducer were located at the base of the transducer unit. The diameter of the metal transducer was 50 mm and the total diameter of the unit was 95 mm. It was possible to clip a range of premade and custom reactors on top of the transducer using four clamps arranged around the edge of the transducer unit. An O-ring of diameter 83 mm and thickness 2 mm sat in a groove around the transducer and formed a water tight seal between the transducer unit and the reactor when the reactor was tightened in place.

In the course of this work two reactors were used. Most commonly for single frequency work a jacketed kettle-shaped Pyrex vessel was used. For dual frequency work an open Pyrex® cylindrical reactor was used.

Figure 3.2: Photo of 515 kHz setup

The custom kettle-like reactor had a height of 99 mm and a width of 78 mm. The lip on the base of the reactor which was used to clamp the reactor onto the transducer unit had a diameter of 91 mm and a thickness of 5 mm. The jacket of the reactor was approximately 7 mm thick around the reactor. The reactor was capable of holding up to 250cm^3 of water. Two B19 Quickfit® joints were affixed to the top of the reactor. One was stoppered with an ungreased ground glass joint which the other was sealed with a rubber Subaseal®. Gas was introduced where necessary through the Subaseal® using a stainless steel needle with a second needle inserted to allow gas flow out of the reactor. Cooling water was introduced into the jacket from the lower left side of the reactor and exited from the top right side via two grooved ports. The air flow to cool the inside of the transducer was pumped using an Aqua Air Mini by Interpret.

The cylindrical reactor had a total height of 125 mm, an internal diameter of 70 mm and a thickness of 4 mm. The lip on the base used to attach the reactor to the transducer had a diameter of 93 mm and a thickness of 4 mm. The attached reactor had a maximum capacity of 466 cm^3. This reactor was unjacketed.

3.1.3: Dosimetry of the ultrasonic systems

Various methods and techniques have been created by scientists studying ultrasound to quantify operational aspects of ultrasonic systems. In this work the ultrasonic power was measured by standard calorimetry, the oxidative power of the system was quantified using Fricke dosimetry and the hydroxyl radical (•OH) production rate using the terephthalic acid dosimeter. The methodologies employed for these are described below along with calibration data.

3.1.3.1: Calibration of Ultrasonic Intensity

Both of the generators used had power setting dials with arbitrary values. This made it necessary to measure the ultrasonic power transmitted into the system for each power setting employed in the study. This was easily done by measuring the temperature increase over time of a known volume of liquid of known and/or measurable specific heat capacity, in this case water.

This technique is also necessary since the power which is delivered from the generator, although easily readable, is not the same as the ultrasonic power transmitted from the tip of the horn. This in turn may also not be the same as the energy actually absorbed by the system due to conversion into other energy forms and losses due to impedance and attenuation of the sound wave.

Calculating the specific heat capacity of distilled water

It was first necessary to accurately calculate the specific heat capacity of the water used. To do this 100 mL of distilled water was placed in a flask and stirred using a magnetic stirrer and flea. A resistor with resistance of 90 Ω connected to a Thandar TS3021S power supply with adjustable voltage was immersed in the water. The voltage was set to the desired value and the temperature of the water was measured using a Digitron thermocouple every 30 seconds for 5 minutes. The experiment was performed 3 times for three different voltage settings.

The data obtained is shown below in Table 3.1.

Voltage = 6 V		Voltage = 9 V		Voltage = 12 V	
Time / s	**Water Temperature / °C**	**Time / s**	**Water Temperature / °C**	**Time / s**	**Water Temperature / °C**
0	16.4	0	16.9	0	17.7
30	16.4	30	17.0	30	17.8
60	16.5	60	17.0	60	18.0
90	16.5	90	17.1	90	18.1
120	16.5	120	17.2	120	18.2
150	16.6	150	17.2	150	18.3
180	16.6	180	17.3	180	18.4
210	16.6	210	17.4	210	18.5
240	16.7	240	17.4	240	18.6
270	16.7	270	17.5	270	18.6
300	16.7	300	17.5	300	18.7
ΔT / °C	0.3	**ΔT / °C**	0.6	**ΔT / °C**	1.0

Table 3.1: Data used to calculate the heat capacity of water

The energy delivered by the generator was calculated from the current (I), voltage (V) and time of delivery (t) using equation 3.1 below.

$$"E = IVt" \tag{3.1}$$

Therefore, the energy inputted in the above experiments were 119 J at 6 V, 262 J at 9 V and 457 J at the 12 V setting.

The specific heat capacity was calculated from the energy calculated above (E) and the measured temperature rise (ΔT) using equation 3.2

$$"C = E/\Delta T" \tag{3.2}$$

Therefore, the calculated specific heat capacities of water are 396.67 J K^{-1} at 6 V, 436.67 J K^{-1} at 9 V and 457.00 J K^{-1} at 12 V setting. An averaged specific heat capacity of water of 430.1 J K^{-1} or 4.301 J $g^{-1}K^{-1}$ was then obtained.

The quantifiable errors in measuring the heat capacity of water were the temperature measurements using the stopwatch and the temperature measurements using the thermocouple.

Since the timer was readable in seconds the error in measuring the time of experiment was ±0.5 seconds. This gives an uncertainty of

$$\sqrt{(0.5)^2 + (0.5)^2}$$

= 0.7070 s.

Since the thermocouple reads to 1 decimal place the error in measuring the temperature was ±0.05 °C. This gives an uncertainty of

$$\sqrt{(0.05)^2 + (0.05)^2}$$

= 0.0707°C.

The uncertainty in the specific heat capacity value above is therefore:

$$430.1\sqrt{\left(\frac{0.707}{300}\right)^2 + \left(\frac{0.0707}{0.63}\right)^2}$$

= 48.27JK^{-1}

Therefore the calculated specific heat capacity is 430.1 ± 48.3 J K^{-1}
or 4.301 ± 0.48 J g^{-1} K^{-1}.

Calibration of generator power scales

To measure the ultrasonic power dissipated into solution at a given power setting on both generators the following was carried out. 100 mL of water was placed into the appropriate reactor using a volumetric pipette. The temperature of the water was measured using the same thermocouple. The probe was inserted one inch below the surface of the water and always in the same location in the reactor. The generator was then switched on. The initial temperature of the water was read and a digital stop watch was then set counting down 5 minutes. After the stopwatch was started, the generator was

set to the desired setting and the water temperature read every 30 seconds. Each power setting was measured 3 times.

The data obtained for both the Sonic Systems 20 kHz system and the Undatim 515 kHz system (at both 25W and 100W settings) with the ultrasonic intensities derived from the data are summarised below in tables 3.2, 3.3 and 3.4. Where temperature differences are quoted they are averages of 3 repeats. The ultrasonic power transmitted during an experiment was calculated using equation 3.3

$$"q = m.\Delta T.C" \quad (3.3)$$

where q is the power dissipated into the system and m is the mass of water used in the experiment. The ultrasonic intensity was calculated by dividing the ultrasonic power calculated previously by the area of the radiating surface. These areas were 1.567 cm^{-2} for the Sonic Systems horn tip and 18.1 cm^{-2} for the Undatim transducer.

	Arbitary power setting shown on generator			
	2	4	6	8
ΔT / °C	2.90	5.40	7.30	9.60
Power (W)	4.04	7.53	10.22	13.34
Intensity (W cm^{-2})	2.58	6.84	9.30	12.13

Table 3.2: Calibration of the power scale of the Sonic Sytems 20 kHz generator.

	Arbitary power setting shown on generator				
	2	4	6	8	10
ΔT / °C	16.2	20.3	26.8	32.9	34.3
Power (W)	22.63	28.35	37.36	45.87	47.87
Intensity (W cm^{-2})	1.25	1.56	2.06	2.53	2.64

Table 2.3: Calibration of the power scale of the Undatim 515 kHz generator (100W setting).

	Arbitary power setting shown on generator				
	2	4	6	8	10
ΔT / °C	1.2	3.0	5.8	9.2	14.8
Power (W)	1.67	4.18	8.09	12.83	20.64
Intensity (W cm^{-2})	0.09	0.23	0.45	0.71	1.14

Table 3.4: Calibration of the power scale of the Undatim 515 kHz generator (25W setting).

These data are presented graphically in figures 3.3a-c. The power outputs are described in Watts.The error bars represent the error from three results for each data point (n=3). Figure 3.3b has been curtailed since the power output from the generator fell away from linearity at power setting 10 (the highest setting on the generator). Therefore, only the linear portion is described in figure 3.3b and it was decided not to use power setting 10 on the 515 kHz system. Similarly it can be seen from figure 3c that the relationship between the dial setting and the ultrasonic power was not linear (gave a good fit to an exponential function, as shown) at the 25 W setting on the 515 kHz system. It was decided therefore to avoid this setting for degradation work.

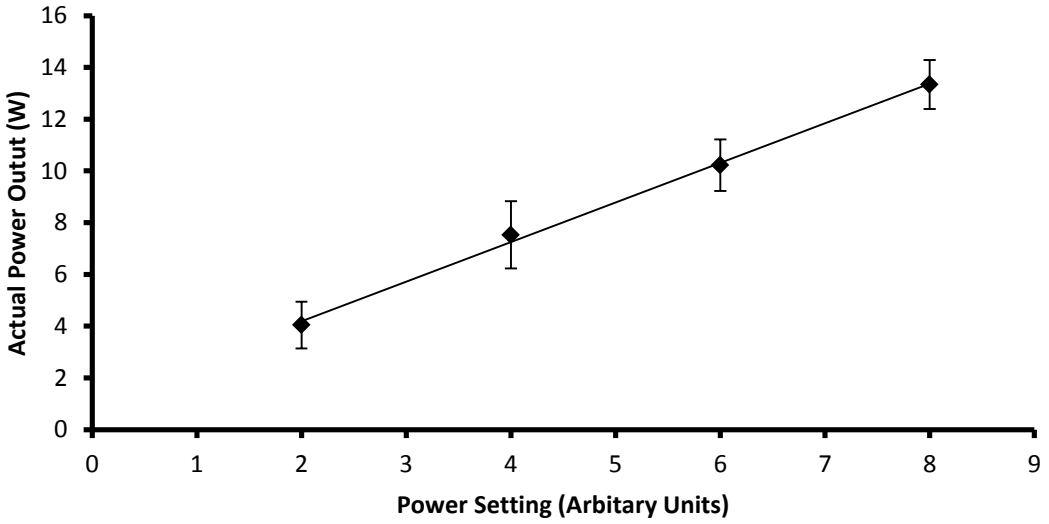

Figure 3.3a: Calibration data for 20 kHz horn (n=3)

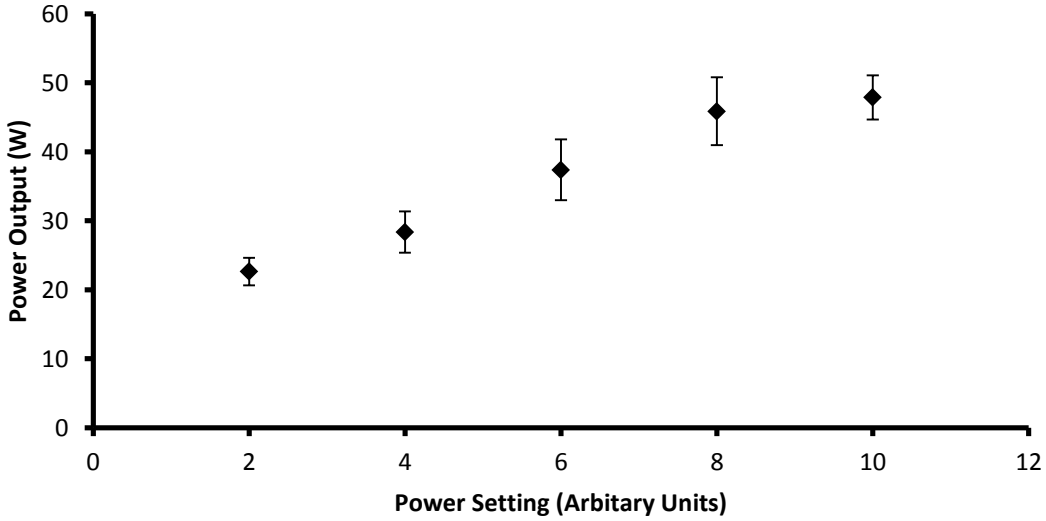

Figure 3.3b: Calibration data for 515 kHz transducer (100 W setting) (n=3).

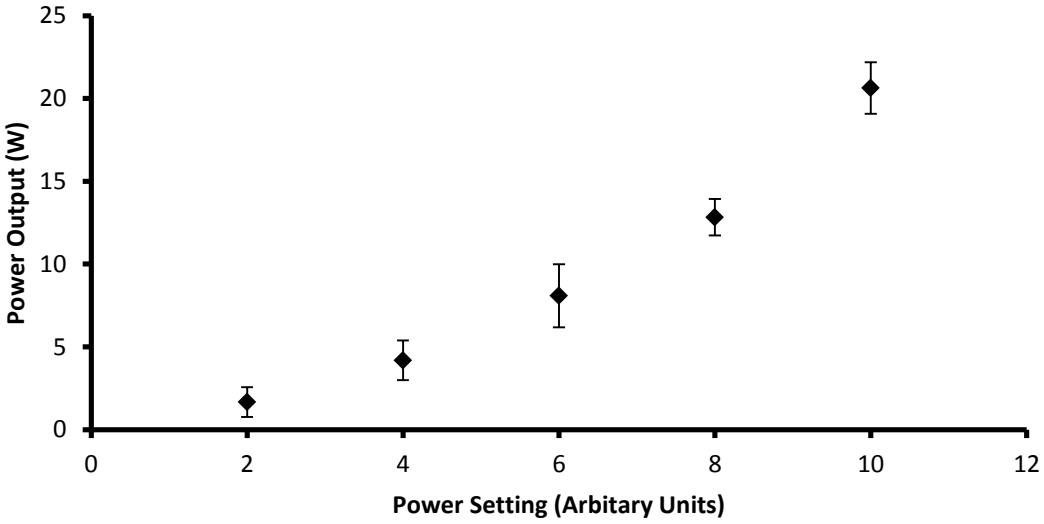

Figure 3.3c: Calibration data for the 515 kHz transducer (25 W setting) (n=3).

3.1.3.2: Calibration of the oxidative power

The oxidative power of both systems was measured using the Fricke dosimeter. This dosimeter utilises the oxidation of Fe^{2+} to Fe^{3+} by various oxidising species (such as hydroxyl radicals and hydrogen peroxide) produced by the sonolysis of water to enable comparison of the total oxidative power of ultrasonic systems. For the chemistry to be stable and reliable acid has to be added. This is illustrated in scheme 3.1.

$$\cdot OH + Fe^{2+} + H^{+} \rightarrow H_2O + Fe^{3+}$$

$$H_2O_2 + Fe^{2+} + H^{+} \rightarrow H_2O + Fe^{3+} + \cdot OH$$

Scheme 3.1: The reactions that make up the Fricke dosimeter.

The Fe^{3+} ions formed are easily quantifiable using a UV-Vis spectrophotometer. In this study an Agilent 8453 spectrophotometer fitted with mercury and tungsten lamps was used.

Calibration of the spectrophotometer response to Fe^{3+} ions.

The Fe^{3+} ion has a UV response with a maximum at 305 nm. To calculate the extinction coefficient and therefore the relationship between UV response and Fe^{3+} ion concentration the following method was used.

In 100 mL of distilled water was dissolved $FeCl_3.6H_2O$ (27.4 mg, 1.014 mmol). A dilution series of this solution was prepared ranging between 0.005 mmol and 1 mmol of Fe^{3+} ions. The UV blank was distilled water. To measure the UV spectrum of a given sample, a quartz cell was filled with the solution to be analysed. The solution filled cell was then analysed in the spectrophotometer. The peak maximum height @ 305 nm was thus obtained. The data obtained is presented in table 3.5 and a graph of this data in figure 3.4.

[Fe^{3+}] / milimoles	**UV response @ 305 nm / Arbitrary units**
1.000	1.8468
0.750	1.3827
0.500	0.9066
0.250	0.4633
0.100	0.1948
0.050	0.1175
0.010	0.0236
0.005	0.0164
0.000 (blank)	0.0003

Table 3.5: Data for calibration of the UV spectrophotometer.

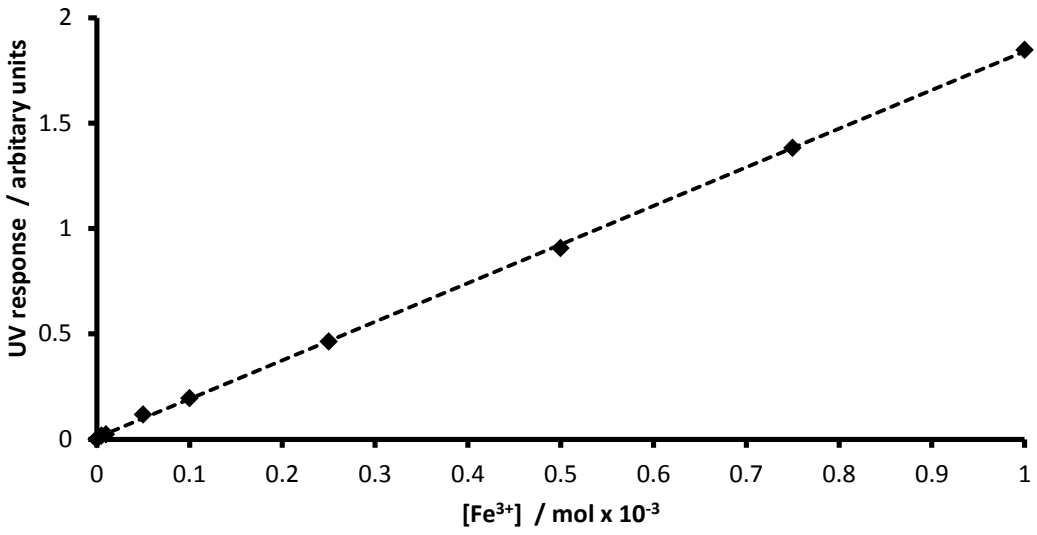

Figure 3.4: Calibration curve used to calculate the extinction coefficient of $FeCl_3.6H_2O$

Using this data the extinction coefficient was calculated using equation 3.4, the Beer-Lambert law

$$"A = \varepsilon cl" \tag{3.4}$$

where A is the UV absorbance, ε is the molar extinction coefficient, c is the sample concentration (in mol L^{-1}) and l is the path length (in cm). Using the above data and the fact that path length equalled the cell thickness (1 cm) the molar extinction coefficient of Fe^{3+} was calculated to be 1831 ± 42 L mol^{-1} cm^{-1}.

Fricke dosimetry of ultrasonic systems.

To perform Fricke dosimetry on both the 20 kHz horn and the 515 kHz transducer employed, $FeSO_4.7H_2O$ (139 mg, 1 mmol) and H_2SO_4 (245 mg, 5 mmol) were dissolved in 500 mL distilled water. A solution consisting of H_2SO_4 (245 mg, 5 mmol) in distilled water was used for the UV blank. In all experiments 100 mL of the Fe^{2+} containing solution was placed in the appropriate reactor and the appropriate power set on the generator. All sonications were performed in air with cooling water flowing. The solution was

sampled every 15 minutes for 1 hour for UV analysis. A quartz UV cell was filled with the solution sample by direct pipetting from the reactor. A UV spectrum obtained for the sample and the peak height maximum at 305 nm obtained. Using the calibration graph above this could be converted to [Fe^{3+}].

Figure 3.5a shows the relationship between the ultrasonic intensity employed and the k(Fe^{3+}), the rate of production of Fe^{3+} ions in the 20 kHz system and 3.5b shows the same for the 515 kHz system. The error bars represent errors calculated from triplicate measurements for each point.

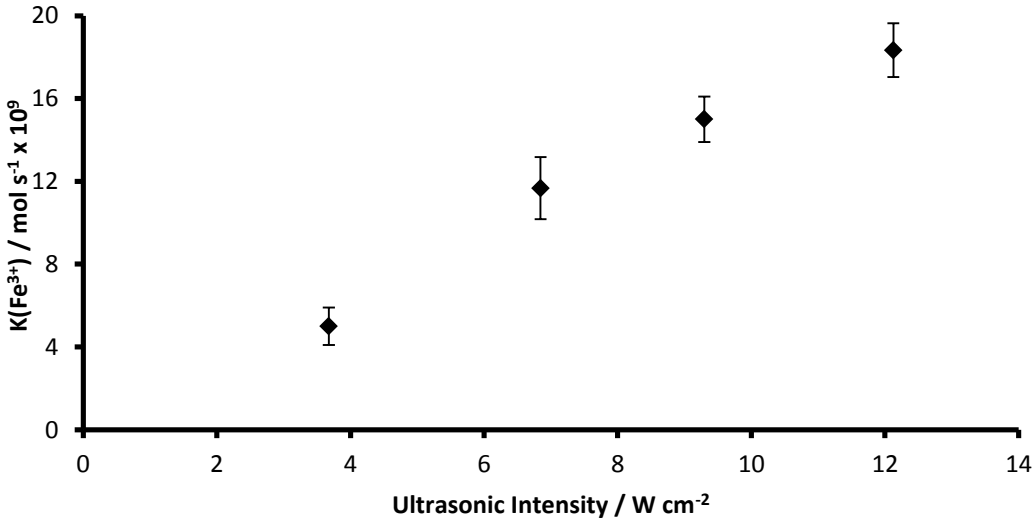

Figure 3.5a: Rate of production of Fe^{3+} ions at differing intensities for 20 kHz horn (n=3).

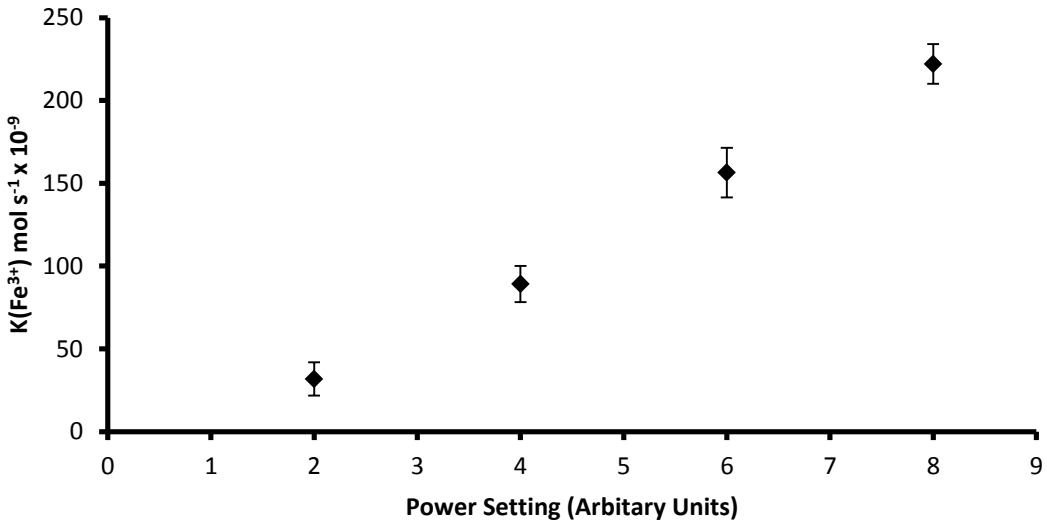

Figure 3.5b: Rate of production of Fe^{3+} ions at differing intensities for 515 kHz reactor (n=3).

3.1.3.3: Calibration of the production of hydroxyl radicals

The rate of production of hydroxyl radicals produced through the sonolysis of water was measured using the terephthalate dosimeter. The dosimeter works by trapping the hydroxyl radicals produced with terephthalic acid forming hydroxyterephthalic acid which is strongly fluorescent. This fluorescence was measured using a Jenway 6200 fluorimeter using an excitation wavelength of 315 nm and an emission filter of 425 nm. These values correspond to the wavelengths of light that excite HTA and that which it emits.

Synthesis of hydroxyterephthalic acid

To calibrate the fluorescence response produced it was necessary to synthesise and purify a sample of hydroxyterephthalic acid as it was not commercially available at the time of this work being conducted (this has recently changed however). The method of Field[1] was followed.

Using a solution of NaOH, 2-bromoterephthalic acid (1.3 g, 4.5 mmol) was neutralised to form the disodium salt of the acid. To this was added water (20 mL) sodium acetate (0.81 g, 10 mmol), copper powder (6 mg) and 3 drops of phenolphthalein solution (acid indicator). The resulting suspension was heated to reflux for 10 hours overnight. The reaction slowly increased the acidity of the solution as shown by the indicator turning the liquid phase a pink colour. When

the solution turned slightly pink, 5% (W/V) KOH solution was added until the solution lost its pink hue.

After 10 hours the suspension was filtered. The solution was then stirred vigorously while a 10% (W/V) solution of HCl was added in a drop wise fashion. This resulted in a creamy precipitate forming. Acid was added until no further precipitate formed, after which the solution was filtered. The resulting liquor had further HCl solution added drop wise to ensure no further precipitation occurred. The solids were washed with water and then smeared onto a watch glass and dried at 100°C in an oven for 24 hours. This resulted in 1.2 g of crude HTA as beige solids. The product was confirmed using ^{1}H NMR only since ^{13}C gave poor spectra even when using 50 mg of HTA.

Hydroxyterephthalic acid

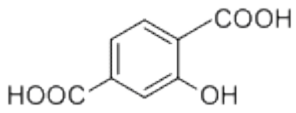

NMR: ^{1}H (D_2O/NaOH, 300 MHz): 7.509 (H, d, ArH), 7.081 (2H, d, ArH)

Purification of HTA

It was necessary to purify the crude HTA produced before its use. To do this the crude HTA (1.2 g) was dissolved in H_2O adjusted to pH 8 with sodium acetate. This was vigorously stirred while a 1% (W/V) solution of HCl was added drop-wise to the HTA solution. As soon as a precipitate formed this was filtered, washed with additional water and dried for 24 hours at 100°C. Further acid was then added to the remaining liquor until the next precipitate formed. This process was repeated to yield 6 crops of purified HTA as an off white solid (total mass of 705 mg). Each crop was analysed using ^{1}H NMR. Some crops gave rise to poor quality spectra where the doublets detailed above were poorly resolved. These crops were discarded. The crops which resulted in spectra showing the coupling details were then used for making a HTA solution for fluorimeter calibration (total mass HTA= 353 mg).

Preparation of HTA solution for fluorimeter calibration

In one litre of distilled water was dissolved HTA (353 mg, 1.95 mmol), NaOH (200 mg, 5 mmol) and 25 mL of pH buffer. The suspension was stirred for 16 hours until fully dissolved. The solution must be alkaline for the HTA to dissolve in water and this concentration had been found by Lenz *et al* to be the optimum concentration for work on terephthalate dosimetry[2].

Calibration of Fluorimeter

The freshly prepared HTA solution was then used to fill a plastic cuvette and the fluorescence measured. The HTA solution prepared above gave a fluorescence above that measureable by the fluorimeter used. It was found that HTA solution diluted with water 25 times to yield a 0.08 mmol solution gave an intensity of fluorescence within measurable limits.

A dilution series of this solution was then analysed by measuring the fluorescence of each dilution in a clear plastic cuvette (path length 1 cm). The same cuvette was used for each measurement and was washed several times with distilled water before being used for the next sample.

A graph showing the results of this calibration is shown in figure 3.6.

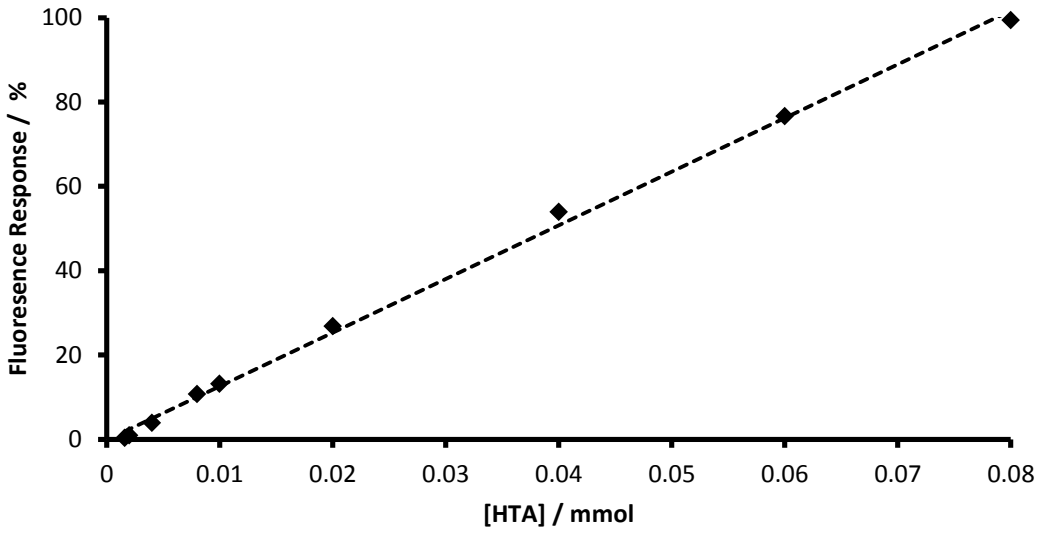

Figure 3.6: Calibration of measured fluorescence to HTA concentration

Terephthalate dosimetry

In 1L of distilled water was dissolved terephthalic acid (330 mg, 2 mmol), NaOH (200 mg, 5 mmol) and 25 mL of pH 7 buffer. This suspension was stirred for 16 hours until fully dissolved.

100 mL of this solution was placed in the appropriate reactor and sonicated for 30 minutes. Samples were taken every 5 minutes for fluorescence analysis in a plastic cuvette and replaced after measurement. The dosimetry was performed for both the 20 kHz system and the 515 kHz system (100 W setting only). In the case of the 515 kHz system the jacketed kettle-like reactor was used.

The results of this are shown in figures 3.7a and 3.7b. The y-axis shows the rate of hydroxyl radical production, k(•OH) calculated from the fluorescence data by converting the measured fluorescence to [•OH], the concentration of hydroxyl radicals, using equation 3.5, derived from figure 3.6.

$$[\bullet OH] = ((f + 0.1797)) \,/\, 1273.1 \qquad (3.5)$$

where f is the measured fluorescence. The gradients of the plots of [•OH] against time gives k[•OH] as a zero order rate constant with dimensions mmol L^{-1} min^{-1}.

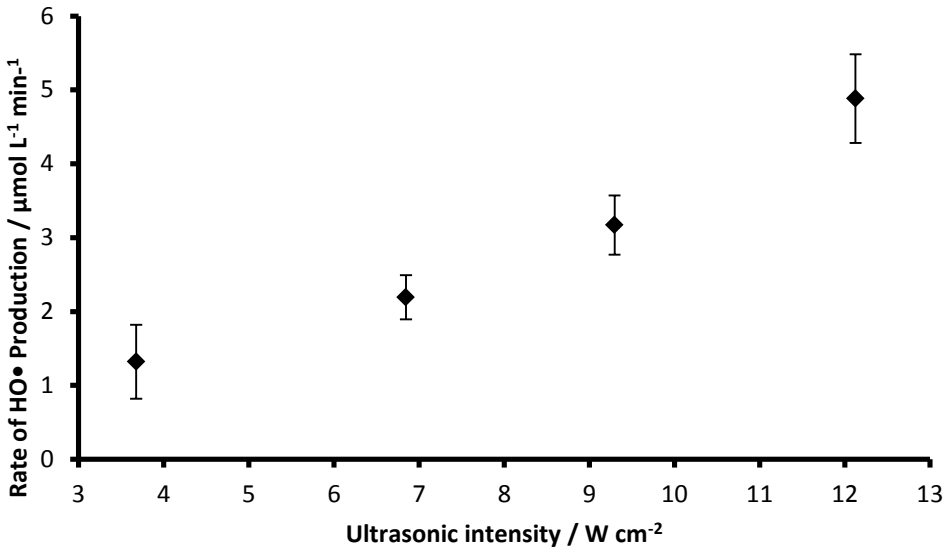

Figure 3.7a: Terephthalate dosimetry of 20 kHz system (n=3).

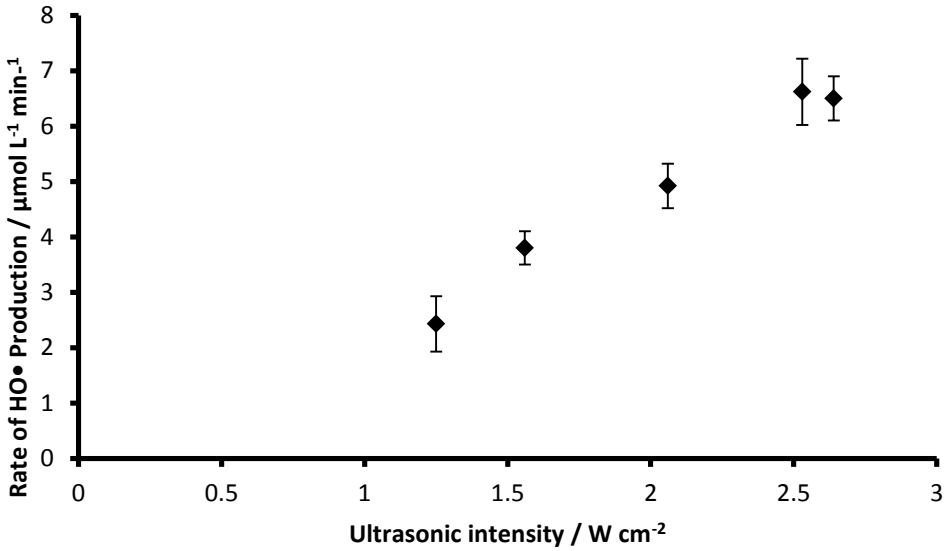

Figure 3.7b: Terephthalate dosimetry of 515 kHz system (n=3).

3.2 Liquid Chromatography - Mass Spectrometry

Below are given the details of the instrumentation used to the acquire mass and chromatography information used to calculate phthalate concentration and investigate phthalate degradation products. Also given are details of the methods used to analyse samples and to quantify phthalate concentrations. For details on how these methods were developed, see section 4.

3.2.1: Instrumentation

All mass spectrometry was performed using a micrOTOF electrospray time of flight (ESI-TOF) mass spectrometer (Bruker Daltonik GmbH, Bremen, Germany). Nitrogen supplied at a pressure of 1 bar was used as the nebulising gas. Nitrogen was also used as the drying gas, supplied at a flow rate of 8 L min^{-1} at a temperature of 200°C. To detect positive ions a capillary voltage of -4000 V was used. For negative ions +4000 V was used. Only full scan data was acquired.

The mass spectrometer above was coupled to an Agilent 1200 LC system (Agilent Technologies, Waldbronn, Germany). The mass spectrometer acted as the detector for the LC system. In each acquisition 10 μL of a 5 mM sodium formate solution was injected before the sample and passed through a bypass loop rather than the LC column. This was used to calibrate the mass scale of the spectrometer between masses of 50 – 700 m/z, using the High Precision Calibration (HPC) algorithm. Data acquisition and automated processing was controlled using Compass OpenAccess 1.2 software (Bruker Daltonik GmbH, Bremen, Germany). Mass and isotope patterns observed from the calibrant perfectly matched those calculated from the expected elemental formula using the DataAnalysis data processing suite (Bruker Daltonik GmbH, Bremen, Germany).

3.2.2: LC Condtions

Since an open access system was used, the working conditions were fixed by the mass spectrometrist and are as follows. The mobile phase employed was water/acetonitrile. This was pumped with a flow rate of 0.4 mL/min during acquisitions. For separations, a Phenomenex lunar 5μ C18 column was used. The dimensions of the column stationary phase were 50 mm x 2 mm. The oven temperature of the LC was set to 25°C.

Two methods were employed with differing lengths. The “Standard LC” method has a LC run time of 11 minutes while the “Long LC” method had a LC runtime of 20 minutes.

The solvent ramp conditions for the “Standard LC” method are shown in table 3.6 and those of the “Long LC” method in table 3.7. Solvent ramps were same in both positive and negative ion modes.

Elapsed time / min	Solvent Composition
0	95% H_2O 5% AcN
7	5% H_2O 95% AcN
8.1	95% H_2O 5% AcN

Table 3.6: Ramp conditions for the “Standard LC” method.

Elapsed time / min	Mobile Phase Composition
0	95% H_2O 5% AcN
7	5% H_2O 95% AcN
18.1	95% H_2O 5% AcN

Table 3.7: Ramp conditions for the “Long LC” Method.

3.2.3: Sample processing

After being removed from the reactor, aqueous samples were aliquoted into either clear LC vials (kinetic measurement experiments) or amber LC vials (product determination experiments), to prevent possible interactions of unknown degradation products with light. Screw tops with a high quality rubber

septum were used. Samples were stored below 10°C until they were analysed. The time between sampling and analysis was kept as short as possible, but data collection had to occur overnight due to limitations from using an open access system. Because of this sonications were typically performed in the afternoon.

Prior to analysis of samples in kinetic measurement experiments, 10 μL of a 1 μg μL^{-1} methanolic solution of thiabendazole was added to each sample to act as an internal standard for phthalate quantification. For product determination experiments no internal standard was added. The sample was then mixed thoroughly for 5 seconds using an IKA “lab dancer” vortex.

For analysis of samples containing the more water soluble phthalates (DMP, DEP, DBP) the “Standard LC” method was used to process the samples. For the less soluble phthalates the “Long LC” method was required.

3.2.4: Quantification of phthalate concentration

Phthalate solutions were prepared using the method in section 3.3.1. Once prepared, a dilution series was made from the base solution. Typically, 6 dilutions were prepared at 0, 20, 40, 60, 80 and 100% of the concentration of the base solution. For each concentration 3 samples were prepared. Once diluted, samples were thoroughly mixed for 5 seconds using an IKA “lab dancer” vortex. 10 μL of a 1 μg μL^{-1} methanolic solution of thiabendazole was then added to each sample, acting as an internal standard for quantification. The samples were then mixed using the vortex a second time for 5 seconds. Samples were then processed on the LC-MS system described above.

The ratio between the internal standard LC-MS trace peak and the phthalate LC-MS trace peak were analysed using the QuantAnalysis quantitative analysis suite (Bruker Daltonik GmbH, Bremen, Germany). This software allowed for the recording of calibration curves of a solution of known concentration and then used the calibration curve produced to calculate the concentration of samples of unknown concentration.

Each time a new phthalate solution was prepared a new calibration curve was produced for the solution, typically this was weekly.

3.3: Methods for kinetic analyses of phthalate degradations.

Below are presented the methods used for making phthalate solutions and details of sonication experiments performed for kinetics studies. These methods are the result of several months of method development work. The work that produced the methods is discussed separately in chapter 4.

3.3.1: Method for preparing aqueous phthalate solutions.

Preparation of methanolic stocks

For a stock used to make aqueous phthalate solutions of 100 μg L^{-1} or less, 10 mg of phthalate was dissolved in 10 mL of methanol in a 10 mL volumetric flask. The flask was inverted 10 times and mixed thoroughly using a Grant Bio PV-1 vortex before being left to stand for 1 hour to allow the phthalate to dissolve and form a homogenous solution. The resulting solutions had a concentration of 1 μg $μL^{-1}$.

For a stock intended to make aqueous phthalate solutions above 100 μg L^{-1}, 1 g of phthalate was dissolved in 10 mL of HPLC grade methanol. The same procedure as above was then followed. This produced a stock with a phthalate loading of 100 μg $μL^{-1}$.

All stock solutions were stored below 10°C and discarded after 2 weeks.

Preparation of aqueous phthalate solutions from a methanolic stock

An appropriate amount of methanolic stock was then dissolved in just under 1L of MiliQ quality water (resistivity 18.2 MΩ), supplied from an Elga Purelab Classic, in a 1L volumetric flask using a 100 μL variable volume automatic pipette (e.g. 100 μL stock to produce a 100 μg L^{-1} solution). After the stock had been added, a cloudy emulsion was formed near the air-water interface for phthalates with solubility less than that of DBP. For DBP and shorter chain

phthalates this emulsion was not seen but a slightly oily character to the water close to the interface could be seen.

The flask was then inverted 10 times to mix the phthalate into the solution. Additional water was then added to make the solution exactly up to 1L as shown by a graduated mark on the flask. The flask was then inverted an additional 10 times. A plastic stirrer bar was added and the solution stirred for 16 hours using a magnetic stirrer. After this time the solution was checked for any visual signs of emulsified phthalate (bubble-like small droplets). If any were found the solution was stirred for another 4 hours and checked again.

After passing a visual check, a 1 mL sample of the solution was taken for LC-MS analysis. This was particularly important for phthalate solutions of 40 $\mu g\ L^{-1}$ or less, since depending on the phthalate employed certain phthalates could not be visualised below this concentration. If the analysis showed a peak with a retention time consistent with the known retention of the phthalate and reasonable Gaussian shape, the solution was accepted, if not the solution reanalysed. If the sample failed the analysis criteria 3 times out of three it was rejected. A solution that failed twice was analysed a 4^{th} time and accepted or failed on analysis of that sample. Solutions accepted on the first analysis were not reanalysed.

Once analysed successfully, the flask was wrapped in tin foil and the solutions stored in the dark below 10°C until needed. Solutions were discarded after 1 week. Solutions were typically prepared just ahead (typically one day) of when they were needed.

3.3.2: General method for phthalate degradations

The below method was used when assessing the kinetics of the sonolysis of individual phthalates in aqueous solution unless otherwise stated.

100 mL of aqueous phthalate solution was placed into the appropriate reactor using a measuring cylinder. Cooling water was flowed through the jacket of the reactor. The solution then was purged with argon for 15 minutes. The argon flow rate was monitored via a silicone oil filled bubbler. While purging the reactor, the flow rate was 10 mL min^{-1}. After 15 minutes the needle used to

introduce gas into the reactor was lifted into the headspace of the reactor and the flow of the argon gas was reduced to a minimal slow flow of 2-5 mL min^{-1}. An initial (t=0) sample from the reactor was taken. The generator was then turned on and set to the appropriate power setting. In the case of 515 kHz degradations the transducer was then tuned to the solution. This meant adjusting the tuning dial on the generator until the disturbance of the solution surface was maximised. This also resulted in the formation of intense visible bubble streamers when done correctly. The solution was sonicated for 3 hours with samples being taken from the reactor every 15 minutes for the first hour and then every half an hour in the 2^{nd} and 3^{rd} hours. The samples were placed in LC vials and then analysed using LC-MS.

After 3 hours, the water and gas flow were turned off and the remaining solution decanted into a screw top glass bottle and stored in the dark at room temperature.

3.3.3: Method for investigating the effect of ultrasonic intensity

As per 3.3.2. Degradations were performed at both 20 kHz and 515 kHz using DBP solutions at two concentrations: 10 mg L^{-1} and 100 μg L^{-1}. The experiments at 20 kHz and 515 kHz ultrasonic frequency were performed separately using different DBP solutions. All experiments were done within a week of the solution being prepared.

3.3.4: Method for investigating the effect of dissolved gas

As per 3.3.2, except single experiments were performed with air, argon, carbon dioxide, nitrogen and oxygen purged solutions. The purge time was kept the same regardless of the gas being dissolved. The study was performed using solutions of DBP with concentrations of 10 mg L^{-1} and 100 μg L^{-1} at both 20 kHz and 515 kHz ultrasonic frequencies. For a given concentration, the same solution was used to investigate each gas at both frequencies .All sonications were performed within a week of the solution being prepared.

3.3.5: Method for investigating the effect of ultrasonic frequency.

As per section 3.3.2. Degradations were performed on DBP solutions with concentration of 100 μg L^{-1} at 20 kHz and 515 kHz ultrasonic frequencies using a range of ultrasonic intensities. A single solution was used to test both 20 kHz and 515 kHz ultrasound to allow for accurate comparison between the effects of two frequencies. All experiments were performed within a week of the solution being prepared.

3.3.6: Method for DBP degradations with additives.

3.3.6.1: Method for DBP degradation in the presence of H_2O_2

100 mL of 100 μg L^{-1} DBP solution had 56 μL of H_2O_2 (5 mmol as calculated by titration) added and the two were mixed by swirling the reactor for 1 minute. The solution was sonicated in air for 3 hours and 990 μL samples were collected for LC-MS analysis periodically.

Once the experiment was over and all samples were collected the samples were heated to 45℃ for 45 minutes to reduce the residual peroxide concentration as it was thought high levels may be damaging to the LC column. Samples were then spiked with 10 μL of 1 mg mL^{-1} of thiabendazole which acted as an internal standard. Samples were then analysed using the LC-MS methodology described above.

3.3.6.2: Method for DBP degradation in the presence of *tert*-butanol

100 mL of 100 μg L^{-1} DBP solution had 143 μL of t-BuOH (1.49 μmol) added and the two were mixed by swirling the reactor for one minute. The solution was then sonicated in air for 3 hours and 990 μL samples were collected for LC-MS analysis periodically. These samples were then spiked with 10μL of 1 mg mL^{-1} of thiabendazole solution which acted as an internal standard. Samples were then analysed using the LC-MS methodology described above.

3.4: Methods for assessments of phthalate degradation products.

3.4.1: Assessment of aqueous phase products from DBP degradation

As per section 3.3.2. LC-MS samples did not have internal standard added to them. Degradations were carried out initially at 10 mg L^{-1} and later at 100 μg L^{-1} to check for any effect of concentration on the sonolysis products. Samples were analysed initially in positive ionisation mode overnight and then in negative ion mode the next night.

3.4.2: Assessment of gas phase products from DBP degradation.

The below method was used to determine gas phase products of DBP degradation using 20 kHz ultrasound.

100 mL of 10 mg L^{-1} DBP solution was placed in the appropriate reactor. An initial (t=0) sample was taken from the reactor, cooling water was turned on and the solution was purged with argon gas for 15 minutes. The reactor was then completely sealed using ungreased glass stoppers, leaving the Subaseal® used to introduce gas into the reactor. The generator was then set to power setting 8 (12.12 W cm^{-2} (20 kHz) and the solution sonicated for 3 hours.

After 3 hours, a 100 cm^3 gas syringe was filled to extract a sample from the headspace. This was immediately injected into the gas chromatograph. A second liquid sample was taken (t=180) and the two samples analysed using mass spectrometry to confirm degradation had occurred and to what extent.

For GC analysis the gas sample was analysed via GC with helium at the flow gas. Gas samples were analysed on a Hewlett Packard 5890 GC with a CP-LowOx column (10 m by 0.53 mm) and analysed via FID.

For GC-MS analysis Gas typically 30 ml of gas was sampled using a gas syringe and injected into an Agilent 7890A gas chromatography mass spectrometry with a HP-PLOT/Q, 30 m long 0.530 mm diameter column.

The same temperature ramp was used on both machines. A starting temperature of 50℃ was applied for 5 minutes. After this time the temperature was increased to 200℃ at a rate of 10℃ min^{-1}. This maximum was applied for 5 minutes before the end of the sequence.

3.4.3: Synthesis of monobutyl phthalate.

The method of Leung[3] was adapted. In a 25 mL single necked round bottomed flask was placed phthalic anhydride (2.5g, 16.9 mmol) and 20 mL of 1-butanol. A small stirrer bar and a couple of anti bumping granules were added. A water condenser was fitted into the neck of the flask and cooling water circulated through the condenser. Using an aluminium block placed on a magnetic heater/stirrer the flask was heated to 125°C as recorded and controlled by the heater's thermometer, which measured the temperature of the aluminium block. All the phthalic anhydride had dissolved by the time reflux had started. The solution was allowed to reflux for 4 hours. After 4 hours any remaining 1-butanol was removed by vacuum evaporation using a Büchi R-215 Rotavapor connected to a Büchi B-491 water bath. This required the water bath to be set to 40°C and yielded a pale yellow oil.

Analysis by ^{1}H and ^{13}C NMR confirmed the oil product as monobutyl phthalate with an amount of 1-butanol remaining. The product was also confirmed using LC-MS in positive ionisation mode. Complete removal of 1-butanol proved very difficult so it was decided to use the monobutyl phthalate "as is" and so included some 1-butanol. This crystallised over the course of several days to yield a waxy white solid.

Monobutyl phthalate

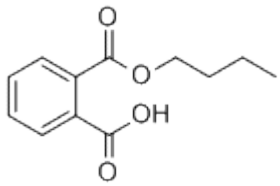

NMR: δ_H - ($CDCl_3$, 300 MHz): 7.846 (H, m), 7.637 (H, m), 7.516 (2H, m), 4.268 (2H, t), 2.041 (2H, quintet), 1.373 (2H, sextet), 0.871 (3H, t)

Lit[3]: ($CDCl_3$, 300 MHz): 7.86 (H, d), 7.66 (H, d), 7.4 – 7.59 (2H, m), 4.31 (H, t), 1.67 – 1.74 (2H, m), 1.35-1.47 (2H, m), 0.91 (3H, t)

δ_C - ($CDCl_3$, 300 MHz): 172.59, 168.28, 133.57, 132.248, 130.815, 129.944, 129.859, 128.801, 65.923, 30.430, 19.190, 13.714

Lit[3]: 172.66, 168.12, 133.48, 132.07, 130.64, 129.90, 129.61, 128.62, 65.75, 30.30, 19.05, 13.55

Masses found by LC-MS: 149.025 I% = 86 (phthalic anhydride + H^+), 161.129 I% = 11 (phthalic anhydride + Na^+), 245.079 I% = 100 (MBP + Na^+), 467.168 I% = 24 (2MBP + Na^+)

A second batch was synthesised during the course of experiments when needed. This yielded white crystals from a yellowish oil after vacuum evaporation and standing in a fume cupboard for 48 hours. The NMR and mass spectra were in agreement with those reported above.

3.4.4: Assessment of liquid phase products from MBP degradation.

A 10 mg L^{-1} aqueous solution of MBP was made using the same method as in section 3.2.1 using one gram of MBP to make the methanolic stock. MBP, being a monoacid was much more soluble than its corresponding di-phthalate, DBP. This meant that no emulsion was seen when making solutions and only 1 hour of stirring was required to form adequate solutions.

100 mL of this solution was degraded using the same method as in section 3.3.1.

3.4.5: Assessment of effect of dissolved gas on DBP degradation products.

Solutions of both DBP and MBP (10 mg L^{-1}) were degraded using the same method as in section 3.3.2. The experiment was performed 4 times using air, argon, nitrogen and oxygen as the dissolved gas. Analysis was the same as in section 3.3.1.

3.5: Method of analyses of reaction model

3.5.1: Effect of phthalate concentration on pH change of bulk solution

A 100 μg L^{-1} solution of DBP was prepared using the method in section 3.3.1. The solution was sonicated as in section 3.3.2. As well as the 1 mL samples taken for LC-MS analysis, 5 mL samples were taken at the same time intervals. These were used to record the pH of the solution using an Oakton Acorn series pH 6 portable pH meter. After pH measurement these samples were replaced. The experiment was performed at both 20 kHz and 515 kHz ultrasonic frequencies.

The experiment was then repeated using the same method above but with distilled water instead of DBP solution.

3.5.2: Effect of DBP addition on the sonoluminescence (SL) output of water.

SL measurement conditions and apparatus

All SL measurements took place inside a custom-built metal dark box of dimensions 89 cm x 48 cm x 51 cm. The box had several ports in it to allow for the feeding of cables and tubes into the box. To ensure a dark environment inside the box, the box sides and apex were sealed using duct tape. The box was then shrouded with two black felt blankets.

Photographs were taken using a Cannon EOS 500D, digital SLR camera fitted with a Cannon “Ultrasonic” EFS 600 mm f/2.8 Macro USM lens. The shutter and aperture of the camera were controlled remotely using EOS Utility software by Cannon.

20 kHz Experiment

A 10 mg L^{-1} solution of DBP was prepared using the method in section 233.1. The required amount of phthalate solution was diluted with distilled water using a 250 cm^3 volumetric flask. The solution was inverted 10 times and poured into a 500 cm^3 glass beaker. The solution was then purged with argon for 5 minutes. The tip of the 20 kHz horn was placed in the centre of the beaker immersed an inch below the surface of the solution. The camera was then focussed onto the centre of the tip. To enable focussing in the right spot, a bubble was initially introduced under the tip and the camera focussed onto the bubble. The correct lens setting was then noted and reproduced. The set up was reproduced exactly for each solution measured. After purging, the flow rate was reduced and the needle used was positioned above the water surface to maintain an argon atmosphere over the solution without disturbing its surface.

For each solution measured, a 5 minute background or “darkframe” was captured. After this, the solution was sonicated at 12.12 W cm^{-2} for 5 minutes. The camera was started collecting for 5 minutes just after sonication was started.

Image and Data handling

The images and darkframes captured above were manipulated using the ImageJ software suite. To produce a working image, the darkframe was mathematically subtracted from the image. This gave images in which the SL of water could clearly be seen. To quantify the amount of SL emitted, the average pixel brightness of a region of interest was calculated. 3 regions of interest were analysed; the whole frame of the image, a column drawn from the horn tip down to the beaker base with the same width as the horn tip, and lastly a smaller region which just incorporated the area closest to the horn tip and which always completely enclosed the cone of SL produced.

Check of experiment using a different container

To check if the peak present was affected by the sound wave present in solution the above experiment was replicated but in a 500 cm^3 conical flask. All other factors in the experiment were kept exactly the same and the experiment was performed identically as above.

3.6: Measuring surface tension of DBP solutions

To measure the bulk phase surface tension of DBP solutions a Sigma 702 tensiometer was used. A 10 mg L^{-1} solution of DBP was prepared as described above and this was diluted to make solutions of various concentrations which were to have their surface tensions measured. This was done by aliquoting the appropriate amount of stock solution into a 25 cm^3 volumetric flask. This volume was then diluted using miliQ quality water to correct volume. The flask was then inverted 10 times after which the solution was transferred into the measuring vessel, a 40 cm^3 round dish made from Pyrex. The experiment was started immediately after the solution had been poured into the measuring vessel.

For each run the experiment was ran until a constant surface tension was reached. Typically this was 3-5 minutes. This tension was then recorded as the surface tension of the bulk solution.

The platinum deNouy ring of the tensiometer was cleaned between each run as follows. The ring was dipped into absolute ethanol and drained 3 times. After this the ethanol was burned off by igniting the residual ethanol using a cigarette lighter. The ring was always held so that the ring itself was never handled directly.

The measuring vessel was cleaned using only miliQ water and special Kimwipe wipes which are designed to leave no residual fibres on the surface of whatever they dry. Care was taken not to handle the sides of interior of the vessel.

3.7: Materials Used

Argon: BOC Pureshield, used as received.

Benzyl butyl phthalate: Sigma Aldrich, 98%, used as received.

n-Butanol: Sigma, ≥99%, melted to form liquid then used.

Carbon dioxide gas: BOC, used as received.

Dibutyl phthalate: Aldrich, Reagent Plus ≥99%, used as received.

Diethyl phthalate: Aldrich, 99.5%, used as received.

Diheptyl phthalate: Aldrich, 99%, used as received.

Dimethyl phthalate: Sigma Aldrich, 99%+, used as received.

Dinonyl phthalate: Fluka, GC stationary phase, used as received.

Di-n-octyl phthalate: Fluka, Oekanal analytical standard, used as received.

Dioctyl phthalate: Sigma Alridch, 99%, used as received.

EDTA: Sigma, supplied as calcium disodium salt, used as received.

Hydrogen perodxide: Fisher, Laboratory Reagent Grade, 100 volumes solution in water, used as received.

Methanol: Fisher, HPLC grade, used as received.

Nitrogen gas: Supplied internally to same specifications as “Zero Grade” BOC nitrogen.

Oxygen gas : BOC, used as received.

Phthalic anhydride: Sigma Aldrich, A.C.S. reagent, 99%+, used as received.

Sodium hydroxide: Fisher, General purpose grade, used as received.

Thiabendazole: Riedel de Haën, Pestanal analytical standard, used as received.

3.8: Calculation of best fit lines and fitted data calculated from such lines

In order to produce accurate best fit lines all shown in figures (dashed and bold) have been calculated as follows:

Firstly a plot of $\ln(C/C_0)$ was produced. A linear best fit line was then fitted using the functions in Microsoft Excel. For most of the data acquired, a linear graph was obtained implying that the degradations followed first order, or more correctly, pseudo first order reaction kinetics. Equation 3.6 shows the appropriate rate law for such a degradation where [DBP] is the concentration of DBP at any moment in time, *t* is the amount of time progressed and *k* is the pseudo first order rate constant.

$$\frac{d[DBP]}{dt} = -k[DBP] \tag{3.6}$$

This rate law has the solution shown in equation 3.7. Therefore a plot of the L.H.S. of the equation verses time should give a straight line with slope equal to *k*.

$$Ln\left(\frac{[DBP]}{[DBP]_0}\right) = -kt \tag{3.7}$$

This initial value of *k* was then recalculated by using a least squares fitting process: From the initial value of *k* and equation 3.8, model data for [DBP] was calculated for each time point (expressed as $[DBP]_i$ in the equation below). The sum of the squared differences between this modelled data and the experimental data was then minimised by varying the value of *k* using the Microsoft Excel Solver function to give a recalculated value of *k*. This final value was the one reported in all instances below. Recalculated model data was then calculated from this rate constant and used to plot the bold and dashed best fit lines in all [DBP] *Vs.* time and/or ln[DBP] *Vs*. time figures shown in this work.

$$[DBP]_i = [DBP]_0 . e^{-kt} \quad (3.8)$$

3.9: Chapter References

1. W. M. Meylan, P. H. Howard and R. S. Boethling, *Environmental Toxicology and Chemistry*, 1996, **15**, 100-106.
2. G. J. Price and E. J. Lenz, *Ultrasonics*, 1993, **31**, 451-456.
3. D. L. Defoe, G. W. Holcombe, D. E. Hammermeister and K. E. Biesinger, *Environmental Toxicology and Chemistry*, 1990, **9**, 623-636.

Chapter 4: Method Development

This chapter discusses how several of the methods in the experimental section came to be. It also describes the rationale behind the development of these methods. Several stages of the analysis procedure will be discussed namely handling requirements, solution preparation, use, choice and making of internal standard solutions, sampling and processing of solutions and a brief method validation.

4.1: Handling requirements and user precautions

Several precautions were taken as to the handling of samples and solutions to avoid contamination by phthalates. Since phthalate esters by design are present in most plastic materials the use of plastics was reduced as much as possible.

Glass stoppers, foil and cork bungs were used in place of plastic stoppers and Parafilm™. One place where plastic could not be avoided is in the use of micropippettes. These were used to measure out phthalate liquid and to measure phthalate methanolic stocks, to sample the reacting solution and to add internal standard to the samples. These use plastic disposable tips and this was the only area where plastic could not be avoided and so was tolerated.

Similarly latex or nitrile gloves were not worn and hands were cleaned thoroughly using warm water and soap before handling any solutions. During the course of this project perfumes were not worn at all by the author as perfume fumes can cause contamination of the solutions and samples even several days after the perfume being applied.

Glasswear was cleaned not with acids nor organics but with copious amounts of distilled water. Surfactant based cleaning products were also avoided as these can help solubilise phthalates in aqueous solution and so were considered a potential cause of contamination.

4.2: Solution preparation

Solution preparation is known to be difficult for phthalate esters. This is due to the low solubility of phthalate esters in water and also the fact that their densities are similar to water. These two factors mean that problems such as surface films and the formation of micro-aggregates are common problems for phthalate ester solutions[1]. In the literature the best method for avoiding the formation of these aggregates is the slow stirring method of workers such as Ellington[2]. Therefore a slow stirring method was developed in this work.

Solutions were made from methanolic stock solutions as in the experimental and then stirred slowly for at least 16 hours (overnight preparation). Upon addition of the methanolic stock, clouds and droplets were often formed in the solution present in the volumetric flask neck, these were always gone by the end of the stirring method.

The use of methanol in making methanolic stocks of both phthalate and internal standard was the only use of organic solvents in the work. It was decided to limit the amount of organics used to as little as possible since such solvents readily accumulate phthalate esters over time from even the atmosphere of a fume cupboard or lab. The use of organics was therefore limited to avoid contamination of samples with extra phthalate.

The stirrer bars used for the stirring were Teflon coated. Two were used and kept aside during this study. One for the creation of low concentration phthalate solutions (<100 µg L^{-1}) and one for high concentration solutions (>100 µg L^{-1}). This was to prevent any possible cross contamination of the low concentration solutions in case the bar was able to adsorb and desorb phthalates present in the high concentration solutions.

Initially efforts were made to use glass rather than Teflon coated stirrer bars in case of contamination of phthalate from the Teflon material. It was found however that the stirring of glass bars on the surface of a glass flask often lead to the solution becoming cloudy, presumably with motes of ground , worn glass. On other occasions the stirrer bar smashed rendering the solution unusably

contaminated. Due to these problems it was decided to use Teflon stirrer bars despite their coating material.

To avoid contamination from the stirrer bars a cleaning procedure was followed. Before each use the bar was first stirred quickly for one hour in 100 cm^3 of methanol and allowed to dry. The same bar was then stirred in 100 cm^3 deionised water for one hour before being used.

4.3: Internal standards

For the work described in this thesis thiabendazole was the internal standard used. Initially diphenyldramine was investigated for use. Both of these compounds differ in mass and retention time to DBP and so are suitable for use as an internal standard. The perfect standards would have been deuterated DBP but these were too expensive to obtain.

Diphenylhydramine was quickly discarded as it was found difficult to isolate the mass information corresponding to DBP in the mass spectrum produced. It was thought therefore that for some reason diphenylhydramine interacted with DBP either directly in solution or inside the mass spectrometer.

Thiabendazole was therefore used in this study and no problems with interaction were noticed. Figure 4.1 shows the chemical structures of both of these compounds. From the structure of diphenylhydramine it could be possible that the interaction and disruption of DBP signals found could be due to Pi-Pi interactions between the phenyl rings on diphenylhydramine and the benzoic acid moiety of DBP.

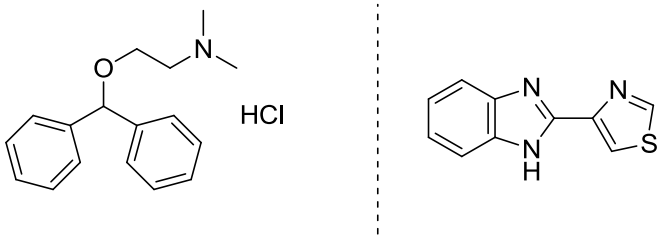

Figure 4.1: Internal standards used: diphenylhydramine on the left and thiabendazole on the right

The retention time of thiabendazole was found to be 6.9 minutes in the LC conditions used and its monoisotopic mass is 202.041 g mol^{-1}.

4.4: Sampling and processing of solutions

4.4.1: Reduction in volume precautions

As mentioned previously analysis samples were taken using a micropipette by Gilsson. Since ultrasound field are influenced by the volume of the solution, it is known that reducing the volume of a cavitating solution by more than 10% during an experiment is undesirable as it may change the bubble dynamics of the system and thus slow or influence the processes occurring as a result of the cavitation process.

During an entire experiment 9 samples were taken at time intervals of 0,15,30,45,60,90,120,150,180 minutes of elapsed sonication. These samples were all 990 µL in volume. Therefore the total amount of solution removed from the reactor was 8.9 mL of an initial 100 mL of phthalate solution. This represents a volume reduction of 9% and so was not thought to influence the cavitation process.

4.4.2: Age of solutions

All phthalate solutions were used in one week. In all cases all the solutions used for a single experiment type e.g. effect of power intensity were performed using the same solution batch. This was so that small changes in solution concentration would not affect the chemistry occurring and was enforced to try

and be precise as possible when calculating the kinetics of the degradation processes.

Similarly phthalate stock solutions were used within one month. De-esterification of phthalate due to being dissolved in methanol for this long was not found to be a problem over these time scales. Often stock solutions were just used for one experiment and then discarded after a single use.

Internal standard methanolic solutions were all discarded after one week. All solutions were kept refrigerated at all times and wrapped in tin foil to avoid any reactions due to UV light.

4.4.3: Samples

Samples were pipetted into glass LC vials. These were prerinsed with deionised water to remove any impurities present in the unused vials during their manufacture and storage. The vials were then dried at 180℃ for 3 hours. Two types of vial were used both of which had a maximum volume of 1.4 mL. For experiments designed for the calculation of kinetic information clear vials were used. For experiments designed for the discovery of degradation products amber vials were used. This was to prevent to reaction of degradation products and intermediates with UV light.

The septa of the lids of these vials were the second unavoidable use of plastic material, however the time for phthalate adsorption from the lid through the vial headspace was quite short in all cases (<12 hours) and so was not thought to occur. There was also no direct contact with the sample itself. Sometimes the analysis resulted in the vial septa being pushed into the vial by the syringe of the LC machinery. Any samples where this happened had their data discounted. This and the occasional failure of automatic processing of sample data resulted in some graphs shown in this thesis not having data for all time points.

Due to processing constraints samples were processed overnight for LC-MS analysis. Experiments were therefore done in the afternoon and evening so that samples were as young as possible when analysed. Samples were vortexed as part of the method which added internal standard to the solutions so any phthalate phase separation which may have occurred post experiment should have been reversed.

Post analysis samples were stored in a fridge for one week in case reprocessing was required. After this time samples were collected together and stored at room temperature. Similarly the left over phthalate solution on which experiments were performed were stored in glass screw top jars in a fridge for one week. After this time samples were stored in cupboards at room temperature.

4.5: Quantification procedures

LC-MS was used to quantify all phthalates studied. For each phthalate studied a 6 point calibration curve was created. The maximum concentration of a given calibration curve was the concentration of the DBP solution to be studied for that experiment. So for example when planning to degrade a 1 mg / L DBP solution the solution itself was diluted appropriately to form the 6 sample concentrations. These 6 samples were at 0% (water), 20%, 40%, 60%, 80% and 100% of the solution concentration. Each point on the calibration curve had 3 samples and so there were 18 samples making up a given calibration curve.

Once diluted the samples were analysed and the data was inputted into Bruker QuantAnalysis software package. QuantAnalysis makes use of 2 main equations to calculate the concentration of unknown samples from calibration curves. The first is for the calculation of theoretical concentrations and this in turn is used to calculate the internal standard concentration. These two equations allow for the calculation of the X,Y pairs which make up the calibration curve and are shown below as equations 4.1 and 4.2.

Firstly the theoretical concentration of a calibration sample is calculated below is equation 4.1.

$$Conc_{theor} = Conc_{level} \cdot \frac{InjVol}{DefInjVol} \quad (4.1)$$

In this equation $Conc_{theor}$ is the calculated theoretical concentration of the sample, $Conc_{level}$ is the standard concentration assigned to the level of the calibration (the calibration level denotes all the samples in increasing concentration of the same concentration and is user defined e.g. level 1in the present case was set to 0 µg L^{-1} and level 3 was set to 40 µg L^{-1} and so on), InjVol is the injection volume (10 µL in the present case) and DefInjVol is the default injection volume and was also 10 µL.

Having calculated the theortical concentration for each sample the relation between these concentrations and the area of the resulting LC-MS peaks can be related using equation 4.2. Here Area is the area of the LC-MS peak, $Conc_{ISTD}$ denotes the concentration of the internal standard, $Area_{Target}$ denotes the area of the target compound (in our case some kind of phthalate e.g. dibutylphthalate) and $Area_{ISTD}$ denotes the area of the internal standard LC-MS peak.

$$(Conc_{theor}, Area)\ resp.\left(\frac{Conc_{theor}}{Conc_{ISTD}}, \frac{Area_{Target}}{Area_{ISTD}}\right) \quad (4.2)$$

From these X,Y information pairs a linear fit was calculated to allow for the calculation of unknowns. Having formed the calibration curve by solving equation 4.2 for the calibration samples unknown samples can have their concentrations calculated by solving the resulting linear fit for the area of the LC-MS peaks resulting from the analysis of each unknown sample. These two steps are performed automatically in QuantAnalysis computing the concentration of unknowns once a sufficient calibration curve has been calculated.

4.6: Method validation

To assess the possibility and extent of contamination of samples by phthalates during both solution preparation and analysis procedures a brief method validation of blanks samples was performed. This was inspired by the work of Tienpont *et al* who studied the effects of several experimental procedural elements on the trace quantification of phthalate esters[3]. A secondary purpose of this experiment was to try to show that phthalate contamination could be reduced by avoiding the use of organic solvents in which phthalates are much more soluble.

To this ends, 4 samples of methanol (1 mL) and 5 samples of water (1 mL) in LC vials were prepared and left uncapped in fume cupboards for 3 hours. At the end of this time the samples were made up to 1 mL to replace any lost solvent and then analysed using LC-MS. A second set were aliquoted and then analysed immediately. Figure 4.2 shows the peak areas obtained for four phthalates determined which were DMP, DEP, DBP and DNP for methanolic samples. Figure 4.3 shows the same for the water samples. In figure 4.2 sample 5 and shows the mean value calculated for the two data sets where samples 1-4 were left uncapped in the fume cupboard and samples 6-9 were analysed immediately. The same is true of sample 6 in figure 4.3 and samples 1-5 were left uncapped in fume cupboard while samples 7-11 were analysed immediately.

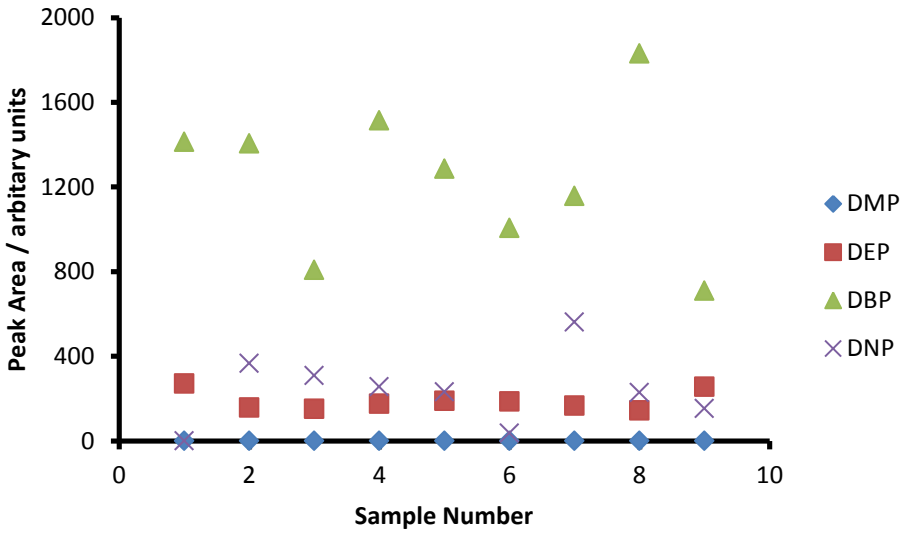

Figure 4.2: Method blank validation for methanolic samples

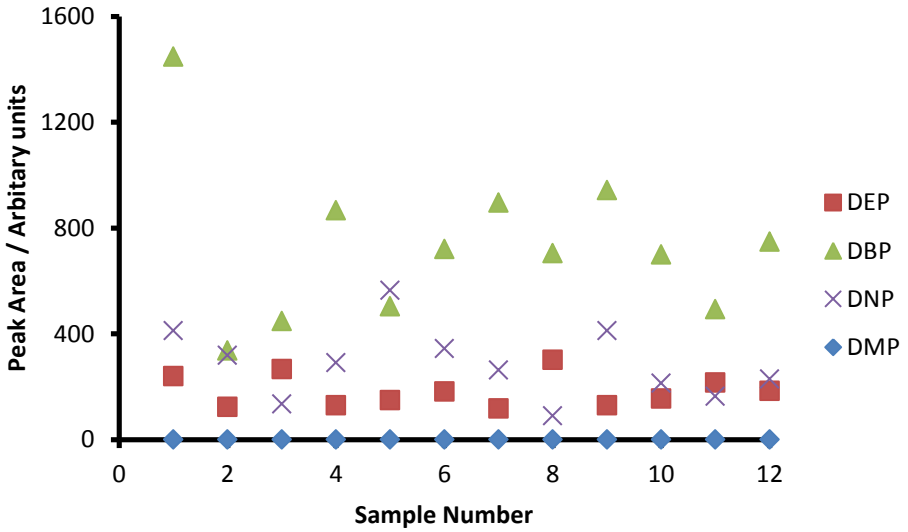

Figure 4.3: Method blank validation for aqueous samples

From these figures it can be seen that phthalate contamination occurs in both data sets for both solvents. From the mean values calculated DEP and DNP contamination are similar for both solvents when exposed in fume cupboards and DBP contamination is 44% lower when using water for this data set. DMP was not detected however this may be due to its found low level of ionisation using the methods employed.

For the samples which were analysed immediately mean contamination values are again similar for DEP and DNP but the mean value for aqueous samples is 37% lower.

The mean values of contamination were similar for both data sets for both solvents employed i.e. fume cupboard exposure made little difference to the contamination of the samples by phthalates. From this it can be deduced that the major contamination routes lie in the handling and processing of the samples which is unavoidable.

4.7: Why DBP was chosen as a model

As discussed in chapter 2 investigating the sonolysis of phthalate esters presents several challenges. These largely arise from their increasing hydrophobicity and decreasing solubility in water with increasing ester chain length/complexity**.** However, the more insoluble the phthalate the more susceptible to ultrasonic degradation it is[4, 5]. Practical problems in making and handling solutions of phthalates have been noted due to the similarity in density of most phthalate esters studied to that of water[6, 7]. These problems make it difficult to make aqueous solutions of phthalate esters reliably.

It was decided to initially study a single phthalate as a model of the homologous series. This model phthalate would be used to study how various parameters affected the degradation kinetics and to provide a baseline for comparison with other phthalates. For the mechanistic study the mechanism of degradation of the model phthalate would first be examined and the degradation products revealed. These degradation products could then be searched for in the mass information obtained from the degradation of other phthalate esters. Any differences between the mechanisms could then be rationalised.

In choosing a model phthalate to study initially, there were three main considerations to make, the first being the phthalate's solubility. Making an aqueous solution of the more soluble phthalates would be simpler and less prone to errors such as formation of residual emulsions[2]. Conversely, starting the work with the more insoluble phthalates such as dinonyl phthalate (DNP), dioctyl phtahalate (DOP) and diethyl hexyl phthalate (DEHP), although attractive due to their increased rate of sonolysis, could prove a very difficult starting point due to their extreme insolubility in water[8].

The second consideration was the varying rate of sonolysis of phthalates. This factor does not make too much difference for the kinetic studies. Indeed, it could be argued that a good way of investigating the effect of changes in experimental conditions would be to work with a reasonably recalcitrant phthalate. Any increases or decreases in degradation rate and removal efficiency should then be greater for more the susceptible phthalates. For the mechanistic study, however, the degradation rate and removal efficiency is a critical factor. Degradations with lower removal efficiency would lead to lower concentrations of sonolysis products in solution. Since we wanted to detect reaction products as completely as possible, a more complete reaction would be favourable to maximise the concentration of all products in solution.

These first two factors also combine in importance for the mechanistic study, since detection of products relies on the absolute concentration of each product formed. Therefore the best option would be to choose a phthalate which degrades reasonably quickly i.e. has a fast conversion to sonolysis products, and of which a reasonably large amount can be dissolved in water.

The third point for consideration was a consequence of our chosen detection method, ESI-TOF-LC-MS (Electrospray Time Of Flight Liquid Chromatography). During the course of this work, it was found that the different phthalates used in the study ionised differently using the conditions fixed by the OpenAccess system. The shorter chain phthalates ionised less easily than the longer chain phthalates and therefore gave rise to smaller MS signals. This was especially true for DMP, which was hard to detect in solution.

Since we were keen to use LC-MS for both the examination of reaction products *and* for phthalate quantification in kinetic studies we wanted to start work with a phthalate which gave rise to a reasonably sized initial LC-MS peak area across the concentration range to be studied i.e. gave rise to a peak with “room to decay” (the peak has a minimum area of several hundred area units and could be visualised well below its original size) before hitting detection limits and quantification limits.

Therefore, in considering the 3 factors above, it was decided to start work using dibutyl phthalate as a model for the homologous series. Dibutyl phthalate is reasonably soluble, current estimations of its solubility lie in the range of 10.1-11.2 mg L^{-1} [9, 10], meaning the concentration in solution could be varied by 3 to 4 orders of magnitude before hitting either the solubility limit (for high concentrations) or the detection/quantification limit (for low concentrations). This was appealing since it would allow us to make high concentration solutions when studying the reaction mechanism to maximise reaction product concentrations while also allowing for solutions of DBP with a starting concentration as low as 10 µg L^{-1} to be degraded, a concentration approaching that found in contaminated waters[11-13].

DBP has also been found to be intermediate in its rate of sonolysis in previous works. Using low frequency ultrasound (80 kHz) Psillakis *et al* found that solutions containing 40 µg L^{-1} DBP (as part of a total loading of 240 µg L^{-1} of 6 phthalates) were removed of DBP within 3 hours[5]. Therefore it was hoped that when using 20 kHz ultrasound, DBP would still be of intermediate, yet useful sonolytic susceptibility.

On top of these three practical factors, DBP is also one of the most heavily used phthalates in the processing and manufacturing industries, along with diethylhexyl phthalate (DEHP) and benzylbutyl phthalate (BBP)[8]. This makes its use in an initial study also relevant to current industrial usage.

4.8: Chapter references

1. M. Thomsen, L. Carlsen and S. Hvidt, *Environmental Toxicology and Chemistry*, 2001, **20**, 127-132.
2. J. J. Ellington, *Journal of Chemical and Engineering Data*, 1999, **44**, 1414-1418.
3. B. Tienpont, F. David, E. Dewulf and P. Sandra, *Chromatographia*, 2005, **61**, 365-370.
4. B. Yim, Y. Nagata and Y. Maeda, *Journal of Physical Chemistry A*, 2002, **106**, 104-107.
5. E. Psillakis, D. Mantzavinos and N. Kalogerakis, *Chemosphere*, 2004, **54**, 849-857.
6. D. L. Defoe, G. W. Holcombe, D. E. Hammermeister and K. E. Biesinger, *Environmental Toxicology and Chemistry*, 1990, **9**, 623-636.
7. J. De Bruijn, F. Busser, W. Seinen and J. Hermens, *Environmental Toxicology and Chemistry*, 1989, **8**, 499-512.
8. D. R. Petersen, C.A. Staples, T.F. Parkerton, W.J. Adams, *Chemosphere*, 1997, **35**, 667-749.
9. W. M. Meylan, P. H. Howard and R. S. Boethling, *Environmental Toxicology and Chemistry*, 1996, **15**, 100-106.
10. F. Leyder and P. Boulanger, *Bulletin of Environmental Contamination and Toxicology*, 1983, **30**, 152-157.
11. G. A. Loraine and M. E. Pettigrove, *Environmental Science & Technology*, 2006, **40**, 687-695.
12. Y. Q. Wang, W. Hu, Z. H. Cao, X. Q. Fu and T. Zhu, *Analytical and Bioanalytical Chemistry*, 2005, **383**, 857-863.
13. H. Fromme, T. Kuchler, T. Otto, K. Pilz, J. Muller and A. Wenzel, *Water Research*, 2002, **36**, 1429-1438.

Chapter 5: Results and discussion of dibutyl phthalate degradation kinetics experiments.

The following two chapters present and discuss results generated from the sonolysis of dibutyl phthalate (DBP) solutions. The work is split into two themes: kinetic studies and mechanistic studies. The kinetic studies were performed to investigate how various factors affected DBP degradation. The mechanistic studies were performed on DBP (as a model for general phthalate degradation) to elucidate the products of sonolysis. These could then be searched for in the degradations of other phthalate esters. This chapter discusses the kinetic data only. The product analysis is presented in chapter 6.

Having decided on initially studying DBP, solutions were made at two concentrations to probe the effects of ultrasonic intensity, entrained/dissolved gas and ultrasonic frequency on the rate of DBP degradation. The initial concentration / loading of DBP was then varied to investigate its relationship to the degradation rate. These data will be presented with discussion included with each data subset. Lastly, the data is used to describe a model for the sonolysis of DBP.

5.1: Starting work; a basic check of the sonolysis of DBP

At the start of this work, the degradation of DBP (and some other phthalates) had already been shown to follow pseudo first order kinetics at both high (200 kHz) and low (80 kHz) ultrasonic frequencies[1, 2].

In this work 20 KHz and 515 kHz ultrasound frequencies were employed based on the equipment available. Initially, degradations were performed on 10 mg L^{-1} DBP solutions using 20 kHz ultrasound. The experiments were then repeated using 100 µg L^{-1} solutions. It should be noted that the use of these DBP concentrations was largely for academic and practical reasons. DBP is never

found in the aqueous environment or even in massively contaminated waters at these concentrations[3].

The first work done was a simple degradation experiment to show that DBP sonolysis occurred using the equipment and setup described in the experimental. Figures 5.1 a and b show the data for degradations of 10 mg L^{-1} and 100 µg L^{-1} DBP solutions using 20 kHz ultrasound. These graphs show a linear fit to the natural log function of $[DBP]/[DBP]_0$, indicating first order (or rather, pseudo first order) kinetics for the degradation process. It can be seen in these initial degradations that the sonolysis was slower when using the higher concentration DBP solution.

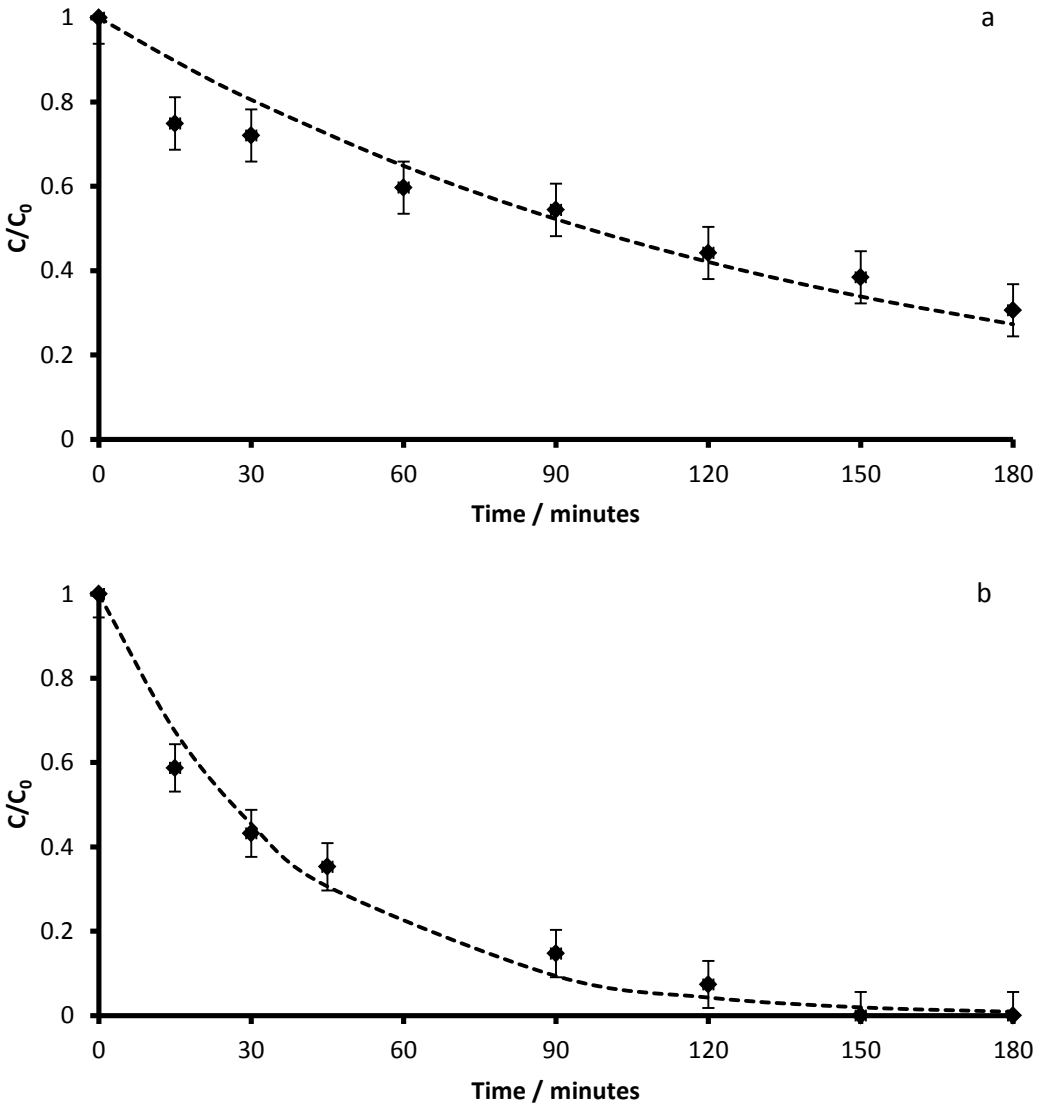

Figure 5.1: Degradation curves of DBP solutions at 10 mg L^{-1} (a) and 100 µg L^{-1} (b). The sonications were performed using 20 KHz ultrasound with an intensity of 12.1 W cm^{-2} under an atmosphere of argon at room temperature. Error bars represent the average standard deviation across the experiment time (n=3).

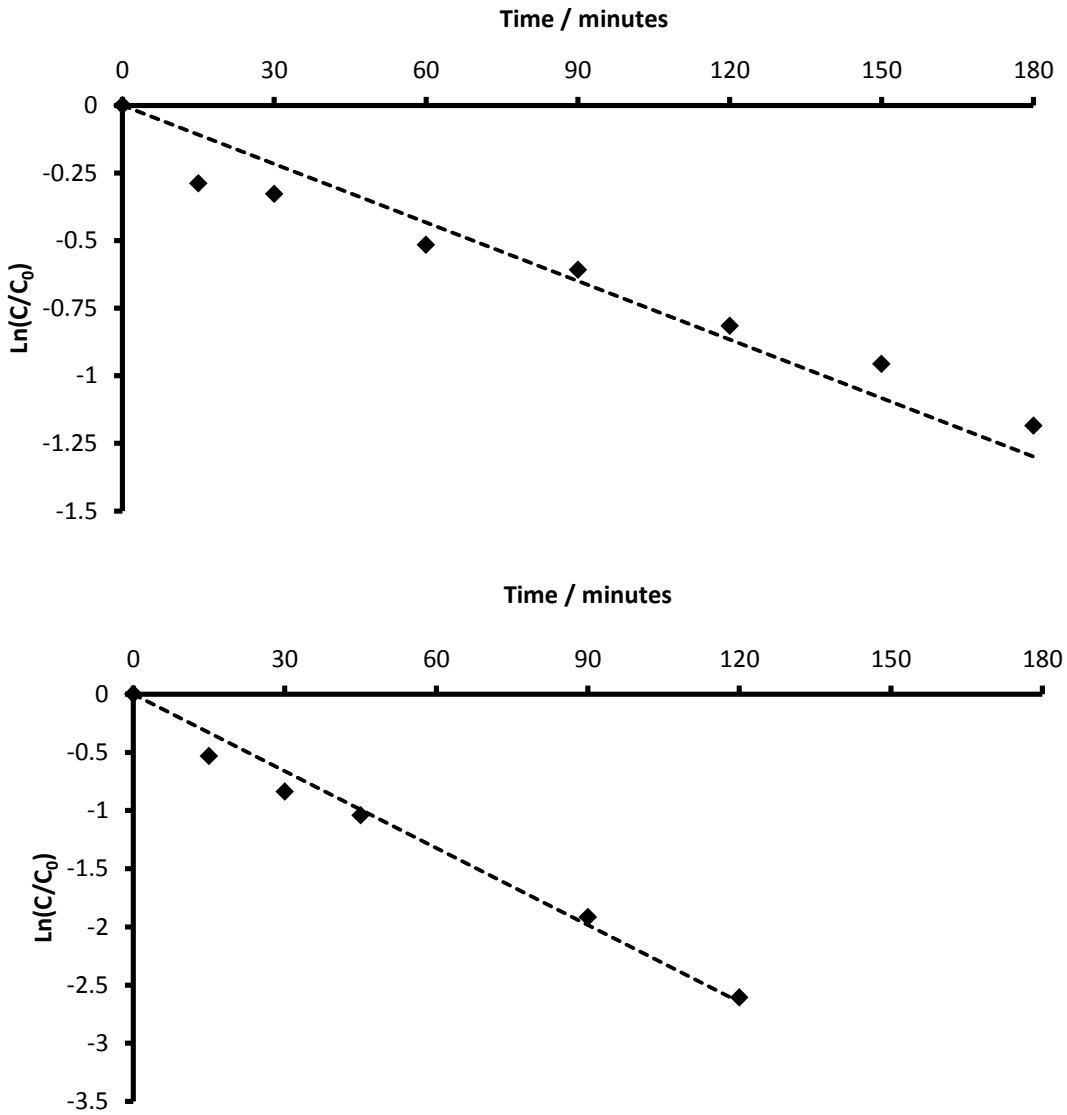

Figure 5.2: First order linear reduction plots for the degradation data shown in figure 5.1.

Using the slopes of the best fit lines above pseudo first order rate constants of 0.0072 and 0.0261 min^{-1} were calculated. The psueo first order degradations agree with the litrature for phthalate degradations however the rate constants are not directly comparible due to the different frequencies used and different initial concentrations used in this study and the two references given[1, 2].

Having established that degradations occurred using the equipment available, studies into various aforementioned parameters were conducted and are presented and discussed next.

5.2: Varying ultrasonic power.

The first effect to be studied was the changing of the ultrasonic power, expressed as ultrasonic intensity. The ultrasonic intensity can be calculated by using equation 5.1 below:

$$I = P_a/A \qquad (5.1)$$

Where *I* is the acoustic intensity, P_a is the acoustic power and *A* is the area of the radiating surface i.e. the area of the horn tip or flatbed transducer surface.

5.2.1: 20 kHz Degradations

5.2.1a: Degradation of 10 mg L^{-1} DBP solutions

Figure 5.3 shows the data from degradations using a range of ultrasonic intensities. It can be seen that increasing the ultrasonic intensity and therefore the power inputted into the system increases the degradation rate of DBP from 0.00 mg min^{-1} (for 3.6 W cm^{-2}) to 2.29 mg min^{-1} (for 12.1 W cm^{-2}).

Solutions irradiated with higher ultrasonic intensities therefore showed more complete degradations with respect to the final calculated DBP concentration. The minimum final concentration of DBP remaining after 3 hours of sonication was 3.12 mg L^{-1} or 31% remaining DBP using an intensity of 12.1 W cm^{-2}. It can also be seen that as well as the degradation rate increasing with higher intensities, that there is a minimum intensity required for DBP sonolysis to occur at all.

To calculate this threshold intensity the calculated pseudo first order rate constants were plotted against ultrasonic intensity as in figure 5.4. There is an apparent linear increase in rate constant with increasing ultrasonic intensity and the intensity threshold value for this system can be seen to be around 5.5W cm^{-2}. This threshold intensity was calculated as being 5.48W cm^{-2} by finding the X-intercept of the fitted line.

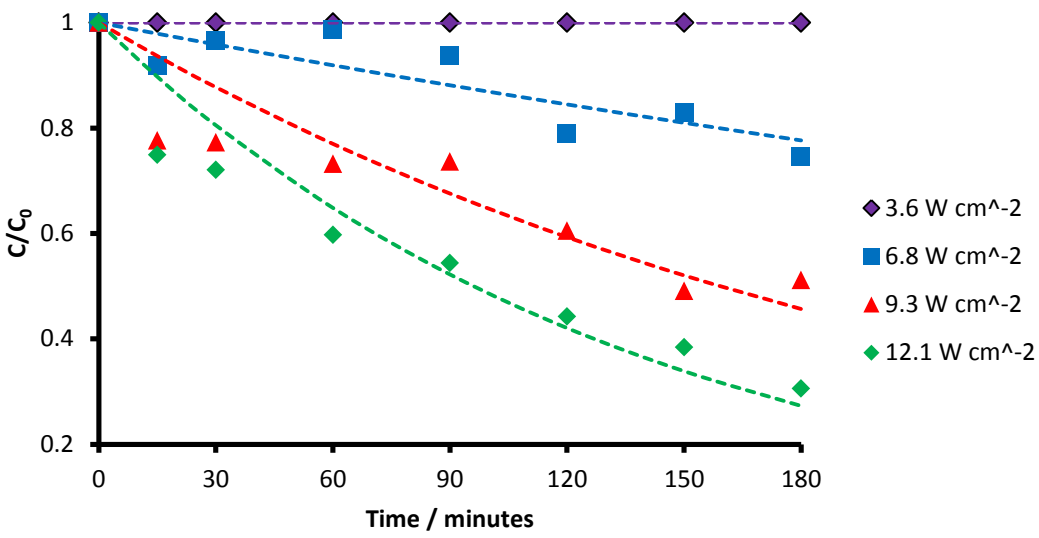

Figure 5.3: The effect of increasing ultrasonic intensity on DBP degradation. Experiments were conducted using 10 mg L^{-1} solution irradiated with 20 kHz frequency ultrasound under an atmosphere of argon. The temperature was controlled to be 18 ±2°C.

Several studies have concluded that due to changes in solution conditions during sonolyses the initial rate best describes the degradation process[4]. This is due to the system being complicated over time by the increased concentration of degradation products (volatile or otherwise) which also degrade and compete with the main substrate thus derailing the reaction kinetics. Due to this, the initial degradation rates were calculated from the first 60 minutes of data.

The effect of ultrasonic intensity on this rate is shown in figure 5.5. The appearance of figure 5.5 is very similar to that of figure 5.4. A threshold intensity is again seen as is a linear increase of rate above a certain threshold intensity. Using the best fit line shown, a threshold intensity of 6.46W cm^{-2} was calculated. Although these estimates of threshold vary, neither the rate constant plot nor the degradation rate plot show any signs of a plateauing of the kinetic rate as the ultrasonic intensity is increased (although this may well occur if higher intensities are used).

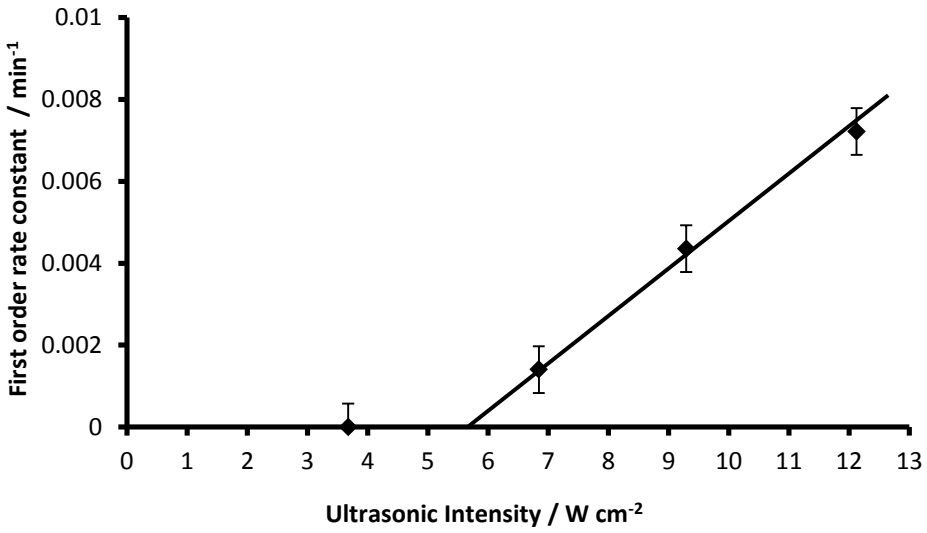

Figure 5.4: The relationship between ultrasonic intensity and pseudo -first order reaction rate constants calculated from data in figure 5.3.Error bars are representative of instrumental error calculated for the mass spectrometer used.

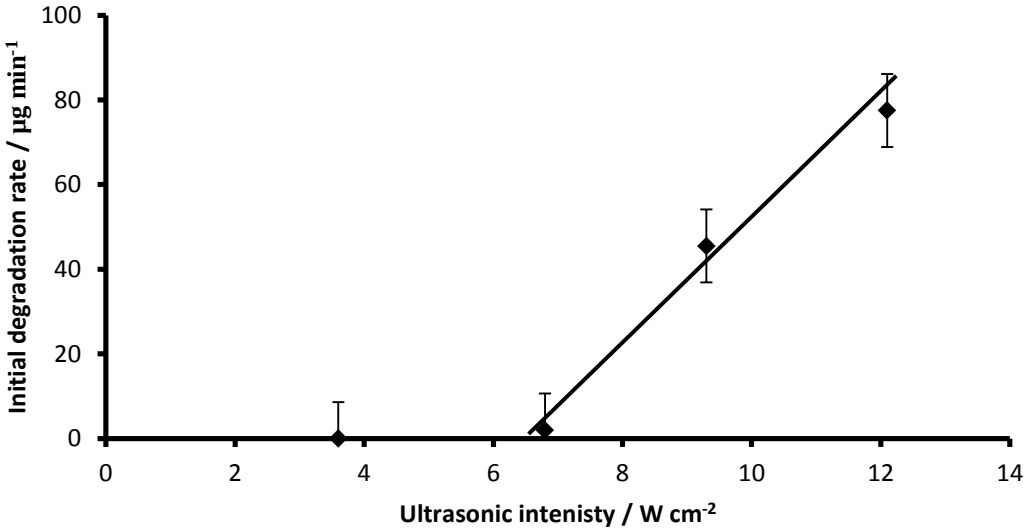

Figure 5.5: The relationship between initial degradation rate and ultrasonic intensity.

The linear increase in degradation rate can be explained by an increase in the total amount of cavitation events occurring in solution. As the intensity is increased more of the liquid structure ruptures creating more bubbles in the solution[5]. This creates a larger surface area for the binding of DBP and

subsequent sonolysis when a bubble DBP is adsorbed onto collapses. This data shows that the degradation process of DBP at high concentrations is limited by the total amount of bubble surface available in solution.

5.2.1b: Degradation of 100 µg L^{-1} solutions

Repeating the experiment above using 100 µg L^{-1} DBP solutions produced the data shown in figure 5.6. Here a similar linear increase of rate constant can be seen with increasing ultrasonic intensity. Again an apparent threshold intensity can be seen. Using the x-intercept of the best fit line shown, this was calculated to be 1.8 W cm^{-2}. It can also be noticed that the rate constants are larger using this lower concentration of DBP. This implies that the rate of reaction becomes more sensitive to the concentration of DBP as the amount in solution is decreased.

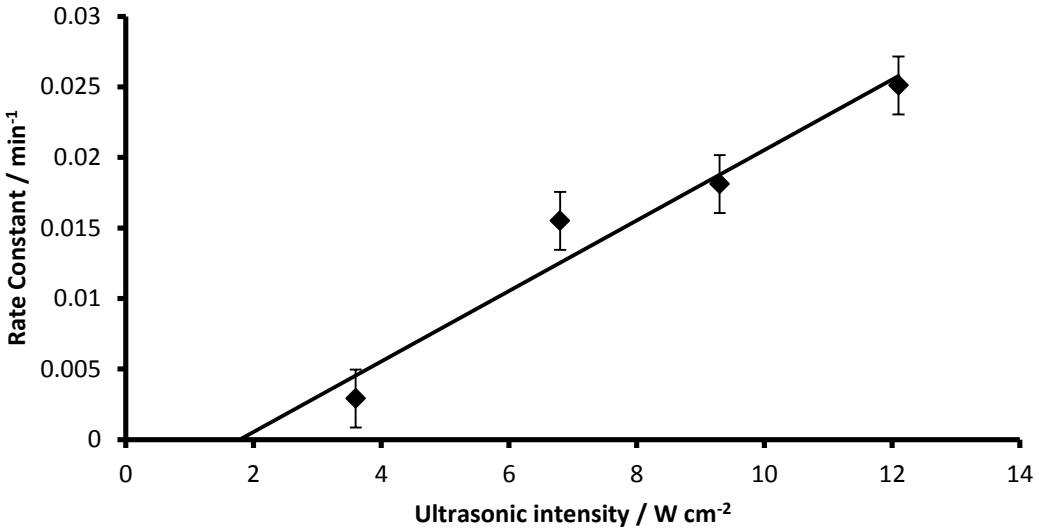

Figure 5.6: The effect of increasing ultrasonic intensity on first order reaction rate constants for 100 µg L^{-1} DBP solutions. Experiments were performed under argon and at 18 ±2°C using 20 kHz ultrasound.

The initial rates of degradation were also calculated for each intensity setting used. This data is shown in figure 5.7. Here a very different trend is seen with increasing intensity. The rate of degradation increases linearly at first, then plateaus and then decreases slightly with increasing ultrasonic intensity.

It can also be noted that although the rate constants are larger for degradations using 100 µg L^{-1} DBP solutions, the absolute rates of degradations are slower with less DBP being removed per unit time than when degrading 10 mg L^{-1} solutions.

Regression of the linear portion of figure 5.7 gave a calculated intensity threshold value of 1.58W cm^{-2}, which is in good agreement with the value calculated from the rate constant data above.

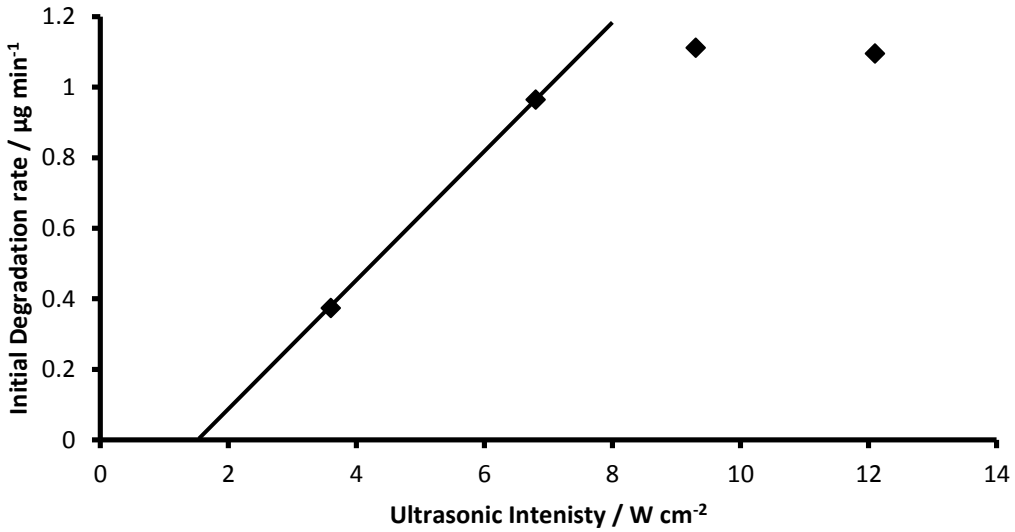

Figure 5.7: The evolution of degradation rate with increasing ultrasonic intensity. Experiments were performed under argon using 100 µg L^{-1} solutions and 20 kHz ultrasound.

The linear portion of figure 5.7 reflects an increase in rate due to an increase in the amount of bubble surface area present in the solution. The plateau effect can be explained by remembering that the concentration of DBP in solution is now quite low. The plateau suggests that the rate becomes limited by the

amount of DBP in solution and by the rate at which DBP molecules can move to a bubble interface and be degraded.

From figure 5.7 this can be seen to occur at roughly 8 W cm^{-2}, the existence of the plateau suggests that the process at intensities higher than this threshold is now diffusion (of DBP) limited rather than bubble surface area limited. This hypothesis is supported by the fact that no plateauing was seen for degradations performed using 10 mg L^{-1} solutions where there is enough DBP in solution to take advantage of the increased amount of bubble surface area.

Thus, when degrading solutions of increasing concentration, a plateau effect of the rate would still be expected to occur but at higher total bubble surface areas / ultrasonic intensities. Since this is not seen from figure 5.5 it can be assumed that the process was surface area limited within the range of intensities employed.

5.2.2: 515 kHz degradations

To examine the effect of a change of the ultrasound frequency on the intensity effect found above the same experiments were performed using 515 kHz ultrasound. Direct comparison of the two systems is difficult due to the fact that the two reactors used differ in geometry however some deductions can be made.

5.2.2a: Degradation of 100 µg L^{-1} DBP solutions

The effect of varying the ultrasonic intensity was performed using only 100 µg L^{-1} solutions of DBP. The reason for this was that the above work on 10 mg L^{-1} was less relevant and had less importance to the context of this work. The data from these experiments is shown in figure 5.8 below.

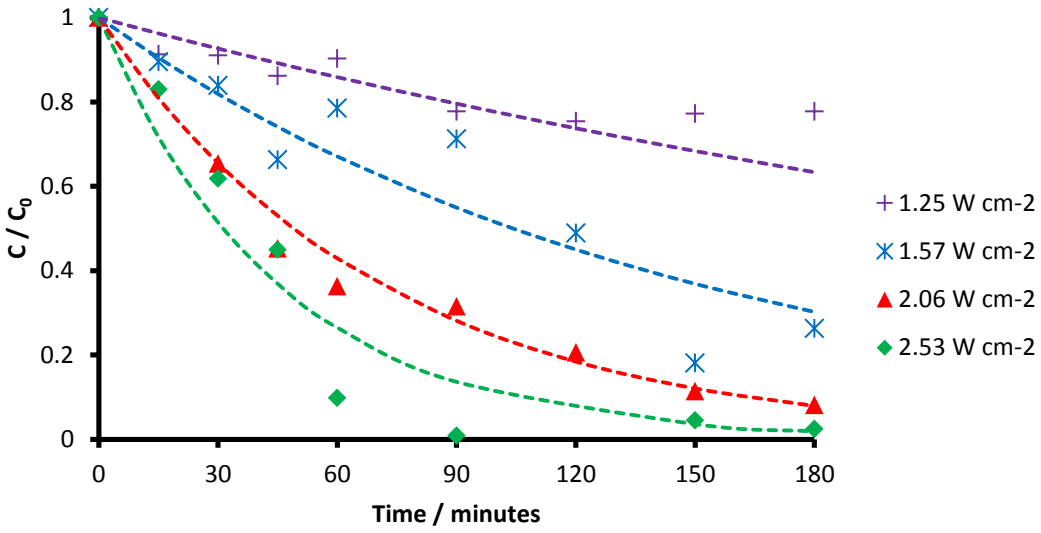

Figure 5.8: Degradations of 100 µg L^{-1} DBP solutions at differing ultrasonic intensities (515 kHz). Degradations were performed under argon and at a temperature of 18±2°C.

A plot of ultrasonic intensity verses rate constant is shown below in figure 5.9 and a plot of initial rate verses ultrasonic intensity is shown in figure 5.10. As with 20 kHz degradations a linear increase of rate constant is seen. From regression of the best fit line shown an apparent intensity threshold of 1.11 W cm^{-2} exists for degradation to occur.

In contrast with experiments using 20 kHz ultrasound there is no plateauing of degradation rate with ultrasonic intensity, which increases linearly. This can be attributed to the much lower intensities being used in the 515 kHz system. This implies that there is either a smaller bubble population in solution when 515 kHz ultrasound is used or that there is more efficient micro-scale mixing if the bubble population size is assumed to be similar.

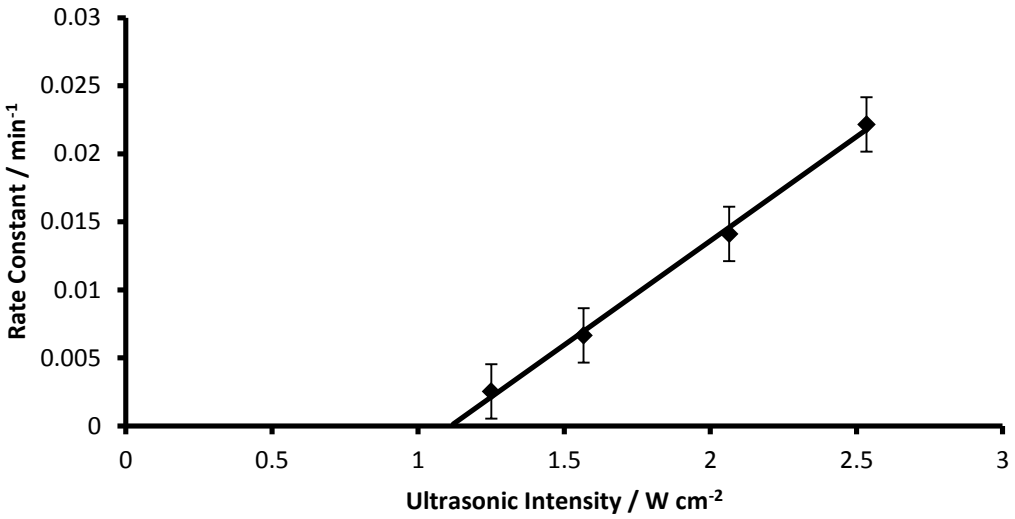

Figure 5.9: The effect of intensity on the rate constants calculated from data in figure 5.8. Error bars are representative of instrumental error of the mass spectrometry system used

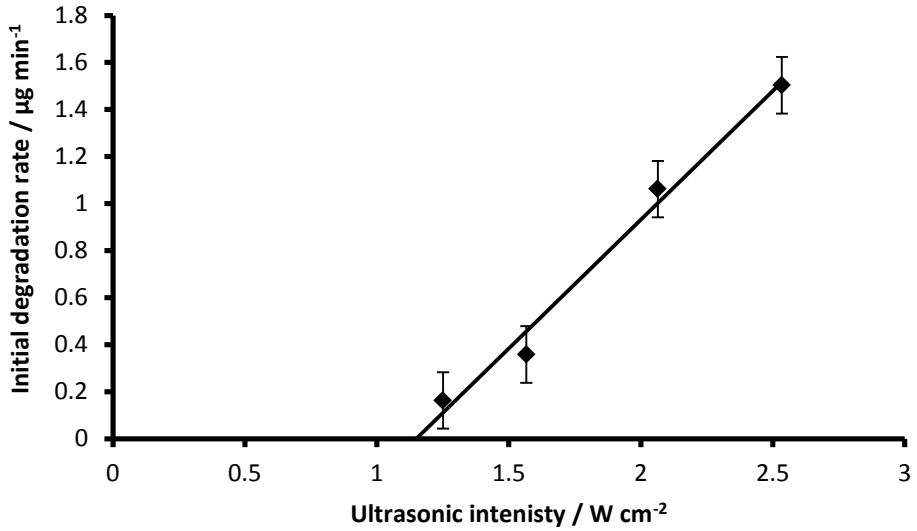

Figure 5.10: Variation of degradation rate with increasing ultrasonic intensity

Given the intensity is much lower in the 515 kHz system due to its' larger radiating surface, the bubble population was assumed to be lower discounting the possibility of more efficient mixing. From the best fit line shown an apparent intensity threshold of 1.14 W cm^{-2} exists which is in agreement with that calculated from the rate constant data. The fact that this threshold appears to

be lower for 515 kHz degradations suggests that it is not a cavitation threshold, since cavitation is known to be harder to induce as the frequency of the ultrasound employed is increased[6].

Most likely, it is a threshold at which there are sufficient OH radicals produced to effect a measureable degradation of DBP. This would explain why this threshold is higher for the 20 kHz systems since all other factors being the same higher frequency systems can be expected to produce a higher radical yield. This hypothesis also explains why the threshold is higher when starting with solutions of higher initial DBP concentration as when [DBP] >> [·OH] the amount of DBP needed to be degraded to be "noticeable" would be higher.

5.3: Changing the gas dissolved in solution

The gas dissolved in a solvent be it aqueous, organic, ionic liquid or otherwise has a profound impact on the violence of collapse of cavitation microbubbles. Changing the gas content of a solution will therefore affect the efficiency and nature of any chemistry performed in that solution *via* the use of ultrasound [7-9]. In the context of DBP degradation, it was expected that changing the dissolved gas would affect both the rate of DBP degradation and also, possibly, the products formed by the sonolysis of DBP. The investigation of the latter is discussed in chapter 6, and the former is explored below.

Experiments were performed using 10 mg L^{-1} DBP solutions and then using 100 µg L^{-1} DBP solutions. The gases employed were air, argon, carbon dioxide, nitrogen and oxygen. Studies were performed using 20 kHz and 515 kHz frequency ultrasound. For this subsection all the data will first be presented and described, a discussion then follows.

5.3.1: 20 kHz degradations

5.3.1a: Sonolysis of 10 mg L^{-1} DBP solutions

Figure 5.11 shows the effect of changing the dissolved gas on the degradation of DBP. It can be seen that altering the dissolved gas had a massive effect on DBP degradation. The experiments performed using air and argon both degraded around 78% of the initial DBP loading. Sonication under oxygen degraded 39% of the initial loading, while dissolving nitrogen lead to 22% degradation of DBP. No degradation occurred when carbon dioxide was dissolved into solution.

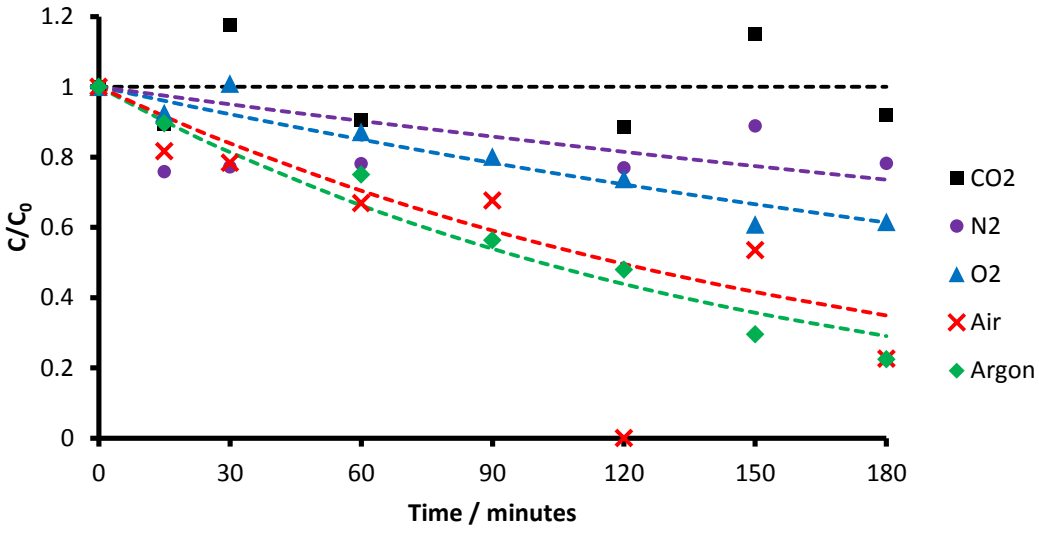

Figure 5.11: The effect of changing the gas dissolved in 10 mg L^{-1} DBP solutions. An ultrasonic intensity of 12.1 W cm^{-2} was used. The temperature was controlled at 18 ±2°C.

Table 5.1 shows the calculated rate constants and initial degradation rates for the above experiments along with thermodynamic data for the gases employed. It was found that neither the polytrophic ratio, solubility in water nor the thermal conductivity of the gases nor a simple transform of the three could explain the ordering of rates seen in table 5.1.

Gas employed	Polytropic ratio[10]	Thermal conductivity[11] / mW m^{-1} K^{-1}	Solubility in H_2O[10] / Molar	First order rate constant / min^{-1}	Initial degradation rate / µg min^{-1}
Argon	1.66	17.9	0.0180	0.0069	40.1
Air	1.40	26.2		0.0059	43.0
Oxygen	1.39	26.3	0.0176	0.0027	16.8
Nitrogen	1.40	26.0	0.0194	0.0017	12.1
Carbon Dioxide	1.30	16.8	0.0181	-	-

Table 5.1: Thermodynamic and degradation rate information for degradations using differing gases described in figure 5.11

5.3.1b: Sonolysis of 100 µg L^{-1} DBP solutions

The experiment was then repeated using 100 µg L^{-1} solutions of DBP. The results from these sonolyses are shown in figure 5.12. From figure 5.12 it can be seen that changing the DBP concentration had two effects. Firstly the degradation rate constants and therefore extent of degradation were increased when degrading the more dilute solutions of DBP. The second effect is that there is a slight change in the ordering of the reactivity resulting from changing the dissolved gas.

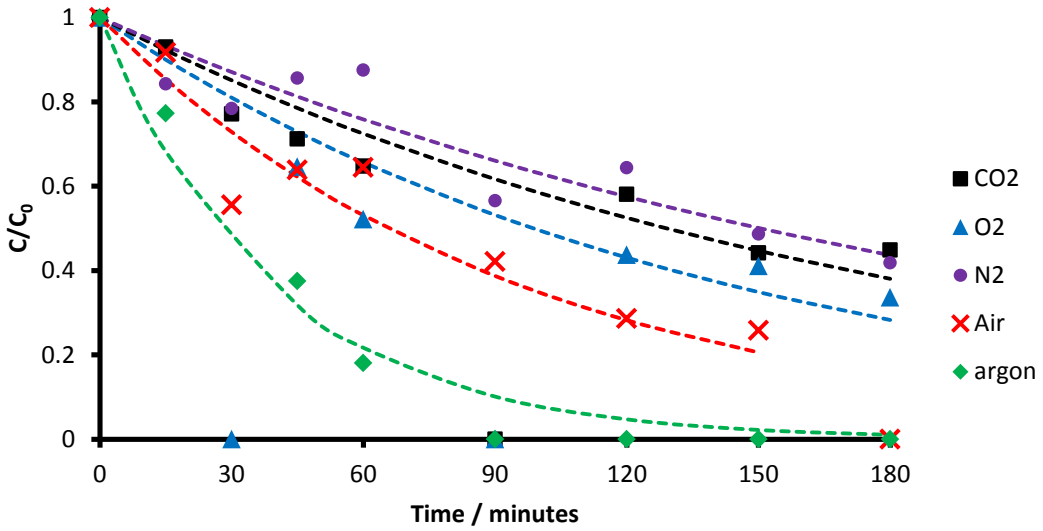

Figure 5.12: Effect of changing the dissolved gas. Degradations were performed using 20 kHz ultrasound, 100 µg L^{-1} DBP solutions and an ultrasonic intensity of 12.1 W cm^{-2}. The temperature was controlled at 18±2°C.

The difference between the reaction rates of degradations using nitrogen and carbon dioxide is reduced when degrading the more dilute solutions. When degrading 100 µg L^{-1} solutions the reactions proceed similarly when using these two gases and this is reflected in the rate constants calculated from the data. These constants along with the calculated initial rates are shown in table 5.2.

For the 10 mg L^{-1} experiments the initial rate of degradation increased along the series $CO_2 < N_2 < O_2 <$ Argon < Air. For 100 µg L^{-1} experiments this series became $N_2 < CO_2 < O_2 <$ Air < Argon.

Similarly the series of rate constants are Argon > Air > O_2 > N_2 > CO_2 for 10 mg L^{-1} DBP experiments and Argon > Air > Oxygen > CO_2 > N_2 for 100 µg L^{-1} DBP experiments.

Gas	Rate Constant / min^{-1}	Initial rate of degradation / $\mu g\ min^{-1}$
Argon	0.0255	1.3649
Air	0.0105	0.5922
Oxygen	0.0070	0.7969
Carbon Dioxide	0.0054	0.5872
Nitrogen	0.0046	0.2070

Table 5.2: Data for degradations shown in figure 4.12

5.3.2: 515 kHz driven degradations

Using 515 kHz ultrasound 10 mg L^{-1} and 100 µg L^{-1} solutions of DBP were degraded using the same gases as for the work using 20 kHz ultrasound.

Sonolyses of 10 mg L^{-1} solutions of DBP

Figure 5.13 shows the degradation plots produced from experiments using 10 mg L^{-1} DBP solutions. It can be seen that by far the most effective gas is now oxygen with argon and air being very different in the degradation rate constants they give rise to. Nitrogen is still more effective than CO_2 however. These rate constants along with the initial rates of degradations are described in table 5.3.

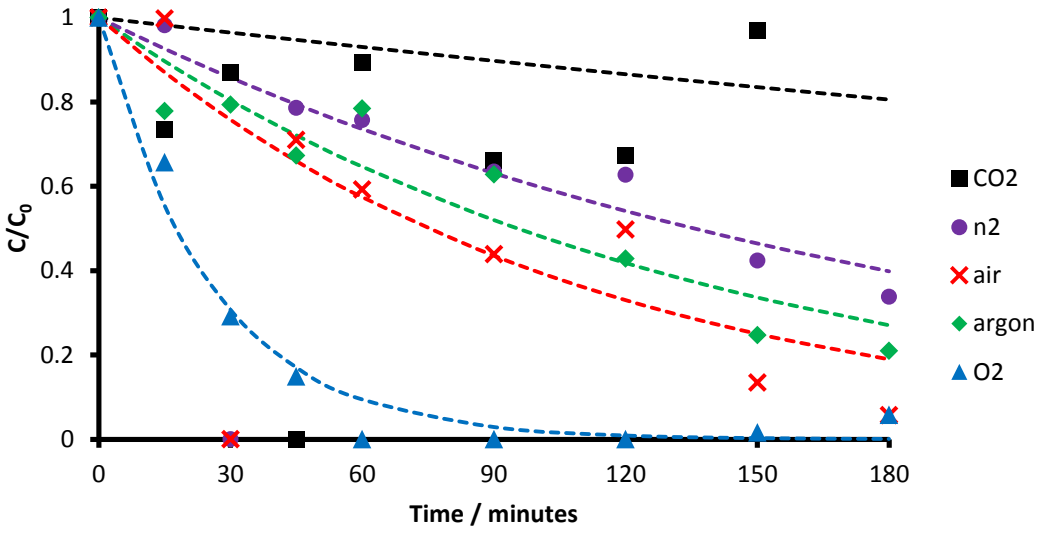

Figure 5.13: Degradations of 10 mg L^{-1} DBP solutions with different dissolved gas contents. Degradations were performed using 515 kHz ultrasound at an intensity of 2.5 W cm^{-2}. The temperature was controlled to be 18±2°C.

Dissolved gas	Rate constant / min^{-1}	Initial degradation rate / μg min^{-1}
Oxygen	0.0393	150.9
Argon	0.0073	35.9
Air	0.0090	68.0
Nitrogen	0.0051	40.5
Carbon Dioxide	0.0012	17.7

Table 5.3: Rate data for degradations shown in figure 4.13.

The apparent initial degradation rates are much greater for the 515 kHz system than for the 20 kHz system. The initial rate of the degradation employing oxygen gas was 9 times faster using 515 kHz than 20 kHz ultrasound. The rates for argon infused degradations were much the same within a 10% boundary. Air showed a 50% increase in rate whereas nitrogen is four times as effective when using 515 kHz ultrasound. Nitrogen is also just as effective using 515 kHz ultrasound as using argon with 20 kHz ultrasound. Finally, CO_2 infused

solutions degraded much more effectively even at this high concentration of DBP. This is in contrast to using 20 kHz ultrasound where no degradation occurred at all for a similar experiment.

Sonolyses of 100 µg L^{-1} solutions of DBP

Figure 5.14 shows the data from experiments using 100 µg L^{-1} solutions of DBP. Compared to the experiment above using 10 mg L^{-1} solutions, the rates of degradation are much more similar between the gases used as described in table 5.4.

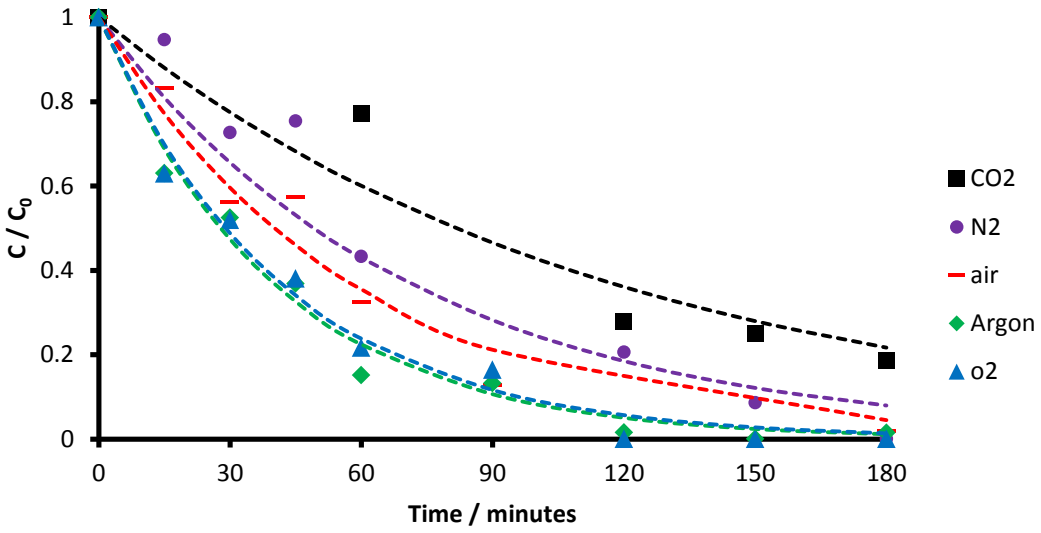

Figure 5.14: Degradations of 100 µg L^{-1} DBP solutions with different dissolved gas contents. Degradations were performed using 515 kHz ultrasound at an intensity of 2.5 W cm^{-2}. The temperature was controlled to be 18±2°C.

As with 20 kHz experiments the initial degradation rate is much higher for the higher concentration solutions of DBP. Interestingly the rate constants of both 10 mg L^{-1} and 100 µg L^{-1} solution experiments are of similar magnitude, possibly implying that the rate of degradations using 515 kHz ultrasound are less sensitive overall to the initial DBP concentration than those using 20 kHz ultrasound.

For 10 mg L^{-1} experiments the rate constants increase along the series $CO_2 < N_2 <$ Air $< Ar << O_2$. For degradations using 100 µg L^{-1} DBP solutions the rate constants decrease along the series $Ar > O_2 >$ Air $> N_2 > CO_2$.

Gas	Rate Constant / min^{-1}	Initial degradation rate / µg min^{-1}
Oxygen	0.0172	1.305779
Argon	0.0248	1.414706
Air	0.0239	1.174547
Nitrogen	0.0140	0.944856
Carbon Dioxide	0.0084	0.281667

Table 5.4: Kinetic information for degradations of 100 µg L^{-1} DBP solutions using 515 kHz ultrasound

Similarly the initial rates of degradation increase along the series $CO_2 < N_2 <$ Argon < Air << O_2 for 10 mg L^{-1} DBP solutions and $CO_2 < N_2 <$ <Air < O_2 < Ar for 100 µg L^{-1} DBP solutions.

Again it was found that the rate of degradation did not depend on a single thermodynamic property of the gases used nor a simple transform.

4.3.3: Discussion

The differing degradation rates of DBP brought about by changing the dissolved gas content is a measure of two factors: the total amount of radicals expelled from the bubble after its collapse and also the violence of the collapse itself. Each gas shall now be considered in turn and the reactivity seen in sections 5.3.1 and 5.3.2 will be explained.

CO_2

The ineffectiveness of degradation of CO_2 purged solutions in all experiments can be simply explained with reference to its low polytropic ratio value. It is the lowest of the gases employed and so the heat generated upon collapse is much lower than with the other gases used. This means much fewer •OH radicals are

formed from water hydrolysis in CO_2 – water vapour filled bubbles and so the degradation of DBP is slow for 100 µg L^{-1} solutions and immeasurably low for 10 mg L^{-1} solutions.

Argon

Inversely to the case for carbon dioxide, argon has the highest polytropic ratio of the gases employed and so the heat of collapse is high. This means that a large amount of •OH radicals are formed from argon –water vapour filled bubbles in all experiments and so the degradations are always effective.

Nitrogen

The sluggish degradations effected by nitrogen filled bubbles were initially a surprise when considering the fact that it has a quite high polytropic ratio value. From this value it would be expected that the heat upon bubble collapse would be quite high leading to a large amount of water lysis into radicals and effecting a fast degradation of DBP. The reason for the sluggish reaction rates in all reactions is due to the chemistry which can occur between nitrogen and the •OH radical.

For bubbles driven by low frequency ultrasound such as the case for the 20 kHz reactions the bubble wall is known to collapse in 10^{-5}s[6]. According to Margulis the lifetime of the OH radical is of the order of 10^{-6} seconds[12]. Therefore in 20 kHz systems there is enough time during bubble collapse for intra-bubble chemistry to occur before the contents of the bubble is ejected into solution. For bubbles driven by high frequency ultrasound such as in the 515 kHz systems, the time for collapse is roughly 4 x 10^{-7} seconds, 10 times faster than the proposed lifetime of the radical species initially generated by water sonolysis. This means that for 515 kHz systems there is much less time for intrabubble chemistry to occur.

This means that for the two systems studied in 515 kHz driven degradations, radical attack is likely to occur mainly by primary radical species from the sonolysis of water. For 20 kHz driven degradations, the radicals and reactive species which initiate attack on DBP will be those resulting from intrabubble

chemistry between the initially formed •OH radicals and any radicals and molecules present in the gas/vapour content of the collapsing bubble.

Unlike argon, despite the nitrogen triple bond being quite strong and typically inert, nitrogen is known to undergo a range of chemistry with the •OH radical at high temperatures and pressures. Misik *et al* collected together the rate information for 46 reactions which occur from the sonolysis of nitrogen in a water vapour – nitrogen filled bubble[13] From examination of these reactions it can be seen that although some reactions involve the formation of reactive species such as ·N, ·NO, $\cdot NO_2$ and O: and H_2O_2, most of the reactions result in the formation of unreactive species such as N_2, NH, HNO_2, HNO_3, N_2O and N_2O_3. It can also be noticed that for many of the reactive species formed that further reactions exist which convert these reactive species into inactive ones.

Therefore nitrogen acts mainly as a radical scavenger and so the degradation of DBP in nitrogen purged solutions is very slow compared to oxygen with which it shares similar physical properties (of the ones considered in table 5.1).

The proposal that less intrabubble chemistry occurs for 515 kHz ultrasound can be supported by noticing that nitrogen retarded the degradation of DBP to a greater amount when using 20 kHz ultrasound than when using 515 kHz ultrasound. Since there is less time for •OH radical scavenging chemistry to occur during bubble collapse driven by 515 kHz ultrasound the initially formed •OH radicals are scavenged less. These then are expelled into the bubble interfacial region where they react with the DBP present there.

Oxygen

Conversely to nitrogen, oxygen was found to effect very efficient degradations when using 515 kHz ultrasound and reasonable degradations when using 20 kHz ultrasound. The oxygen – oxygen double bond is readily cleaved in conditions within a collapsing bubble driven by ultrasound. As such, a mixture of chemistries occur some of which generate reactive species such as oxygen atoms and peroxides, and some of which result in the formation of additional ·OH radicals. The rate information for several of these reactions are given in scheme 5.1.

$O_2 \rightarrow 2O$: ($k = 3.20 \times 10^{-11}$ cm^3 $molecule^{-1}$ s^{-1} @ 5000 K)[14]

$O_2 + H\cdot \rightarrow \cdot OOH$ ($k = 9.92 \times 10^{-17}$ cm^3 $molecule^{-1}$ s^{-1} @ 2000 k)[15]

$O_2 + \cdot OH \rightarrow \cdot OOH + O$: k = 2.6 x 10-15 cm3 molecule-1 s-1 @ 2100 K)[16]

O: + H· → ·OH (k = 7.11 x10-[17] cm3 molecule-1 s-1 @ 3700 K)[17]

O: + $H_2O \rightarrow 2\ \cdot OH$ ($k = 6.37 \times 10^{-12}$ cm3 molecule-1 s-1 @ 2500K)[18]

O: + ·OH → ·OOH (no rate information available)

O: + $O_2 \rightarrow \cdot O_3$ ($k = 5.2 \times 10^{-12}$ cm3 molecule-1 s-1 @ 2100 K)[19]

Scheme 5.1: The reactions of oxygen with the OH radical

The rates of all these reactions are much faster than the collapse time of either 20 kHz or 515 kHz driven bubbles. Therefore during the collapse period a large amount of these reactive species can be expected to be produced. For 20 kHz ultrasound driven bubbles there is also sufficient time for the recombination of most of these radicals and so much of the oxidative strength is lost once the bubble contents is expelled into the bubble interfacial region. Since the collapse time is shorter for 515 kHz driven bubbles there is much less radical recombination and more reactive species are expelled from the bubble. This explains why oxygen does not affect as effective degradations when using 20 kHz ultrasound as when using 515 kHz ultrasound. It also explains why, for 515 kHz systems, oxygen effects the fastest degradations of DBP.

Air

Since air is 78% nitrogen and 21% oxygen, it is likely that the intrabubble chemistry which occurs is likely to be a combination of the two sets of chemistry already described for these gases. The mixture of N_2 and O_2 will exhibit a very complex set of chemistries as the chemical pathways of both gas's sonolysis will be available. Typically however, as described above, O_2 will tend to increase the •OH radical yield whilst N_2 will tend to reduce it and form unreactive by products. The overall effect of the two mixed along with the small

amount of argon also present cannot easily be estimated and, likely, has to be deduced from experiment.

Therefore from the data presented it can be seen that air generally affects quite efficient degradations. For 20 kHz driven experiments, purging the solution with air leads to faster degradations than with either nitrogen or oxygen. From this it can be deduced that the addition of 21% oxygen with 78% nitrogen is overall beneficial to the degradation rate and that the extra reactive species produced by the lysis of this oxygen is not entirely scavenged by the nitrogen present in the bubbles cores. For 515 kHz driven degradations air still leads to more effective degradations of DBP than nitrogen but is now less effective than oxygen. Since the bubble would contain more nitrogen than oxygen it can be concluded that the initial radical and reactive species yield is lower for the air filled bubbles than the oxygen filled bubbles and so the reaction rate is slower. This observation leads to the conclusion that much of the radical concentration expelled comes from intrabubble chemistry for air-water filled bubbles.

Fitting the degradation rate

In section 5.3.1a it was mentioned that the degradation rate could not be rationalised by a single thermodynamic property of the gases employed. It was found however that the data for degradations using 100 μg L^{-1} DBP solutions could be fitted using a transform of two properties of the gases employed; their molar volume and their solubility in water.

Figure 5.15 shows a plot of DBP degradation rate versus the ratio of the solubility of the gas employed divided by the molar volume of the gas using the data from table 5.2. Due to the fact that air is not a pure gas but a mixture of several, it was excluded from this plot. This was also partly due to data of molar volume and solubility of air not being available, again due to the fact it is a mixture of several gases.

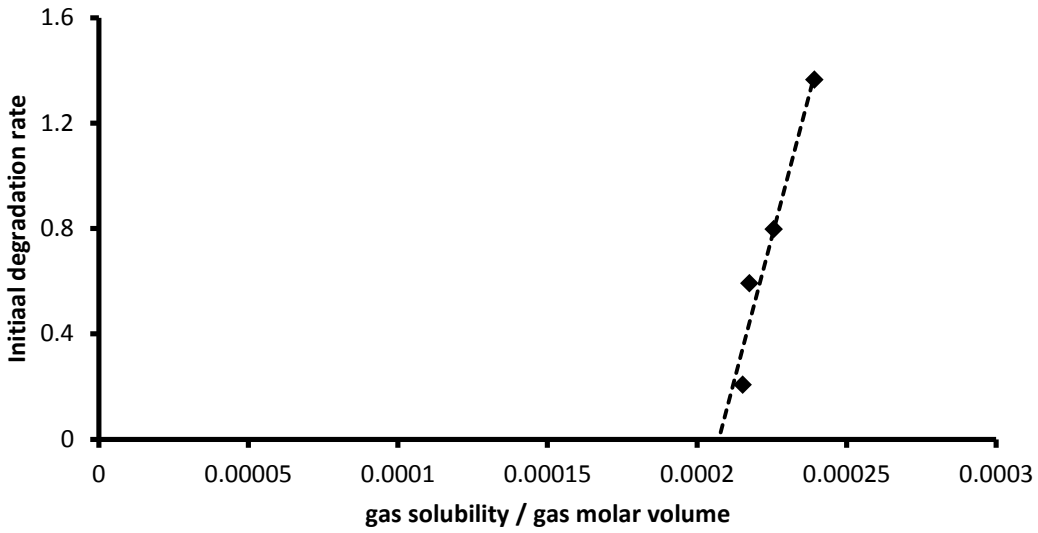

Figure 5.15: The relationship between the DBP degradation rate and the ratio of the solubility of the gas divided by its molar volume for degradations driven by 20 kHz ultrasound.

From figure 5.15. it can be seen that there is a good linear agreement between the degradation rate and the solubility divided by the molar volume for each gas. As the value of this ratio increases so does the degradation rate. The same can be seen to be true for the data from the 515 kHz degradations shown in figure 5.13, this relationship is shown in figure 5.16.

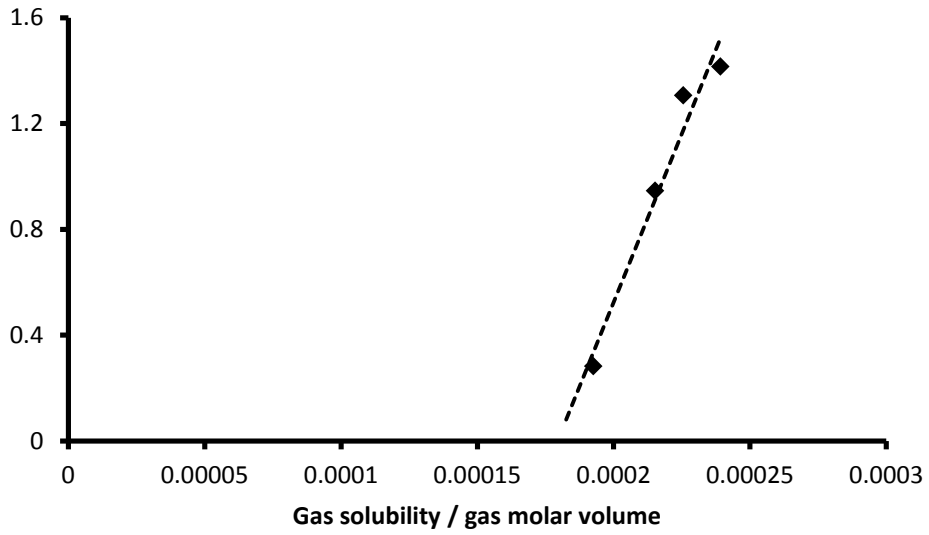

Figure 5.16: The relationship between the DBP degradation rate and the ratio of the solubility of the gas divided by its molar volume for degradations driven by 515 kHz ultrasound.

The proposed reason for the positive correlation between the degradation rate and the ratio (now referred to as α) is that α describes the amount of gas which escapes during a bubble collapse.

A bubble filled with more gas has its collapse cushioned more by its contents and so the violence of collapse is less. This leads to less heat is being created in the bubble core upon bubble collapse so less radicals are formed from water lysis and so less DBP is degraded. For polyatomics such as CO_2 O_2 and N_2 used in this study, energy of collapse is also consumed by endothermic chemical processes as well as energy loss due to rotational and vibrational excitement of the polyatomics[20].

From the positive correlation seen this means that as α increases in value there must be less gas inside the collapsing bubbles for the reasons explained next.

An increase in the solubility of the gas in water would mean that the gas favours a dissolved state more, so gas readily escapes the bubble during each collapse period. The molar volume can be used to describe the diffusion of the gas molecules across the bubble interface and so describes the concentration of gas that can escape within the finite time of collapse. Since the molar volume is

known to scale inversely with the diffusion of a molecule through a liquid[4], an increase in the molar volume of the gas would decrease its diffusion through water and thus its flux across the bubble interface. Therefore an increase in molar volume decreases the amount of gas that is able to escape the bubble by diffusion during collapse phases.

The correlation of degradation rate with α appears to be influenced by frequency since the gradient of the two lines found is different. This is most likely due to the increase in surface area to volume that occurs as bubbles get smaller at higher frequencies[21]. This hypothesis is supported by noticing that the gradient of the line is greater for 20 kHz degradations (m~43000), which would contain larger radius bubble populations, than for 515 kHz degradations (m ~ 25000), which would contain smaller bubble populations. However the correlation applies equally well to both frequencies used and so describes an effect which occurs in bubble dynamics regardless of the frequency used to drive the system i.e. the escape of gas contents during bubble collapse.

5.4: Varying the initial concentration of DBP

Comparison of the experiments in the previous two sections showed that the rate of sonolysis of DBP using fixed conditions decreased when a more dilute solution of DBP was used. To investigate this further, sonolyses of DBP solutions were performed using an ultrasonic intensity of 12.1 W cm^{-2} under argon, as these conditions lead to the fastest degradations when using 20 kHz ultrasound.

5.4.1: Degradations using 20 kHz ultrasound

The degradation curves produced from the degradations of 7 DBP solutions ranging in concentration between 10 mg L^{-1} and 20 μg L^{-1} are shown in figure 5.17.

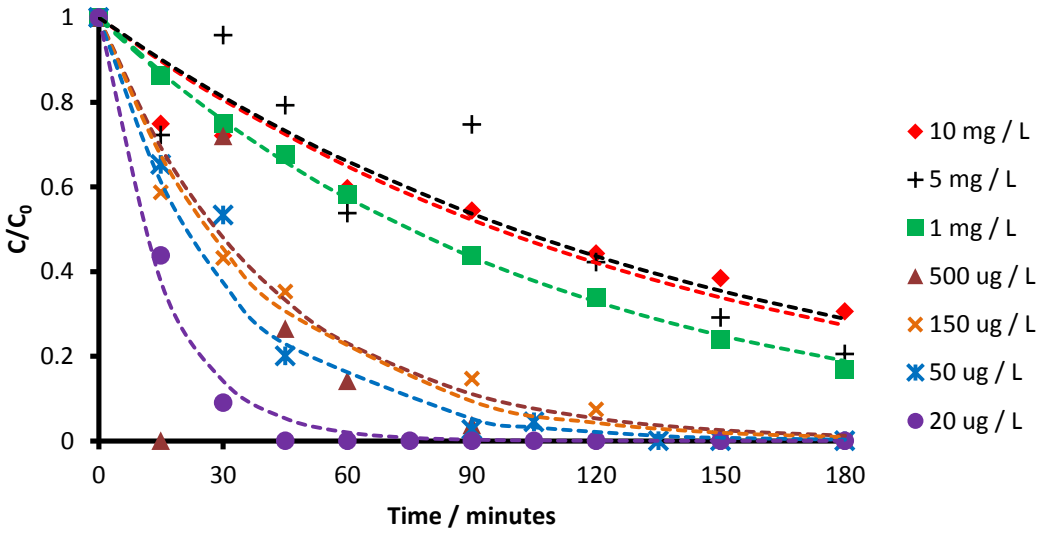

Figure 5.17: Degradations of DBP solutions with a wide range of initial concentrations. All degradations were performed using 20 kHz ultrasound with an intensity of 12.1 W cm^{-2} under an atmosphere of argon. The temperature of was controlled to be 18±2°C.

It is clear that the degradation rate constant increases with decreasing DBP concentration, although the reactions of several concentrations appear to be clumped into groups. 10 and 5 mg L^{-1} degradations behave similarly as do 50, 150, and 500 µg L^{-1} solutions. Figure 5.18 shows the pseudo first order linear reduction plots for the above data. The initial rates and rate constants for the degradations are shown in table 5.5.

Concentration of DBP / mg L^{-1}	Rate Constant / min^{-1}	Initial rate of degradation / mol L^{-1} min^{-1}
10.000	0.0072	2.4610E-08
5.000	0.0054	1.3832E-08
1.000	0.0093	2.5149E-09
0.500	0.0245	2.5747E-09
0.150	0.0263	6.3471E-10
0.050	0.0328	2.2454E-10
0.020	0.0652	1.1975E-10

Table 5.5: Kinetic data for degradations of DBP solutions with different initial concentrations.

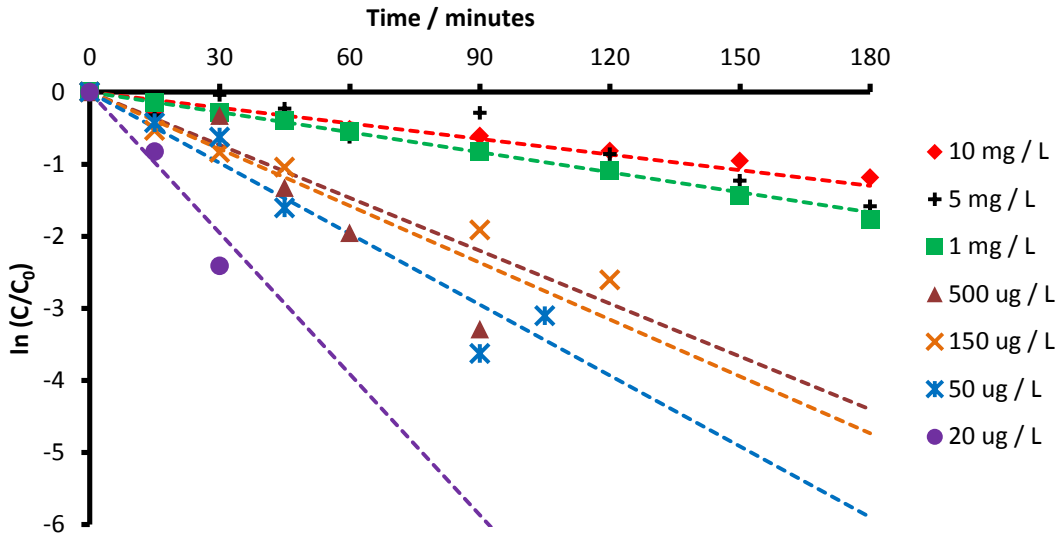

Figure 5.18: First order linear reduction plots for the DBP degradations in figure 5.17

From table 5.5 it can be seen that generally the rate constant increases with decreasing concentration and initial rate of degradation decreases with decreasing concentration. The rate constants for 10 mg L^{-1} DBP and 5 mg L^{-1} DBP concentration are contrary to this trend.

From figure 5.18 and the rate constants quoted, it is clear that the degradation of DBP cannot truly be a first order reaction, since the rate constant (the slope of the lines shown) varies with DBP concentration[22].

To examine the possible rate order of the reaction, the initial rates method of determining reaction orders was used[23]. In order to be able to use this method the likely rate equation for the degradation has to be found.

If we assume that the majority of degradation under the conditions used occurs via radical attack[1] then we can state that the rate of DBP degradation is likely to depend on ·OH radical concentration and also on DBP concentration. This statement leads to equation 5.2 being the rate equation.

$$v = k\,[DBP]^a\,[\cdot OH]^b \qquad (5.2)$$

Where *v* is the rate of degradation, *k* is the rate constant of the reaction and *a* and *b* are factors relating to the order of the reaction with respect to DBP and ·OH. The overall order of the reaction is the sum of *a* and *b*.

Over the course of the experiment it can be assumed that the overall rate of production of ·OH radicals is constant. This assumption has been widely used in work by other authors[4] and was found to be true by terephthalate dosimetry at the relevant power setting for experiments in water (see experimental section, chapter 4) and so will be assumed to apply to aqueous solutions of DBP.

This means that the rate equation becomes pseudo first order as expressed in equation 5.3.

$$v_{app} = k'[DBP]^a \qquad (5.3)$$

Where v_{app} is the apparent rate of degradation, *k'* is the pseudo first order rate constant. Using this equation, the plot of Log [DBP] against Log (initial rate of DBP degradation) should behave linearly with the slope of the line equalling the order of reaction with respect to DBP. The y intercept at x = 0 would then equal Log (k') and subsequently *k'* can be calculated. Such a plot is shown in figure 5.19 where initial rate means the rate of reaction for the first hour of the experiment only.

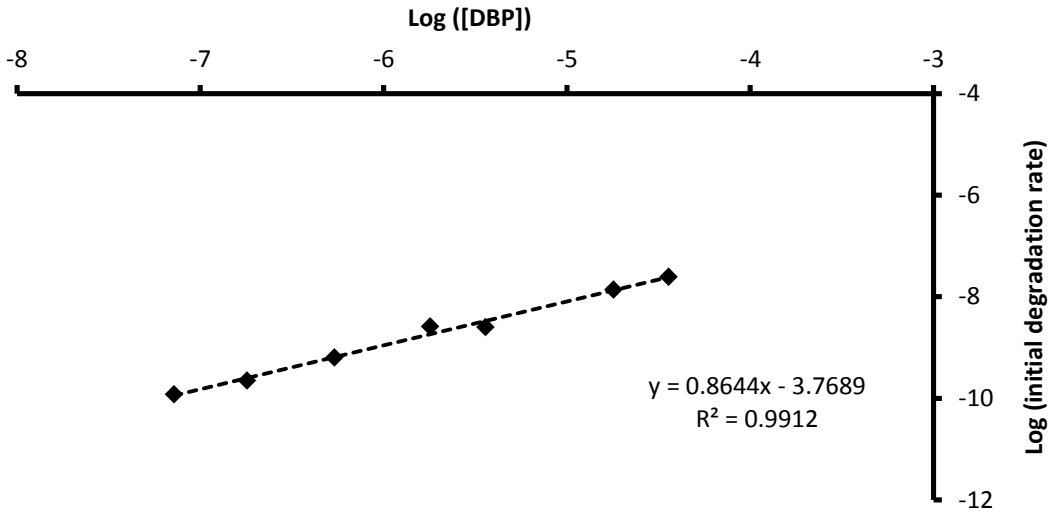

Figure 5.19: Initial rates study for degradations of DBP using 20 kHz ultrasound

Figure 5.19 shows that the plot produced is indeed linear. The apparent reaction order is 0.86 with respect to [DBP] as given by the gradient of the line shown with an apparent rate constant of 0.00017 min^{-1}.

5.4.2: Degradations using 515 kHz ultrasound

As with 20 kHz ultrasound, a series of solutions of different initial DBP concentration were prepared and degraded using 515 kHz ultrasound. An ultrasonic intensity of 2.53 W cm^{-2} was employed and the solutions were first purged with argon gas. The data produced are shown in figure 5.20.

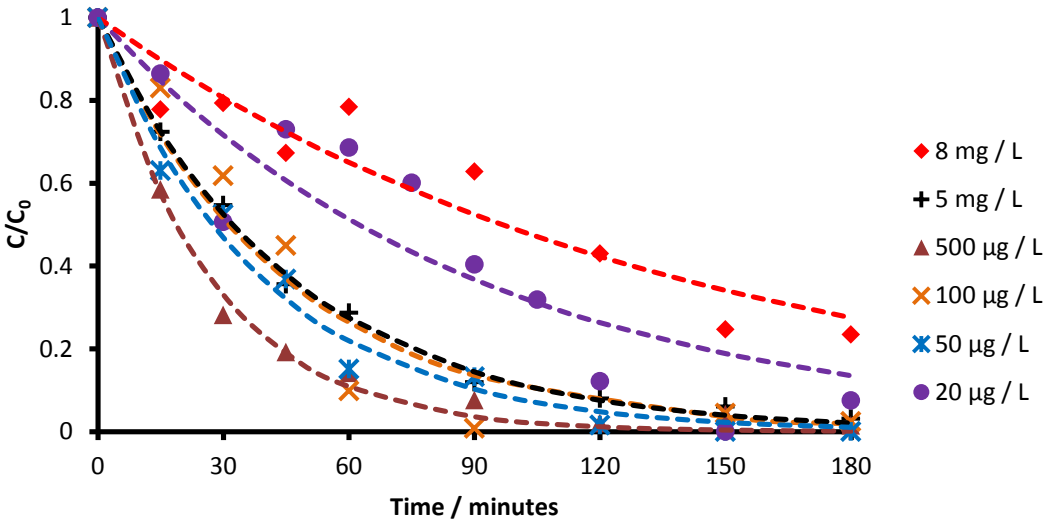

Figure 5.20: Degradations of DBP solutions of differing initial concentrations (515 kHz)

As with 20 kHz experiments it can be seen from figure 5.20 that degradation rate constants increase with decreasing initial DBP concentration, as seen by the increasing angle of the degradation curve arcs. In order to calculate the degradation rate constants, first order linear reduction plots of $\ln(C_i/C_0)$ verses time were produced as shown in figure 5.21. These rate constants are presented in table 5.7 along with the initial rates of the degradations.

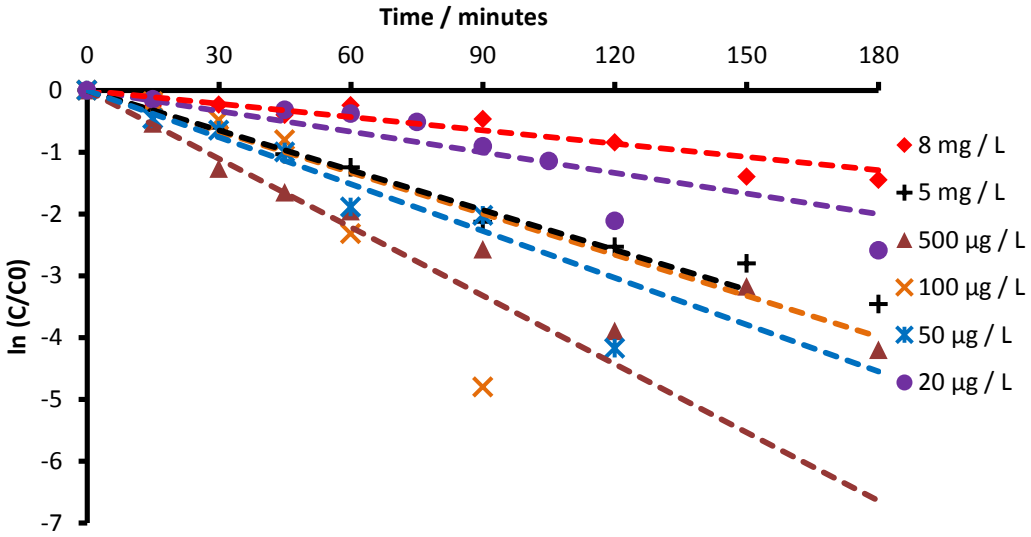

Figure 5.21: First order linear reduction plots of degradation on DBP solutions of varying concentration (515 kHz).

[DBP] / mg L^{-1}	First order rate constant / min^{-1}	Initial rate of degradation / mol L^{-1} min^{-1}
8.00	0.0072	1.0179E-08
5.00	0.0215	2.1376E-08
0.50	0.0369	2.5304E-09
0.10	0.0221	5.4489E-10
0.05	0.0297	2.9939E-10
0.02	0.0111	3.754E-11

Table 5.7: Kinetic data for degradations of DBP solutions with varying concentrations (515 kHz).

From table 5.7 it can be found that the initial rate of DBP degradation generally decreases with decreasing concentration of DBP. The rate of degradation for the 8 mg L^{-1} DBP solution bucks this trend however. The rate constants increase up to a point with increasing concentration with a maximum of 0.0369 min^{-1} at a DBP loading of 0.5 mg L^{-1}. Beyond this concentration the rate

constants calculated decrease with the value of k being similar at both the highest and lowest concentrations studied.

Using the same theory as previously a plot of Log (initial rate) *verses* Log ([DBP]) was produced as in shown in figure 5.22. In this plot the highest concentration studied was left out of the calculation, since it decreased erroneously.

From the equation shown for the best fit line in figure 5.22, a rate order of 1.09 was apparent with an apparent rate constant of 0.00379 min^{-1}. Both of these values were higher than those calculated for the 20 kHz degradation process

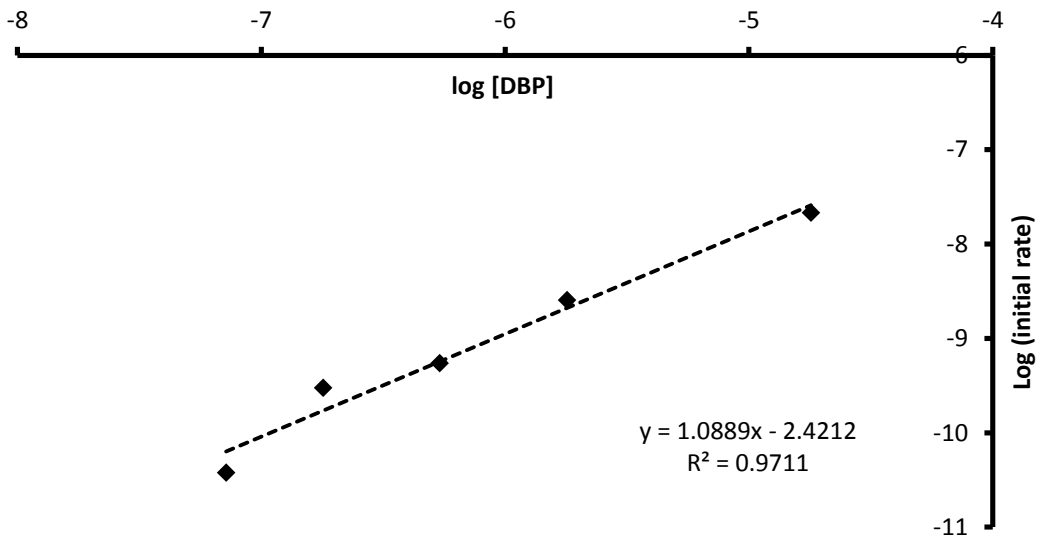

Figure 5.22: Log-Log plot for the calculation of rate order (515 kHz)

5.4.3: Modelling of the data using Langmuirian surface theory.

Since simple first order kinetics, although apparent due to a mathematical simplification of the system, do not adequately describe the chemical system of a molecule being destroyed on or near a bubble surface, several studies have tried to make use of Langmuirian kinetic models. These models draw analogies between the bubble interface and an infinite air-water flat surface. Since it is likely that DBP is degraded at the bubble interface (from its' log K_{ow} and lack of vapour pressure) it was decided to try and model the degradation rates above using a Langmurian model identical to that of Okitsu[24-26].

Okitsu *et al* proposed a simple model where the Langmuirian surface is the air/water interface and the surrounding interfacial region of a cavitation bubble. Their model made use of several assumptions in order to be able to use a Langmurian model: Firstly the rate of movement of the organic species into the bubble interfacial region, $r_{1,}$ is proportional to the concentration of the species in the bulk solution. Secondly, this rate also depends on the term (1-θ) where θ describes the ratio of species within the bubble interfacial region to that in the entire solution. Thirdly the rate of movement from the bubble interfacial region into the solution bulk, r_{-1}, depends on θ

These 3 assumptions can be mathematically expressed as equations 5.4 and 5.5, where *[C]* is the solution concentration of the organic species and the *k* terms are the rate constants for the adsorption and desorption processes. The development of the rest of the model relies on the assumption that the system approaches a steady state equilibrium where $r_1 = r_{-1}$. While this is probably not strictly true for cavitation bubbles which are in rapid motion and too short lived for their surroundings to reach equilibrium, this assumption has still lead to good fits of data by Okitsu and Serpone[27].

This assumption allows for equations 5.4 and 5.5. to be set equal to each other, allowing θ to be expressed in terms of k_1, k_{-1} and *[C]* as in equation 4.6, where the term $K = k_1/k_{-1}$.

$$r_1 = k_1[C](1-\theta) \tag{5.4}$$

$$r_{-1} = k_{-1}\theta \tag{5.5}$$

$$when, k_1[C](1-\theta) = k_{-1}\theta$$

$$\theta = \frac{K[C]}{1+K[C]} \tag{5.6}$$

Having defined how *θ* is related to the bulk solution and to the bubble interfacial region it is then assumed that *θ* is the dominant factor is deciding the rate of the decomposition/reaction of the species. In traditional Langmurian models θ is the number of free surface sites. Since bubbles do not have free chemical sites as a catalyst may do θ represents the amount of DBP already around the bubble divided by the maximum amount that theoretically could be i.e. the bulk concentration of DBP.

Making that assumption the rate of decomposition, *r*, can then be described as in equation 5.7, where *k* is the rate constant of the degradation reaction.

$$r = k\theta = \frac{kK[C]}{1+K[C]} \tag{5.7}$$

Having described the situation using a Langmurian model Okitsu linearised the model as in equation 5.8. This allows for a linear plot to be created from experimental information of the initial concentration and rates of degradation experiments. A plot of *1/r verses 1/c* should yield a linear plot from which *k* and *K* can be calculated. From such a plot *k = 1/intercept* and *K = intercept / slope*.

$$\frac{1}{r} = \frac{1}{kK}\cdot\frac{1}{C} + \frac{1}{k} \tag{5.8}$$

Additionally, Serpone *et al* also described a similar system which took into account the likelihood of reactions also occurring in the solution bulk[27]. Since DBP is much more hydrophobic than the majority of species previously studied by others, this was concluded not to happen. Most radicals produced by the collapse of ultrasonically driven bubbles will be assumed to have reacted with the DBP present around the bubble, so that insufficient concentrations arrive into the bulk solution to effect degradation.

Figure 5.23 shows the data from 20 kHz ultrasound degradations in figure 5.17 which is to be fitted to equation 5.8. Figure 5.24 shows the data as 1/r versus 1/c for which a very good linear fit was found. From this plot *k* was calculated to be 3.94 $x10^{-9}$ mol^{-1} L min and the Langmuir constant K was calculated to be 418507 M^{-1}. For this calculation the lowest concentration value i.e. the highest 1/C value was omitted as it was found to be erroneous compared to the other data, its value was much higher than the linear model predicted.

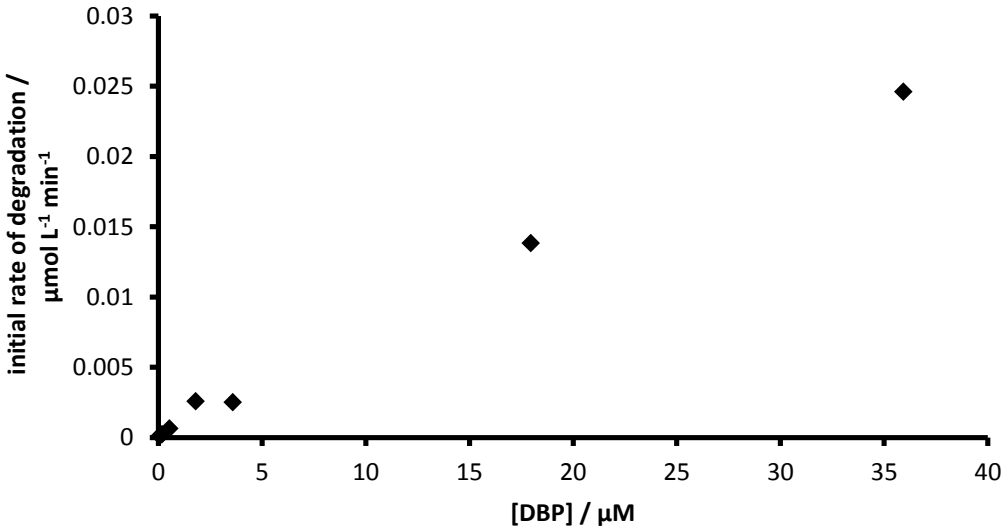

Figure 5.23: Data from 20 kHz DBP degradations to be fitted using a Langmuirian kinetic model.

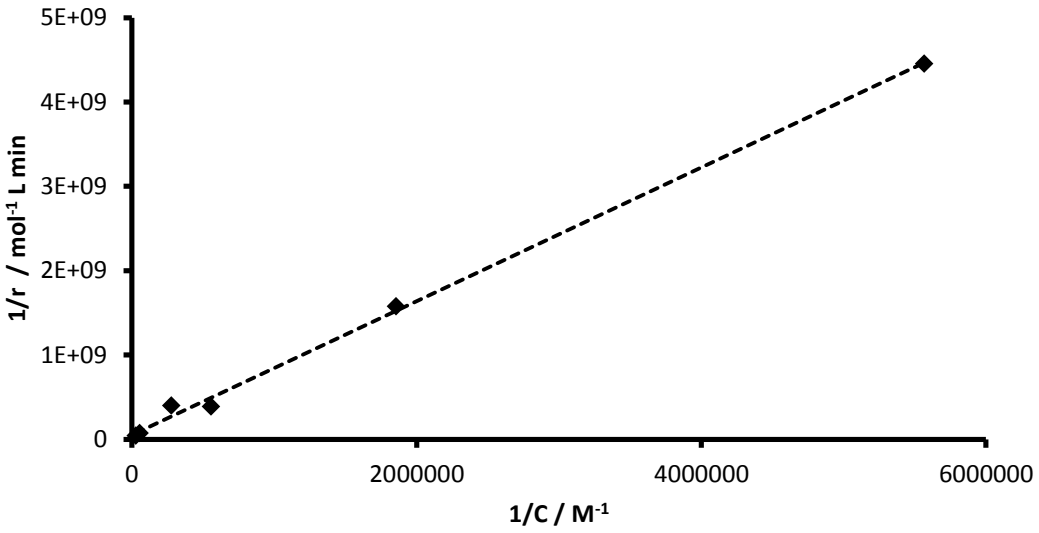

Figure 5.24: Plot used to determine *k* the rate constant and *K* the Langmuir constant for DBP degradations driven by 20 kHz ultrasound. The dashed line represents the line from which *k* and *K* were calculated.

This calculation process was repeated for the data from 515 kHz driven degradations in figure 5.21 and the same 1/r versus 1/C plot is shown in figure 5.25. From this plot k was calculated to be 5.64 x 10^{-9} mol^{-1} L min and K was calculated to be 296123 M^{-1}.

It was found that the linear fit was less good for the 515 kHz data and that again the lowest concentration data had to be omitted as its value of 1/r was much greater than the linear fit predicted.

It can be seen that the Langmuirian model fits the data well apart from at very low concentrations. The values of K are very much larger than the value Okitsu calculated for various azo dyes (K = 28,000-72,000 mol^{-1}) and for butyric acid (K = 11,000 mol^{-1}). This is not surprising when the hydrophobicity of these compounds is considered. Table 5.8 lists the octanol-water partition coefficients for the compounds previously fitted by others to Langmuirian models.

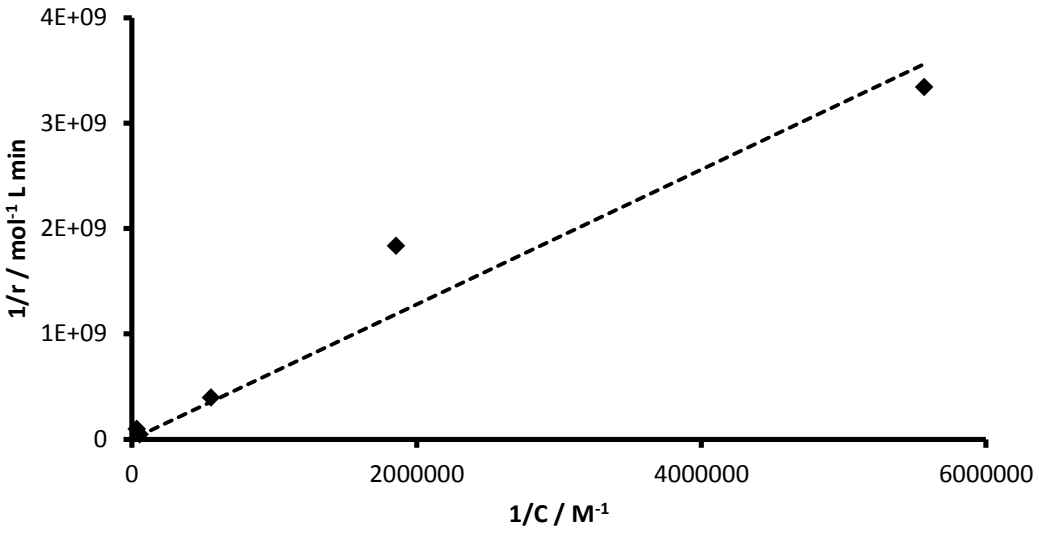

Figure 5.25: Plot used to determine *k* the rate constant and *K* the Langmuir constant for DBP degradations driven by 515 kHz ultrasound

Chemical Species Studied	Octanol Partion Coeffcient Value
Reactive red (azo dye)	0.92[28]
Butyric Acid	0.79[29]
Benzoic Acid	1.87[29]
Phenol	1.46[30]
4-*iso*-propyl phenol	2.8[31]
Rhodamine B	2.2[32]
Dibutyl phthalate	4.63[33]

Table 5.8: Chemicals previously modelled by Langmurian kinetics

DBP is much more hydrophobic than butyric acid and the azo dyes studied by Okitsu. Therefore it can be expected to partition to the bubble air-water interface much more than the compounds studied by Okitsu. This amount of partitioning is the real meaning of *K* as it represents the rate of absorption to the bubble interface divided by the rate from the bubble interface.

For species such as azo dyes and organic acids it would be expected from their hydrophobicity that a reasonable flow from the bubble interface would exist. This is not so obvious for DBP which is much more hydrophobic. From this it can be reasoned that the reason of *K* being comparatively large is that there is a quick rate of partition to the bubble interface (*k*) and a very slow or possibly non-existent rate of flow from the bubble interface (k_{-1}) to the bulk, leading to K (k/k_{-1}) being very large.

The reason for the value of *K* being lower for 515 kHz driven degradations is proposed to be due to the longer apparent bubble lifetimes. One of the reasons k_{-1} is small for 20 kHz driven degradations is that there is not much time for desorption from the bubble interface before bubble collapse since the type of cavitation can be expected to be transient. For the 515 kHz driven degradations stable cavitation is expected to occur and so there is more time for some desorption of DBP to occur. This makes k_{-1} larger. The values of *k* are likely to be similar for the two frequencies studied as it is mainly the bubble size and bubble lifetime which is affected by the change in frequency. This was found to be true for the value of k calculated above.

In summary the Langmuirian model of Okitsu successfully described the change of rate of degradation of DBP with concentration for both high and low frequencies of ultrasound. The values of *K* were much larger than those of other previously studied compounds and this was reasoned to be due to the net accumulation of more DBP than the other compounds on the bubble surface as a result of its comparatively high hydrophobicity. This was thought to occur due to a much slower rate of desorption as opposed to a faster rate of sorption.

One final use of k and K is that we can use them to calculate θ at any concentration. As mentioned before θ is thought by Okitsu to describe the amount of substance (in the present case DBP) present at the bubble interface compared to the total amount in solution. The author does not agree with this conclusion for the present work and surmises that it represents the amount of DBP present on the bubble interface compared to the maximum amount which could be adsorbed if all the bubble surface area was occupied.

5.4.4: Measuring the surface activity and surface excess of DBP

The high value of *K* showed that DBP was expected to accumulate significantly around bubble interfaces. This was also predicted from the hydrophobicity and low vapour pressure of DBP. It was decided to quantify this accumulation by measuring the change of the surface tension of bulk solutions of DBP with increasing solution concentration. This lead to the determination of the surface excess of DBP at any concentration, Γ_{DBP}.

The data from this experiment is shown in figure 5.26. It can be seen that the surface tension of DBP solutions decreased significantly with only micromolar amounts of DBP present at the air-water interface of the solution.

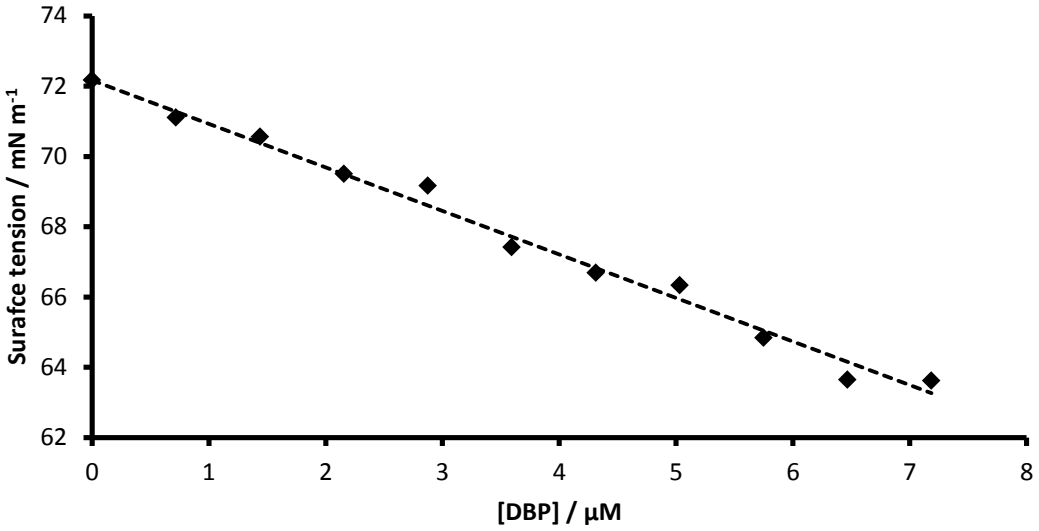

Figure 5.26: The reduction of surface tension of DBP solutions with increasing DBP bulk solution concentration

The surface excess was calculated by using the above data and the Gibbs-Duhem equation which is shown in equation 5.9.

$$\Gamma_{DBP} = -\frac{1}{RT}\frac{d\gamma}{d(\ln(C_{DBP})} \quad (5.9)$$

The accumulation of DBP at an air-water interface as measured by its surface excess is shown in figure 5.27. The surface excess of DBP was found to range between 1.0 x 10^{14} molecules cm^{-2} and 2.0 x10^{15} molecules cm^{-2} for the concentration range studied.

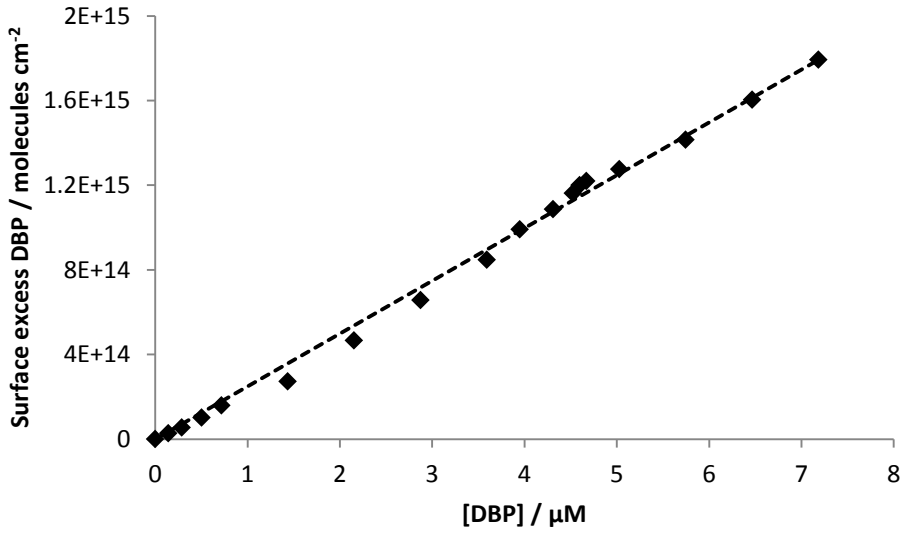

Figure 5.27: The increase in surface excess of DBP with increasing DBP bulk solution concentration

Within the context of ultrasound, sonochemistry and surface excesses of molecules on a bubble interface several species have already been studied. As a comparison Yang *et al* calculated the surface excess of octyl benzene sulfonic acid, a surfactant, as 1.9 x 10^{14} molecules cm^{-2} at the C.M.C point of OBS, 6.3 mM. Similarly, they also reported the surface excess of dodecyl benzene sulfonic acid to be 3.7 x 10^{14} molecules cm^{-2} at its C.M.C point, 1.2 mM.

Comparing these quantities to the surface excesses of DBP shown in figure 5.27 it can be seen that DBP is much more surface active than even these well known surfactants. The surface excess of DBP at the same quantities as the C.M.C. of OBS above would be expected to be 1.57 x 10^{18} molecules cm^{-2} assuming a continuation of the linear trend in figure 5.27. This is 4 orders of magnitude i.e. 10,000 times higher. Similarly for the C.M.C point concentration

of DBS a surface excess of DBP of 2.99 x 10^{17} is expected. This clearly illustrates how effectively DBP adsorbs to air-water interfaces due to its extreme hydrophobicity.

To show that the rate of DBP degradation is related to the surface excess of DBP at given concentrations the surface excesses for the concentrations shown in figures 5.18 and 5.21 were calculated. The rates of DBP degradation were then plotted against these surface excess values as in figure 5.28 for 20 kHz degradations and figure 5.29 for 515 kHz degradations.

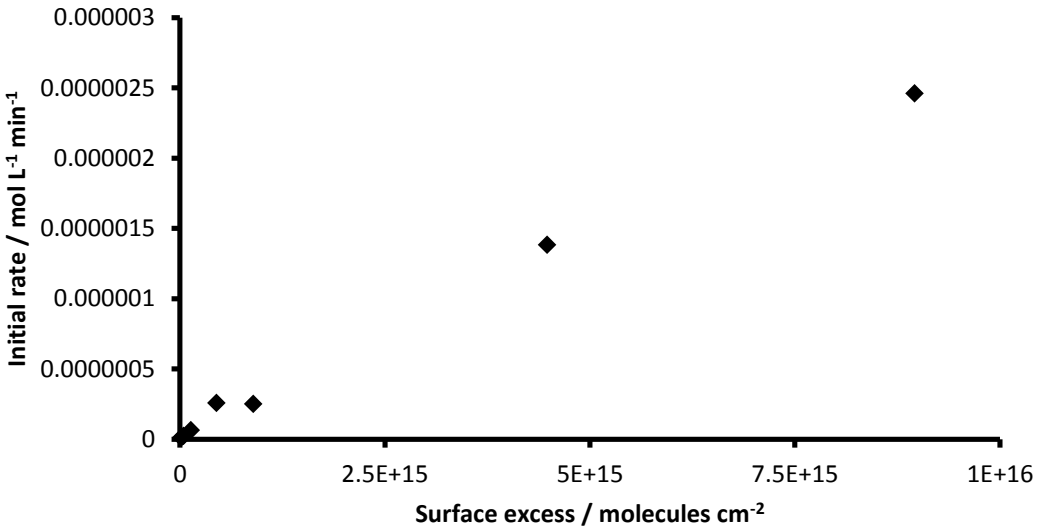

Figure 5.28: The relationship between surface excess and DBP degradation rate of 20 kHz driven degradations

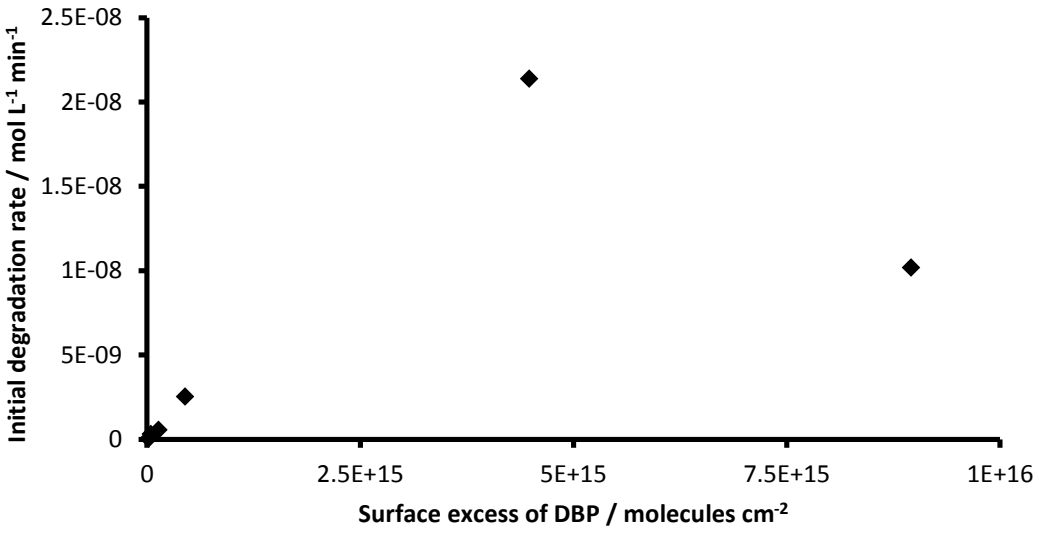

Figure 5.29: The relationship between surface excess and DBP degradation rate of 515 kHz driven degradations.

Again a good linear relationship between the two can be seen and shows that the rate of degradation of DBP relies on the amount of DBP adsorbed at the bubble air- water interface as measured as surface excesses.

5.5: Relating the rate of degradation of DBP to the ·OH radical yield

In the discussions of the above data, it had been assumed that the degradation of DBP occurred mainly due to attack by ·OH radicals. This finding is confirmed in chapter 6 from the degradation products found. This chapter however is about kinetic and rate information obtained from DBP degradations and it was thought necessary to be able to show this through such data as well.

In order to do so, figure 5.30 shows the data in figures 5.6 and 5.9 plotted on the same axis. Figure 5.31 shows the rate of ·OH radical output at each of the same intensity settings employed as calculated from terephthalate dosimetry. In both plots black diamonds represent 515 kHz data and black squares 20 kHz data.

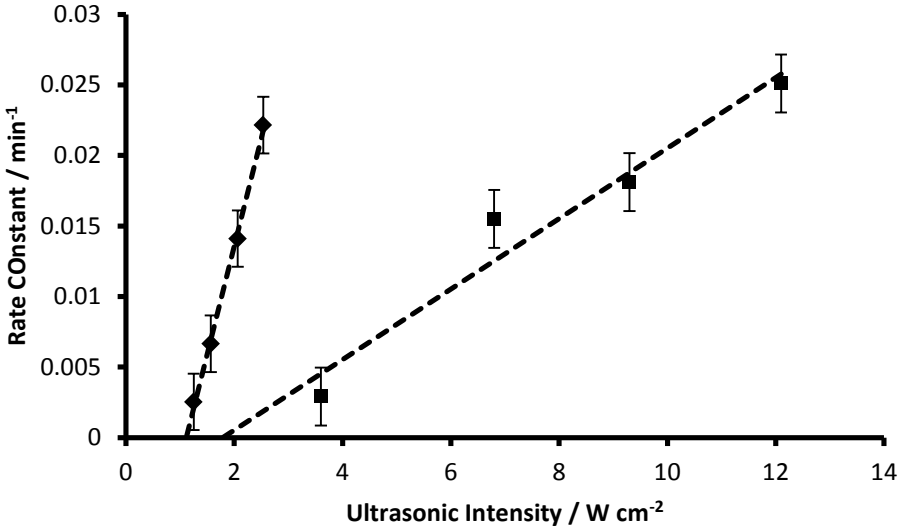

Figure 5.30: Rate constant information for 20 (black squares) and 515 kHz (black diamonds) ultrasound driven degradation experiments

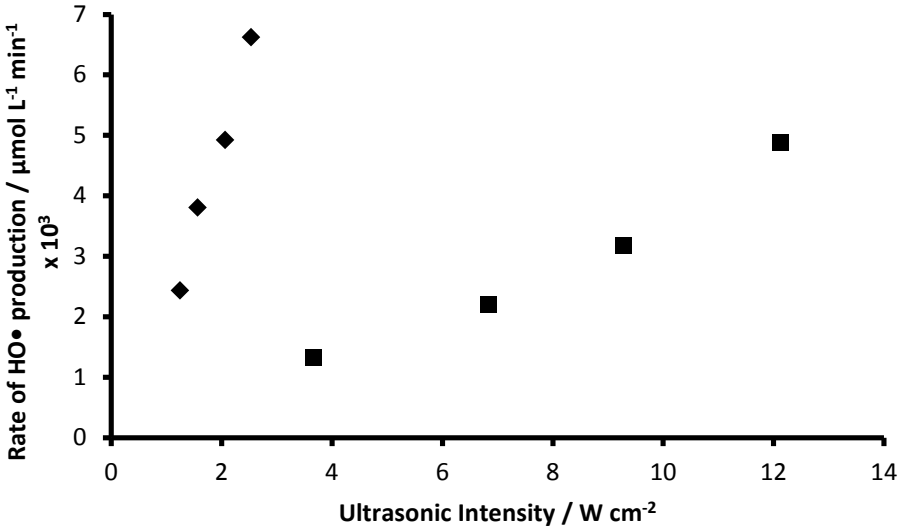

Figure 5.31: The increase in the rate of OH radical production with increasing ultrasonic intensity. Black diamonds represent data for 515 kHz ultrasound and black squares that for 20 kHz ultrasound.

From inspection of the two figures it can be seen that the shapes and gradients of the rate constants for DBP degradations and the rates of ·OH radical production are very similar for both frequencies studied. This similarity shows that it is the ·OH radical which primarily degrades the DBP present at the bubble wall interface.

It can also be seen from figure 5.30 and 5.31 that the intensity thresholds calculated earlier are not cavitation thresholds. At the intensities calculated previously (1.58 W cm^{-2} and 1.14 W cm^{-2} for 20 kHz and 515 kHz driven degradations respectively) it can be seen from figure 5.31 that some ·OH radicals should be formed. This is assuming that due to being a micromolecular solution DBP solutions should behave similarly to pure water. Therefore the thresholds in power are not cavitation thresholds but the thresholds intensity at which enough ·OH radicals are produced to effect a noticeable degradation of DBP.

From figure 5.31 ·OH radical production thresholds can be calculated. These intensities were calculated as 1.06 W cm^{-2} for the 20 kHz system and 0.43 W cm^{-2} for the 515 kHz system. From this it is clear that at the intensity thresholds mentioned in the previous paragraph that ·OH radicals should be produced at a rate of 0.22 µmol L^{-1} min^{-1} using the 20 kHz system and at a rate of 2.21 µmol L^{-1} min^{-1} when using the 515 kHz system. These data themselves suggest that a greater radical density is required to degrade DBP noticeably when using the 515 kHz system.

5.6: Addition of additives to DBP degradation experiments

This section discusses degradations performed on DBP solutions with the presence of additives known to affect the amount of ·OH radicals in solution. The first is hydrogen peroxide which is known to enhance the radical yield over time. The second is t-BuOH which is a well known radical scavenger. The experiments with hydrogen peroxide were performed with both 515 and 20 kHz ultrasound whereas the t-BuOH experiments were performed using 515 kHz ultrasound.

5.6.1: Addition of hydrogen peroxide

Hydrogen peroxide is a well known source of ·OH radicals when irradiated in solution with power ultrasound[34]. The peroxide bond is labile enough that in the presence of ultrasound the bond undergoes homolysis to form two equivalents of ·OH radicals per equivalent of hydrogen peroxide. These extra radicals can then aid the degradation of the contaminant in question, in this case DBP.

To determine whether H_2O_2 would be useful in the degradation of 100 µg L^{-1} DBP solutions had 5 mmol of H_2O_2 added prior to the degradation experiment. Since experiments were also to be relevant to the water processing industry degradations were performed under air. Figure 5.32 shows the data for 515 kHz ultrasound where the plot contains data of degradations both with and without ("plain") H_2O_2 performed under identical conditions.

From figure 4.30 it can be seen that the addition of H_2O_2 greatly enhanced the degradation of DBP which was degraded in 45 minutes. Without H_2O_2 the process took the full length of the experiment to achieve complete transformation of DBP to products. The rate constants calculated from the two best fit lines shown are 0.0215 min^{-1} for the "plain" experiment and 0.0698 min^{-1} for the experiment containing H_2O_2. This shows that the likelihood of a given DBP molecule degrading was more than three times more likely in the presence of 5 mmol H_2O_2 due to the increase in ·OH radical production due to hydrogen peroxide degradation. It is likely therefore that there was a *circa* three-fold

increase in ·OH radical production in the experiment. The initial degradation rate was calculated as 2.11 µg min^{-1}.

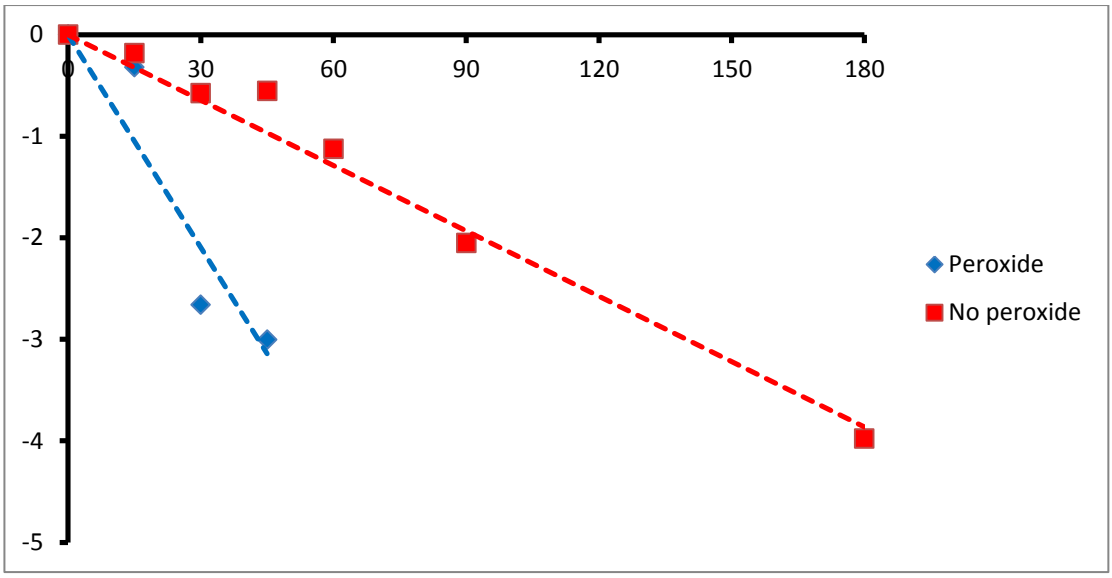

Figure 5.32: The degradation of DBP in the presence of H_2O_2 (515 kHz)

The same as above was performed again using 20 kHz ultrasound, the data for these is shown in figure 5.33. Again it can be seen that the degradation with the addition of peroxide is enhanced albeit by not as large a margin as for the 515 kHz experiment. The pseudo first order rate constants are 0.0096 min^{-1} for the experiment without peroxide and 0.0197 min^{-1} for the experiment with peroxide. The initial degradation rate was calculated as 0.61 µg min^{-1}, which is under 3 times of that of the 515 kHz reaction.

The reason for the enhancement not being as great can be explained by the process of radical recombination. As explained previously, the length of bubble collapse is longer for 20 kHz ultrasound driven bubbles than those driven by 515 kHz ultrasound. This means that there is more time for intrabubble chemistry when using 20 kHz ultrasound. Hence for 515 kHz ultrasound most of the ·OH radicals formed are able to attack DBP as intended. For 20 kHz ultrasound the enhancement is lessened by radicals recombining to form H_2O_2

or other products. This may then be converted back into ·OH radicals in the hot interfacial region but the effectiveness of the system is lessened.

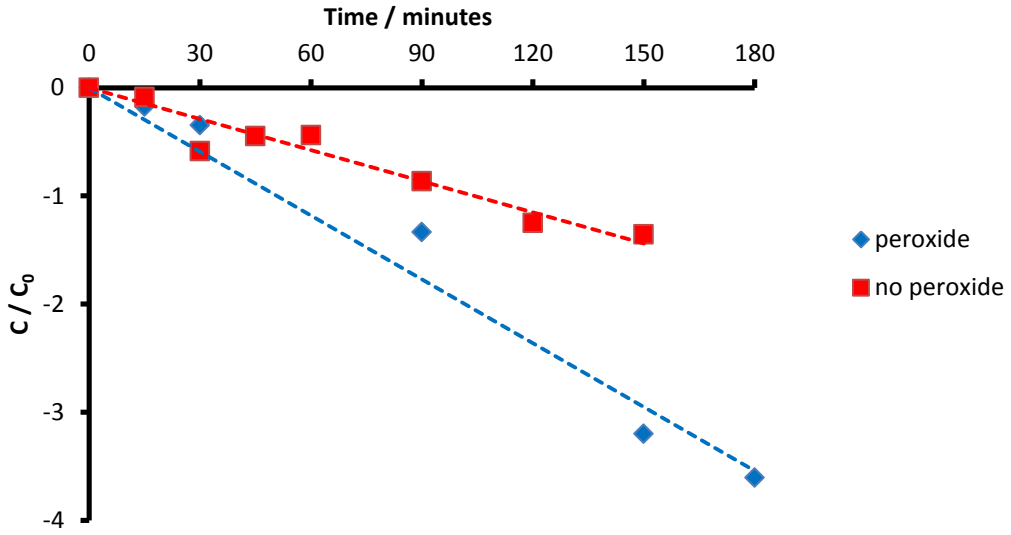

Figure 5.33: Degradation of DBP in the presence of H_2O_2 (20 kHz)

5.6.2: Addition of t-BuOH; a free radical quencher

In ultrasound research it is common to prove that a reaction follows a radical mechanism. This is usually done by the addition of a radical scavenger to the solution which is to be quenched. For this t-BuOH is a popular choice due to its affinity of the ·OH radical and its ability to form t-BuO· radicals with low reactivity in solution[35]. This happens by the ·OH radicals produced extracting a proton to form t-BuO· radicals. This radical centre is stabilised by hyperconjugation from the t-Bu methyl protons and so is much less reactive and does little degradation chemistry. To this end, a 100 µg L^{-1} DBP solution was sonicated using 515 kHz ultrasound with the addition of 1.5 mmol t-BuOH. In this experiment type the scavenger is always added in large excess so that it should out-compete the substrate for radicals and reaction should be quenched. This was not found to be the case however for DBP degradation as shown in figure 5.34.

Under the conditions used it was found that DBP still was able to degrade even in the presence of the radical quencher. The rate constant for the no t-BuOH experiment was 0.215 min^{-1} and 0.0267 min^{-1} in the presence of t-BuOH. The initial rate with t-BuOH was calculated as 1.33 µg L^{-1}, the rate without t-BuOH was 1.12 µg L^{-1}. The increase in rate must be within the error for the experiment, as an enhancement of rate is not expected. It does however show that t-BuOH does not compete well for ·OH radicals with DBP.

This can be explained entirely by the difference in hydrophobicity between DBP and t-BuOH. The octanol-water partition coefficient of t-butanol has not been measured since it is widely miscible with water. The solubility of the two substrates will therefore be used as a measure of their hydrophobicity. The solubility of DBP in water is estimated to be around 11.2 mg L^{-1}, this value is the high limit to current estimations, the solubility of t-butanol in water is known to be much higher than this[36-38] .

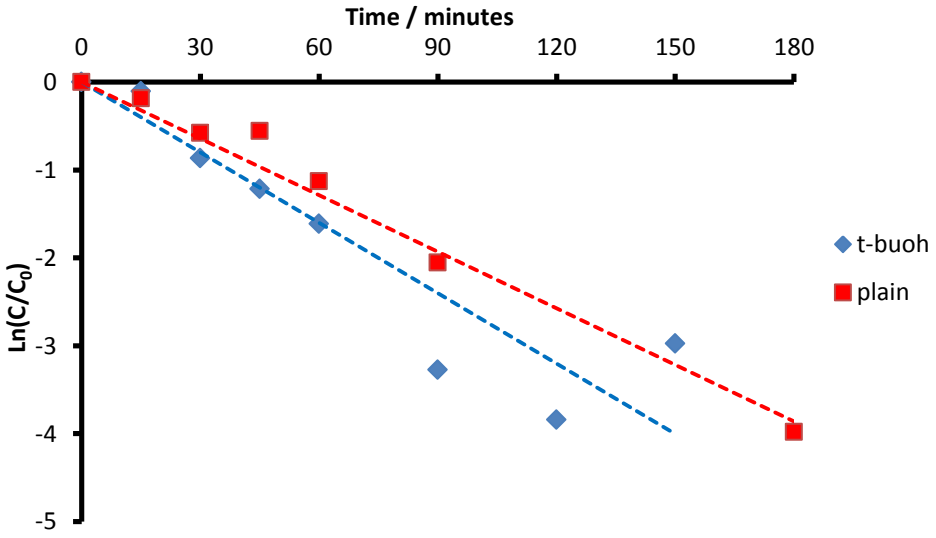

Figure 5.34: Degradation of DBP in the presence of t-BuOH

Therefore it is thought that the interface of a collapsing bubble is still is surrounded by mainly DBP with little or no t-butanol present due to its lower hydrophobicity. This means that the radical degradation of DBP occurs as if

t-BuOH was not present at all and so the reaction is not quenched. This is in contrast to the finding of Yim *et al* where DEP was successfully out competed for OH radicals by t-BuOH[1]. DEP is however much less hydrophobic than DBP[33] (pK_{ow} of 2.42 for DEP compared to 4.62 for DBP) and so in high concentration t-BuOH does successfully retard the degradation, although it did still continue. This was, according to Yim *et al* due to the amount of hydrolysis and pyrolysis occurring in the system and may well be the case.

From the finding in this section it appears that the addition of peroxides particularly hydrogen peroxide (due to it forming environmentally benign products i.e. water) would be beneficial as an efficient way to remove DBP and hopefully other phthalate esters from water sources. The rates found were akin to the use of oxygen as a dissolved gas and would allow for degradations to be performed under air which is practically much more simple when scaled up to an industrial scale. These two methods could either be combined while using high frequency ultrasound or the most economically and practically viable method could be used.

5.7: Drawing up a model for the degradation of DBP

This final subsection aims to gather together the findings of the previous 6 subsections to describe a model for the degradation of DBP. Since previous degradation studies and countless other works have cited the chemical effect of ultrasound arising from bubble collapse and so the same is deduced here. This has already been done when discussing the previous results.

Due to DBP's hydrophobicity and vapour pressure we would expect DBP to accumulate around the bubble interface and in the wider interfacial region of the bubble. This can also be surmised from the data in figure 5.26, DBP is surface active as it reduces the surface tension of the air-water interface. How DBP (and phthalates generally) could gather and pack around an air-water interface can be thought of in two ways.

Firstly, similarly to surfactants the ester chain tails of DBP could protrude into the bubble core leaving the phthalic acid moiety traversing the interface with some of the phenyl ring exposed to the water bulk phase. Otherwise since DBP is a planar molecule, the most favourable packing is if the molecules of DBP are flat against the bubble surface, again possibly contained within the interfacial boundary. This arrangement would allow for more of the DBP molecules to escape the water bulk phase and so lower the energy of the system more and so would be favoured.

The difference between these two packing modes are likely to be driven by the amount of DBP compared to the amount of bubble space i.e. θ as mentioned in section 5.4.3. In the present work the highest concentration employed was 10 mg L^{-1} of DBP. At this concentration the dimensionless θ can be calculated as 0.9376 for 20 kHz degradations and 0.9141 for 515 kHz degradations. Following the author's belief that this represents the amount of DBP bound compared to the maximum amount which could be bound the bubble surface at this concentration is quite crowded, therefore at this concentration maximum the DBP will be expected to partially traverse the bubble interface. The two possible packing modes mentioned are shown diagrammatically in scheme 5.2. At high concentrations of DBP additional DBP can be expected to exist around the first layer of DBP which is in contact with the bubble

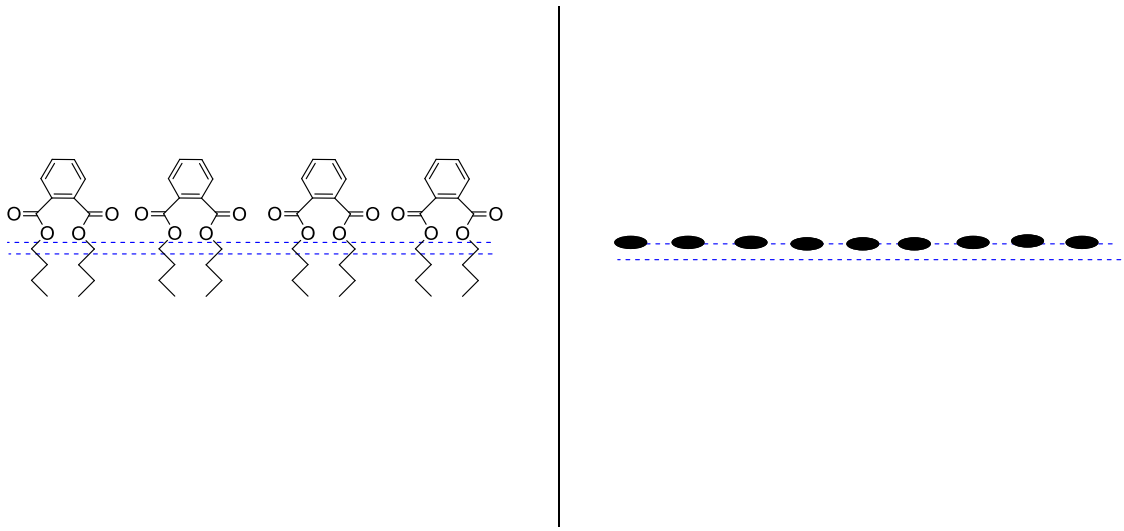

Scheme 5.2: Two possible packing modes of DBP on a bubble interface. The dashed blue lines represent the bubble interface while the black obloids on the right hand side denote DBP in plane to the viewing angle.

At any concentration a DBP gradient can be expected to exist with high concentration of DBP close to the bubble and decreasing amounts of DBP further away from the bubble. There can be expected to be a rate of flux of adsorption onto the bubble surface and theoretically a flux away from the bubble surface. This second flux with rate constant k_{-1} was postulated in section 5.4.3 to be very small for 20 kHz degradations, possibly non-existent due to DBP's hydrophobicity and larger than this for 515 kHz systems. These ideas are expressed diagrammatically in scheme 5.3.

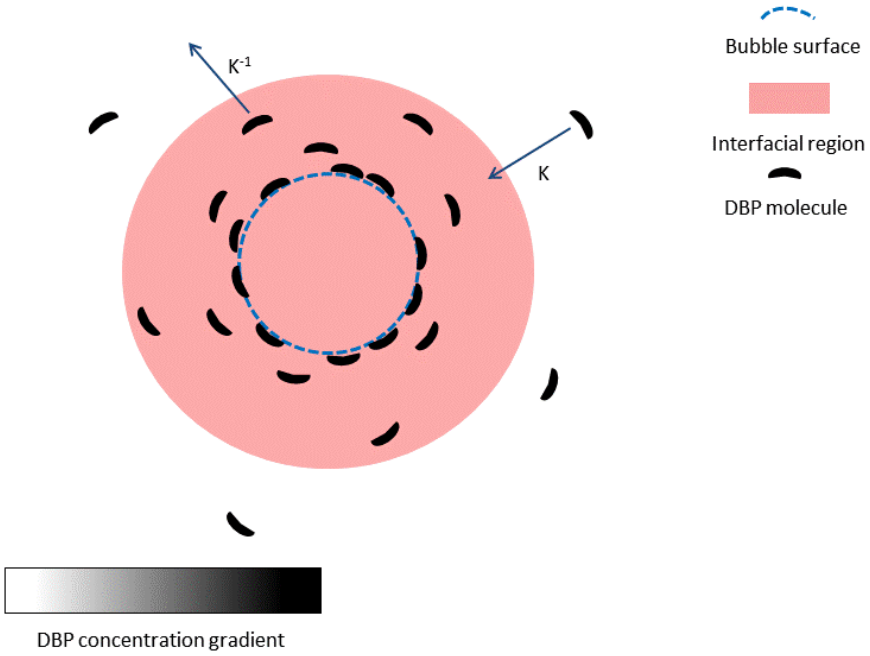

Scheme 5.3: A depiction of the accumulation of DBP around a bubble interface.

Having described how the stable bubble becomes coated with DBP the collapse phase now has to be considered. Upon bubble collapse the radius of the bubble first grows exponentially then collapses. The growth period is relatively long and so it is possible that extra DBP adsorbs onto the bubble interface as θ diminishes during the growth period. The collapse itself is very quick and so a great outwards force is exerted on DBP as the bubble shrinks. This would force DBP away from the bubble interface and into the now interfacial region of the bubble forming a “sea” of DBP around the bubble.

The speed of collapse would be faster for 515 kHz degradations due to the difference in frequency (there is less time for the collapse to occur) and so this force can be expected to be greater. This would result in the DBP to be thrown further off the bubble interface upon collapse. This part of the model would explain why figures 5.30 and 5.31 and the calculated ·OH radical productions necessary to effect noticeable DBP degradation are higher for the 515 kHz

system. Since the DBP now present around the bubble is further away the probability of an ·OH radical encountering the DBP is lower and so a higher initial concentration of DBP or a higher concentration of radicals is required.

Having collapsed, the contents of the bubble experience very high temperature and pressure for a very short amount of time. The magnitude of the temperature reached is a function of the concentration of gas and water vapour present within the bubble. A more vaporous bubble will generate a lower collapse temperature due to the collapse being cushioned as well as endothermic processes consuming the heat energy created. During bubble collapse there is however time for mass transfer and so water vapour as well as the gas contents can be expelled from the bubble as it collapses due to the reduction in bubble volume. Some gases will be able to diffuse faster across the bubble interface and so if the gas contents of the bubble is varied while all other factors stay the same some bubbles will be closer to a vacuum than those filled with a different gas. This model would account for the finding in section 5.3 that the rate of degradation is a function of the solubility of the dissolved gas divided by its molar volume (a model for its diffusivity in water).

Whatever the temperature reached water is lysed into ·OH radicals and ·H radicals. These are then ejected from the bubble into the interfacial region where they can encounter and react with the DBP now present there. As a result degradation products are formed. Degradation products can be expected to arise mainly due to ·OH as ·H is known to not to be able to diffuse from bubbles in aqueous solution as well as ·OH radicals can[39].

The next chapter discusses the degradation products of DBP sonolysis and draws up a degradation process for the sonolysis of DBP as a model of the family of phthalate esters.

5.8: Chapter references

1. B. Yim, Y. Nagata and Y. Maeda, *Journal of Physical Chemistry A*, 2002, **106**, 104-107.
2. E. Psillakis, D. Mantzavinos and N. Kalogerakis, *Chemosphere*, 2004, **54**, 849-857.
3. J. Schwarzbauer, S. Heim, B. Krooss and R. Littke, *Organic Geochemistry*, 2006, **37**, 2026-2045.
4. G. Y. Pee, J. F. Rathman and L. K. Weavers, *Industrial & Engineering Chemistry Research*, 2004, **43**, 5049-5056.
5. R. J. Emery, M. Papadaki and D. Mantzavinos, *Environmental Technology*, 2003, **24**, 1491-1500.
6. J. P. Lorimer and T. J. Mason, *Chemical Society Reviews*, 1987, **16**, 239-274.
7. Supeno and P. Kruus, *Ultrasonics Sonochemistry*, 2000, **7**, 109-113.
8. D. Drijvers, H. Van Langenhove and K. Vervaet, *Ultrasonics Sonochemistry*, 1998, **5**, 13-19.
9. M. H. Uddin and S. Hayashi, *Journal of Hazardous Materials*, 2009, **170**, 1273-1276.
10. R. W. G. Robert H. Perry, *Perry's Chemical Engineers' Handbook*, 5th Edition edn., McGraw-Hill Professional, 1997.
11. *CRC Handbook of chemistry and physics*, 61st Edition edn., Boca Raton, Florida, USA.
12. M. A. Margulis, *Ultrasonics*, 1985, **23**, 157-169.
13. V. Misik and P. Riesz, *Journal of Physical Chemistry*, 1996, **100**, 17986-17994.
14. N. A. Maksimenko and M. A. Margulis, *Zhurnal Fizicheskoi Khimii*, 1991, **65**, 3310-3316.
15. D. L. Baulch, C. T. Bowman, C. J. Cobos, R. A. Cox, T. Just, J. A. Kerr, M. J. Pilling, D. Stocker, J. Troe, W. Tsang, R. W. Walker and J. Warnatz, *Journal of Physical and Chemical Reference Data*, 2005, **34**, 757-1397.
16. N. K. Srinivasan, M. C. Su, J. W. Sutherland and J. V. Michael, *The Journal of Physical Chemistry A*, 2005, **109**, 7902-7914.
17. S. Javoy, V. Naudet, S. Abid and C. E. Paillard, *Exp. Therm. Fluid Sci.*, 2003, **27**, 371-377.
18. W. Tsang and R. F. Hampson, *Journal of Physical and Chemical Reference Data*, 1986, **15**, 1087-1279.
19. C. J. Cobos and J. Troe, *Journal of Chemical Physics*, 1985, **83**, 1010-1015.
20. J. Franck, Nobel Institute, 1926.
21. M. Ashokkumar, J. Lee, Y. Iida, K. Yasui, T. Kozuka, T. Tuziuti and A. Towata, *Chemphyschem : a European journal of chemical physics and physical chemistry*, 2010, **11**, 1680-1684.
22. A. DeVisscher, P. VanEenoo, D. Drijvers and H. VanLangenhove, *Journal of Physical Chemistry*, 1996, **100**, 11636-11642.
23. A. P. a. d. P. J, Oxford University Press, Seventh Edition edn., 2002, pp. 869-870.
24. K. Okitsu, K. Iwasaki, Y. Yobiko, H. Bandow, R. Nishimura and Y. Maeda, *Ultrasonics Sonochemistry*, 2005, **12**, 255-262.
25. B. Nanzai, K. Okitsu, N. Takenaka and H. Bandow, *Journal of Physical Chemistry C*, 2009, **113**, 3735-3739.
26. K. Okitsu, B. Nanzai, K. Kawasaki, N. Takenaka and H. Bandow, *Ultrasonics Sonochemistry*, 2009, **16**, 155-162.
27. N. Serpone, R. Terzian, H. Hidaka and E. Pelizzetti, *The Journal of Physical Chemistry*, 1994, **98**, 2634-2640.
28. B. Kuhn, P. Mohr and M. Stahl, *Journal of Medicinal Chemistry*, 2010, **53**, 2601-2611.
29. I. V. Perminova, F. H. Frimmel, D. V. Kovalevskii, G. Abbt-Braun, A. V. Kudryavtsev and S. Hesse, *Water Research*, 1998, **32**, 872-881.
30. G. Boge and H. Roche, *Bulletin of Environmental Contamination and Toxicology*, 1996, **57**, 171-178.
31. A. R. Jacobson, S. T. Moe, P. D. Allen and J. D. Fessenden, *Molecular Pharmacology*, 2006, **70**, 259-266.

32. E. J. R. Ngen, Pallavi; You, Youngjae *Bioorganic and Medicinal Chemistry*, 2009, **17**, 6631-6640.
33. D. R. Peterson, C.A. Staples, T.F. Parkerton, W.J. Adams, *Chemosphere*, 1997, **35**, 667-749.
34. Y. Nagata, M. Nakagawa, H. Okuno, Y. Mizukoshi, B. Yim and Y. Maeda, *Ultrasonics Sonochemistry*, 2000, **7**, 115-120.
35. A. Tauber, G. Mark, H. P. Schuchmann and C. von Sonntag, *Journal of the Chemical Society-Perkin Transactions 2*, 1999, 1129-1135.
36. K. Abdur-Rashid, T. P. Dasgupta and J. Burgess, *Transition Metal Chemistry*, 2005, **30**, 948-956.
37. S. C. Dutta, A. K. Bhattacharyya and S. C. Lahiri, *Journal of the Indian Chemical Society*, 2001, **78**, 729-738.
38. P. X. Li, Y. L. Wang, B. X. Han, H. K. Yan and R. L. Liu, *Journal of Solution Chemistry*, 1996, **25**, 1281-1289.
39. A. Henglein, Advances in Sonochemistry, ed. Mason. TJ, JAI Press, London, 1993, vol. 3, pp. 17-83.

Chapter 6: Studies on the products of the degradation of DBP

6.1: Chapter summary and initial explanations

Chapter summary

This chapter discusses the results from experiments designed to probe the products of the degradation of DBP. As discussed in chapter 5, DBP was chosen as a model phthalate as its physical properties and rate of sonolysis made it the most useful choice for maximising the concentration of products in solution.

All the data in this section comes from detection with LC-MS (Electrospray ionisation – time of flight (ESI-TOF)) systems and also GC and GC-MS systems. As discussed in chapter 4, LC-MS is particularly suited to and useful for detecting *and* quantifying trace amounts of non-volatile compounds in aqueous solutions. This made the ESI-TOF systems available in the department invaluable in conducting the product analysis studies discussed in this section.

While elucidating the products of DBP sonolysis, firstly the liquid phase products detectable directly from DBP degradations were identified. Then, one of the major products was synthesised and solutions containing high concentrations of this intermediate were then degraded under identical conditions. This allowed for many more products to be identified. Where possible these products were then searched for in direct degradation studies on DBP itself.

Next, experiments were conducted to identify any gas phase products that were produced from sonolysis using 20 kHz ultrasound. These could have either resulted directly from DBP due to direct pyrolysis (microinjection of DBP into the bubble core) or from the more volatile degradation products of DBP.

Once the degradation products had been identified the distribution of the various products over time was studied. Finally, the effect of dissolving different gases into DBP solutions was examined. This was to check whether the product distribution changed at all due to a change in sonolysis conditions and was focussed on the use of air rather than argon as the dissolved gas. The reason for this is that in an industrial setting sonolysis under air would be much more attractive due to practical and economic reasons (the use of argon on a large scale would be expensive).

6.2: The products of DBP degradation under argon: liquid phase

6.2.1: Products found from degradation of 10 mg L^{-1} DBP solutions using 20 kHz ultrasound.

Using the methodology presented in chapter 4, the products from the degradation of DBP were studied. All products were identified using degradations on 10 mg L^{-1} DBP solutions purged with argon. The reasoning for this was that it was thought that the concentration of products would be higher for increasing concentrations of DBP. This decision was made in spite of the fact that the degradation would be less complete with respect to the final amount of DBP remaining in solution. Argon was used to make the degradation process more efficient with respect to the sonolysis conditions[1, 2] to maximise the OH radical yield. In starting with these conditions, it was assumed that sufficient DBP would be degraded fully to allow for the detection of products all the way down the degradation process.

When searching for degradation products a few assumptions were made based on the type on chemistry occurring.

1: Degradation products would generally be lower in mass than the parent compound, DBP. This excludes two important classes of products which were found during the study:

a: products arising from hydroxylation of DBP without any resulting fragmentation of the molecule. These products were known to exist from the start of the study and so searched for routinely.

b: dimers of the parent compound. These were discovered quite late into the study, following a conversation with the mass spectrometrist, Dr Anneke Lubben.

2: It was assumed that the main method of degradation would be radical attack by hydroxyl radicals. While searching for products radical attack by hydrogen atoms was kept in mind, however it was not expected that much evidence would be found of this due to the lifetime and diffusivity of the hydrogen radical in water[3].

3: Due to point 2, we assumed that the formulae of products would only contain C, H and O. Na was also considered due to a consequence of the detection method. In ESI-TOF ions are formed by addition of H^+ and Na^+ to molecules[4], so sodium adducts had to be searched for in addition to hydrogen adducts.

4: To be a valid product the compound ideally had to have zero concentration at t = 0 and increase substantially during the experiment. Several proposed products were in solution at t = 0 but their concentration always increased by a large proportion and so it was rationalised that they were being formed during the degradation process.

Armed with these four assumptions to aid product detection 10 mg L^{-1} solutions were degraded with the resulting samples being analysed by ESI-TOF in both +ve and –ve ionisation modes.

The routine method for product detection was as follows:

1: The “fingerprint” of the deionised water used in making DBP solutions was first ascertained. This was done by identifying which mass peaks were always found to arise from water samples. These peaks could not be identified most of the time, as doing so required some knowledge of what elements are contained within the compounds described. The important point was to identify those peaks which always occurred so that they could be discounted from being a possible product peak.

2: Having described the water “fingerprint” mass profile, samples arising from degradation experiments were analysed in both +ve and –ve ionisation modes. Initially these did not contain any internal standard to make sure the products fully ionised and so would be detected as fully as possible. This precaution was due to a feature of ESI-TOF where compounds tend to be preferentially ionised based on their concentration in solution and their surface activity[5].

This effect can be imagined by assuming that the mass spectrometry system provides a fixed, finite amount of H^+ and Na^+ which could ionise compounds in the ionisation chamber. Once these are used up further ionisations do not occur. Therefore swamping the samples with an unneeded compound, in relatively high concentration, could mask compounds present in the sample at much lower concentrations. With LC-MS systems this is less likely to occur as the samples are separated in time pre-ionisation due to the LC system. However any compounds eluting at the same time as the standard most often used (thiabendazole (TBZ)) could still be masked.

3: The first step in finding products was to try and discover which regions of the LC-MS trace compounds were eluting in. This was done by using some of the built in functions of the OpenMS Bruker Daltonics Data Analysis package particularly the “dissect compounds” routine.

4: Having discovered the time frames during which new compounds were eluting the main isotopic mass giving rise to the LC trace peak was checked to see if it could be accurately described using combinations of C, H, O and Na. If it could not it was assumed to not be a product from DBP degradation. If it could, the formula was recorded.

5: Having analysed the main mass peak within a given time frame the same process was repeated for all mass peaks in the same time frame. By doing this it was found that several products co-eluted, that is to say that several products were found to enter the MS system from the LC within a narrow time frame. This would be due to their being similar in their physical properties which describe their solubility in water – acetonitrile gradient systems. Again any masses which could be accurately described by combinations of C, H, O and Na were recorded.

It should be noted that this step generated many possible formulae describing a mass which do not make chemical sense e.g. $C_3O_{15}H_{23}$ but made mathematical sense. These were always discarded.

6: The possible formulae were then compared to that of DBP to try and propose structures for the compounds thought to be degradation products. This sometimes required some imagination and several references were of use during this step as shall be discussed.

7: Having proposed masses, formulae and structures for possible degradation products these products were then checked to see if they were formed reliably. Experimentally this meant searching for them in 3 degradation experiments. To count as being a product, mass information had to be found in all three runs, the LC trace peak resulting from the mass of a given product also had to occur in the same region of the LC trace. That is, the compound had to elute in a similar time frame in each run. Lastly the mass of the product had to be repeatable within a fairly narrow confine (10 - 50 mDal). This last requirement existed so that the given formula could be assigned to the resulting mass within the error mentioned for each run.

References used to aid proposal of degradation products.

When discerning degradation products, 3 papers were very useful for generating leads and ideas. These 3 were on hydrothermal oxidation[6], titatium dioxide enhanced UV degradation[7] and UV action alone[8]. All three of these papers had already examined the degradation of DBP by methods for which similar chemistries as those known happen in ultrasonic degradation occurred.

The paper on hydrothermal oxidation by Onwudili *et al*[6] reported degradation of DBP mainly by hydrolysis of the ester chain linkages followed by decarboxylation the resulting of phthalic acid. This was then converted to phenol *via* the loss of CO_2 and then oxidised to benzoquinone. This was then cleaved to form two equivalents of hydroxyl acetaldehyde. The cleavage of the phthalate ester chains proceeded along two reaction paths. Firstly was a simple hydrolysis to form butanol. This was then oxidised directly to H_2O and CO_2. The second pathway followed a disproportionation of the two chains to form 1-butene and 2-butanol. This process is shown in scheme 6.1 below.

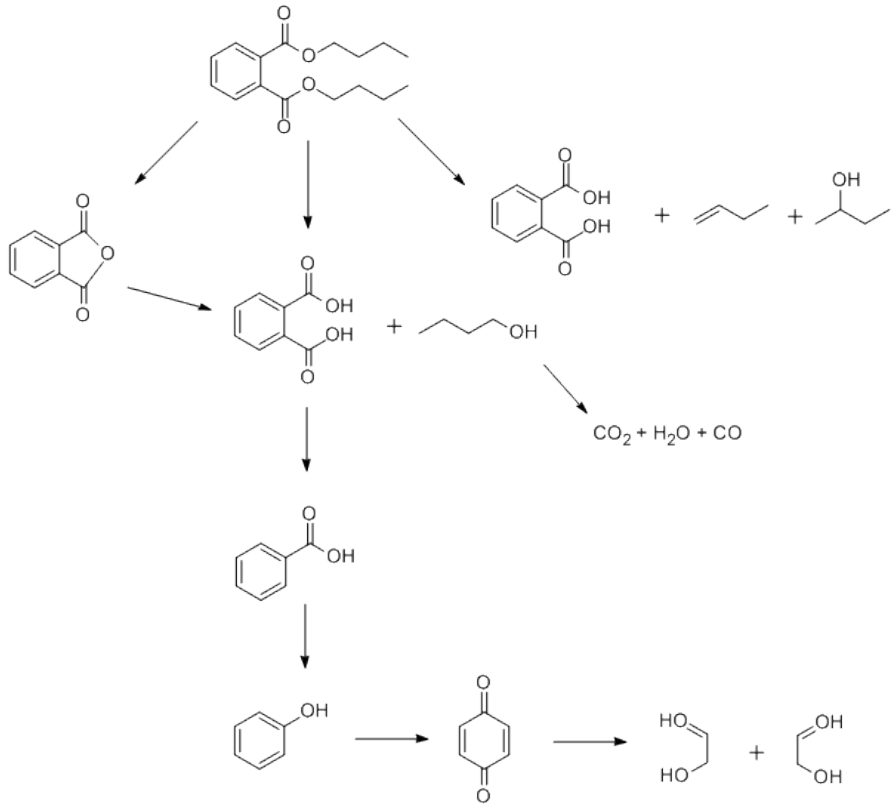

Scheme 6.1: The degradation process proposed by Onwudili *et al*[6].

For the degradation of DBP by UV action, Lau *et al*[8] proposed a simple degredation as shown in scheme 6.2. UV action behaves similarly to ultrasound sonolysis in that the main species for chemical attack are hydroxyl radicals. The two processes are different in that ultrasound also combined hydrolysis and pyrolysis due to the action of bubble implosions which is absent from UV

processes. Also, UV creates ·OH radicals in solution, in the degradation of hydrophobic and surface active pollutants most radicals expelled from cavitation bubbles do not make it into the bulk solution. The main products postulated by Lau were the mono ester of DBP, monobutyl phthalate (MBP) and butyl benzoate. The mono ester product then forms benzoic acid, whereas the MBP forms an aldehyde and then is oxidised to phthalic acid.

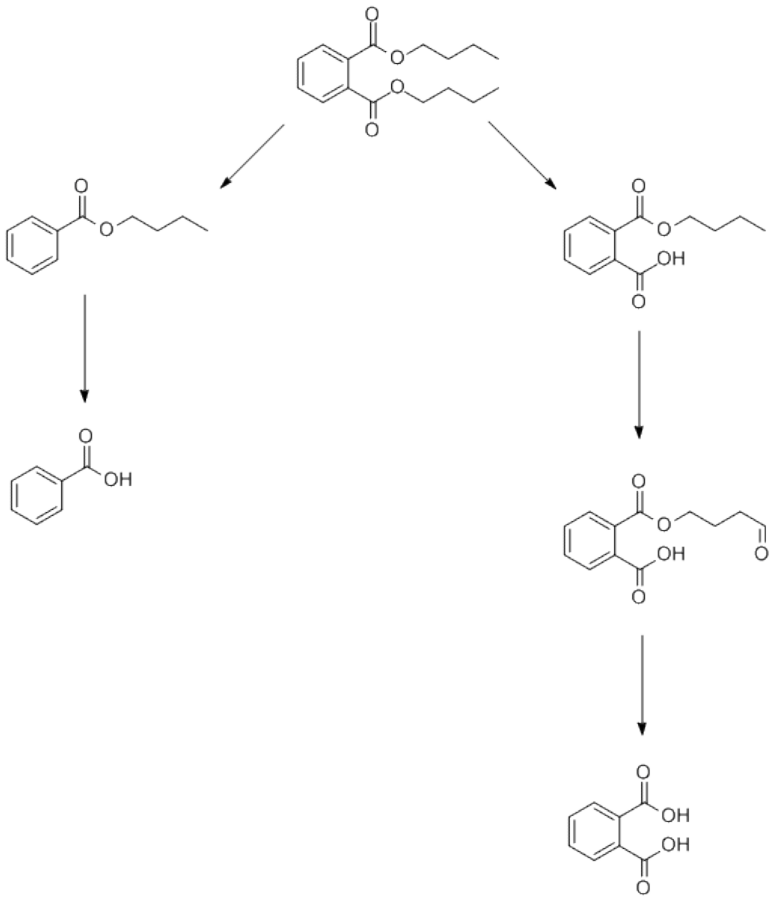

Scheme 6.2: The degradation proposed by Lau *et al*[8].

For the degradation of DBP by UV / TiO_2 systems, Kaneco *et al*[7] proposed a rich and complicated degradation process. TiO_2 acts as a catalyst for the formation of OH radicals upon reacting with UV light. This creates a lot more radicals in solution that UV light by itself and so a more diverse range of

chemistry was seen. This also included more high energy chemistry and radical abstractions as well as additions. Thirteen of the reaction products formed and identified are shown in scheme 6.3.

It was hoped that these three processes generated products might also be found for the sonochemical degradation of DBP. The formulae and structures of the compounds in schemes 6.1 – 6.3 were kept in mind when proposing structures from formulae. Some of the most likely structures were searched for in addition to the peak searching / matching method already described. These are shown in figure 6.1 along with their corresponding ionic masses. The structures searched for were those thought, at the time, to be the ones which would most likely be formed by cavitation bubble mediated ·OH radical attack and hydrolysis.

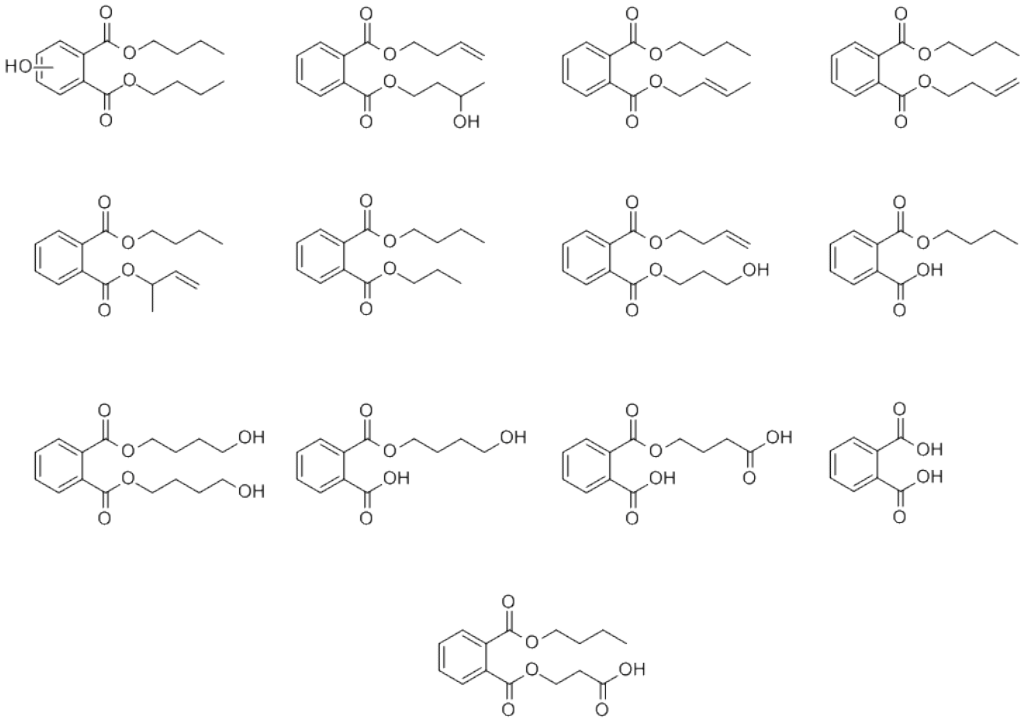

Scheme 6.3: The degradation products identified by Kaneco *et al*[7].

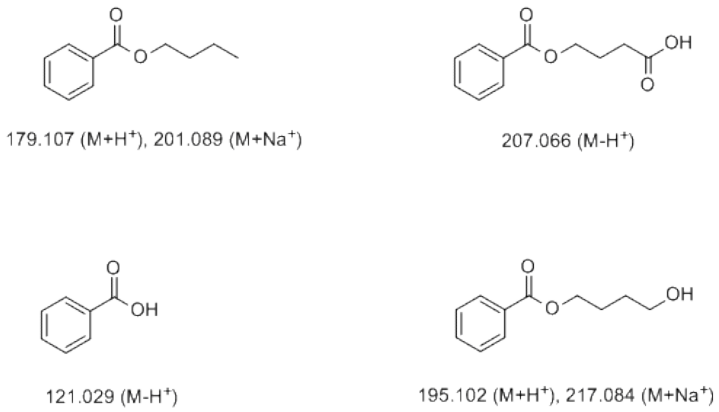

Figure 6.1: Degradation products initially searched for.

Of these products and their corresponding masses it should be noted that none of them were found reliably from direct DBP degradation. Four products were found however, these were hydroxy-dibutyl phthalate, monobutyl phthalate, a product already identified in works by Yim[9] and Psikallis[10], phthalic anhydride and a product arising from hydrogen abstractions on hydroxyl-dibutyl phthalate. The structures of these products along with the masses used to identify them are shown in figure 6.2.

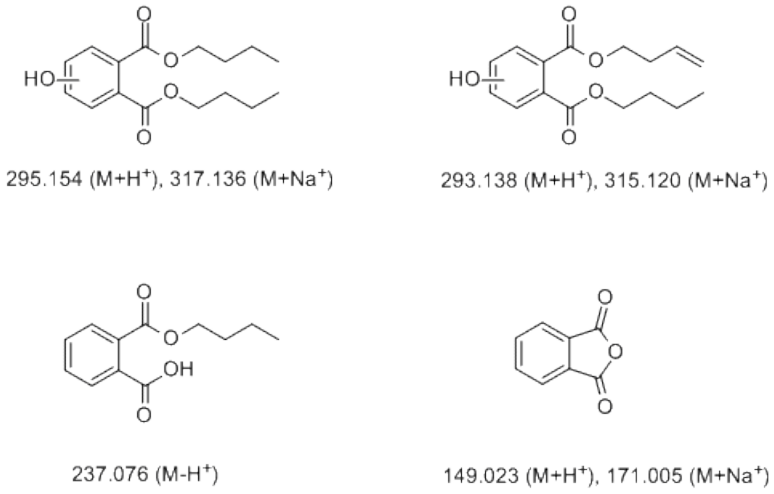

Figure 6.2: Products identified directly from DBP degradations.

So that the reader can gain an appreciation for the size of the mass peaks identified in figure 6.2, figure a.1 – a1.4 in appendix I show typical LC-MS spectra for these compounds. An extracted mass LC chromatogram is shown in the top of the diagram. This peak describes the intensity of the given mass over time. The lower part of the figures show the mass spectrum generated from the time given by the width of the LC peak. Where necessary the product peak is identified by a label.

As can be seen from the figures, the heights of the product mass peaks are often much smaller than even some of the mass peaks seen in pure water and / or random contaminants. This is why it was so important that the information be reproducible both by LC retention time and by the mass of the produced peak.

Having followed the steps discussed earlier only 4 products had been found which matched the necessary criteria. It was obvious that these could not be all the possible degradation products as none of the 4 found increased in concentration over the entire time of the experiment. This also signified that none of these products were the final end point of the degradation.

The reason for other products further down the degradation path not being discovered was that there was a very steep drop-off in the intensity of mass peaks formed even from the four products found in figure 6.2. It was therefore assumed that other products would exist, but that their concentration in solution must be too low to be detected from direct degradation of DBP.

To allow probing of the rest of the degradation products, it was decided to synthesise and make solutions from one of the products already found. Of the 4 products monobutyl phthalate was the best choice. This was mainly due to practical reasons as the synthesis of MBP is quite straightforward. A simple addition reaction of n-butanol from the anhydride made enough MBP for many degradation experiments. The other reason for choosing MBP was that its intensity in the mass spectra produced was the lowest of the products found. This was assumed to mean that it was further down the degradation process “tree” than the other 3. This meant that MBP was the product the furthest along the degradation process which could actually be visualised from DBP degradations.

6.2.2: Synthesising MBP and products found from MBP degradations.

The method used to synthesise MBP is shown in scheme 6.4 and presented more thoroughly in the experimental chapter. The methodology was taken from Leung's work on alkyl and allyl phthalamates where MBP was made as a phthalamate precursor[11].

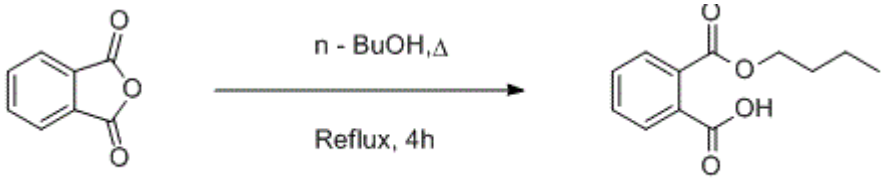

Scheme 6.4: Synthesis of MBP[11]

The synthesis resulted in several grams of a waxy white crystalline product. ^{1}H NMR and LC-MS analysis (see experimental section) confirmed that the product was MBP and was formed in good purity without the need for further workup beyond filtering and solvent removal.

Using the same methods and experiments as for DBP degradations several 10 mg L^{-1} solutions of MBP were degraded and analysed using LC-MS. When comparing the resulting mass spectra to that of pure water further degradation products were found. These are shown in figure 6.3. Products highlighted in blue were found in positive ionisation mode while those highlighted in red were found using negative ionisation mode.

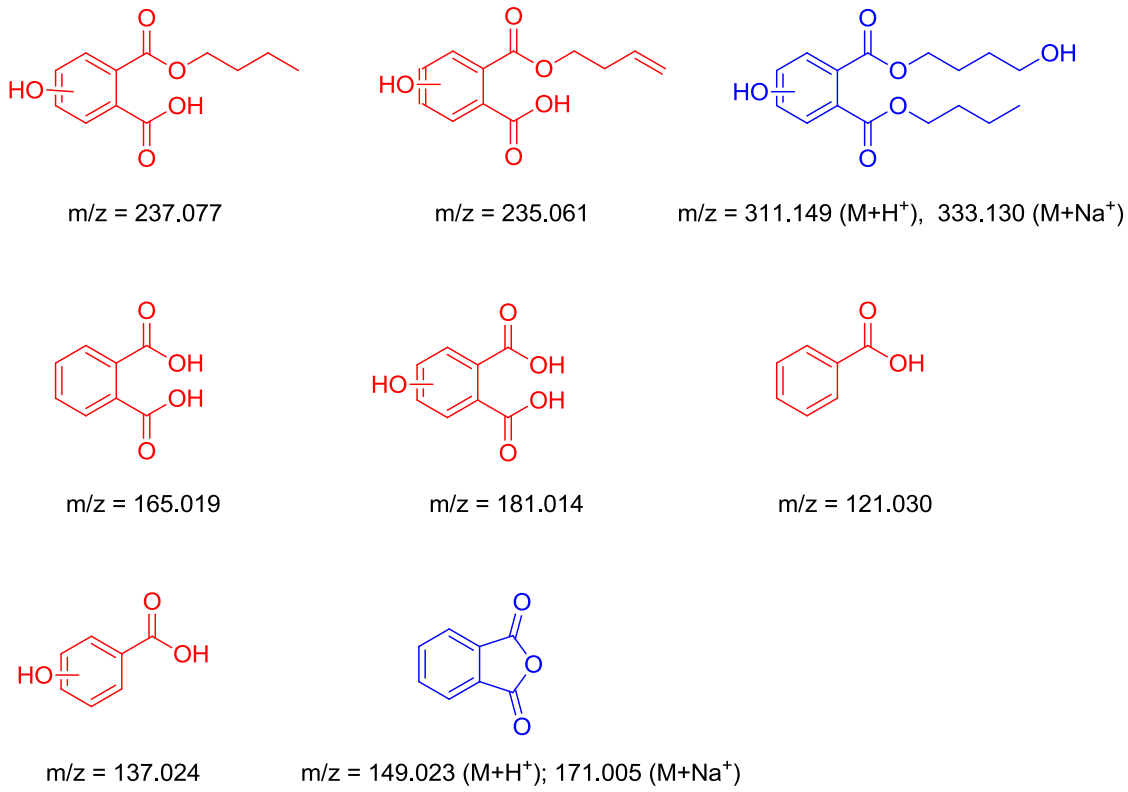

Figure 6.3: Products found from degradation of MBP solutions purged with argon

It should be noted at this point that both benzoic acid and phthalic anhydride were present at t=0, presumably as contaminants from the manufacture of the phthalate used. These were assumed to also be products since their mass spectrum intensities increased and decreased several times in the three hours of the experiments. As above figures a1.5 to a1.11 in appendix I show typical mass spectrum information for the products found and proposed in figure 6.3. Again the low intensity of these peaks compared to that of the “fingerprint” can be noted.

Having found these products in MBP degradations, DBP experiments were then reanalysed to see if any of the newly discovered products could be observed. It was found that none of these could be seen , their supposedly low concentration was assumed to be the reason for this.

From analysis of the products found it was found that the main route of degradation was through ·OH radical substitution and subsequent hydrogen abstractions of the phthalate ester chain tails. Once hydroxylated several times the mono ester is formed from the phthalate. This can also then be attacked further by hydroxyl radicals to then form phthalic acid from a second ester hydrolysis. It then seems that the fate of phthalic acid has two routes to follow. Firstly there is an interconversion with phthalic anhydride arising from formation of the anhydride and subsequent reopening of the anhydride ring. Secondly, the diacid can also decarboxylate to form benzoic acid. This is then further hydroxylated.

Products smaller than benzoic acid could not be found. The concentration of benzoic acid remained low throughout the experiment and it is thought that this is not the end point of the degradation. The reason for not finding further products was thought to be two-fold. As with DBP degradations regarding MBP peak intensities, the intensity of hydroxyl benzoic acid was very low even in the last time sample of the experiment i.e. the time point with the most complete degradation of MBP. This meant that again very low subsequent product concentration hindered further degradation product elucidation. Secondly the products formed were now quite low in weight and so were expected to be reasonably volatile. The ionising chamber in ESI-TOF analysis is heated, in the case of this work to 50°C. This temperature may be enough for products to boil out of the micro droplet spray formed and to be lost to the surrounding vacuum. This meant that using ESI-TOF these and any other volatile compounds would not have been observed. The use of ion chromatography could have remedied this.

The fact that the product arising from hydrogen abstraction on an ester chain before a radical addition is not found suggests that hydroxylation is the favoured attack pathway for the radicals formed within the conditions in the cavitating solutions. Once hydroxylated the product with unsaturated ester chains is found. This behaviour was found in the DBP degradation and also MBP degradation.

It should now be noted that there is some ambiguity as to the site of ·OH radical addition. This is due to the fact that ESI-TOF single MS does not fragment the ionised molecules and so no structural information is obtained just a formula fitting the accurate masses measured. It was assumed that the first ·OH radical would add to the aromatic ring, as this is the area of highest electron density. For the case of products arising from a second radical addition, the case is quite ambiguous. MS-MS experiments are needed to resolve this point but could not be performed using the equipment available in this study.

Having discovered from the MBP degradations that successive radical additions and hydrogen abstractions were found to occur on MBP this method of attack was looked for further in DBP based degradations. It was found that products arising from up to 3 radical attacks and / or abstractions could be found. These additional products are shown in figure 6.4 and were all visualised using the positive ionisation mode.

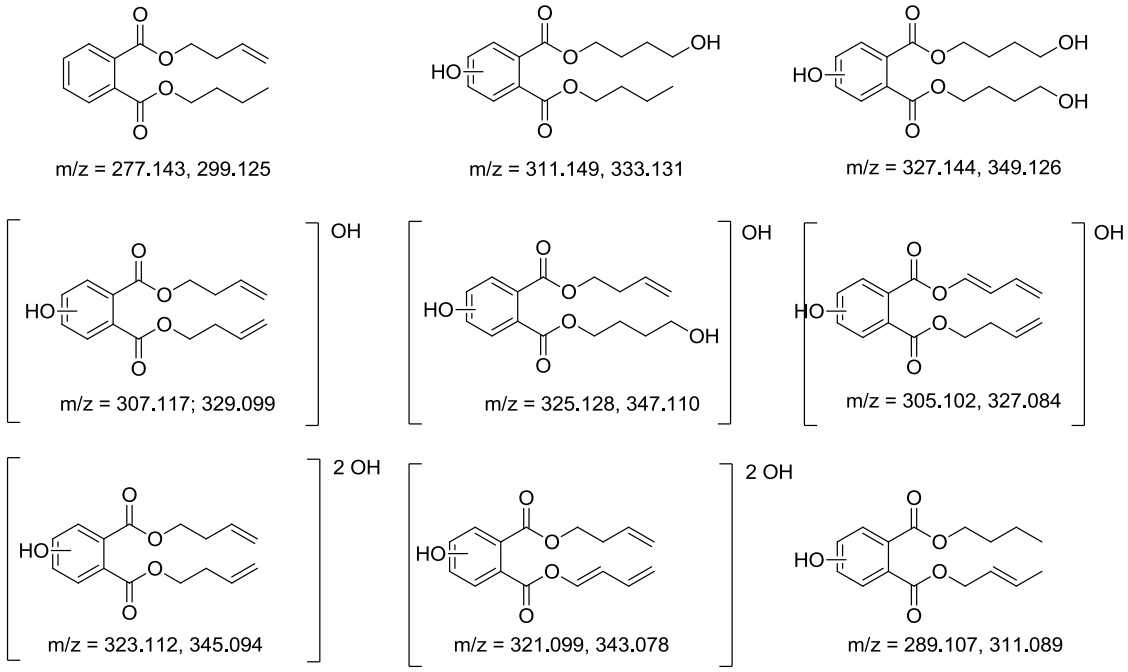

Figure 6.4: Further products found in DBP degradations

The square brackets and OH/2OH denote one or two hydroxyl groups present on the molecule but the position is not certain due to lack of fragmentation / MS-MS information.

6.2.3: Using the known degradation of benzoic acid to complete the evaluation.

In the last subsection it was found that the smallest product which could be assigned with confidence was benzoic acid. Beyond this for the two reasons mentioned no further products could be found. Singla *et al* had previously studied the sonolytic degradation of benzoic acid in 2004[12]. The process proposed is shown in scheme 6.5. It can be seen that the degradation forms several small molecules such as phenol and catechol before the aromatic ring is broken to yield small organic acids.

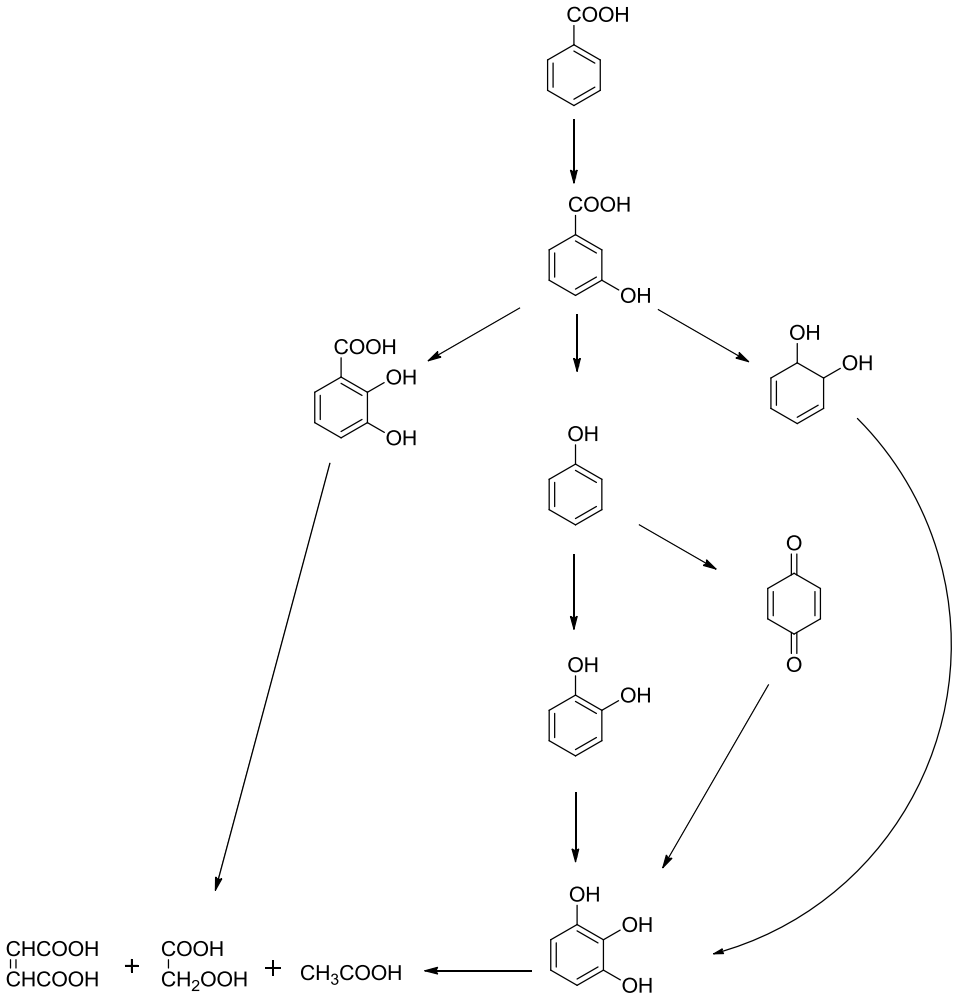

Scheme 6.5: The degradation of benzoic acid according to Singla *et al*[12]

It was not just assumed that this process was identical for DBP/MBP degradations. The products shown were all searched for in the mass information from the degradation of MBP solutions. From these salicylic acid,

2,3 hydroxy-benzoic acid, phenol, catechol and o-hydroxycatchol were found albeit with very low intensity. Given the similarity of the degradations it was noticed with some surprise that benzoquinone was not found in any degradation experiments.

Having confirmed these products we could now describe the degradation of DBP down to the smallest known product before ring cleavage. It is certain from known boiling points that the small acids formed from ring scission would not be observed and so it was concluded that within the limitations of the equipment available the products had been fully described.

It was then possible to draw up a degradation process tree showing the progression of the degradation from DBP right through to o-hydroxy catechol. The completed process is shown in scheme 6.6. The reactions of DBP with hydroxyl radicals are not fully shown as several products were identified as in figure 6.4. After catechol the ring breaks into small acids and then these are pyrolised inside cavitation bubbles to form combustion products , CO_2 and water.

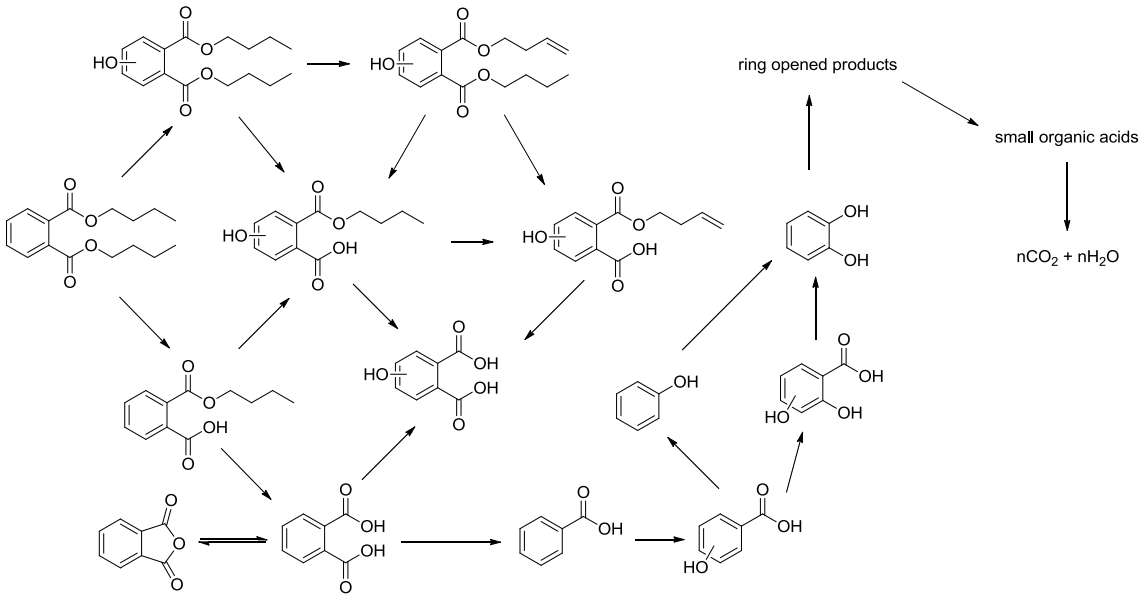

Scheme 6.6: The proposed route of DBP degradation.

6.2.4: Checking for change of products when using 515 kHz ultrasound

The above products were all found using 20 kHz frequency ultrasound to degrade the DBP / MBP solutions. To see if / how the use of a different frequency affected the degradation products, the process was repeated as above for degradations using 515 kHz frequency ultrasound.

For the most part, this simply involved searching for all the products found in figures 6.2 to 6.4 and noting any changes. After this the emerging compounds algorithm in DataAnalysis was then used to check for any other products which could have been formed. It was found that the products were the same. This was not too surprising as a change in bubble dynamics resulting from the increase in frequency does not alter the active radical species at all. It appears the lack of time for intrabubble chemistry did not affect the products found from the qualitative study described so far. Section 6.4 describes a semi quantitative study performed comparing the degradation products' distribution over time using both 20 kHz and 515 kHz ultrasound frequencies.

One difference that was found was the occurrence of dimers of DBP. These were observed for 515 kHz and not 20 kHz experiments purely because, by accident, a different LC routine was used. This other routine ran for much longer c.a. 20 minutes not 10 minutes as for 20 kHz experiment analyses. Two types of dimer were found to occur, one with a mass of 2M-2H signifying that one bond had been formed and another with mass 2M-4H signifying that two bonds or a double bond had been formed between the molecules. Their structures are shown in figure 6.5.

Multiple isomers seemed to be present as shown by the LC traces. This is entirely reasonable. If the bonding was occurring through radicals being formed on the ester chains then the number of ways in which the bonds could be formed is very large. Bonding could be occurring by chain – chain bond formation or chain – ring bond formation. Without MS-MS information it is impossible to analyse this data further.

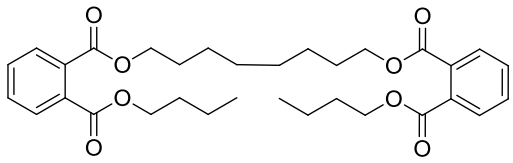

m/z = 555.295, 577.277

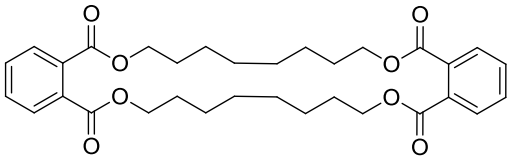

m/z = 553.295, 575.277

Figure 6.5: Dimers of DBP found

6.2.5: Formation of isomers of products

From several of the mass spectra profiles shown in this chapter it can be seen that structural isomers of the product are often formed. This is not surprising given the reactivity and low specificity of the ·OH radicals formed from water sonolysis. The formation of isomers of several of the products is easily seen in the LC traces obtained. The column used in the LC separations seemed to be able to resolve the isomers formed for several products extracted from the mass spectrum information. The products found to form isomers shall now be introduced and the nature of their isomerisation explored briefly.

The first product found to exhibit isomer formation was $C_{16}H_{22}O_5$ which arises from a single hydroxylation of DBP. From examination of the LC traces obtained for this compound 5 isomers can often be seen. This results in hydroxylation occurring in both possible positions on the benzyl ring and also three different locations on the ester chains. In the single MS system used it is however impossible to say which is which as structural information from molecular fragmentation is not obtained. These are shown in figure 6.6

The next product to show isomerisation is $C_{16}H_{22}O_6$. This product showed two main isomers being formed and eluted in equal amounts. This product arises from two hydroxylations on a DBP molecule. From the combination of possible positions of attack and the low amount of isomers seen it is impossible to say what these isomers are without the use of MS-MS experiments.

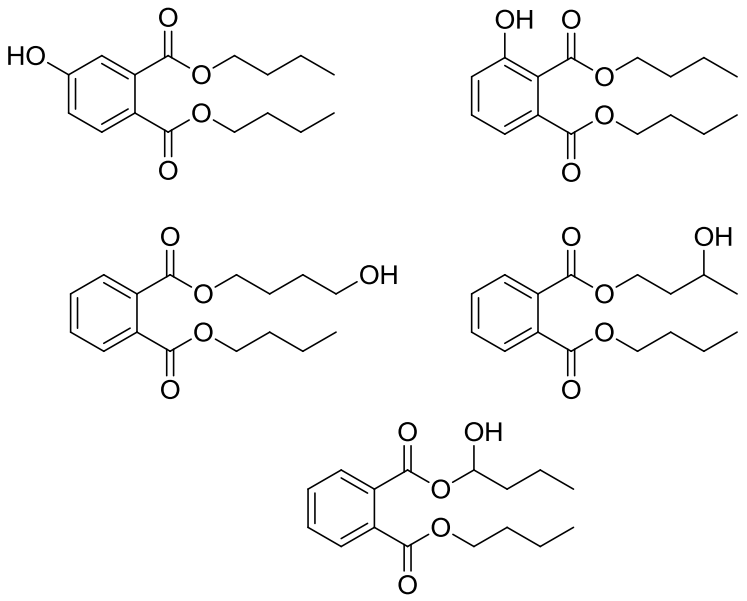

Figure 6.6: Possible isomers of $C_{16}H_{22}O_5$

The products formed from a single hydroxylation and a single double bond formation also showed 2 main isomers. Here we could guess that one arises from hydroxyl attack on the phenyl ring with subsequent unsaturation of one phthalate ester chain and that the other occurs from hydroxylation and double bond formation on a ester chain tail. The fact that the product arising from just double bond formation is not seen, suggests that double bond formation occurs on the position next to the hydroxylation site. Therefore it seems most likely that these two isomers are from terminal hydroxylation with 3-4 unsaturation and hydroxylation on the third carbon with either 2-3 or 3-4 double bond formation. These are shown in figure 6.7.

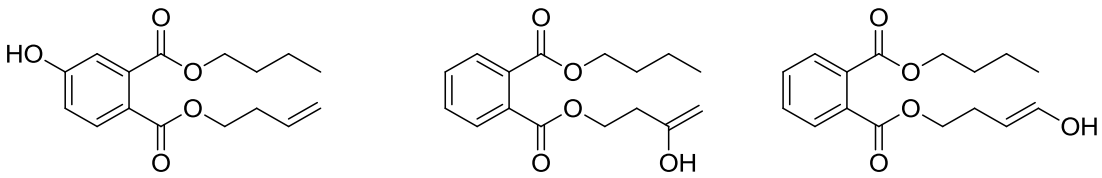

Figure 6.7: Possible isomers of $C_{16}H_{20}O_5$

Similarly $C_{16}H_{20}O_6$ and $C_{16}H_{20}O_7$ showed a lot of structural isomer information in their LC traces. This arises from the large permutations of possible hydroxylation sites and positions for double bond formation. From the amount of sub peaks seen it seems that almost every possible isomer is formed to some extent.

For MBP degradations the MBP molecular structure only contains one ester chain and so the number of sites for chemistry to occur is less. Therefore fewer isomers should be formed. For the product arising from one hydroxyl radical attack two isomers are seen. These are thought to be those arising from attack on either the terminal chain position or the phenyl ring. Conversely the product from two hydroxylations $C_{16}H_{22}O_6$ shows only a single isomer being formed. This would suggest that either this is formed from a separate mechanism of simultaneous dihydroxylations or that once one position is hydroxylated (phenyl or terminal ester chain) the other is in the second hydroxylation resulting in the same product either way.

6.3: Finding gas phase products using GC and GC-MS

Having described the liquid phase products from DBP and MBP degradation, efforts were made to then investigate any gaseous products formed. Previous studies into the degradation of various compounds have found combustion products in the gas phase via GC and GC-MS methods[9]. To study the gas phase initially GC was used. As with liquid phase product detection, 10 mgL^{-1} solutions of DBP were degraded using 20 kHz ultrasound but this time in a sealed vessel. The head space was then sampled after 3 hours of sonication and injected straight into the GC. This simple experiment yielded a gas sample which was found to smell slightly of methane hinting at the presence of small organic gas species.

The GC analysis yielded disappointing results however. The resulting peaks were found to be very small but by comparison of the resulting retention times with samples of known retention the following were proposed to be present in

the gas phase samples collected: methane, ethane, ethylene, butane and 1,3-butadiene.

Later in the course of this work a GC-MS became available in the department. The same experiment described above was performed using this machine to analyse the headspace samples. Disappointingly no peaks were found in the MS profile apart from that of oxygen, nitrogen, argon and other gases found in air. In spite of this the sample was again found to smell of methane

The experiment was repeated using 515 kHz ultrasound and the GC-MS analysis results showed peaks corresponding to CO_2 and methane.

6.4: A semi quantitative study into the effect of frequency on degradation product distributions

Having qualitatively described the degradation products of DBP for both 20 and 515 kHz frequency ultrasound, it was decided to conduct a quantitative study into the degradation process. To do so solutions of DBP and MBP were degraded as above but with the addition of two internal standards. TBZ was added to samples acting as an internal standard during positive ionisation mode analyses. The internal standard used for negative ionisation mode analyses was mandelic acid. This was chosen as it was different in mass to all the products found and so it was thought that it would not interfere in the mass spectra obtained.

The study conducted was actually semi quantitative in that the products are described as [product] / [internal standard], where [*i*] denotes the area of the LC peak in question. The reason for this is that to convert this quantity to an actual concentration, calibration curves of ionisation response *verses* concentration would be needed for each product. This was obviously impossible as several of the products resulting from radical attack are quite exotic and difficult to synthesise. It was therefore decided to describe all products by [product] / [internal standard] even for those products which are easily obtainable in most laboratories *e.g.* phthalic acid and benzoic acid

The first of the two studies conducted was to explore the effect of frequency on the product distribution of DBP and MBP degradation. It should be noted however that only the 515 kHz frequency ultrasound had internal standards added to samples. This was due to the fact that the data from 20 kHz ultrasound was extracted from previous experiments in which no internal standard was added. Therefore the graphs from 20 kHz experiments have a y axis of peak area whereas those from 515 kHz experiments have a y axis of [product] / [internal standard]. Not all of the products described in the complete process were analysed in the product distribution, only the major ones as determined by peak area or [product] / [internal standard]. For the frequency comparison, experiments were done with solutions purged with argon.

Product distribution analysis for 20 kHz degradations

Figure 6.8 shows the product distribution over time of the 8 major products found via positive mode ionisation from degradation of DBP solutions. From this plot we can see that by far the most prominent product is $C_{16}H_{20}O_5$. This product arises from a single hydroxylation and single hydrogen abstraction on DBP. The concentration of this product increases during the entire experiment. There is then a second group of products with very similar concentration over time profiles. These are those arising from a single and a double hydroxylation of DBP and also that arising from a single hydrogen abstraction creating a double bond. The remainder of products are in much lower abundance and are those which are formed from either $C_{16}H_{20}O_5$ or the group of products next lowest in abundance.

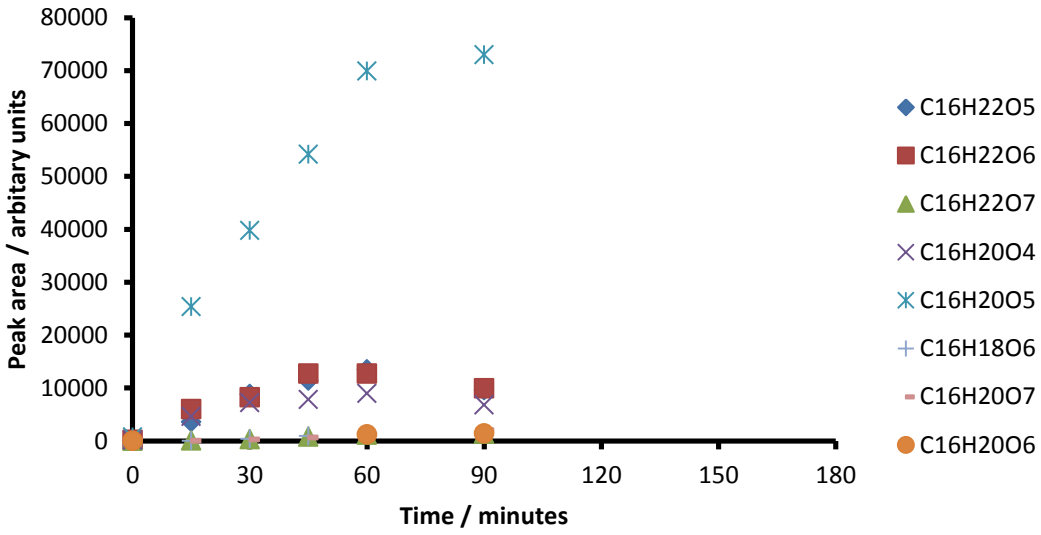

Figure 6.8: Distributions of products visualised in positive ionisation mode

The fact that this lowest concentration group of products comes from degradation of more initial products is easily seen in figure 6.8, from which the curve for $C_{16}H_{20}O_5$ has been removed. It can now be seen that $C_{16}H_{22}O_6$, $C_{16}H_{20}O_4$, and $C_{16}H_{22}O_5$ increase in concentration until 45 – 60 minutes into the degradation. They reach maximum concentration around this time point and are then degraded themselves.

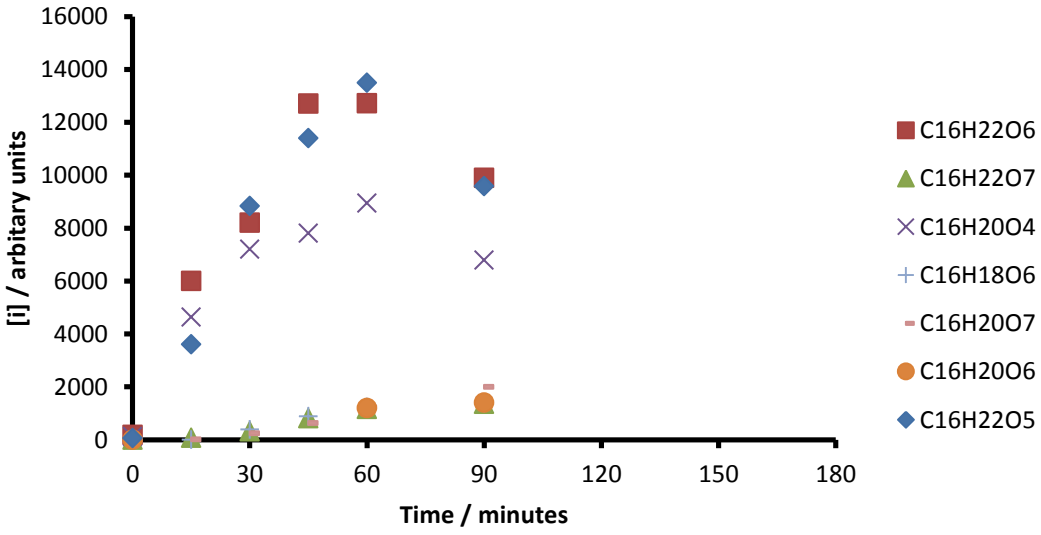

Figure 6.9: Low concentration magnification of figure 5.1

This is reflected in the sharp increase in the profiles of the other products at the same time point, signifying that they are being formed from the more initial products of DBP degradation.

It is surprising to find that the product with the highest concentration was not that arising from a single transformation of DBP but two; a hydroxylation and the formation of a double bond on one of the ester chain tails. If we compare this to the product arising from a single double bond formation then there is a large difference in their abundances in solution, if we assume that being similar structurally that they ionise equally well. This difference suggests that hydroxylation of DBP then encourages the formation of a double bond. This ratio of products also suggests that the initial hydroxylation of DBP occurs on one of the terminal points of an ester chain, not on the phenyl ring as previously thought.

The other surprising point to note is that the products formed from a single and a double hydroxylation of DBP have very similar concentration, i.e. $C_{16}H_{22}O_5$ and $C_{16}H_{22}O_6$. If we compare this to the much lower concentration of $C_{16}H_{22}O_7$, which arises from 3 hydroxylations, it seems that possibly one is not made from the other but that there are both single and double radical attack mechanisms running concurrently. This is possibly not surprising if we consider the fact that DBP exists close to the bubble interface and would be subject to the ejection of a considerable concentration of hydroxyl radicals in a short amount of time upon bubble collapse.

The product visualised using negative mode ionisation, monobutyl phthalate is shown in figure 6.9. Again it can be seen that the abundance of MBP increased to around 90 minutes whereby it then decreases, signifying it is also degraded by ultrasonic action.

It is also interesting to note that it seems from the peak areas obtained that it could be that MBP is not the major product formed from DBP degradation but $C_{16}H_{20}O_5$ is. Care needs to be taken with this statement since concentrations are not being reported but peak areas. It could be that $C_{16}H_{20}O_5$ happens to ionise much better and so has a peak area three times larger for that reason. But from the graphs shown here it is probable that MBP is not the major product.

This finding would conflict with statements by Yim *et al* [9]and Psikallis *et al*[10] who both reported the major product of DBP degradation to be the mono ester, MBP. This finding also suggests that radical attack is the major pathway by which DBP is degraded and that hydrolysis is a much more secondary pathway. This agrees with the same finding by Yim *et al*. It would appear therefore that hydrolysis of DBP occurs mainly after it has been attacked several times by hydroxyl radicals.

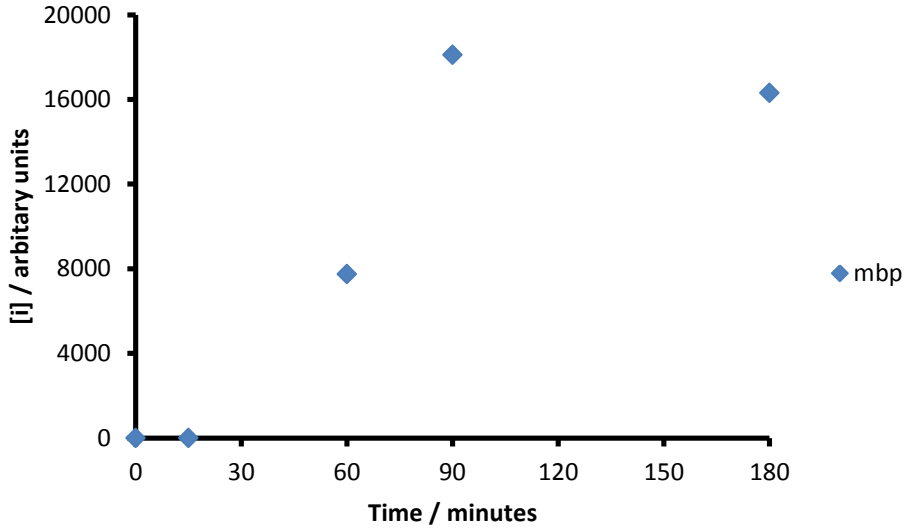

Figure 6.10: Plot of MBP "concentration" over time

Having described the product distributions of those products found from degrading DBP directly those found by degrading MBP solutions shall now be presented. From figure 6.11 it can be seen that the major product found to ionise as negative ions is phthalic acid. This is in much higher abundance than the two products found to arise from radical attack on MBP, $C_{12}H_{13}O_5$, which has been hydroxylated and $C_{12}H_{11}O_4$ where a double bond has been formed. This suggests that the fate of MBP once formed is mainly hydrolysis to form phthalic acid and not further radical attack.

This finding can be rationalised quite easily. Since MBP is a monoester it possesses a free acid group. This moiety would make MBP much more hydrophilic than DBP and so it would be expected that less MBP would be

present close to the bubble interface and so is out competed for ·OH radicals by DBP. There would however be enough MBP in the hot interfacial region for MBP to then be hydrolysed by activated water molecules just after the collapse of a cavitation bubble.

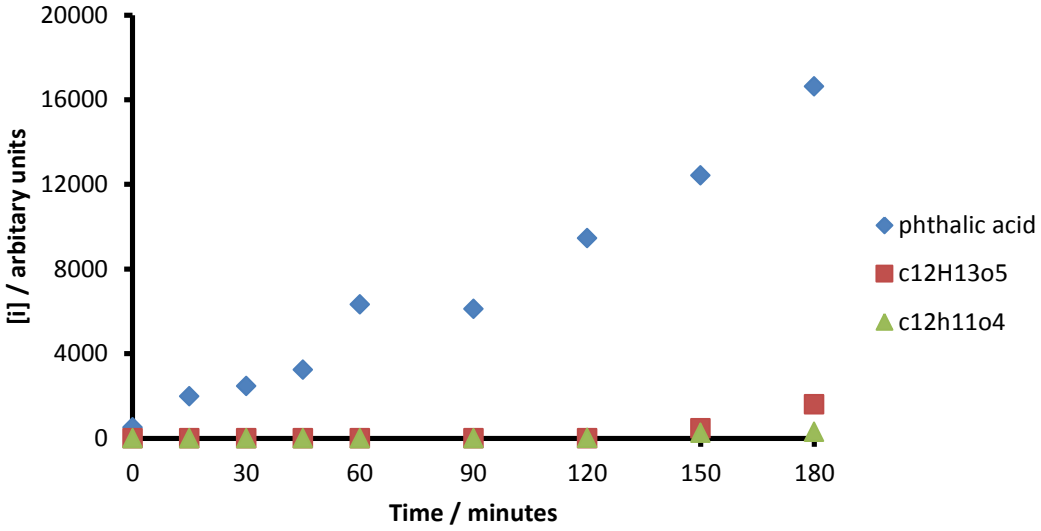

Figure 6.11: Negative ionisation mode products found from MBP degradations

Product distribution analysis for 515 kHz degradations

Having described the degradation of DBP and MBP by 20 kHz ultrasound the same plots shall now be presented using the data from 515 kHz degradations. Figure 6.9 shows the major products found from positive ionisation mode analyses of the degradation of DBP solutions purged with argon.

Similarly to the distributions of degradations brought about by 20 kHz ultrasound, $C_{16}H_{20}O_5$ was again found to be the major product formed. In this experiment its concentration peaks quite early on (t = 30 min) and then generally decreases over time. When using 515 kHz ultrasound the concentrations of all the other products formed is much higher in comparison. It can also be seen that most of the products formed go through several cycles of increasing and decreasing in concentration over the time of the experiment.

Both of these findings are due to the fact that stable rather than transient cavitation is now taking place.

The reasoning for the concentrations of most products being higher is due to the higher radical output from stable cavitation bubbles compared to transient cavitation bubbles. This allows the products arising from several radical attacks to be formed much more readily and quickly. The continual production of radicals is characteristic of stable cavitation and also explains the oscillation in concentration seen for most products in figure 6.12. Products are continually being formed and then attacked and degraded to form the next product. This variation of product concentration shows that the bubbles formed have a longer lifetime over which radicals are continually produced.

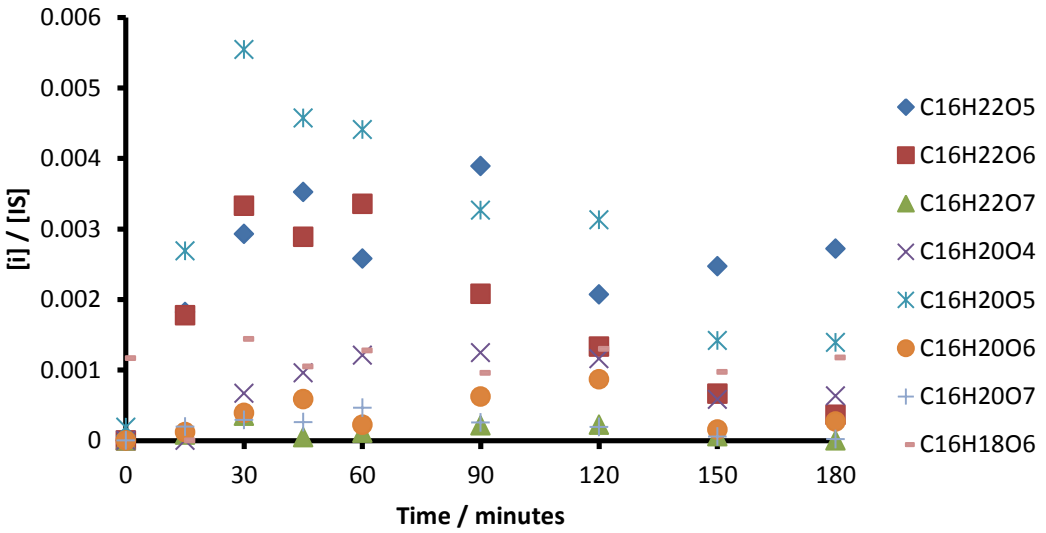

Figure 6.12: Distributions of products visualised in positive ionisation mode

The distribution of products visualised in negative ionisation mode is shown in figure 6.13. Unlike the experiments using 20 kHz ultrasound MBP was not the only product which was visualisable from DBP degradation, phthalic acid could also be detected towards the end of the experiment in very low concentrations. It can be seen that the concentration of MBP goes through two cycles of increasing and decreasing concentration, one minor and one major. The comparatively low concentration of phthalic acid also indicates that hydrolysis is

a minor reaction pathway for 515 kHz as well as 20 kHz ultrasound. The MBP initially created does not seem to be converted to phthalic acid. It is only when a large quantity of MBP is destroyed in the second cycle that phthalic acid is detected.

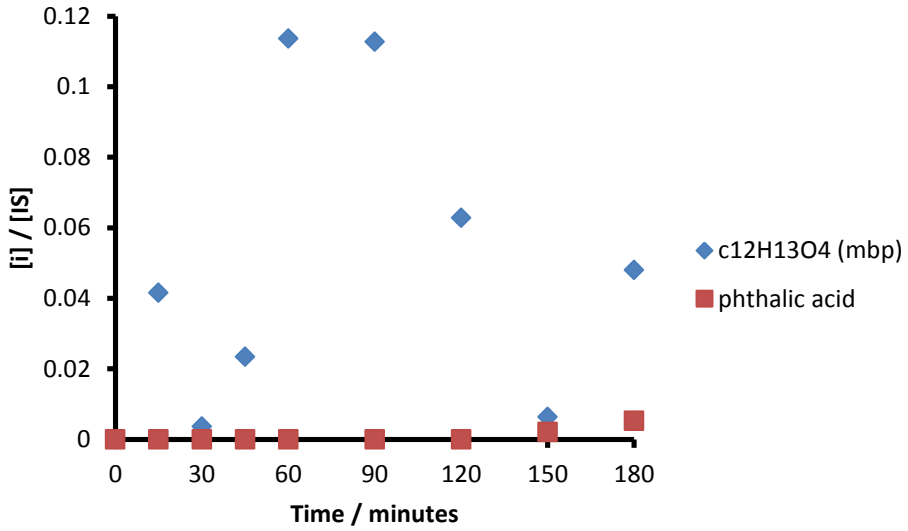

Figure 6.13: Distribution of products found using negative mode ionisation

This suggests that phthalic acid is not created directly from MBP but from transformation products of MBP which have then been attacked by OH radicals before any hydrolysis occurs to form phthalic acid. This behaviour is exactly the same as that seen for the formation of MBP from DBP; hydrolysis is thought to be a minor degradation pathway and only seems to occur once a species (DBP or MBP) has been attacked several times by hydroxyl radicals.

This behaviour would suggest that hydrolysis is occurring further away from the imploding bubble than radical attack since hydroxylated and unsaturated products would be more hydrophilic than DBP and/or MBP and therefore be partitioned further away from the bubble interface.

Figure 6.14 shows the distributions of products found from the degradation of MBP solutions. Phthalic acid and $C_{12}H_{13}O_5$ were again found as with 20 kHz degradations. However $C_{12}H_{11}O_5$ was found for 515 kHz ultrasound instead of $C_{12}H_{11}O_4$ which could not be found. As with the products described in figure 6.13, products undergo more than one cycle of production and degradation.

Unlike 20 kHz ultrasound experiments the major product is now $C_{12}H_{13}O_5$ not phthalic acid and peaks strongly at 45 minutes and is then rapidly consumed. This again shows the higher radical output of 515 kHz ultrasound in comparison to 20 kHz ultrasound.

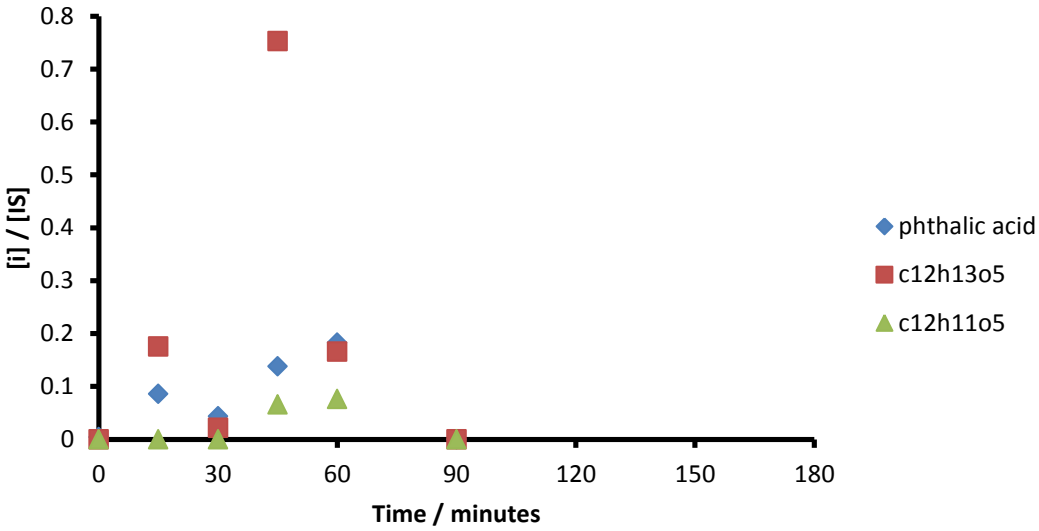

Figure 6.14: Products of MBP degradation found using negative mode ionisation

Summary of comparisons between 20 kHz and 515 kHz ultrasound

Having shown all of the relevant data the following conclusions between 20 kHz and 515 kHz degradations can be made.

1: 515 kHz is effective at transforming DBP, MBP and all of the products formed. 20 kHz ultrasound is not as effective at destroying the initial transformation products of DBP and MBP degradation.

2: Products undergo several cycles of production and consumption during experiments using 515 kHz ultrasound. For 20 kHz degradations only a single cycle is seen and consists mainly of initial product formation and not so much initial product destruction.

3: It may therefore be that 20 kHz ultrasound does not effectively mineralise DBP when compared to 515 kHz ultrasound. This would also explain why only trace amounts of gas phase products were found using GC and GC-MS analysis as 515 kHz ultrasound was not used for this study, only 20 kHz

ultrasound. This could easily be checked using a total organic carbon analyser, which we did not have access to.

4: For both frequencies used hydrolysis seems to be a minor degradation pathway and only appears to occur on species which have been hydroxylated and/or unsaturated several times. This leads the author to believe that hydrolysis is occurring away from the bubble surface in the interfacial zone surrounding the bubble.

6.5: A semi quantitative study into the effect of different gas compositions on the degradation products and their distributions

Having considered the effect that two differing frequencies had on the product distribution of DBP and MBP degradation, the effect of the dissolved gas shall now be investigated. Firstly the effect of air, argon, nitrogen and oxygen shall be examined for 20 kHz ultrasound. After this the same cases for 515 kHz ultrasound shall be discussed along with a brief analysis of results from carbon dioxide purged solutions.

Degradations under different gases using 20 kHz ultrasound

Argon

The case for argon has already been presented in figures 6.8 – 6.11 and shall not be duplicated here.

Air

The product distributions formed when using air as the purging gas is shown in figures 6.15 to 6.17. As with the experiment using argon, $C_{16}H_{20}O_5$ is found to be the major product of the degradation process. In comparison much more seems to be produced than with argon experiments. Care has to be taken with this statement however since no internal standard was used and so the difference in ionisation response could be due to differences with the mass spectrometer. However, the experiments were performed concurrently and so this factor can be thought to be negligible.

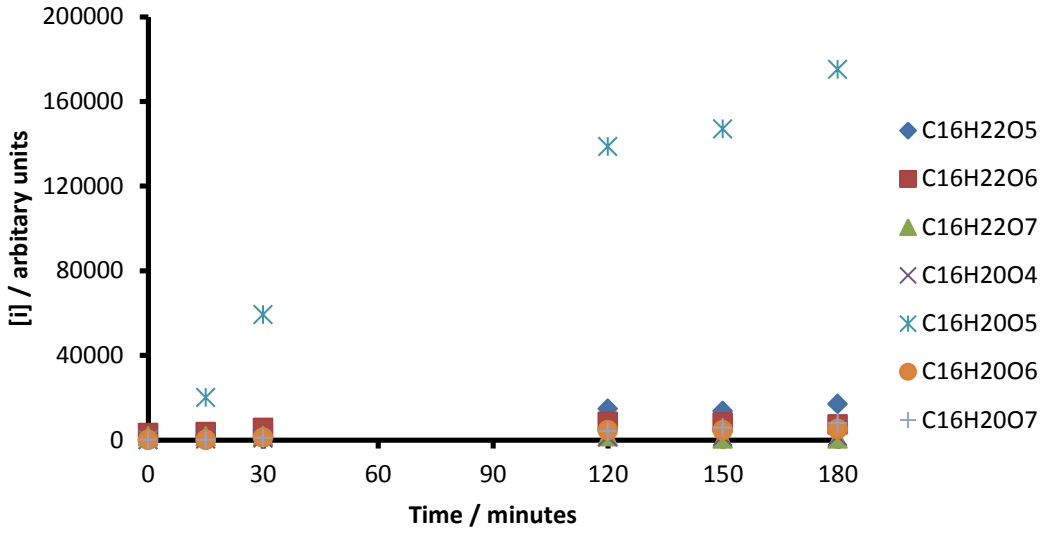

Figure 6.15: Positive ionisation mode products formed using DBP solutions purged with air.

As with experiments using argon $C_{16}H_{20}O_5$ is seen to mainly increase in concentration over time. The amount of other transformation products is in comparison negligible and little $C_{16}H_{20}O_6$ is formed from $C_{16}H_{20}O_5$. This is most likely to be due to $C_{16}H_{20}O_5$ partitioning away from the collapsing bubble interface due to its increased hydrophilictity and therefore being less prone to radical attack compared to the remaining DBP which out competes $C_{16}H_{20}O_5$ for ejected ·OH radicals.

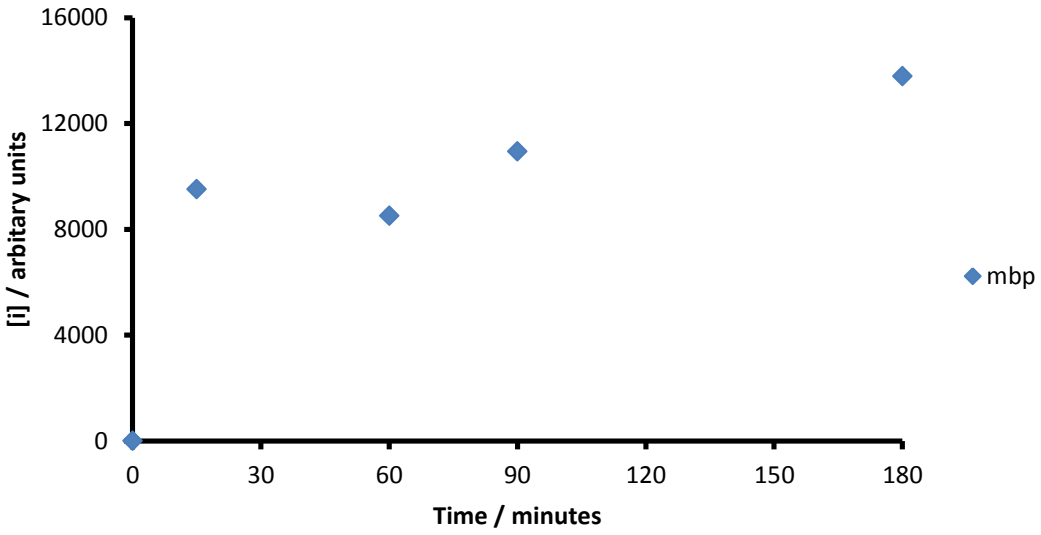

Figure 6.16: Production of MBP over time from DBP solution containing air

From figure 6.16 we can see that MBP is produced throughout the duration of the experiment as with degradations under argon. The concentration over time profile is a bit different however. Under air the concentration rises very quickly within the first 15 minutes. This is then partially degraded further into other products and then continues to increase in concentration again. In comparison, the time profile for MBP concentration in solutions purged with argon increases more steadily over time and more is produced within the time of the experiment as determined by the maximum height of the curve plotted.

Figure 6.17 shows the distributions of 3 products formed by degradation of MBP solutions purged with air. As with argon purged experiments, phthalic acid is the major product seen in negative ionisation mode. Much more phthalic acid is formed however, indicating that the amount of hydrolysis occurring may be higher in solutions purged with air.

The concentration of products arising from degradation of MBP is now much higher than in argon purged solutions. The reason for this is not clear but must be due to a change in the bubble dynamics of the two systems (argon and air purged solutions).

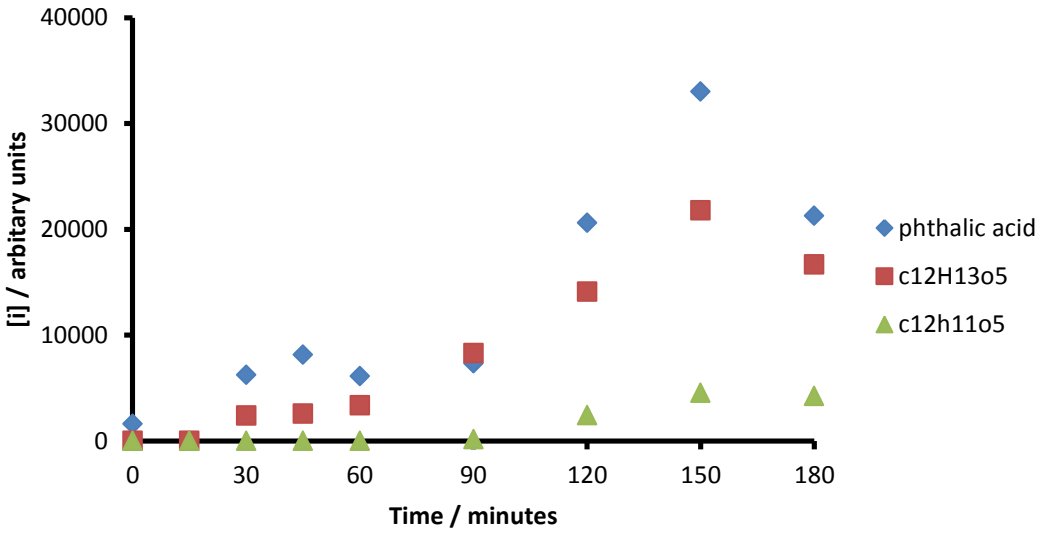

Figure 6.17: Product distribution of products formed from MBP degradations (air).

Oxygen

The same plots as above are shown in figures 6.18 – 6.20 for degradations of DBP solutions purged with oxygen. The plot shown in figure 6.18 is almost identical to that of air. This possibly signifies that the nitrogen content of air has little role to play when considering the concentration of radicals produced from air filled cavitation bubble collapse. From analysis of the products formed it would seem that an air filled bubble acts as if it were filled with only oxygen as the two product distributions are very similar. It should be noted here that surprisingly when searching for new products in oxygen purged solutions no products arising from ·OOH radical attacks were found.

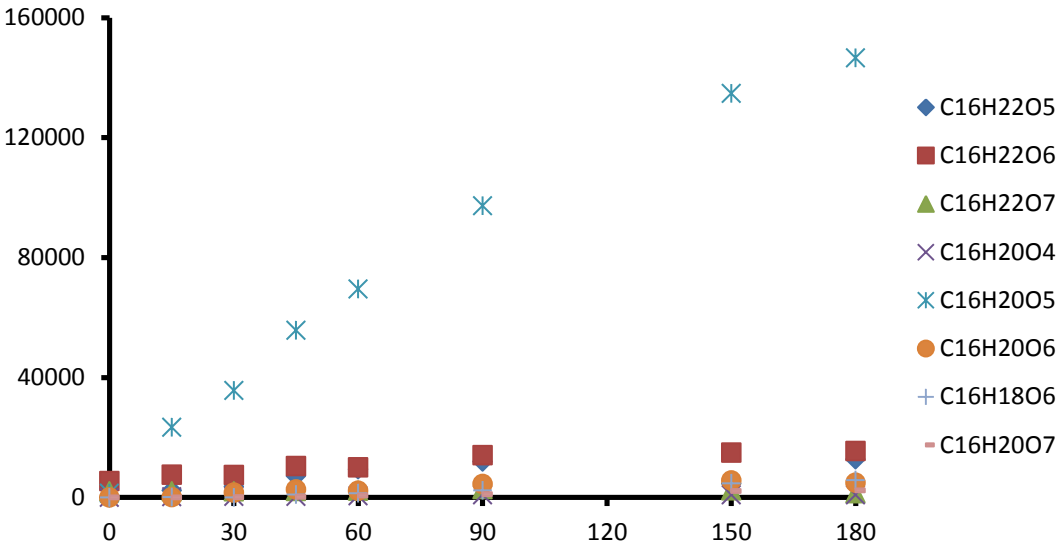

Figure 6.18: Distributions for positive ionisation mode products (oxygen)

Figure 6.19 shows the formation of MBP over time from the degradation of the DBP solution. Again the behaviour is similar to that of air, both experiments show an s shaped profile between 0 and 90 minutes. Under air the concentration then increased to 180 minutes.

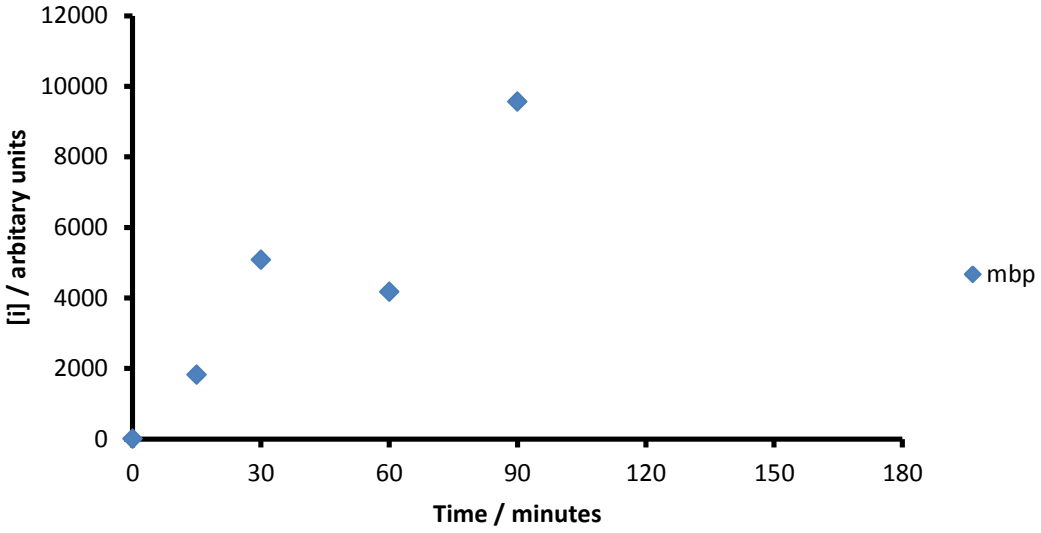

Figure 6.19: Production of MBP over time from DBP degradation. The final time point at 180 minutes is not shown as the data file was corrupted.

The final plot for oxygen experiments shows the degradation products found when degrading MBP solutions. Unlike the other plot this one is dissimilar to

that found from air purged solutions. Phthalic acid is again the major product found in negative ionisation mode and compared to argon quite a lot of products resulting from radical attack on MBP are found. However unlike the profile for air, the concentration of the three products is found to mainly increase over time although the amount of $C_{12}H_{13}O_5$ decreases at t = 180 minutes.

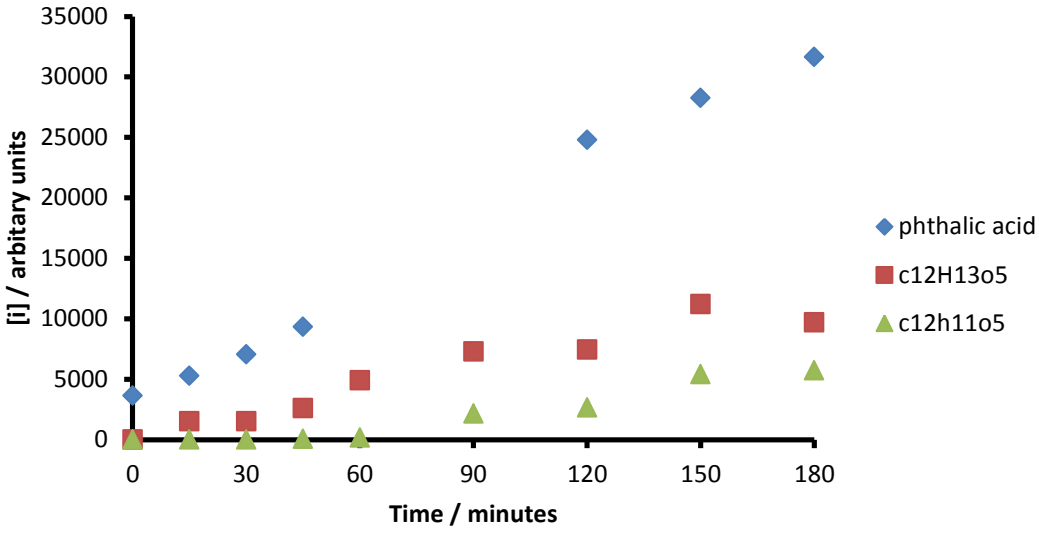

Figure 6.20: Degradation of MBP in oxygen purged solution

Nitrogen

The equivalent graphs as before are shown for nitrogen purged experiments in figures 6.21 – 6.22. As with all the previous experiments the major product found in positive ionisation mode analysis of the degradation of DBP was $C_{16}H_{20}O_5$ which increased strongly over time. By t = 180 the concentration had decreased, at the same time interval one of its transforms $C_{16}H_{20}O_6$ increases in concentration.

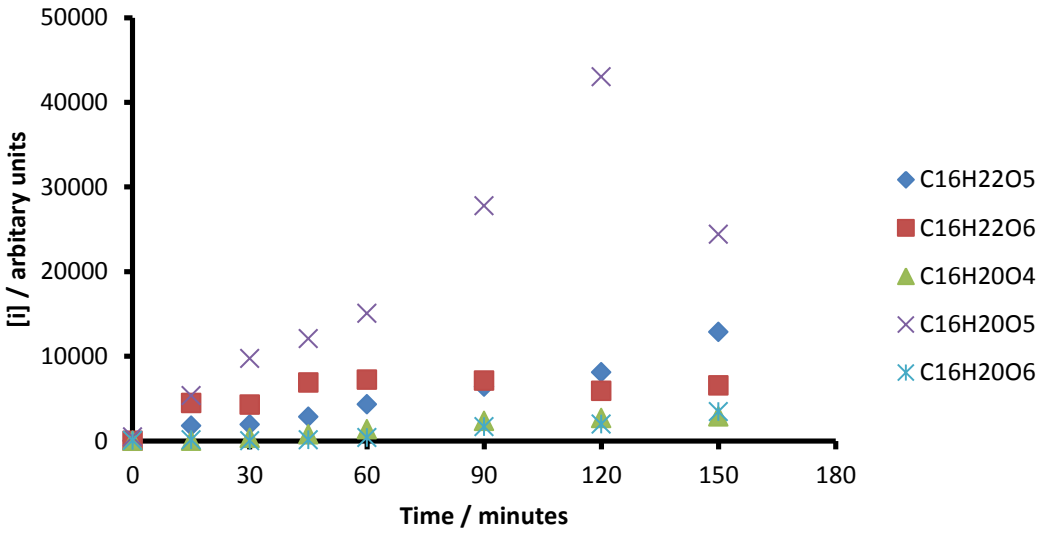

Figure 6.21: Degradation products seen in positive ionisation mode

This is not the only route for $C_{16}H_{20}O_5$ degradation as the increase in $C_{16}H_{20}O_6$ is much smaller than the decrease in $C_{16}H_{20}O_5$. The shortfall is thought to have been converted to MBP by hydrolysis, as the amount of MBP in solution strongly increases from t = 90 to t = 180.

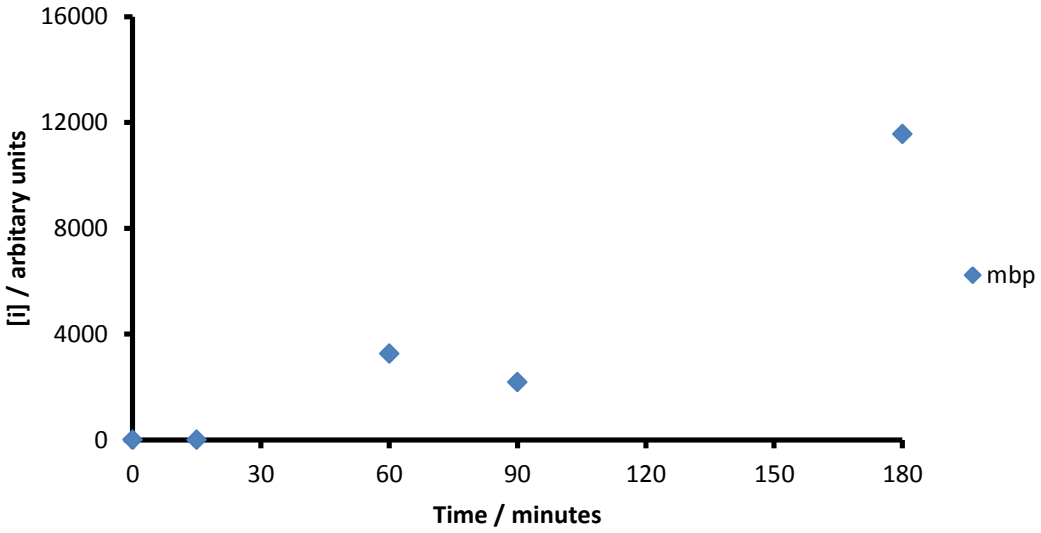

Figure 6.22: Production of MBP over time in nitrogen purged solutions

It has been mentioned previously in chapter 5 that the main radical generated from collapse of nitrogen filled bubbles is the ·NO radical. Therefore in degradation experiments purged with nitrogen adducts of ·NO were also searched for in addition to products arising from ·OH radical addition / attack. These were not found (DBP-NO and MBP-NO) in any time interval for either 20 kHz nor 515 kHz experiments. If produced, it seems that the ·NO radical does not attack DBP molecules.

Degradations under different gases using 515 kHz ultrasound

Argon

As with 20 kHz, the discussion for the case of argon has already been presented and so will not be discussed here further.

Air

Figures 6.23 – 6.25 show the same plots as with argon degradations but for those solutions which have been purged with air. The product profiles were found to be quite different to that of argon. As with all previous degradations $C_{16}H_{20}O_5$ was by far the most prevelant product formed. The other subsequent products were in much lower concentration than for the degradation under argon. This can be rationalised by referring to the kinetic data in chapter 5. Air containing DBP solutions were found to be degraded slower and less completely than argon containing solutions. This was rationalised as a result of the lower concentration of radicals ejected by the cavitation bubbles formed. The same is again true, the lower concentration of products is directly linked to the lower concentration of radicals as the resulting oxidising power arising from the system and conditions is less.

Since less radicals are ejected from the cavitation bubbles it seems that the conversion to products further down the mechanistic chain is much lower and so the DBP might be converted well to primary products but not secondary and tertiary products when air is dissolved in solutions.

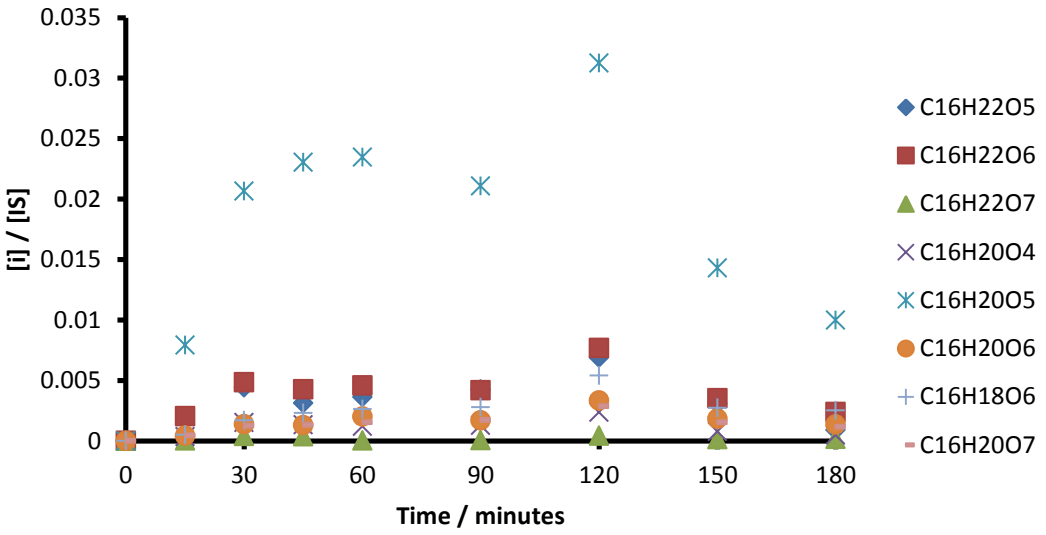

Figure 6.23: Products found via positive mode ionisation of DBP degradation samples (air)

In contrast the amount of MBP formed in solution appears to be higher in figure 6.24 than in figure 6.27. The amount of MBP increases steadily overtime again exhibiting an s shaped profile before decreasing in concentration at t = 150. This finding might suggest that using 515 kHz ultrasound with an air environment encourages the hydrolysis pathway forming more MBP from DBP and primary transforms of DBP.

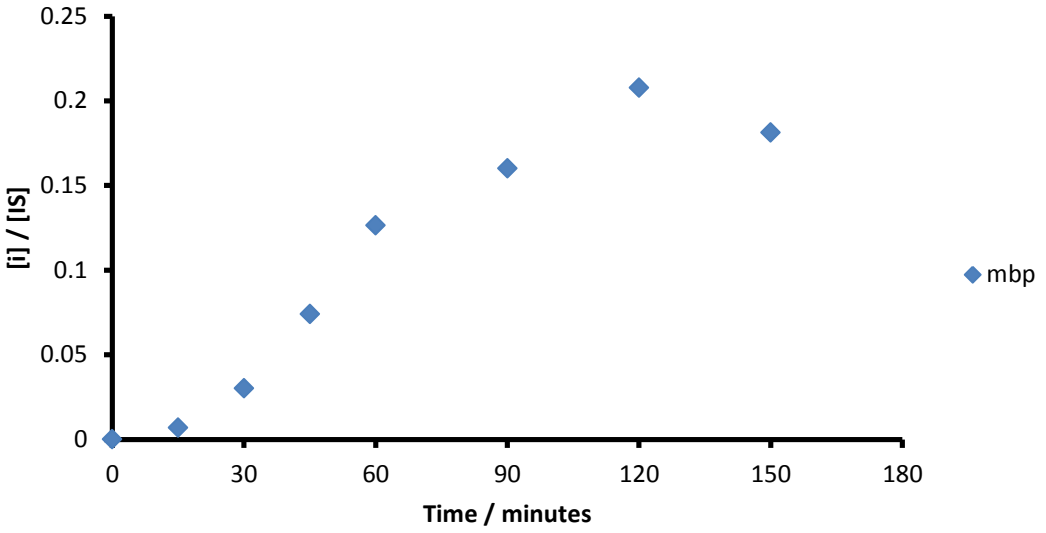

Figure 5.24: Production of MBP in DBP solutions purged with air

The concentration profiles of phthalic acid, $C_{12}H_{13}O_5$ and $C_{12}H_{11}O_5$ are also different under air than under argon. All three profiles go through two cycles of increase and subsequent decrease in concentration over the course of the experiment, with phthalic acid being the most dominant. The graphs also show that all of the products produced from MBP radical attack are destroyed and converted to other products by the end of the experiment, although it seems that $C_{12}H_{13}O_5$ is about to start another cycle of production at t = 180.

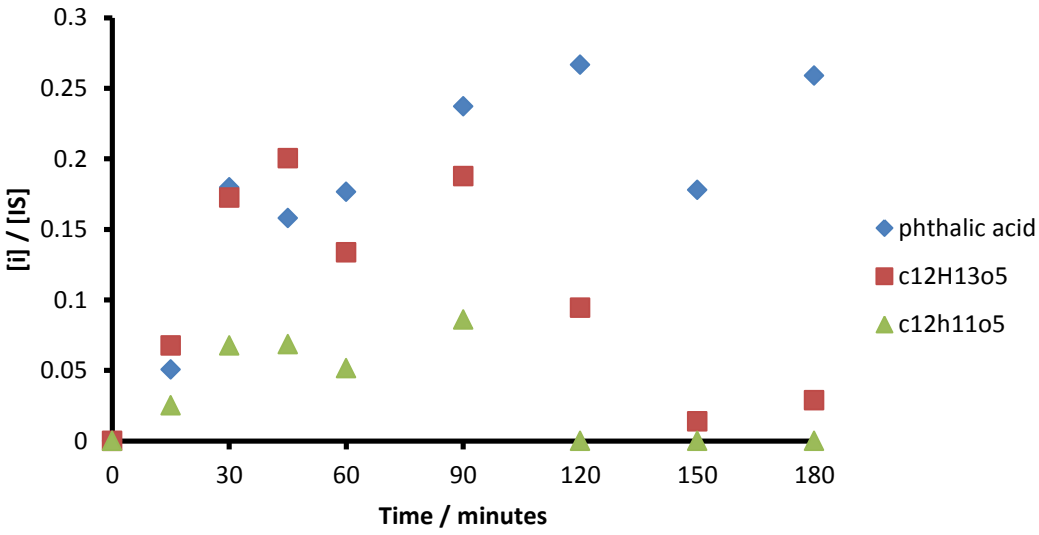

Figure 6.25: Products found through negative ionisation mode of MBP degradations.

Oxygen

The degradations under oxygen are massively different to those of the other gases. When searching for products almost all of the ones used in this study could not be found in any concentration at any of the time intervals. The only product found was $C_{16}H_{20}O_5$ which is at lower concentration than in the other experiments. The reason for this lack of presence of products is attributed to the massive amount of radicals thought to be ejected from a bubble filled initially with oxygen and water vapour undergoing stable cavitation[13-15].

In chapter 5 it was shown that the degradation of DBP solutions purged with oxygen and irradiated with 515 kHz ultrasound progressed very rapidly. This was attributed to a large concentration of ejected OH radicals. This may be the same reason why no degradation products are found. The concentration and activity of the radicals formed could be of such magnitude that the DBP is effectively mineralised resulting in the lack of formation of by-products. Again, use of a TOC analyser would have been able to confirm this understanding.

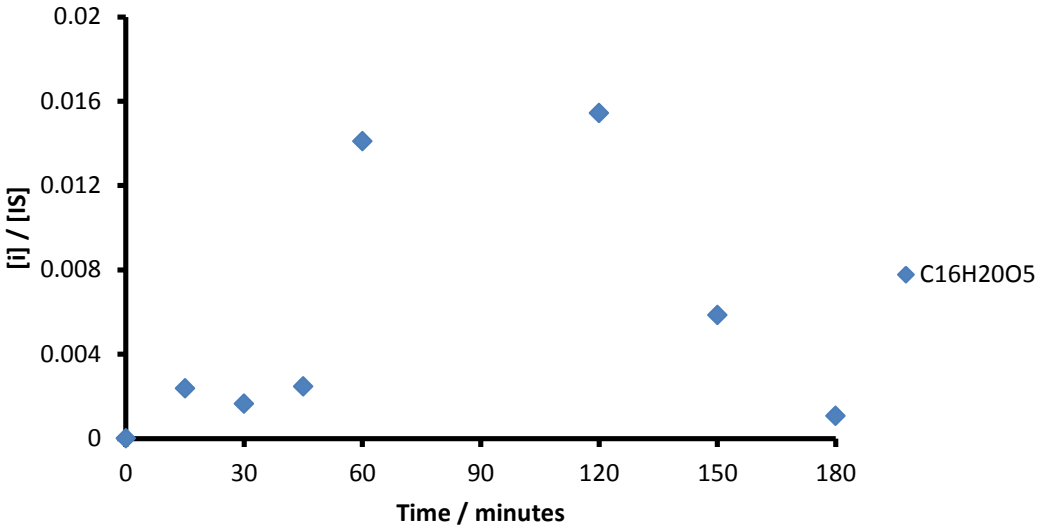

Figure 6.26: The only product found for oxygen purged solutions: $C_{16}H_{20}O_5$

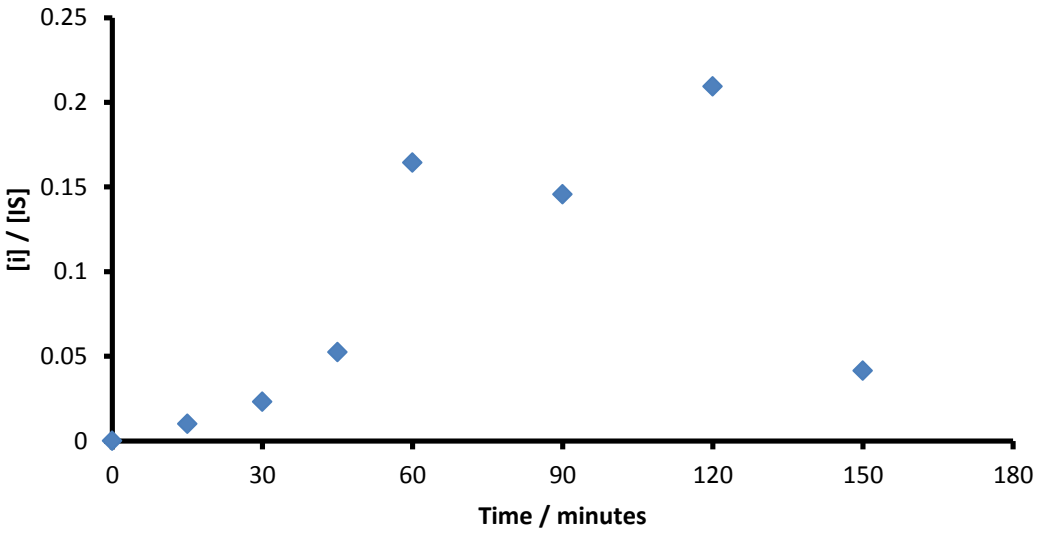

Figure 6.27: The formation of MBP over time in oxygen purged solutions

Figure 6.27 shows that the formation of MBP is however similar to the profile of the other experiments performed using 515 kHz ultrasound. An s shaped profile is again seen and towards the end of the experiment the concentration of MBP seems to be falling sharply so that the final concentration of MBP is much lower than with the other experiments.

Figure 6.28 shows the formation of phthalic acid and the two transforms of MBP studied. As with MBP, the concentrations of the two transforms are approaching zero at the end of the experiment, signifying that they are also being effectively degraded.

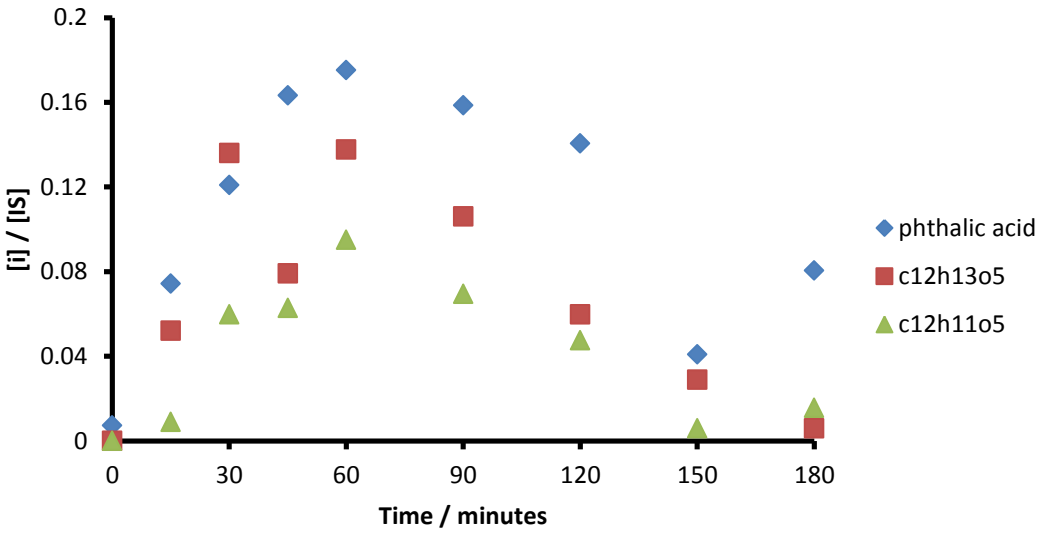

Figure 6.28: The formation of phthalic acid and MBP transforms over time (oxygen)

In summary it seems that oxygen is extremely effective as an entrained gas as all the products studied seem to be mineralised by the end of the experiment or were not detectable at all during the whole experiment.

Nitrogen

Figure 6.29 shows the distribution of products for DBP solutions purged with nitrogen gas. In the kinetic studies discussed in chapter 4, nitrogen purging was found to lead to ineffective degradations, the formation of non-oxidative species being cited as the reason for this. This ineffectiveness is again seen below. The most abundant product was again $C_{16}H_{20}O_5$ much less is found than for the other gases especially air. A similar clustering of the concentration of products as seen in argon is found for nitrogen purged solutions albeit at lower product abundances.

Similarly the amount of monobutyl phthalate formed is the highest of the gases studied. The formation of MBP is much greater than under other gases. This is expected to be due to the fact that since nitrogen filled bubbles eject little by way of OH radicals that hydrolysis now becomes the main pathway for degradation of DBP. Since the collapse of nitrogen filled bubbles still generates a hot bubble core the formation of OH radicals can be expected to be quite efficient. Also the interfacial region where hydrolysis occurs is still heated to

high temperatures and so a lot of DBP hydrolysis could occur in this region. Similarly the formation of phthalic acid from MBP is quite efficient in solutions purged with nitrogen, with a similar amount of transformation products of MBP being created as with air albeit with different time profiles.

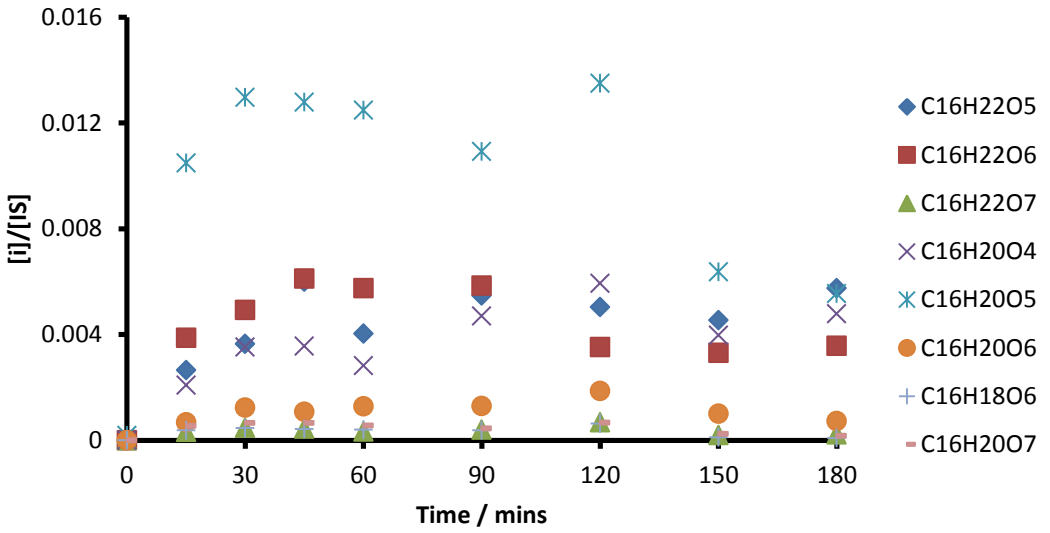

Figure 6.29: Product distributions over time for nitrogen purged DBP solutions

The fact that the hydrolysis reactions appear to be effective is a reminder that cavitation of nitrogen purged solutions still leads to hot cavitation bubbles, for 20 kHz more so than 515 kHz reactions this is just not well translated into OH radical concentration (as seen by the lowered amount of ·OH attack products) due to intrabubble chemistries giving rise to mainly products with little oxidising power. Hydrolysis of DBP to MBP and MBP to phthalic acid would be driven by the heat generated in the interfacial region of the bubble and the fact that nitrogen effectively produces phthalic acid denotes that there exists a hot interfacial region despite poor formation of products from hydroxyl radical attacks.

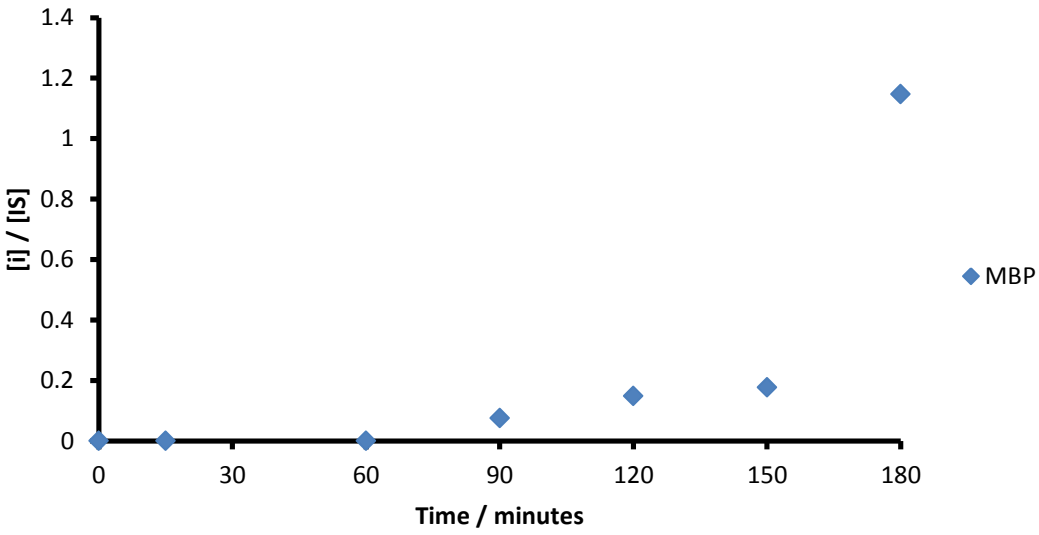

Figure 6.30: The formation of MBP over time (nitrogen purged solution)

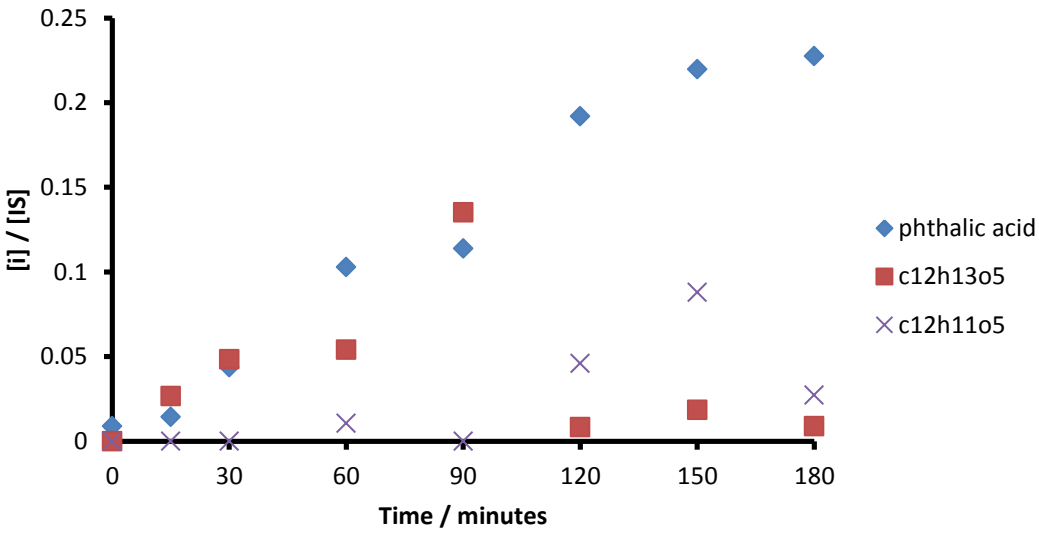

Figure 6.31: Phthalic acid and the products studied arising from MBP degradation

Carbon dioxide

In chapter 5, carbon dioxide had been found to be the least effective gas in degrading DBP. This was due to the very low temperatures attained upon cavitation bubble collapse and subsequent very low concentration of radicals ejected from the collapsed bubble. Nevertheless it was decided to probe the

products formed to see if DBP was degraded at high concentrations and to see if the low temperature of collapse initiated a different sort of chemistry and thus generate different products in solution.

As shown in figure 6.32 only two products were found in solution $C_{16}H_{22}O_5$ and $C_{16}H_{20}O_5$, albeit in very low concentrations. This experiment stands apart from the others in that the major product was <u>not</u> $C_{16}H_{20}O_5$. Instead the product arising from hydroxylation without formation of a double bond is generated as the major and only product found from DBP degradation under CO_2.

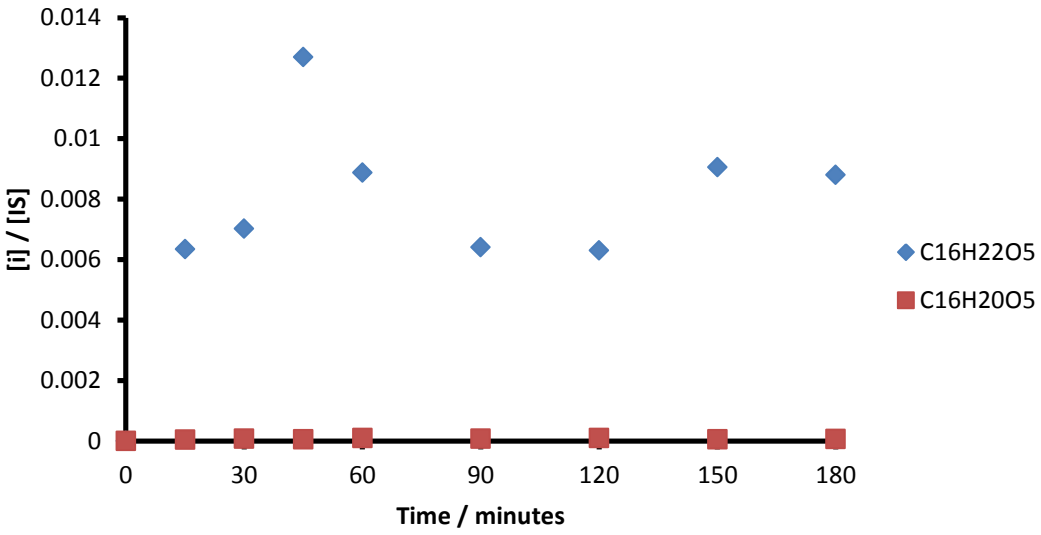

Figure 6.32: The two products found from degrading DBP solutions purged with CO_2

This demonstrates the low temperature of collapse of bubbles filled with CO_2 and subsequent generation of only low radical concentrations. It seems that insufficient radicals are formed to either generate much $C_{16}H_{20}O_5$ (this is in strong contrast with other experiments) or degrade the primary product significantly. In addition when looking for the presence of MBP there was none found in the DBP degradation experiments.

Figure 6.33 shows the distribution of phthalic acid over time for the experiment involving CO_2 purged MBP solutions. The other products of MBP sonolysis were not found (radical attack products of MBP), this again is attributed to the

low concentration of hydroxyl radicals formed from CO_2 filled cavitation bubble collapse. The initial concentration of phthalic acid was found to increase in the first 15 minutes and then was consumed rapidly. After 30 minutes phthalic acid was no longer being produced by the system. This signifies that there is little sonochemical activity with respect to phthalic acid formation much beyond the first 30 minutes. It also suggests that the system is most active in the first few minutes of sonication.

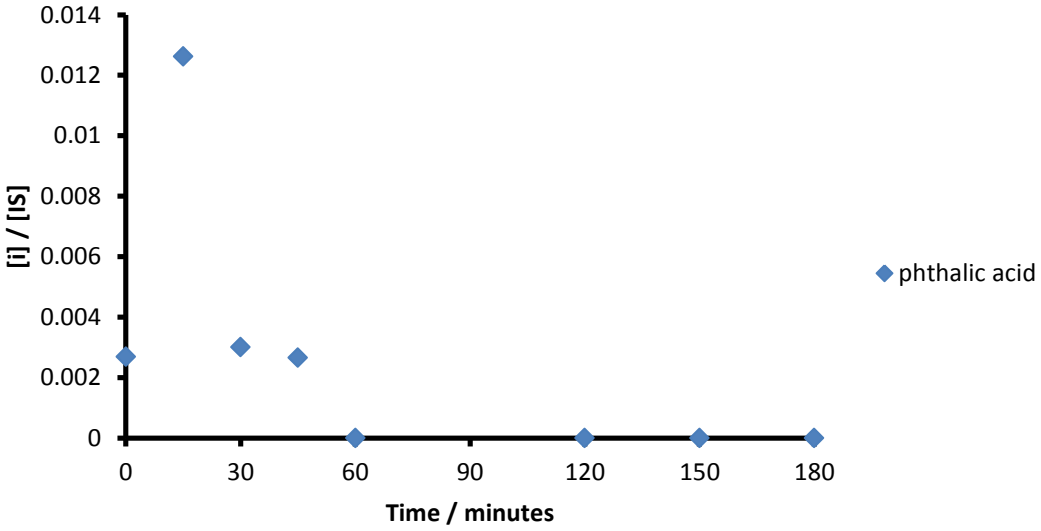

Figure 6.33 Production and consumption of phthalic acid (CO_2)

Summary of findings from changing entrained gas

1: Degradations in air, compared to in argon, produced less complete degradations of DBP and MBP. This was shown by degradation products further down the process tree being much lower in concentration. Conversely there was more DBP hydrolysis to form MBP.

2: Degradations under oxygen were found in chapter 5 to be extremely effective when using high frequency ultrasound. The same is again true when conversion of intermediates is considered. This was found to be extremely high as evidenced by a lack of many degradation products in solution.

3: Similarly to point 1, nitrogen produced less degradation products of MBP and DBP but had a much higher proportion of DBP hydrolysis to form MBP. This, when coupled with the findings for air experiments, seems to be a trend; the less good the conversion to radical based products the more DBP is converted via hydrolysis to MBP. This is quite logical since if DBP is not destroyed via radical attack due to a lack of radicals then there remains more DBP around the hot bubble interfacial region to then be hydrolysed into MBP. The same holds true for MBP hydrolysis to phthalic acid.

4: Carbon dioxide was found to yield much lower product concentrations to the point that most could not be detected in solution. The major product was now $C_{16}H_{22}O_5$ not $C_{16}H_{20}O_5$ as in all other experiments. This was taken as evidence that very few water molecules are lysed to form ·OH radicals in the collapsing bubbles due to the low core temperatures generated.

Final statement

From these data the use of oxygen and 515 kHz ultrasound appears to be the most effective combination of frequency and dissolved gas in rapidly degrading not only DBP but also all of its degradation products. Therefore this combination is recommended to be used if sonochemical treatment is to be used for the removal of DBP and other hydrophobic species from water.

6.6: Chapter references

1. V. Griffing, *Journal of Chemical Physics*, 1952, **20**, 939-942.
2. V. Griffing, *Journal of Chemical Physics*, 1950, **18**, 997-998.
3. K. Yasui, T. Tuziuti, T. Kozuka, A. Towata and Y. Iida, *J Chem Phys*, 2007, **127**, 154502.
4. C. M. Whitehouse, R. N. Dreyer, M. Yamashita and J. B. Fenn, *Analytical Chemistry*, 1985, **57**, 675-679.
5. K. Schug, Chromatography Online, 2011, vol. 2011.
6. J. A. Onwudili and P. T. Williams, *Energy & Fuels*, 2007, **21**, 1528-1533.
7. S. Kaneco, H. Katsumata, T. Suzuki and K. Ohta, *Chemical Engineering Journal*, 2006, **125**, 59-66.
8. T. K. Lau, W. Chu and N. Graham, *Chemosphere*, 2005, **60**, 1045-1053.
9. B. Yim, Y. Nagata and Y. Maeda, *Journal of Physical Chemistry A*, 2002, **106**, 104-107.
10. E. Psillakis, D. Mantzavinos and N. Kalogerakis, *Chemosphere*, 2004, **54**, 849-857.
11. M. K. F. Leung, J. M. J Fretchett, *Journal of the Chemical Society-Perkin Transactions 2*, 1993, **12**, 2329.
12. R. Singla, M. Ashokkumar and F. Grieser, *Research on Chemical Intermediates*, 2004, **30**, 723-733.
13. A. K. Shriwas and P. R. Gogate, *Separation and Purification Technology*, 2011, **79**, 1-7.
14. J. J. Yao, N. Y. Gao, Y. Deng, Y. Ma, H. J. Li, B. Xu and L. Li, *Ultrason Sonochem*, 2010, **17**, 802-809.
15. J. J. Yao, N. Y. Gao, C. Li, L. Li and B. Xu, *J Hazard Mater*, 2010, **175**, 138-145.

Chapter 7: Collected Experiments

This final results chapter collects together work done during the course of this project which does not quite fit into the previous two results chapters. There are two themes of work described herein sonoluminescence (SL) studies on phthalate solutions and degradation work done with other phthalate esters.

7.1: Aqueous sonoluminescence quenching by DBP

Sonoluminescence is the light generated as a result of cavitation bubble collapse and is currently thought to occur due to thermal excitation of the contents of the bubble as the temperature and pressure inside the collapsing bubble core increases during the collapse phase[1].

The amount of light generated by bubbles through sonoluminescence (SL) has been shown to be affected by the presence of several solutes such as organic acids[5], alcohols[2-4], polymers[4] and surfactants[2-4]. Most of these effects have been rationalised by explaining how the solutes affect the temperature of collapse and the number of active bubbles in the bubble population. Since we have shown that DBP also interacts and accumulates on a bubble surface it was decided to see what effect the addition of DBP had on the processes giving rise to SL and how its addition may affect SL intensities.

Figure 7.1 shows the data produced by measuring the amount of light produced when argon purged water is irradiated with 20 kHz ultrasound with the addition of increasing amounts of DBP. The SL intensities shown were reached by calculating the mean pixel brightness of the images produced in a small area below the 20 kHz horn in which a cone of SL was seen. This was done using the ImageJ software package.

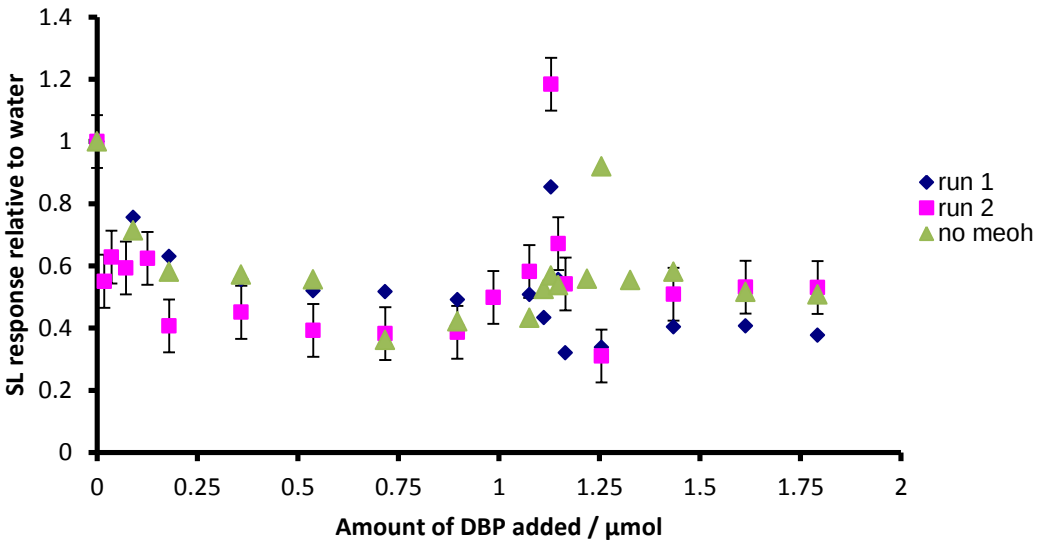

Figure 7.1: The effect of adding DBP on the sonoluminescence of 250 cm^3 argon saturated water. Representative error bars are shown on one data set only for clarity.

From the above figure it can be seen that the SL intensity initially decreases as DBP is added to very low concentrations. As the concentration of DBP increases the SL intensity reaches a constant value. The intensity can be seen to suddenly increase and decrease with a peak in intensity having added just 1.13 µmol of DBP to the water sample. A repeat of the experiment was performed to check that this trend was valid and reproducible and a peak albeit lesser in maximum intensity was found at the same value of added DBP.

A repeat was also performed in which the DBP solution added to the water was prepared without using methanolic stock solutions. This was performed since small amounts of methanol and other alcohols are known to quench the SL response of SL active bubbles and it needed to be confirmed that the peak behaviour arose from DBP based interactions not ones from alcohol. Again the same peak behaviour was seen but at a slightly different value of added DBP.

To explain this data the effect of DBP on the surface tension of the bubble interface needs to be considered. Figure 7.2 shows a plot of the air-water surface tension of DBP solutions of different concentrations. It can be seen from this plot that DBP is surface active due to its hydrophobic nature. As with all

surface active species, binding of DBP to the interface lowers the surface tension of the solution interface.

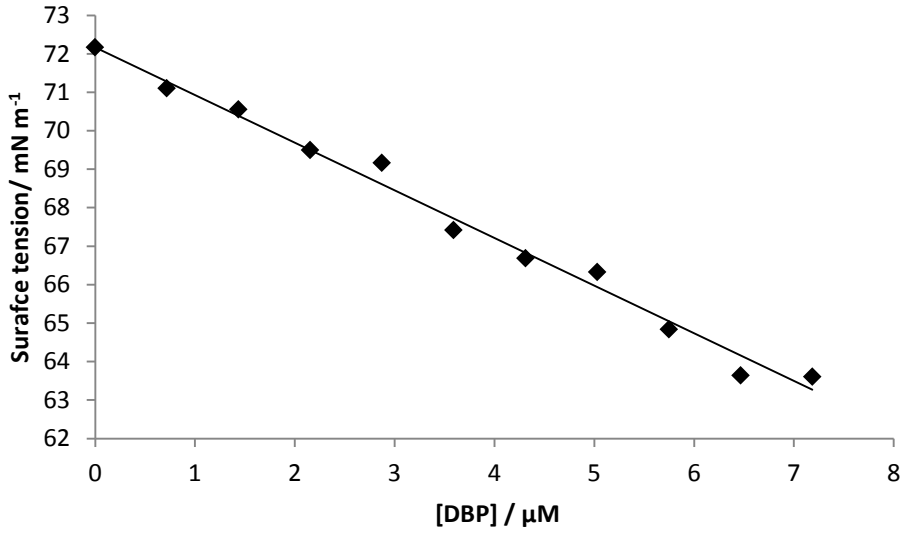

Figure 7.2: The effect of DBP on the surface tension of an air-water interface

This lowering of the surface tension of the bubble air-water interface would also change the resonant frequency range of the bubble population present in the cavitating DBP solutions. The resonant frequency depends in part on the surface tension of the bubble air-water interface as given in equation 7.1[6] where ω_0 is the resonant frequency of a bubble, R_0 is the bubble ambient radius, γ is the ratio of specific heats of the bubble contents, p_0 is the gas pressure in the bubble at equilibrium, ρ is the density of the fluid surrounding the bubble and σ is the surface tension acting on the bubble air-water interface. From this equation we can expect a decrease in surface tension to decrease the resonance frequency of the bubble population present in the DBP solutions.

$$\omega_0 = \frac{1}{R_0}\sqrt{\frac{3\gamma p_0}{\rho}} - \frac{2\sigma}{\rho R_0} \qquad (7.1)$$

A similar behaviour of suddenly peaking SL output was noted by Birkin *et al* [7]. In this paper they increased incrementally the driving frequency of the ultrasound applied to water samples and found that the SL response relative to water peaked suddenly at narrow, specific frequency ranges. To explain this response Birkin *et al* surmised that the response peaks were bought about by the applied frequency matching a resonance frequency of the bubble population. At these specific frequencies the bubble suddenly is driven much more efficiently by the applied ultrasound as its frequency now matches that of a mode of vibration of the bubble population. This matching of frequencies results in a dramatic increase in sonochemical effects, such as SL output.

In the present work a similar effect is being brought about albeit by chemical means. The binding of DBP to a bubble interface reduces its surface tension. From equation 7.1 it can be calculated that this effect also decreases the resonant frequency of the cavitating bubble population. The sudden peaks present in the data occur when the lowered resonant frequency matches the driving frequency applied (20 kHz). The effect of a bubble being brought into resonance occurs in a very specific narrow range and explains both the narrow shape of the SL response peak and the observation that the peak moves slightly due to the omission of methanol from the solution.

The reason for the SL increase at the point at which the bubble is bought into resonance is because suddenly the collapse of the bubble is at its most efficient in terms of the focussing and concentration of the ultrasound energy. This means that at this narrow point the temperature increase inside the bubble is maximal. This leads to more excited species being formed and more SL photons being emitted, so the SL output of the system increases.

The resonance frequency of a bubble population is extremely sensitive to the cell in which the experiment is performed. It was thought that if the SL response effect is due to the bubble population being brought into resonance, then the concentration of DBP which effects the SL response peak should change if the cell is changed. The above data was acquired from experiments in a 500 cm^3 beaker, this was changed to conical flask of the same volume. The data acquired under otherwise identical conditions is shown in figure 7.3

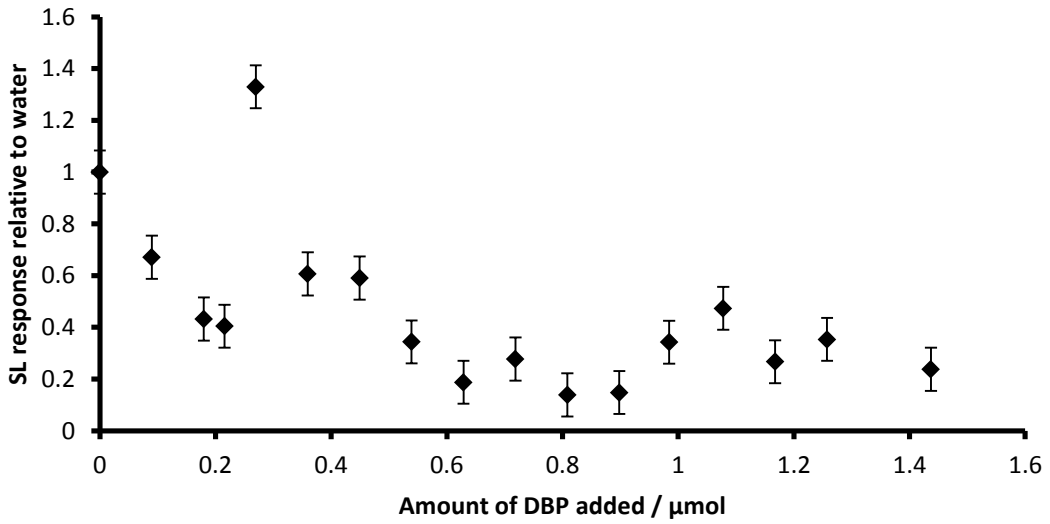

Figure 7.3: The effect of adding DBP on the sonoluminescence of 250 cm^3 argon saturated water in a 500 cm^3 conical flask using 20 kHz ultrasound.

It can be seen from figure 7.3 that a peak in SL response is again seen but arising when a much lower amount of DBP is added. This change in behaviour supports the above hypothesis since changing the cell in which the experiment is occurring should change the initial resonant frequency of the bubble population. Since a much lower amount of DBP needs to be added to bring the system into resonance we can surmise that the initial resonant frequency of the bubble population must be lower in the conical flask system than in the beaker based system.

The same experiment was repeated using 515 kHz ultrasound. The data produced from only a single run is shown in figure 7.4.

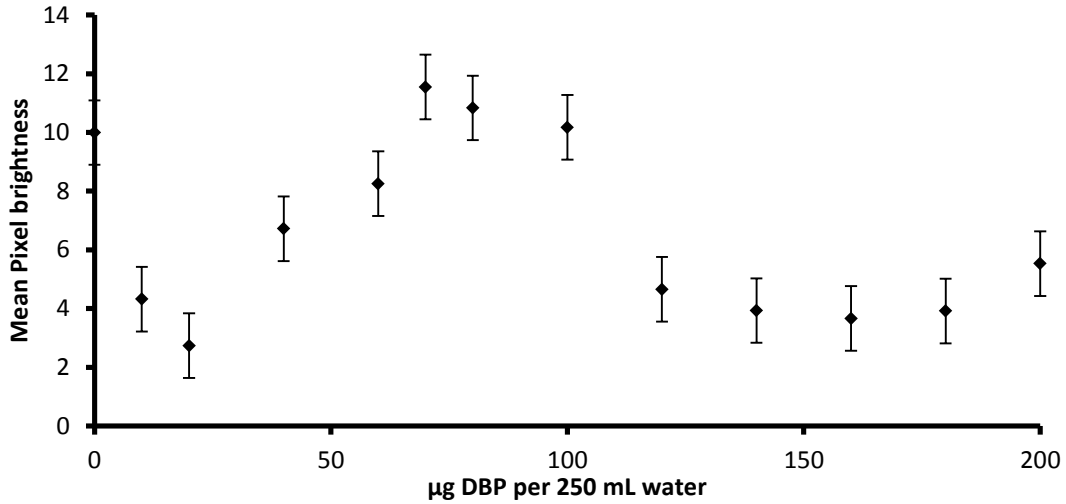

Figure 7.4: Results from SL quenching with DBP when using 515 kHz ultrasound

It can be seen that a different behaviour is seen. There are some similarities however; the response is first quenched as DBP is added up to 25 µg per 250 mL water. A broad peak then develops and then dies away again. At the end of the experiment the signal increases again slightly. The maximum enhancement of the SL signal is about the same as when using 20 kHz, 1.2 times that of pure water. The author is not sure as to the differences when using 515 kHz ultrasound with the available data and literature and this area warrants further study.

7.2: Degradation studies on other phthalate esters

Chapters 5 and 6 presented work on both the kinetics and products of the degradation of DBP as a model for the series of phthalate esters. This subsection presents experiments on the degradations of other phthalates. These were all performed as equal loading i.e. the same µg L^{-1} not as equal molarity. Degradations were all performed in argon and using 20 kHz ultrasound. Firstly 6 alkyl phthalates were degraded under the same conditions. Secondly a non-alkyl phthalate, butyl benzyl phthalate (BBP) was degraded. Lastly, mixtures of both of these types of phthalate were degraded using both 20 and 515 kHz ultrasonic frequencies.

7.2.1: Studies on a range of phthalates as separate aqueous solutions

Solutions of a variety of linear alkyl phthalates were prepared with a concentration of 100 μg L^{-1} of phthalate. The solutions were degraded using 20 kHz ultrasound in an argon atmosphere. Figure 7.5 shows the degradation data obtained from these experiments. It was found that at these conditions DBP was the fastest phthalate to degrade of those studied. Diethyl phthalate (DEP) was next fastest and the two slowest were then dioctyl phthalate and DHP where DHP was the slowest to degrade. The rate constants for the degradations along with the initial rate of degradation are presented in table 7.1.

It seems that there are several forces in effect which create the reactivity found for these degradations. Since the degradation occurs at the bubble interface it would seem reasonable to expect the degradation rate to increase, perhaps linearly, with the hydrophobicity of the phthalate esters. This is not the case as shown in figure 7.5.

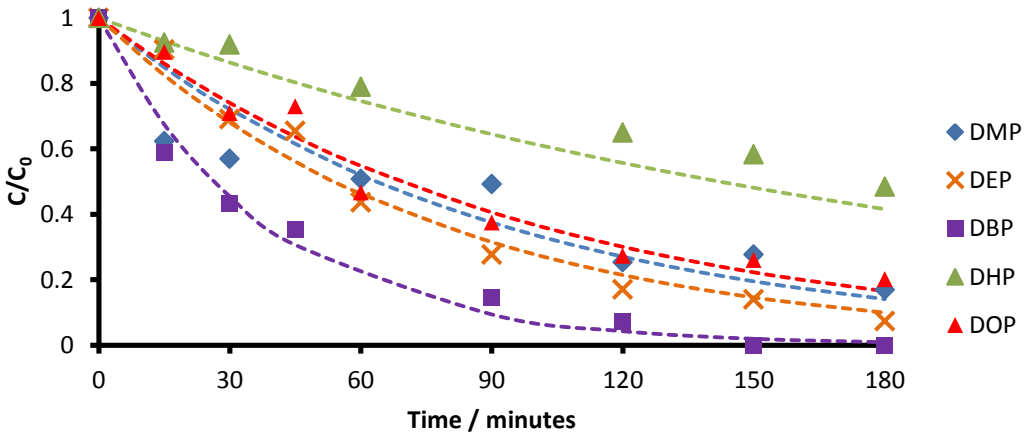

Figure 7.5: Degradations of 5 linear alkyl phthalate esters

Phthalate Ester	Rate Constant / min^{-1}	Initial Degradation rate / $\mu g\ min^{-1}$
DMP	0.0109	0.82
DEP	0.0128	0.94
DBP	0.0262	1.44
DHP	0.0062	0.42
DOP	0.0100	0.89

Table 7.1: Rate information for the degradations shown in figure 6.3

Figure 7.6 shows the degradation rate versus the octanol partition coefficients calculated in the literature[8]. The octanol partition coefficient is a measure of the hydrophobicity of a compound as it described the proportion which partitions into octanol in a water-octanol biphasic system upon efficient mixing. It can be seen that initially the degradation rate increases with increasing hydrophobicity and then decreases after reaching a maximum which occurs for DBP. This suggests that another factor is also at play. From the work on surfactants by Weavers' group, it seems reasonable to suggest that the diffusion of the phthalates to the bubble surface is also affecting the degradation rate[9-11].

As described already for DBP in chapter 5, to degrade a hydrophobic or surface active non-volatile substrate it must accumulate efficiently around the bubble interface to be degraded well by ultrasonic action. The hydrophobicity of the compound describes the activity gradient between the substrate and the bubble interface, i.e. it describes how much the compound "wants" to be on the bubble surface. The substrate then has to move towards the nearest interface through a turbulent "sea" of water molecules. Therefore the diffusion of the substrate through water also affects how much substrate can accumulate on a bubble interface within a given amount of time. Time also becomes a limiting factor when using low frequency ultrasound since bubbles will be transient with short lifetimes. This limits the amount of substrate can accumulate on the bubble before it implodes and subsequently destroys and substrates close to the implosion site. Therefore the degradation rate in a kinetically limited system

depends on both the hydrophobicity of the phthalates being degraded and their diffusivity in water.

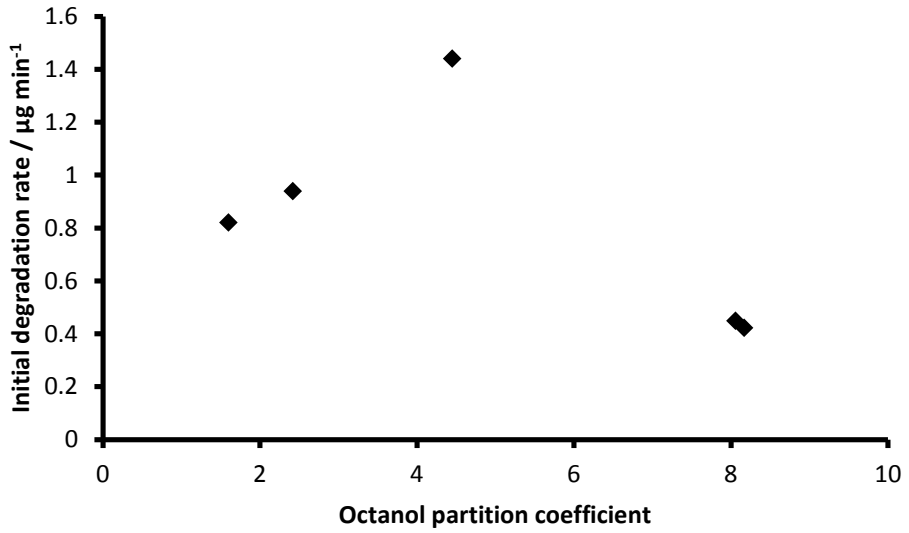

Figure 7.6: Degradation rate *versus* octanol partition coefficient for 5 phthalate esters

Table 7.2 shows the octanol partition coefficients measured for the phthalates used. The diffusivity of most phthalates in water has not been determined. However we can use the Le Bas molar volume of each phthalate as an indicator of their ability to diffuse through water[12].

From this we can see that as the alkyl chain of the phthalates increase their hydrophobicity increases but so does their molar volume. This means that up to a limiting volume the hydrophobicity of the phthalate dictates how quickly it is destroyed. However, once the phthalate volume gets suitably large its own size and subsequent drag in water limits its ability to accumulate on the bubble interface in the limited time available before bubble collapse. Therefore when a plot such as figure 7.5 is produced it displays a parabolic like shape. For the system employed it seems that the limiting volume described is around that of DBP since this was the phthalate which was destroyed the fastest.

Pthalate ester	Octanol Partition Coefficient	Le Bas Molar Volume[12] $cm^3 mol^{-1}$
DMP	1.60	206.4
DEP	2.42	254
DBP	4.45	342.8
DHP	8.17	476
DOP	8.06	520.4

Table 7.2: Octanol partition coefficients and molar volumes of the phthalate used in this study

7.2.2 Studies on aqueous mixtures of phthalate esters

Up until this subsection studies had been on single phthalates in solution. From this it was found that several factors affect the degradation of phthalates esters in solution. This is however not a good model of contaminated water, which would contain several species at the same time.

To this end, a solution was prepared to mimic groundwater which had been contaminated generally by phthalate esters. One of these (BBP) was added in greater concentration (*circa* 0.25 µM) whereas the others were added in equal concentration (*circa* 0.13 µM). The sonolysis experiments were carried out under an atmosphere of air and using both 20 kHz and 515 kHz frequency ultrasound separately. The results of the experiments are shown in figures 7.7 and 7.8 respectively.

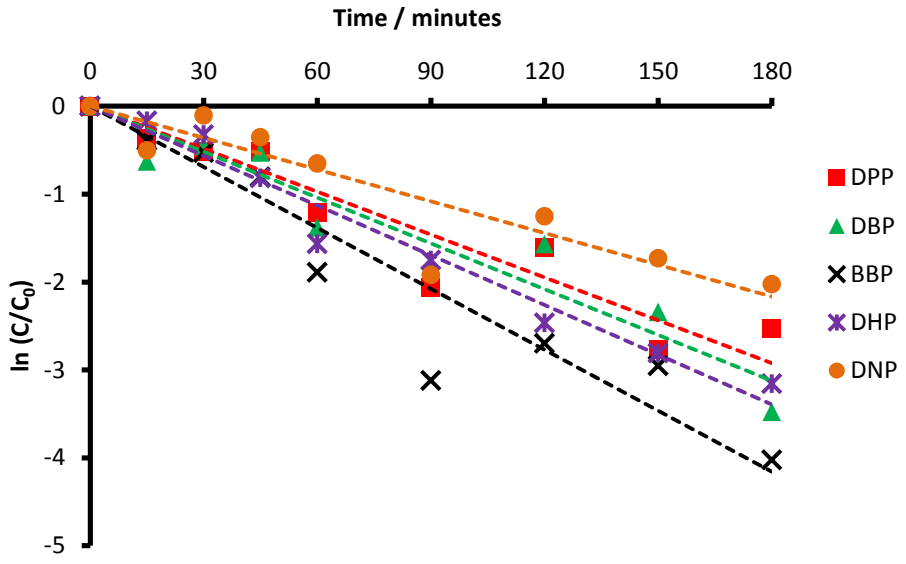

Figure 7.7: Degradation of a mixture of phthalates (20 kHz)

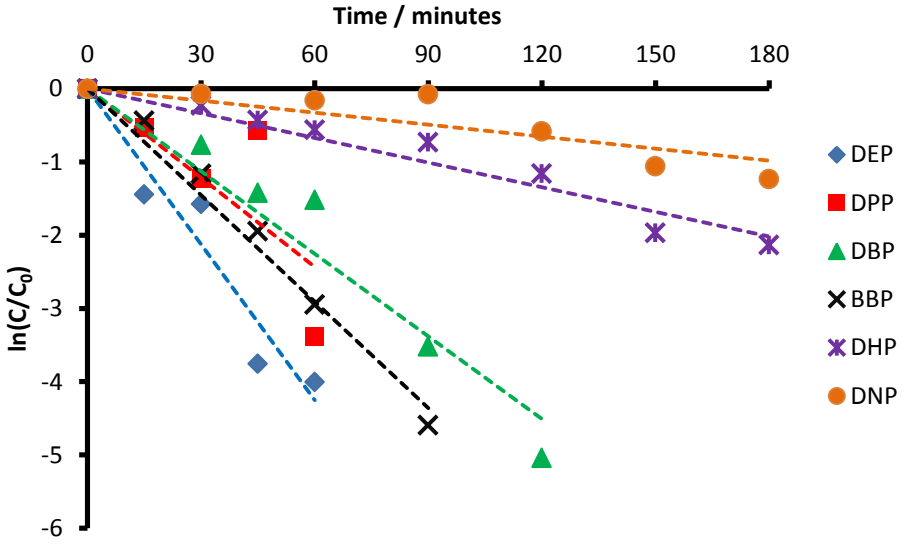

Figure 7.8: Degradation of mixtures of phthalates (515 kHz)

20 kHz driven degradations

Figure 7.7 shows the degradation of the 6 different phthalates studied. DEP does not have a curve although it was added to the solution. This is because for this experiment the DEP could not be quantified in the MS data recorded. DEP was quantifiable for the 515 kHz experiment even though the same solution was used for both experiments and so is included in figure 7.8.

From figure 7.7 it can be seen that BBP degraded the quickest. This makes logical sense since it was present in solution in greater quantities and so is more likely to encounter and absorb onto a bubble interface. All of the other phthalates degraded with very similar rates and rate constants. This was surprising given the range of rates found for a range of phthalate previously and shown in figure 7.5. Although different phthalates were used for the experiments leading to both sets of data one might expect the process to be similar in mechanism and so one might expect a similar reactivity trend. This is clearly not the case.

Since the solution matrix is now much more complicated it is possible that the driving force for the absorption onto bubble interfaces has changed and that the limiting condition to the process has changed. Since all the phthalates other than BBP degrade with very similar rates regardless of hydrophobicity or molar volume, the degradation process is concentration controlled.

Since all of the phthalates other than BBP are present in solution in equal concentration we can expect the solution to be a homogeneous blend of each phthalate throughout its volume. 20 kHz ultrasound gives rise to short lived transient bubbles at the intensity setting used and so there is not much time for absorption to a bubble interface before the bubble implodes. If we assume the solution is homogenous with respect to phthalate balance then we can imagine that their rates of degradation could be similar.

In a homogeneous solution, a bubble appearing randomly into solution can be expected to be surrounded by an equal amount of each of the phthalates in solution. Since the time before implosion is short only the phthalate immediately surrounding the bubble will have time to absorb onto its interface. Since the

distance to travel is now very short driving forces such as hydrophobicity and factors such as diffusion speed have little effect on the amount of each phthalate which coats the bubble successfully and thus degrades. The important factor now becomes with balance of each phthalate which is immediately surrounding a seeded bubble. Since we are assuming the solution to be homogenous then there should be an equal amount of each phthalate near to a bubble in a random location and so their degradation rates are very similar. This was what was found in figure 7.7.

515 kHz driven degradations

From figure 7.8 it can be seen that unlike for the 20 kHz degradation, the rates of degradation are now very different for the phthalates in the mixture. Again, ignoring BBP , the rate of degradation can be seen to decrease with increasing phthalate ester chain length. The reason for this difference of rates is due to the stable cavitation present. Since the bubble lifetime is relatively long the process is now diffusion controlled.

The solution can be thought of as being relatively crowded containing several organic species and so to degrade a given phthalate molecule has to diffuse through the “crowd” of water and other phthalate molecules to reach the bubble interface. It was mentioned in the previous subsection that the Le Bas molar volume can be used as a measure of diffusivity. Hence, figure 7.9 shows the relationship between initial rate of degradation and the Le Bas molar volume of the phthalates studied other than BBP.

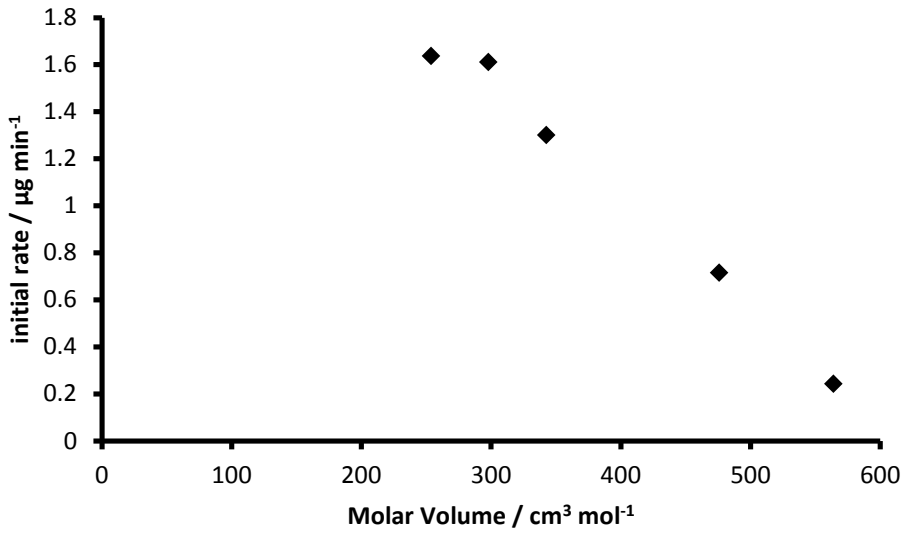

Figure 7.89 The effect of molar volume on phthalate degradation rate

In figure 7.9 it can be seen that there is a good linear fit between molar volume and rate of degradation. As the volume occupied by the phthalate increases then its rate of degradation decreases. It can be inferred from this that the more mobile, smaller phthalates are more able to diffuse through the solution to reach a bubble interface and so are degraded more quickly despite differences in hydrophobicity. The ability to move through the solution to an interface has now become the limiting factor to the degradation reaction.

The results in this subsection show that it is important that mixtures of pollutants are studied as well as the target pollutant(s) by itself. Figure 7.7 shows a different reactivity than expected based on the data shown in figure 7.5 and illustrates that as a matrix becomes more complicated different factors will drive the degradation process. If a novel technology such as ultrasound is to be used by the water processing industry greater efforts need to be focussed on more complicated yet more relevant matrixes.

The use of ultrasound should be considered for use by the water industry as it has the ability to mineralise otherwise difficult to treat pollutants. It is also especially suited to the removal of low concentrations of hydrophobic pollutants, as particular problem for current treatment methods. However, it is quite energy intensive and so is best used as a final polishing step to remove recalcitrant pollutants. It is also therefore best coupled with a low energy process such as ozonation or addition of peroxides to increase the degradation rates achieved and to aid the mineralisation process

7.3: Chapter References

1. K. S. Suslick, N. C. Eddingsaas, D. J. Flannigan, S. D. Hopkins and H. Xu, *Ultrason Sonochem*, 2011, **18**, 842-846.
2. M. Ashokkumar, R. Hall, P. Mulvaney and F. Grieser, *Journal of Physical Chemistry B*, 1997, **101**, 10845-10850.
3. R. Tronson, M. Ashokkumar and F. Grieser, *Journal of Physical Chemistry B*, 2002, **106**, 11064-11068.
4. M. Ashokkumar, J. F. Guan, R. Tronson, T. J. Matula, J. W. Nuske and F. Grieser, *Physical Review E*, 2002, **65**.
5. M. Ashokkumar, P. Mulvaney and F. Grieser, *Journal of the American Chemical Society*, 1999, **121**, 7355-7359.
6. T. Leighton, *The Acoustic Bubble*, Academic Press, London, 1994.
7. P. R. Birkin, J. F. Power, A. M. L. Vincotte and T. G. Leighton, *Physical Chemistry Chemical Physics*, 2003, **5**, 4170-4174.
8. D. R. P. C.A. Staples, T.F. Parkerton, W.J. Adams, *Chemosphere*, 1997, **35**, 667-749.
9. L. Yang, J. Z. Sostaric, J. F. Rathman and L. K. Weavers, *Journal of Physical Chemistry B*, 2008, **112**, 852-858.
10. L. Yang, J. Z. Sostaric, J. F. Rathman, P. Kuppusamy and L. K. Weavers, *Journal of Physical Chemistry B*, 2007, **111**, 1361-1367.
11. L. Yang, J. F. Rathman and L. K. Weavers, *Journal of Physical Chemistry B*, 2006, **110**, 18385-18391.
12. I. Cousins and D. Mackay, *Chemosphere*, 2000, **41**, 1389-1399.

Chapter 8: Conclusions and Future Work

This chapter serves to sum up the work and findings of this thesis. Each results chapter shall be discussed separately and an overall summary at the end. Following from these conclusions is a future work section in which the author discusses work he feels would be useful continuing from the work presented in this thesis.

8.1: Conclusions arising from chapter 5, kinetic results

Chapter 4 ended in presenting a model of DBP degradation. Due to its hydrophobicity it is highly likely that DBP is degraded at the bubble interface and possibly inside the bubble core through microinjection. It was found as with other studies that DBP degradation is affected by several parameters such as acoustic intensity, the nature of gas dissolved and the initial concentration of DBP.

From these results, ultrasound treatment could be a useful tool for the degradation of phthalates in general not just DBP. Ultrasound however is quite an energy intensive method and so the following setup based on the kinetic results should be used to maximise energy efficiency.

Firstly high intensity ultrasound should be used since the radical yield per unit energy is greater.

Secondly since high frequency ultrasound is being used air or oxygen should be used as the dissolved gas. From an industrial processing point of view air is more convenient and still affects efficient degradations when using 100 μg L^{-1} solutions. Oxygen lead to extremely efficient degradation of DBP especially at higher DBP concentrations and this gas may be useful when trying to treat highly contaminated water sources.

From the study into the effect of initial rate it was found that decreasing the DBP concentration lead to an increase in rate constant. This is good news in the context of phthalate remediation since phthalates are present typically in low μg L^{-1} quantities and from the data in this study an efficient and speedy removal of phthalates at these concentrations can be expected.

Experiments also showed that hydrogen peroxide could be useful as an additive for accelerating the degradation rate of DBP and hopefully therefore other phthalates.

Since ultrasound is quite energy intensive its best use would be to combine it with a much more energy unintensive AOP such as ozonation or the addition of peroxides or Fenton reagents. The combination of ultrasound with UV and/or electrolysis/electrocoagulation may prove to be too energy intensive and therefore expensive to be useful as an AOP. The use of oxygen as a dissolved gas is an interesting alternative to the use of ozone but is only useful when using higher ultrasonic frequencies.

In a water processing plant context ultrasound could either be used at the start of the treatment process when the water is quite contaminated or as a tertiary, polishing treatment. It is the opinion of the author that ultrasound is best employed as a tertiary treatment for removing only those pollutants which are not removed by the rest of the treatment process. This opinion comes from the fact that the treatment processing time and therefore cost is likely to be higher when treating water with more organic loading as the amount of TOC in these waters would be much higher and so processing times are likely to be longer.

Ultrasound, due to the fact that it works by action of microbubbles, would be best employed for cleaning waters which are contaminated by hydrophobic compounds which are attracted to bubble interfaces due to hydrophobic interactions. These are also difficult to remove by other methods making ultrasound attractive for their treatment.

The other class of compounds for which ultrasound works well as a remediation tool is volatile species which easily enter the bubble core and are pyrolysed. However for the case of these chemicals simple aeration is likely to remove the majority of the organic loading, is much less energy intensive and is already widely used.

8.2 Conclusions from chapter 6, product analysis

The main conclusion to make from chapter 5 is that the products found to be formed by ultrasonic action on DBP in the liquid phase resulted mainly from radical attack by ·OH radicals and ester hydrolysis. The ·OH radical was found to interact with DBP in two ways; substitution on either the aromatic ring or on the ester chain tails of DBP and also radical mediated hydrogen abstraction. This lead to several products being hydroxylated and being unsaturated, these were typically transforms of DBP. Formation of high weight dimers of DBP were also found in some cases and these must have resulted from the formation of DBP radicals after a hydrogen abstraction and the combination of two of these radicals.

DBP is completely transformed by ultrasound. The lowest mass product which was found in the liquid phase was phenol and this did not build up significantly in solution over time and so must be degraded. Due to the heating up of the ESI ionisation chamber smaller compounds could not be detected although the formation of small organic acids is inferred from the known products of degradation of benzoic acid which was one of the products formed from DBP sonolysis. It was disappointing that gas phase products were not seen when using 20 kHz ultrasound, this could be remedied by trying the same experiment using 515 kHz ultrasound which may produce more gaseous products.

From analysis of the product distributions at both frequencies the product distribution of the degradation is largely unaffected by ultrasound frequency. The major product found was $C_{16}H_{20}O_5$ which results from one hydroxyl addition to DBP and the removal of one molecule of hydrogen leaving a single double bond on one of the ester chain tails. MBP was not the major product found as proposed by Yim[1] and by Psillakis[2].

Several products were found in which there had been unsaturation of DBP and/or MBP and also addition of hydroxyl species. Products including up to 3 hydroxyl additions and 3 double bonds were found. The structures of these however could not be conclusively proved since the MS systems used were not able to perform MS-MS and so no fragmentation and therefore structural information was able to be obtained.

When using different gases similar products were found, no evidence of attack by nitrogen or oxygen containing radicals (other than ·OH) were found when using nitrogen and oxygen as the sparge gas respectively. When using oxygen as a sparge gas very few products were found and this was attributed to the radical yield being very high and the complete degradation and the mineralisation of DBP occurring rapidly close to the bubble. This finding adds weight to the usefulness of oxygen as a dissolved gas for degradation reactions of organic species in a processing plant context.

In conclusion ultrasound effectively degrades DBP and its transformation products to presumably CO_2 and H_2O.

8.3: Conclusions from chapter 7, collected data

In this chapter two unrelated sets of work were presented, the quenching of SL by DBP and the degradation of other phthalates both separately and as a mixture.

The quenching of SL by DBP was found to occur at very low initial concentrations of DBP however as the DBP concentration was increased a sudden peak in SL intensity was seen. This was attributed to DBP bringing the bubble into resonance with the acoustic field by lowering the surface tension of the bubble interface. This peak was found to move when the reaction vessel was changed adding weight to this theory.

This result is the first of its kind Birkin *et al* had achieved similar results when changing the acoustic frequency in a stepwise fashion and bringing the bubble population into resonance that way[3]. The author believes this is the first example of a chemical effect bringing a bubble population into resonance. This finding shows that the effectiveness of bubble collapse can be “fine tuned” using chemical means and may have use in some context later on.

The work on a range of phthalates consisted of these as separate solutions and as a mixture. When using separate solutions it was found that the degradation rate was affected by two factors the hydrophobicity of the phthalate and its diffusivity in water as expressed by its molar volume. The rate which was observed was a balancing act of these. The phthalate which was found to degrade the fastest when using 20 kHz ultrasound was DBP. For DEP and DPP the rate increased with hydrophobicity. For phthalates more hydrophobic and more bulky than DBP however the rate decreased. This was thought to happen due to the diffusivity of the phthalate in water decreasing due to an increase in its size as expressed as its molar volume.

The picture was quite different when degrading a mixture of phthalates. When using low frequency ultrasound degradation rates were very similar. When using 515 kHz ultrasound the rates were very different and were found to rely solely on the ability of the phthalate to diffuse to the bubble surface i.e. the rate decreased with increasing molar volume hence decreasing diffusivity in water.

This finding is very important as most of the work published in the area has been on single contaminants in solution. This is not a realistic situation however as contaminated water contains many tens of if not hundreds of compounds. There is a real possibility therefore that the sonolysis efficiency of chemicals in a complex mixture will be very different to those reported in the literature as single contaminant solutions. This could have very real implications when adopting ultrasound as a water processing tool. Hence more work needs to be done in the area of mixtures of compounds starting with binary mixtures and working upwards. This also would need to include the mixing of different contaminant classes e.g. surfactants and phenols, which to the author's knowledge has not yet been done extensively.

8.4: Proposals for future work

This subsection describes the work that the author would have liked to have carried out and that which should be done building on the results obtained.

1. Perform MS-MS experiments to determine the structures of products formed from DBP sonolysis, especially those which had several hydroxyl additions and hydrogen abstractions.
2. Determine the products for the degradation of other phthalates other than DBP to confirm whether these are the same.
3. Quantify fully the concentration of intermediates and sonolysis products. This may actually be impossible for products which were the result of several hydroxyl additions and hydrogen abstractions.
4. Measure the change in TOC of the phthalate solutions in response to sonication at both 20 and 515 kHz ultrasound.
5. Measure the evolution of gas phase products over time and identify what the gas phase products of phthalate sonolysis are.
6. Perform the DBP SL quenching experiment at 515 kHz frequency to see how a change in frequency affects the phenomenon of chemically derived resonance and whether it occurs regardless of ultrasonic frequency.
7. Perform the same SL experiments but for a phthalate more hydrophilic than DBP such as DMP and one more hydrophobic than DBP. Since the SL peak was brought about by DBP binding to the bubble surface and reducing the surface tension a change in phthalate hydrophobicity should change the effect seen.
8. Perform degradations on phthalates other than DBP at 515 kHz frequency as it was only performed using 20 kHz frequency during this study.

8.5 Chapter references

1. B. Yim, Y. Nagata and Y. Maeda, *Journal of Physical Chemistry A*, 2002, **106**, 104-107.
2. E. Psillakis, D. Mantzavinos and N. Kalogerakis, *Chemosphere*, 2004, **54**, 849-857.
3. P. R. Birkin, J. F. Power, A. M. L. Vincotte and T. G. Leighton, *Physical Chemistry Chemical Physics*, 2003, **5**, 4170-4174.

Appendix I : LC-MS Spectra of products found to occur from DBP degradation

This first appendix contains LC-MS spectra referred to in Chapter 5. Each figure shows the extracted mass of the ion in question in the top window. The lower window(s) show the mass spectrum obtained by averaging over the full width at half maximum of the LC peak. Figures are in the same order as species are encountered in chapter 5 and are named after the species in question. Spectra were produced by exporting the display view directly from Bruker's Data Analysis software package. For each species two masses are reported for those found in positive ionisation mode. These correspond to ions formed by proton and Na^+ addition respectively. For negative ions a single mass is reported where the species has lost a proton.

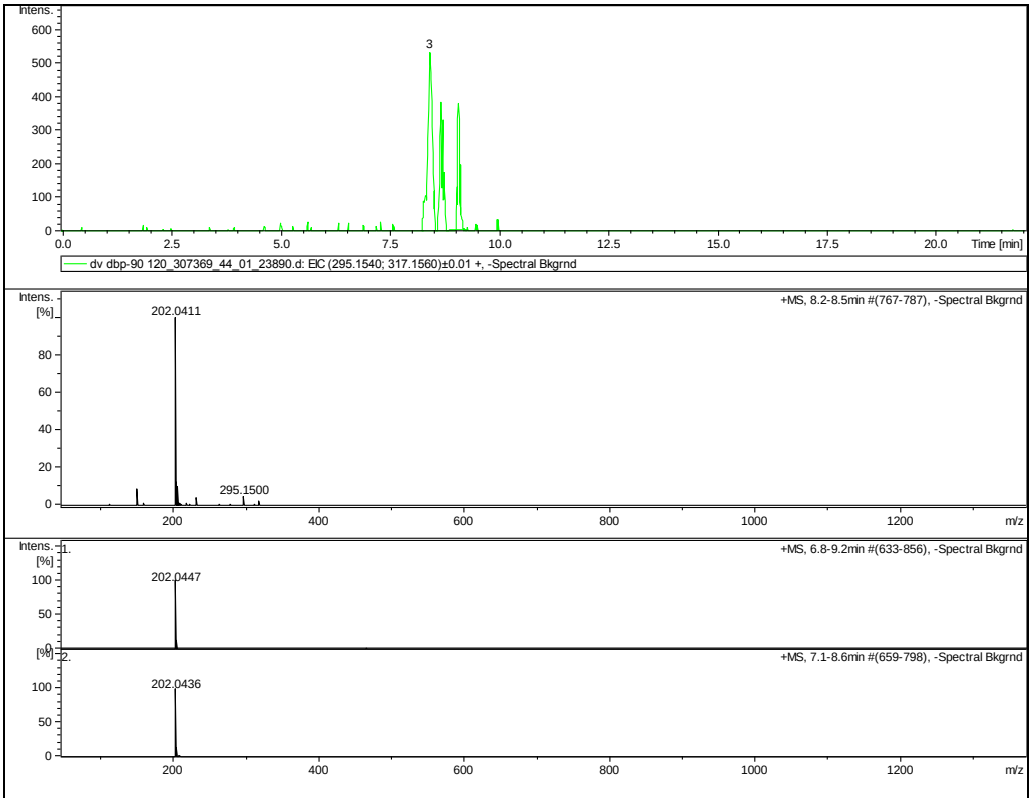

Figure a1.1: $C_{16}H_{22}O_5$ (m/z = 295.194; 317.136)

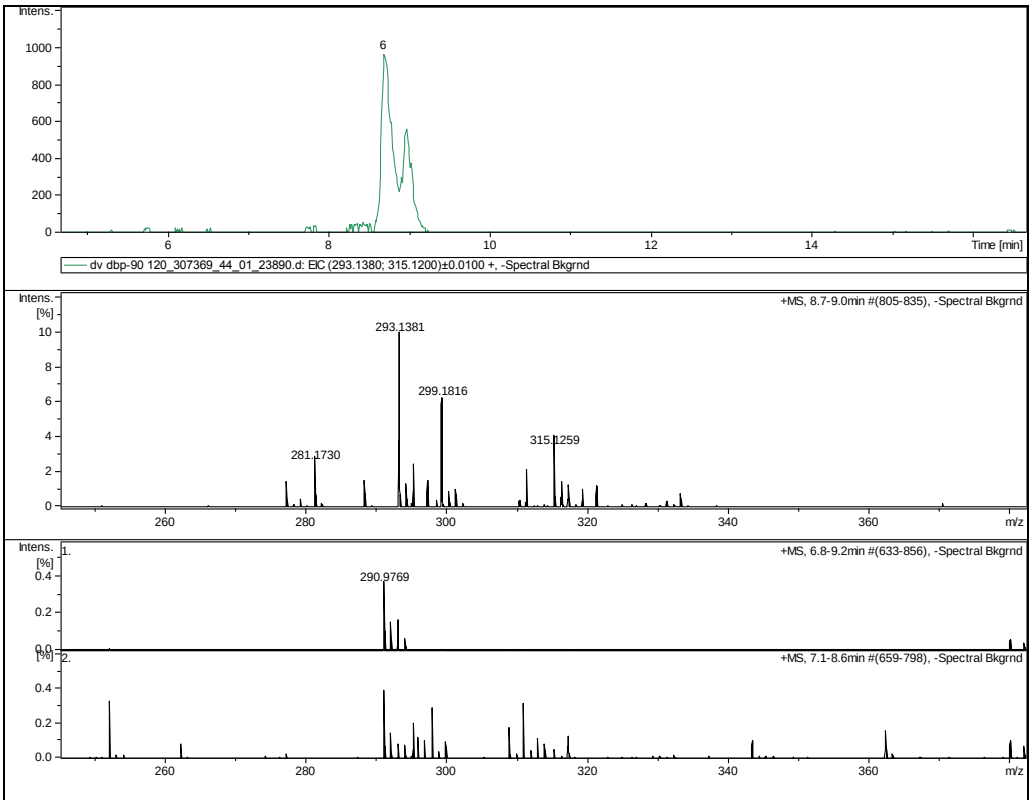

Figure a1.2: C16H20O5 (m/z = 293.138; 315.120)

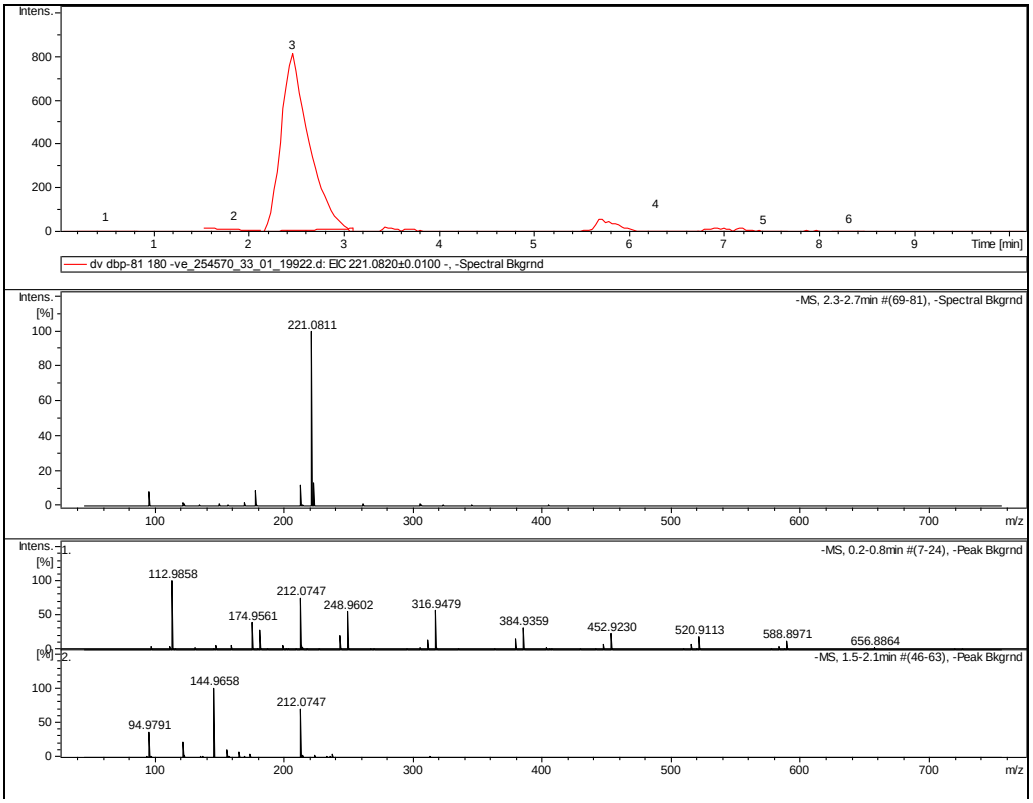

Figure a1.3: $C_{12}H_{13}O_5$ (m/z = 221.082)

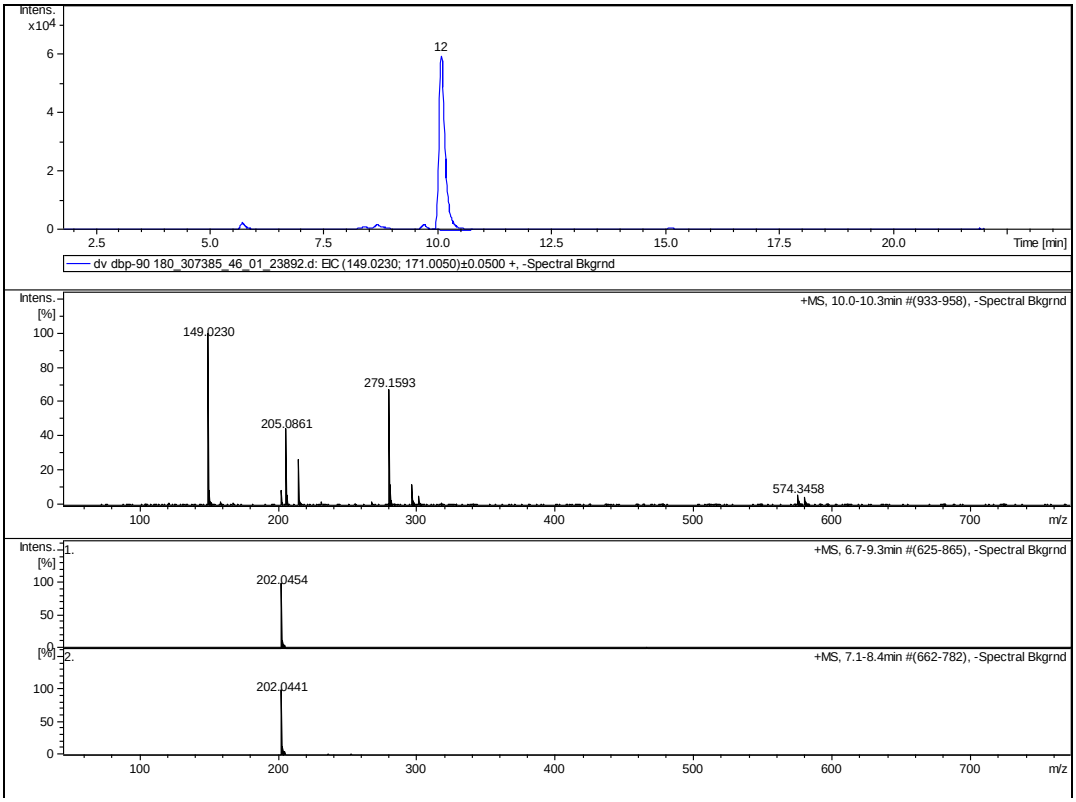

Figure a1.4: Phthalic anhydride (m/z = 149.023; 171.005)

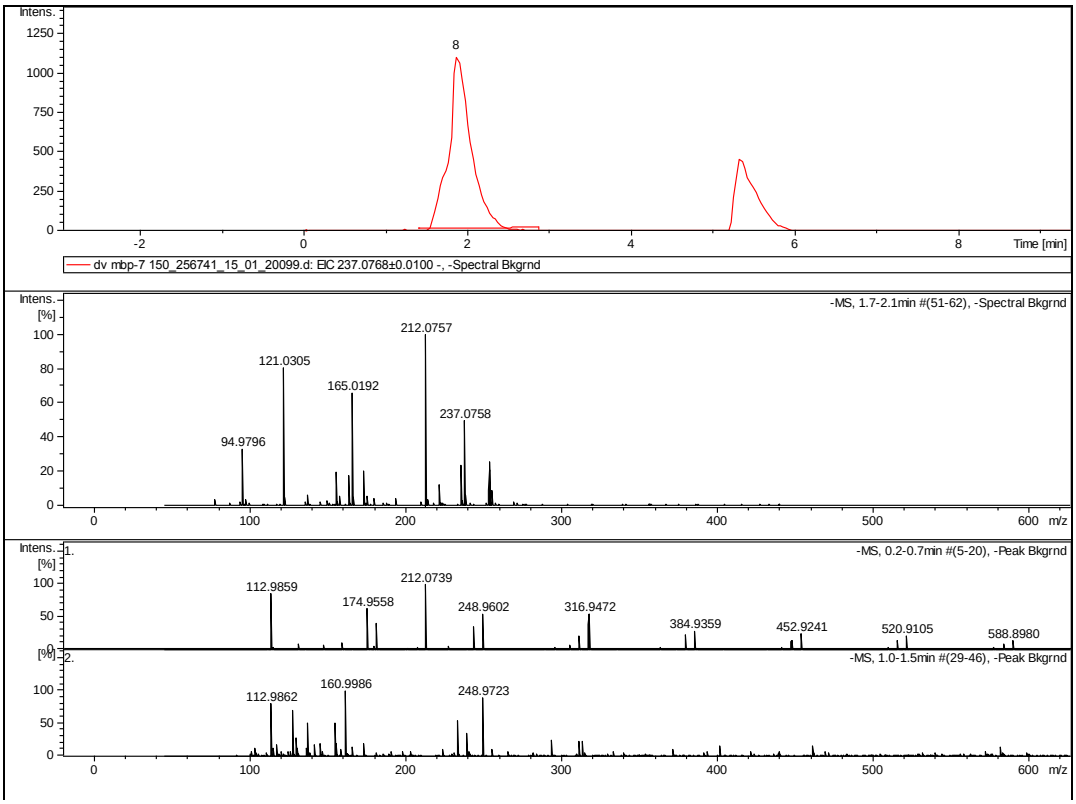

Figure a1.5: $C_{12}H_{13}O_5$ (m/z = 237.077)

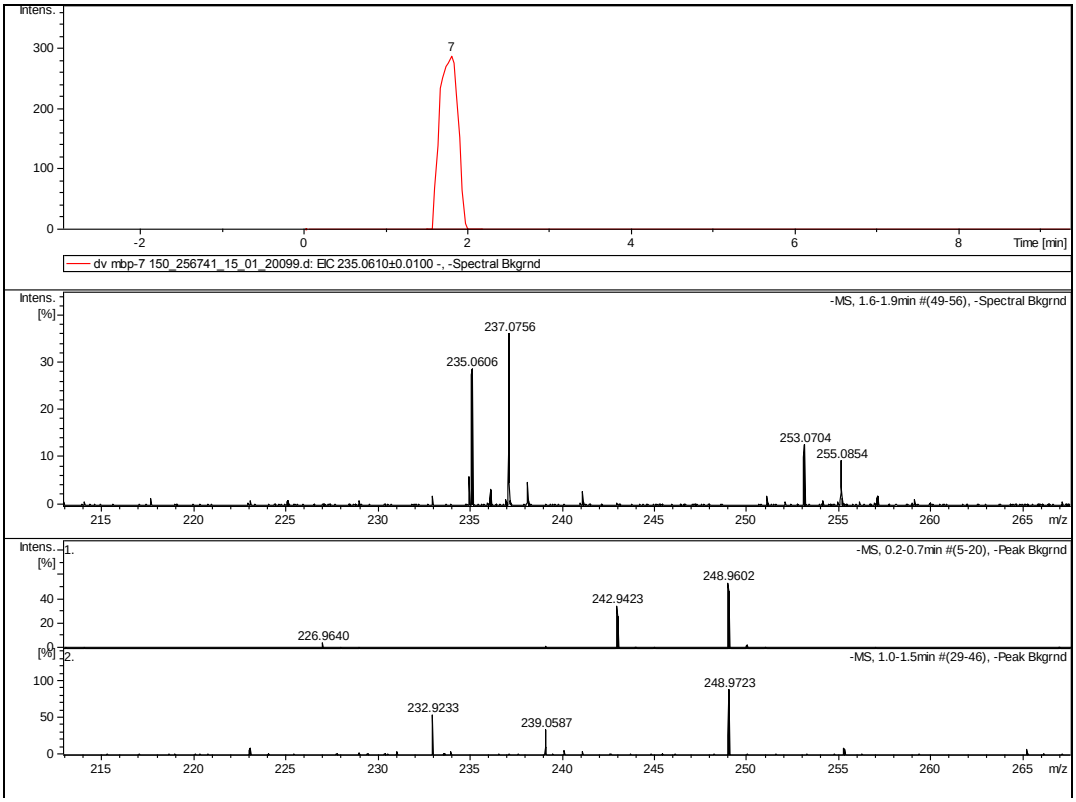

Figure a1.6: $C_{12}H_{11}O_5$ (m/z = 235.061)

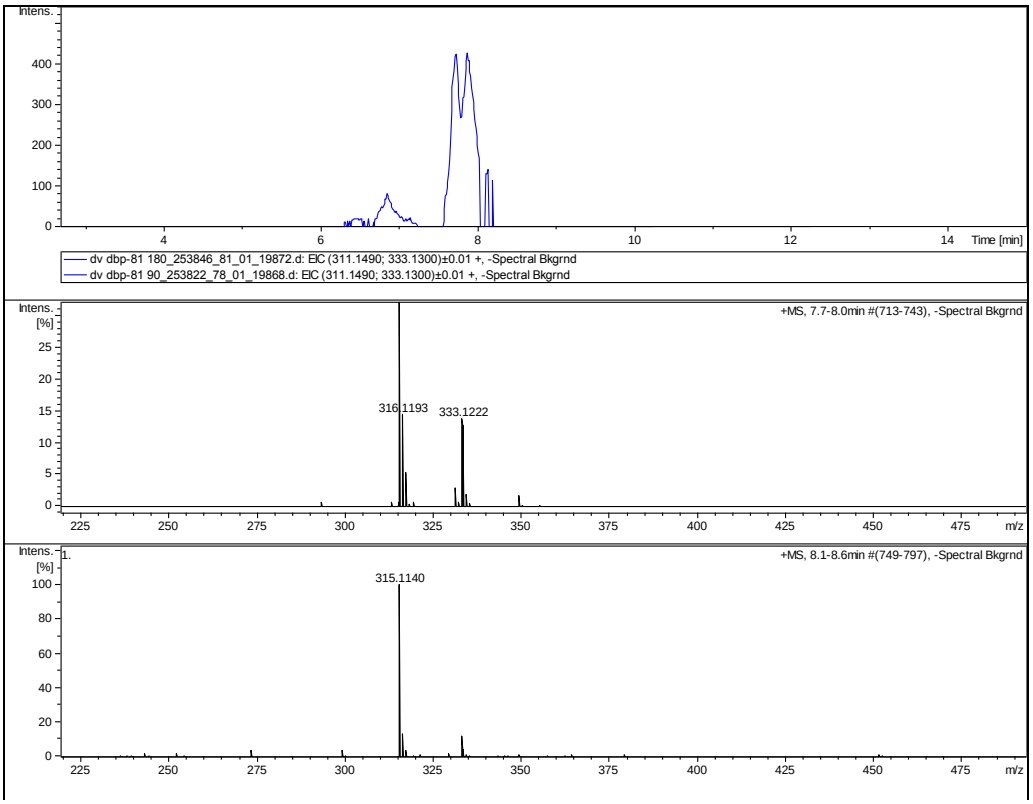

Figure a1.7: $C_{16}H_{22}O_6$ (m/z = 311.149; 333.130)

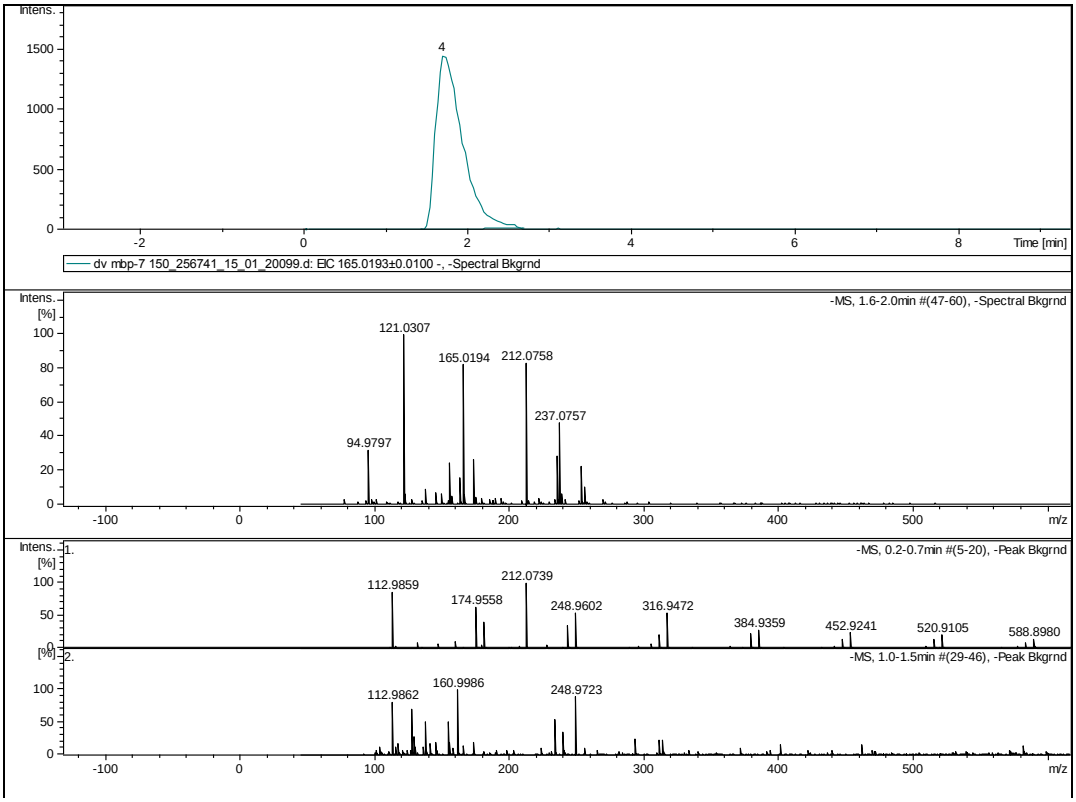

Figure a1.8: Phthalic acid (m/z = 165.019)

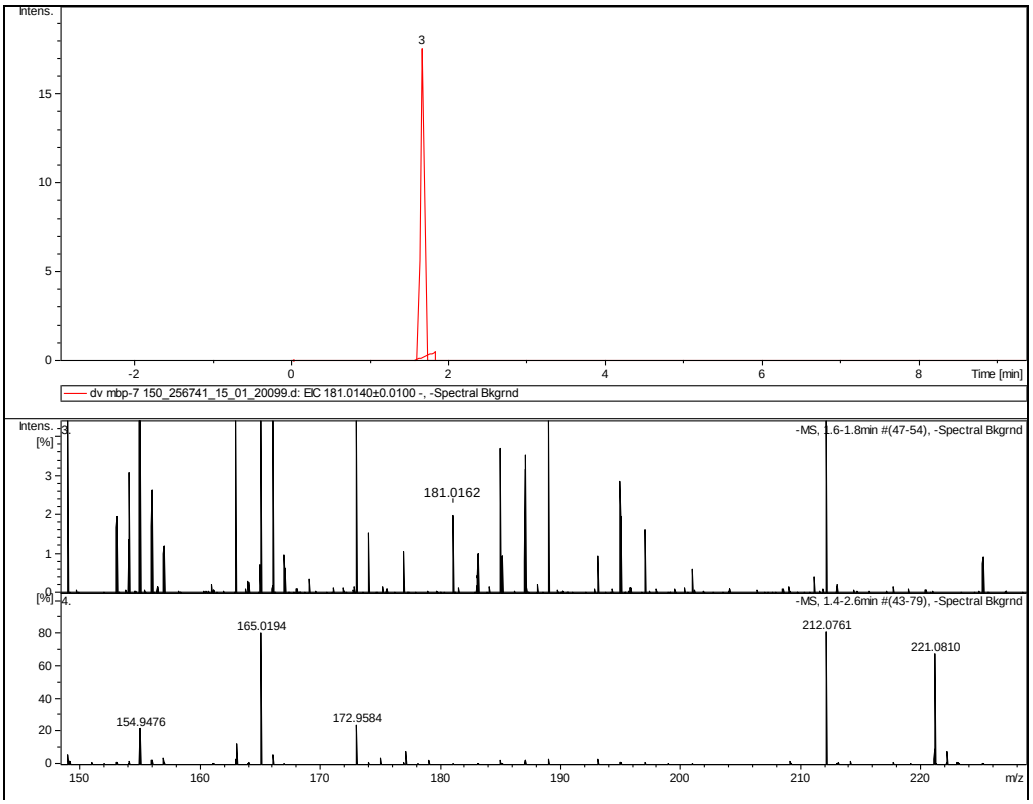

Figure a1.9: Hydroxy phthalic acid (m/z = 181.014)

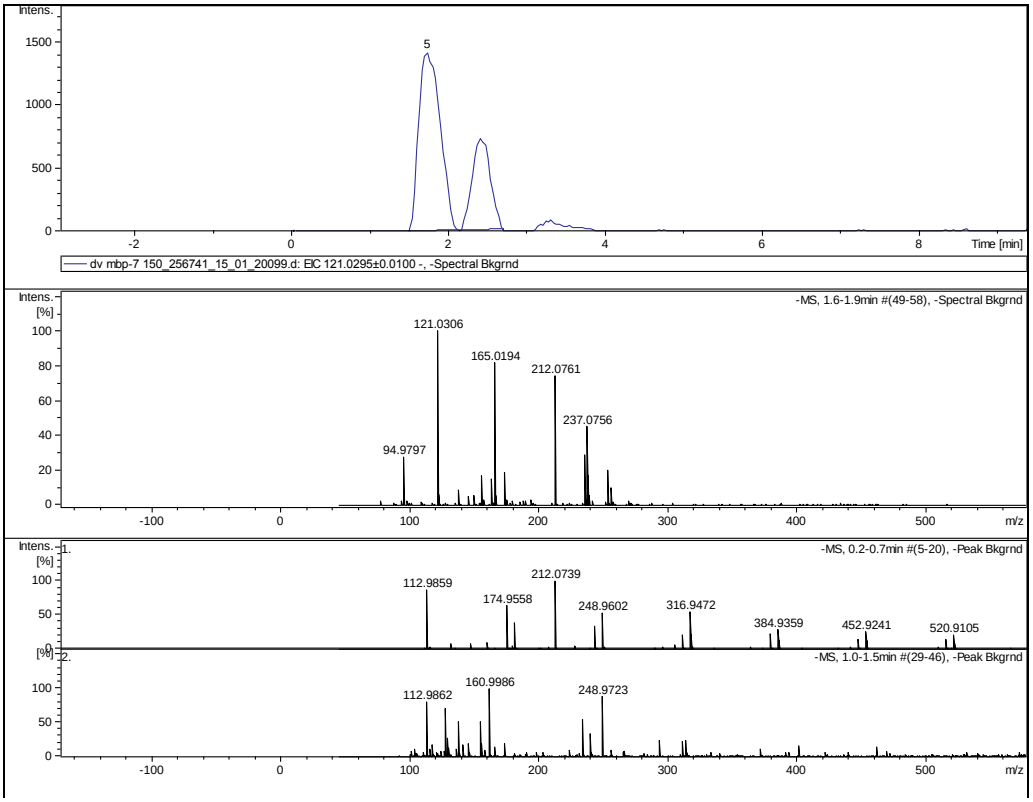

Figure a1.10: Benzoic acid (m/z = 121.030)

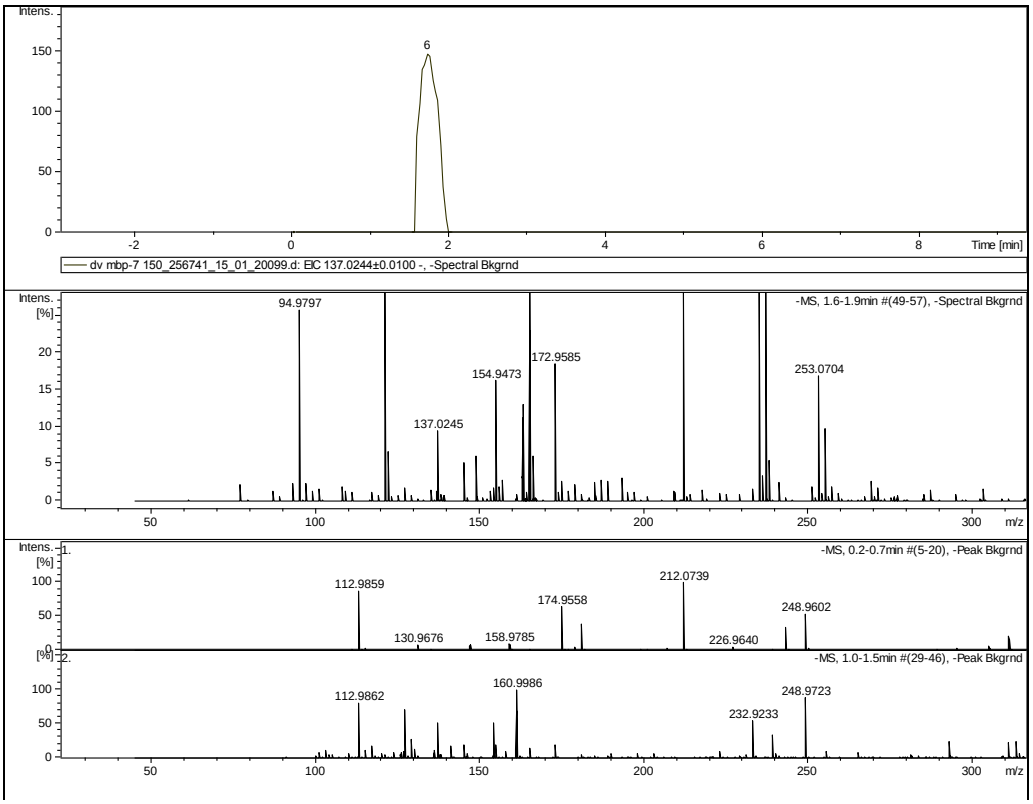

Figure a1.11: Hydroxy benzoic acid (m/z = 137.024)

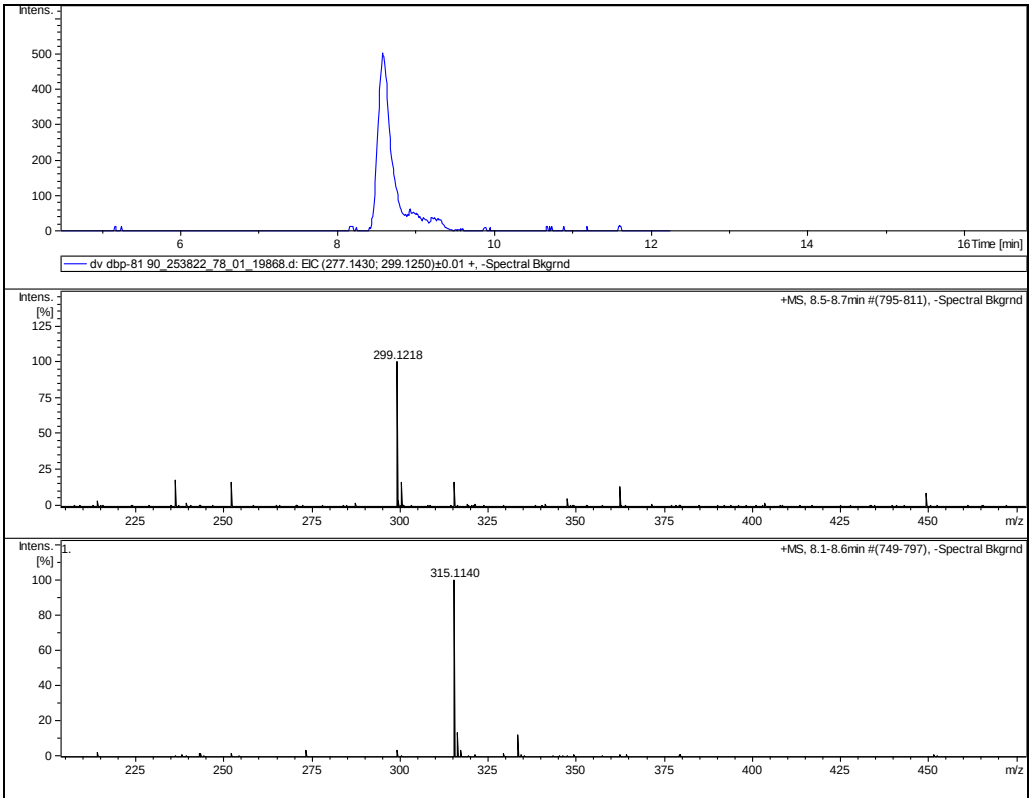

Figure a1.12: $C_{16}H_{20}O_4$ (m/z = 277.143; 299.125)

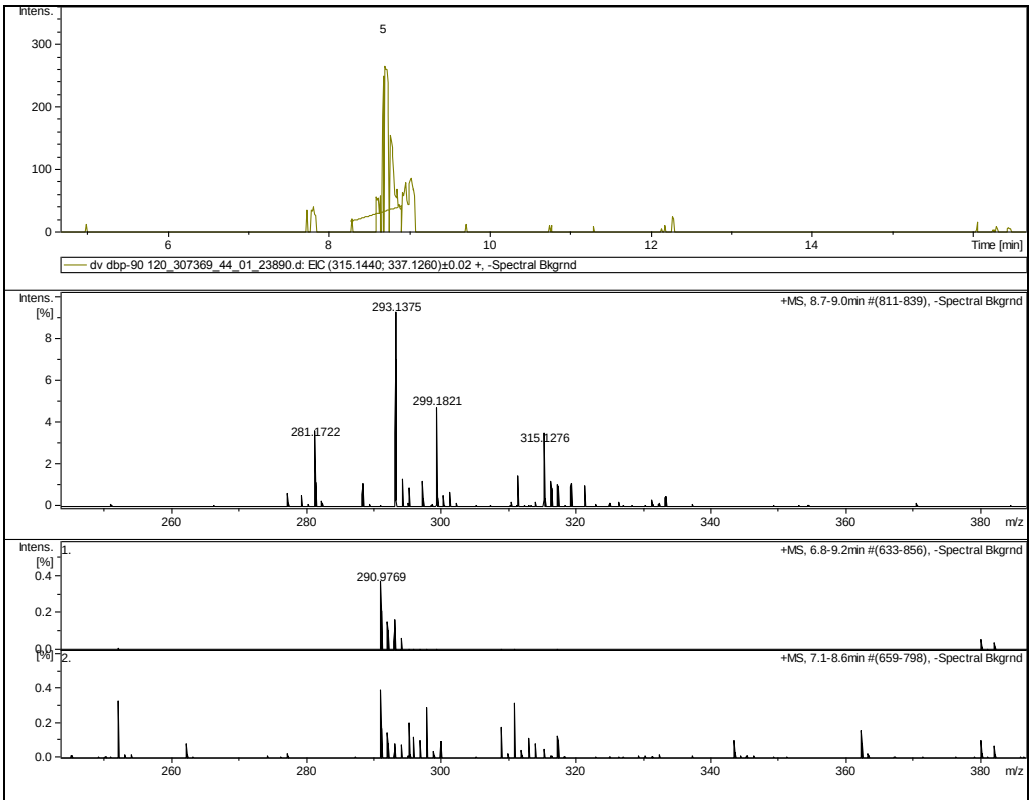

Figure a1.13: $C_{16}H_{22}O_7$ (m/z = 327.144; 349.126)

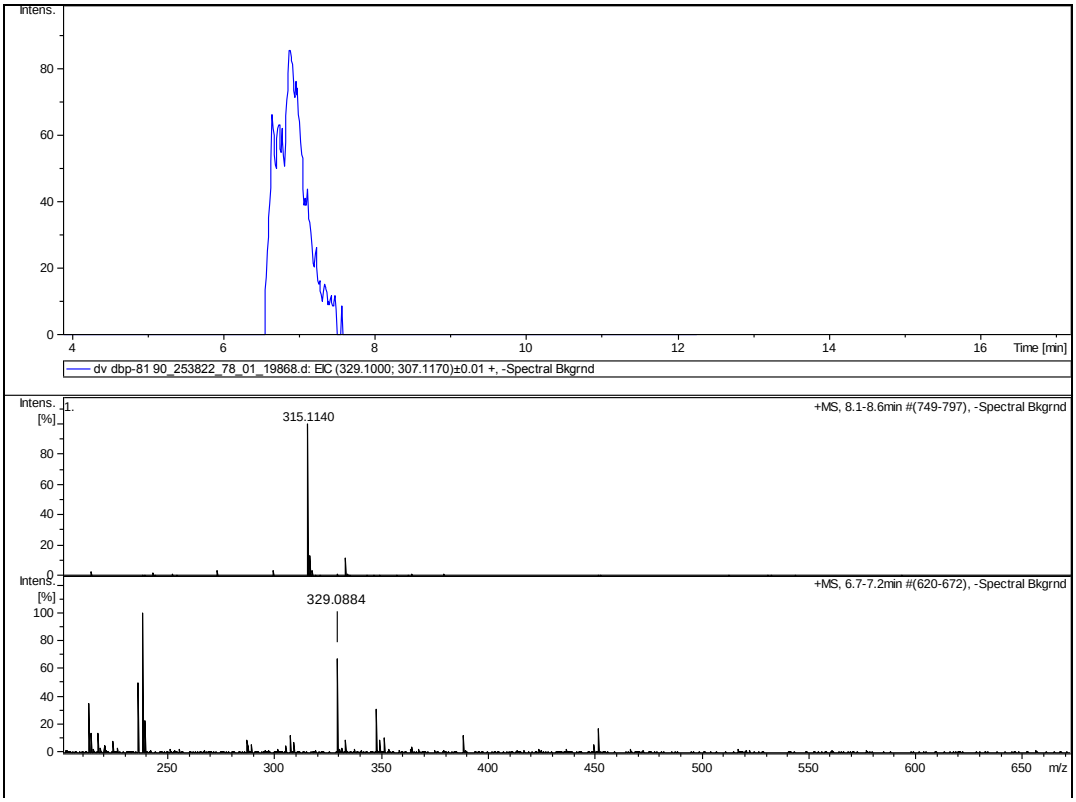

Figure a1.14: $C_{16}H_{18}O_6$ (m/z = 307.117; 329.099)

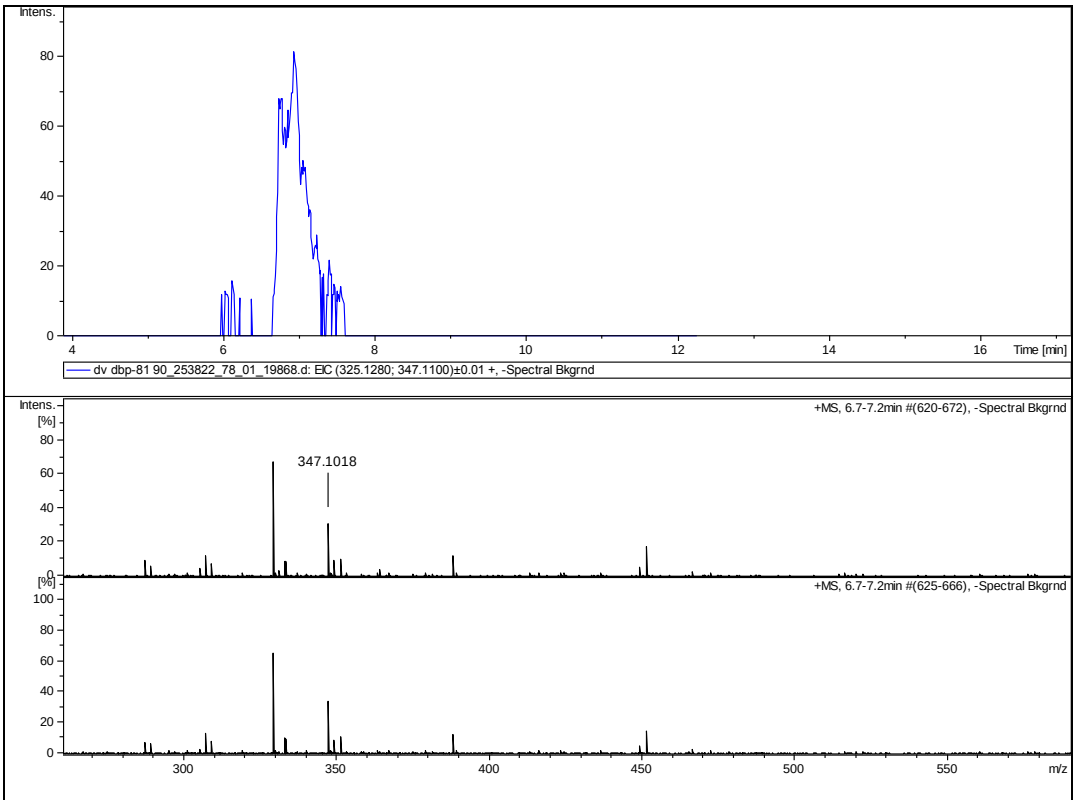

Figure a1.15: $C_{16}H_{20}O_7$ (m/z = 325.128; 347.110)

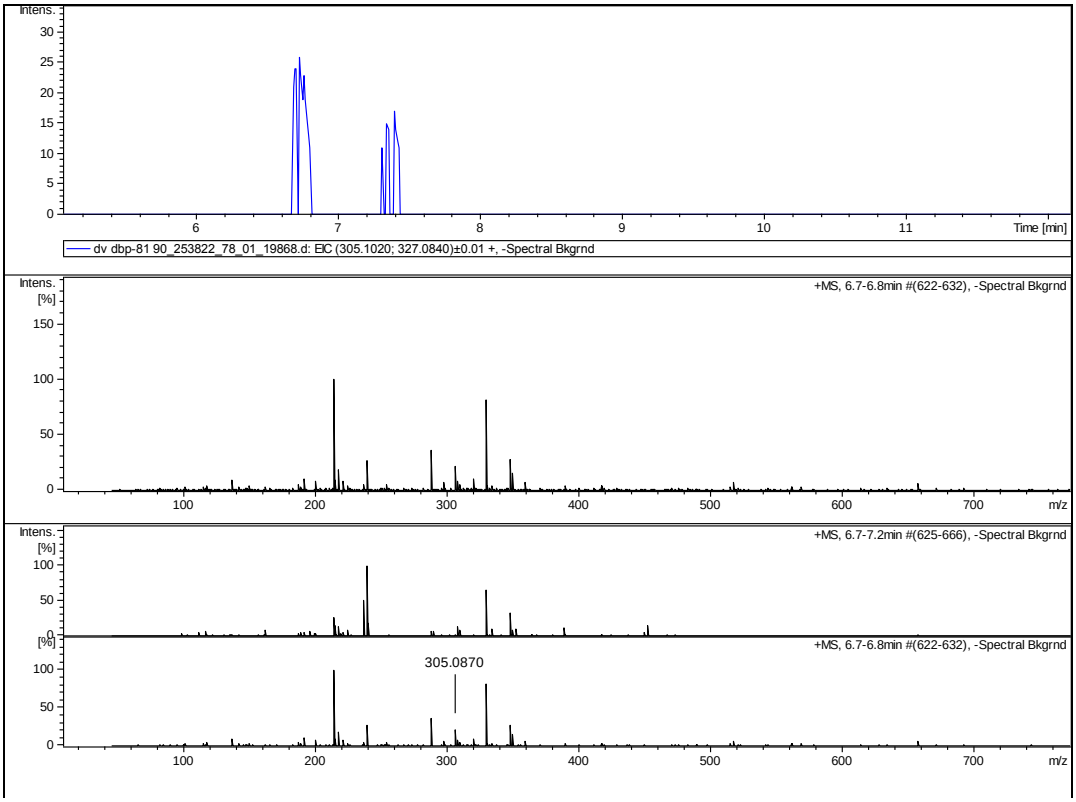

Figure a1.16: $C_{16}H_{16}O_6$ (m/z = 305.102; 327.084)

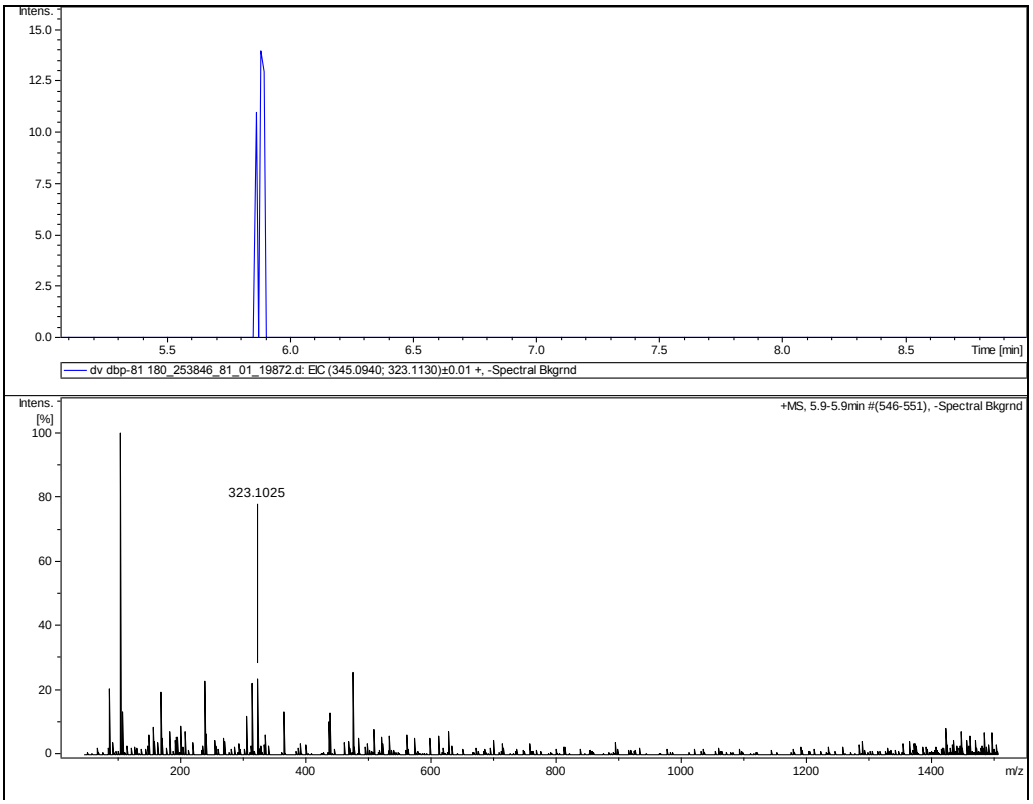

Figure a1.17: $C_{16}H_{18}O_7$ (m/z = 323.112; 345.094)

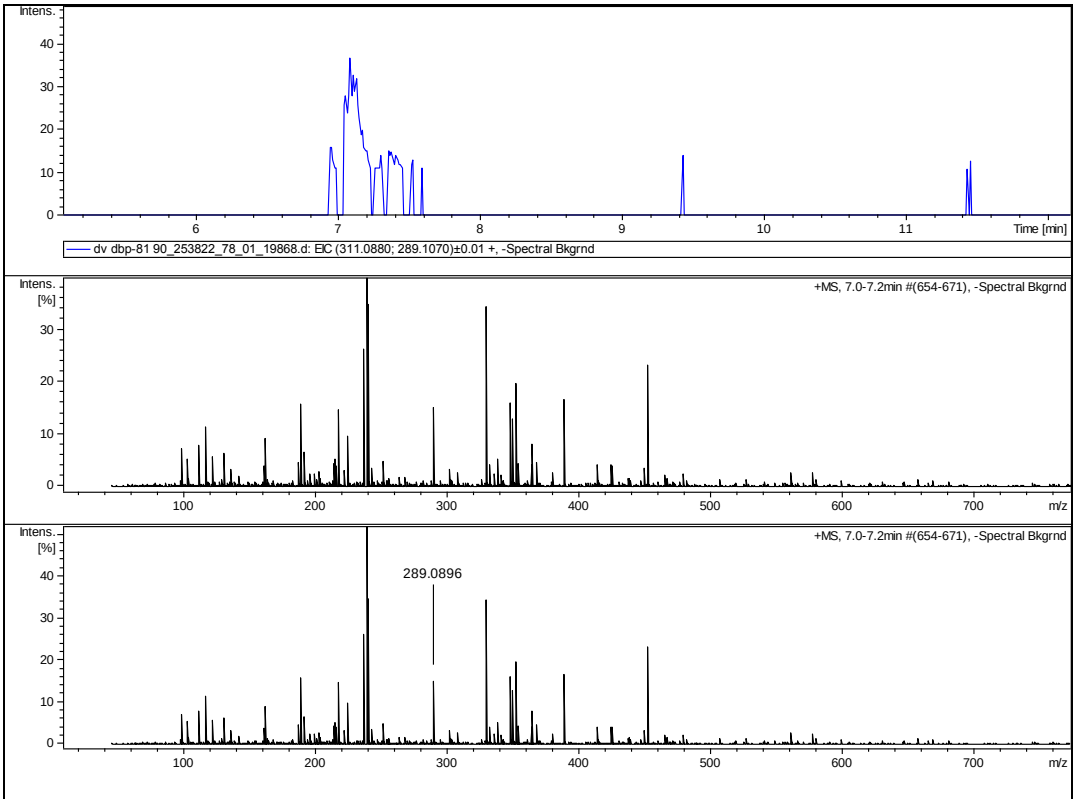

Figure a1.18: $C_{16}H_{16}O_5$ (m/z = 289.107; 311.089)

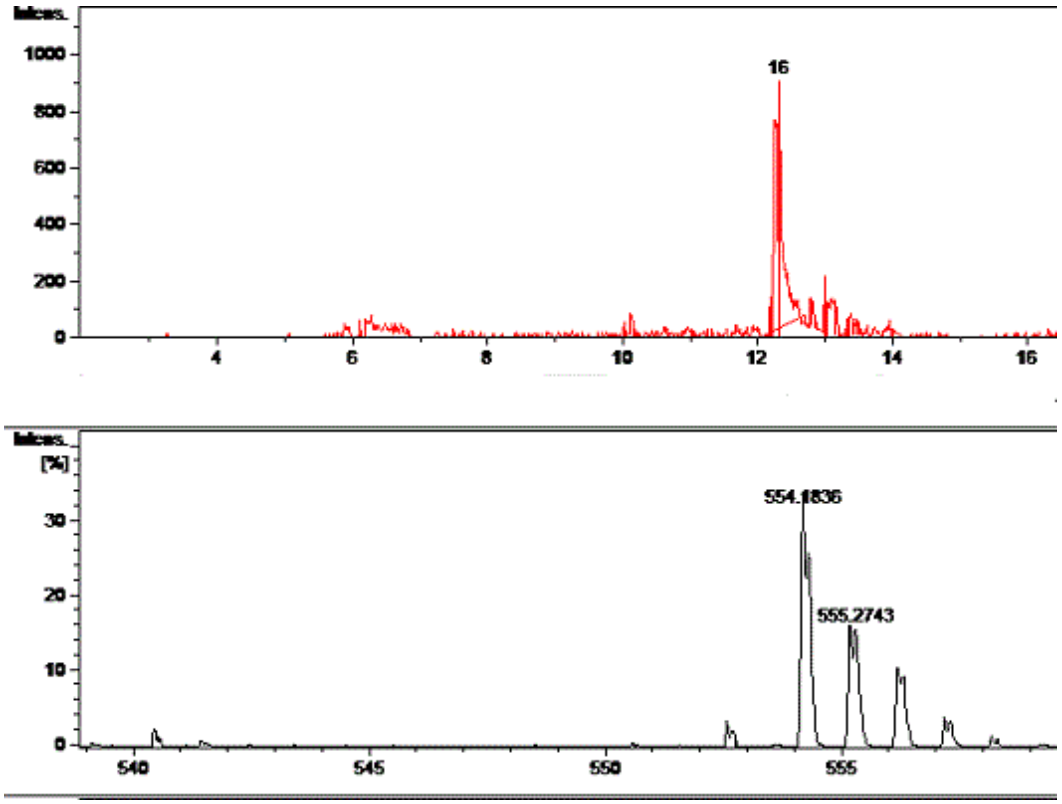

Figure a1.19: C32H42O8 (m/z = 555.295; 577.277)

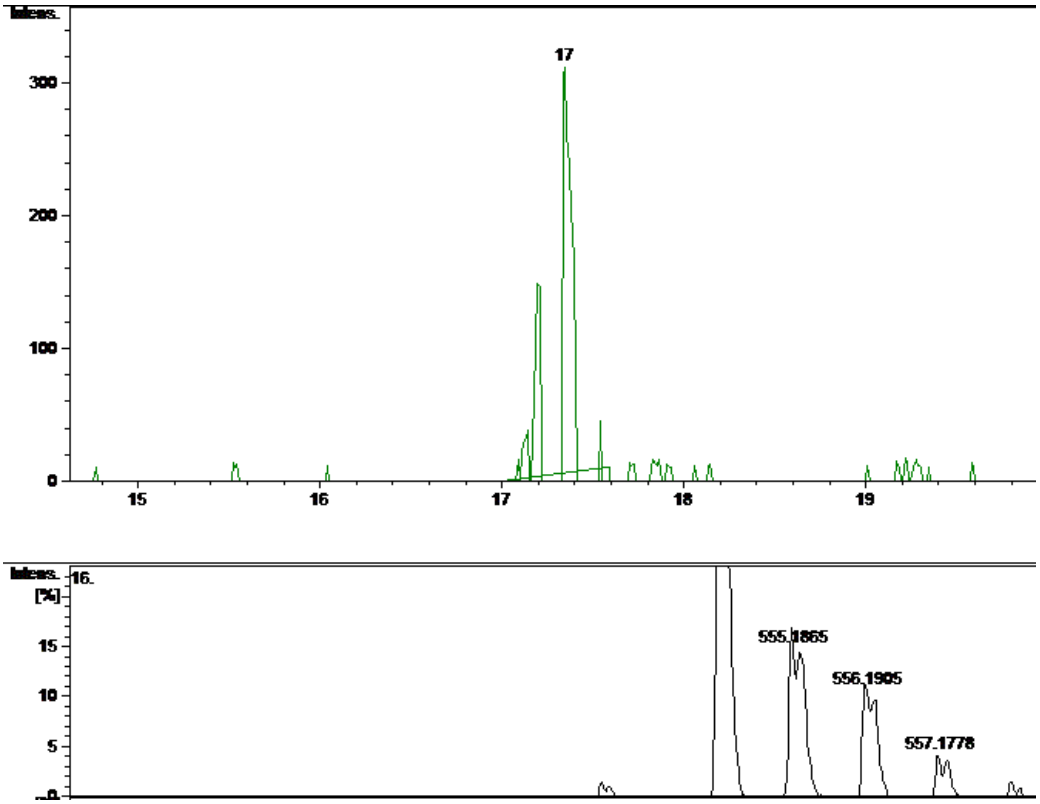

Figure 1.20: C32H40O8 (m/z = 553.295; 575.277)